Direct Analysis Soil-Structure Interaction Case Studies for the ATC-144 Project

Boris Jeremić, Han Yang, Hexiang Wang

University of California, Davis, CA, USA

Bret Lizundia

Rutherford + Chekene, San Francisco, CA, USA

Report version: January 24, 2021, 20:23

Contents

List of Figures

List of Tables

Chapter 1

Executive Summary

This report, conducted as part of the studies for the Applied Technology Council (ATC) ATC-144 project, presents modeling and simulation of Earthquake Soil-Structure Interaction (ESSI) response for three buildings. The first building, the Ventura Hotel building, is excited by the Northridge, Ridgecrest, and Ojai Earthquakes. The second building is a low, steel building that was designed by following ASCE-7 guidance. This building features variations in foundation type, spread foundation versus mat-slab foundation, and is excited with two orthogonal components of an earthquake (2C) using coherent and incoherent seismic motions. In addition, the linear elastic and full nonlinear analyses are performed for both coherent and incoherent seismic excitations. The third building is a tall, concrete frame building on an embedded foundation, designed by following ASCE-7 guidance. This building was also excited using 2C coherent and incoherent seismic motions. In addition, the linear elastic and full nonlinear analyses are done for both coherent and incoherent seismic excitations.

A fourth building, the Loma Linda Veterans Hospital, was initially considered. However, the building's finite element model showed that the building is very stiff, and the first 50 natural modes (eigenmodes) are local oscillations of floor plates. Loma Linda Veterans Hospital building was thus left for future modeling efforts.

It is noted that finite element models for buildings were developed early on and finalized during the early summer of 2019. Early modeling and simulations used Northridge earthquake records. However, in order to address various issues in ESSI response for these buildings, particular new seismic motions had to be developed and scaled for each building.

ESSI results for Ventura Hotel response to Northridge, Ridgecrest, and Ojai earthquakes are available in Section 4.3 on Page 93. It is noted that a very good agreement of simulated and measured seismic motions was obtained for all earthquakes. It is also noted earthquake motions for all three earthquakes were actually very weak, and only minor inelasticity, elasto-plasticity of soil was observed. That is, the behavior was, for the most part, fully elastic. In addition, ESSI analysis results for a set of stronger seismic motions are available for both low, steel braced frame building, Section 4.5 on Page 186, and tall, concrete frame building, Section 4.6 on Page 234,

A number of observations are made below.

- Based on result of analysis of all buildings using Northridge motions as well as set of newly developed motions, it is concluded that nonlinear, inelastic effects in the soil significantly contribute to the reduction of seismic response of buildings.

- It is also observed that spatially variable motions alone, without inelastic effects, do contribute to reducing dynamic response, however, reductions are less than those observed from models that feature nonlinear, inelastic response of soil.

- Deconvolution of seismic motions for soil response that is nonlinear, inelastic, cannot be properly done using linear elastic (equivalent elastic) modeling. For soil response that is nonlinear, inelastic, research is needed to develop better approaches to deconvolution of surface seismic motions to the depth.

- Type of foundations, spread foundations, versus mat-slab foundations, versus embedded foundation, versus pile foundations, play an important role in dynamic response of SSI system. Further work is needed to develop models and gain better understanding on that influence.

- Nonlinear response of structural components can significantly affect overall dynamic response of the SSI system. This is particularly true for use of yielding by design components, for example buckling restrained braces (BRBs). It is recommended to further investigate SSI response for structures with RBRs.

It is hoped that this report, models developed and understanding of Earthquake-Soil-Structure Interaction (ESSI) response developed here will help design and assessment engineers in their everyday work. All models developed for and used in this report are available for the Real-ESSI Simulator program, on the Real-ESSI web site `http://real-essi.us/`.

Chapter 2

Introduction

This report presents details of the analysis of earthquake soil structure interaction behavior for a number of buildings. All modeling and simulation was performed using the Real-ESSI Simulator system (Jeremić et al., 1988-2020).

Models used are available in Jeremić et al. (1989-2021) and can be analyzed and re-analyzed using the publicly available Real-ESSI program. Please see `http://real-essi.us/` for more details on how to obtain Real-ESSI program.

2.1 Seismic Motions Modeling

Seismic motions are developed from prescribed, available surface motions through deconvolution of one component (1C) of motions to a certain depth, and then propagating those motions vertically into the soil structure model using the Domain Reduction Method (Bielak et al., 2003; Yoshimura et al., 2003). More details about the approach used for seismic input are available in Jeremić et al. (1989-2021), Chapter 502.5. Free-field seismic motions development, including seismic wave deconvolution, is described in some detail in Jeremić et al. (1989-2021), Chapter 502.3.

Note that deconvolution is based on a linear elastic methodology. When deconvolution is used for inelastic wave propagation, it has to be done by adjusting the inelastic soil properties and scaling of motions to match observed results. The actual solution to the inelastic deconvolution/convolution problem is an ongoing research topic that needs more work. Most current methods use linear elastic (equivalent elastic) properties, so it is not too hard to match measured surface motions for weak earthquakes. However, when the earthquake is a bit stronger and when soil does plastify, classical methods do not work. Scaling of motions and adjusting elastic soil material properties are actually trial and error methods used to get approximate matching of motions on the ground surface. Simulation results and discussion are presented in Section 4.2.

2.2 Ground Motion Selection and Scaling

This section was written by Bret Lizundia, RUTHERFORD + CHEKENE, San Francisco, CA, USA

The section summarizes the selection and scaling of the baseline ground motions used for direct analysis in the ATC-144 project of two archetype buildings: (1) a low, steel building and (2) a taller, concrete building.

2.2.1 Site Class and Spectral Parameters

Site geotechnical characteristics and soil models are described in Section 2.1.2. ASCE/SEI 7-16 site class and spectral parameters are assumed as follows.

- Low, steel building: The building is assumed to be at the same location as the Loma Linda Hospital in Loma Linda, California (Latitude 34.049601^o, Longitude -117.250073^o) with the same soil conditions, with sands and gravels, with increasing density at depth. The soil profile at the site comes from Stewart and Stewart (1997). The shear wave velocity in the upper 30m is $V_s = 290\,$m/s, resulting in a site classification per ASCE/SEI 7-16 of Site Class D, as it is between $V_s = 183\,$m/s and $V_s = 366\,$m/s. USGS ground motion parameters at the site per online web applications yield $SS = 2.355, S1 = 0.943, SMS = 2.355g$, and $SDS = 1.570g$. Without a site response analysis and with Site Class D, an exception in ASCE/SEI 7-16 Section 11.4.8 allows consideration of a conservative spectral shape with CS taken as the value determined by Eq. 12.8-2 for periods up to 1.5TS and taken as 1.5 times the value computed by ASCE/SEI 7-16 Eq. 12.8-3 for longer periods considering Fv=1.7.

- The 12-story concrete building is assumed to be located in Antioch, California (Latitude 38.0021^o, Longitude -121.7976^o). The soil profile was defined for the example and includes loose sand/fill for $2\,$m, then soft clay to $9\,$m, underlain by medium dense sand to $30\,$m. The average shear wave velocity in the upper $30\,$m is $V_s = 275\,$m/s, yielding Site Class D. Site-specific ground motion parameters are $SS = 1.537, S1 = 0.525, SDS = 1.0g$ and $SD1 = 0.7$.

2.2.2 Ground Motion Selection Process

A key aspect of the direct analyses of the short steel and tall concrete archetype buildings is loading of the systems at various shaking levels. Because the instrumental recordings that are available do not reach the design earthquake level, a suite of ground motions are selected and scaled to the design earthquake (DE) level and beyond. For each building, three records were identified from the FEMA P-695 (FEMA,

2009) far-field suite and amplitude scaled at the building fundamental period to the DE and MCE levels. The three records were selected by examining the RotD50 (Boore, 2010) spectral acceleration amplitude of each ground motion pair in the FEMA P-695 far-field suite and identifying the record pairs at the high end, low end, and at the median at a period 1.5 times the fixed-base fundamental period (Lizundia et al., 2021).

2.2.3 Selected Records

Table 2.1 summarizes the earthquake name, station name, site class, and Vs30 for each of the selected ground motions (Star, 2019, 2020) The information comes from Tables A-4A and A-4B in FEMA P-695 (FEMA, 2009).

Table 2.1: Information on selected earthquake records. Tables A-4A and A-4B are from FEMA P-695 (FEMA, 2009)

				Table A-4A*			Table A-4B*	
		Earthquake Index		ID Number	Earthquake	Site	Site Class	Vs30 (m/s)
Short Building	Medium	120711	120712	7	Kobe, Japan	Nishi-Akashi	C	609
	High	121411	121412	19	Chi-Chi, Taiwan	CHY101	D	259
	Low	121711	121712	22	Friuli, Italy	Tolmezzo	C	425
Tall Building	Medium	120111	120112	1	Northridge	Beverly Hills - Mulholland	D	356
	Low	120121	120122	2	Northridge	Canyon Country-WLC	D	309
	High	120821	120822	10	Kocaeli, Turkey	Arcelik	C	523

Table 2.2: Recorded PGA and PGV for Selected Earthquake Records. From Table A-4C pf FEMA F-695 (FEMA, 2009)

Building	ID Number	PGA_{MAX} (g)	PGV_{MAX} (cm/sec)
Short Building	7	0.51	37
	19	0.44	115
	22	0.35	31
Tall Building	1	0.52	63
	2	0.48	45
	10	0.22	40

2.2.4 Scaling of Ground Motions

For each building, scaling was done to both the DE and MCE$_R$ level and is from Star (2019, 2020).

Figure 2.1 shows four spectra for the low, steel building site: (1) site specific MCE$_R$, (2) site specific Design Earthquake, (3) code Design Earthquake ASCE/SEI 7-16 Section 21.3, and (4) the 80% code minimum for the Design Earthquake in ASCE/SEI 7-16 Section 21.3. The three selected records have been scaled to the Design Earthquake level at the building fundamental period $T = 0.65$ seconds, shown by the red star. Figure 2.2 shows similar plots, but with the records scaled to the MCE$_R$ level at the building fundamental period. Table 2.3 summarizes the scale factors needed to convert the seed record to the Design Earthquake and MCE$_R$ levels at the site. For example, for Records 120711 and 120712, the scale factor at the Design Earthquake level is 1.82.

Table 2.3: Scaling Factors for the Short Building.

	Scaling Factors		
	EQ Index	MCEr	Design
High	121411/2	7.57	5.05
Medium	120711/2	2.74	1.82
Low	121711/2	2.09	1.39

Figure 2.3 shows similar spectra at the tall, concrete building site. The three selected records have been scaled to the Design Earthquake level at the building fundamental period $T = 1.85$ seconds, shown by the red star. Figure 2.4 shows similar plots, but with the records scaled to the MCE R level at the building fundamental period. Table 2.4 summarizes the scale factors needed to convert the seed record to the Design Earthquake and MCE$_R$ levels at the site. For example, for Records 120111 and 120112, the scale factor at the Design Earthquake level is 1.94.

Table 2.4: Scaling Factors for the Tall Building.

		Scaling Factors	
	EQ Index	MCEr	Design
High	120821/2	5.327	3.5482
Medium	120111/2	2.9165	1.9426
Low	120121/2	2.7185	1.8107

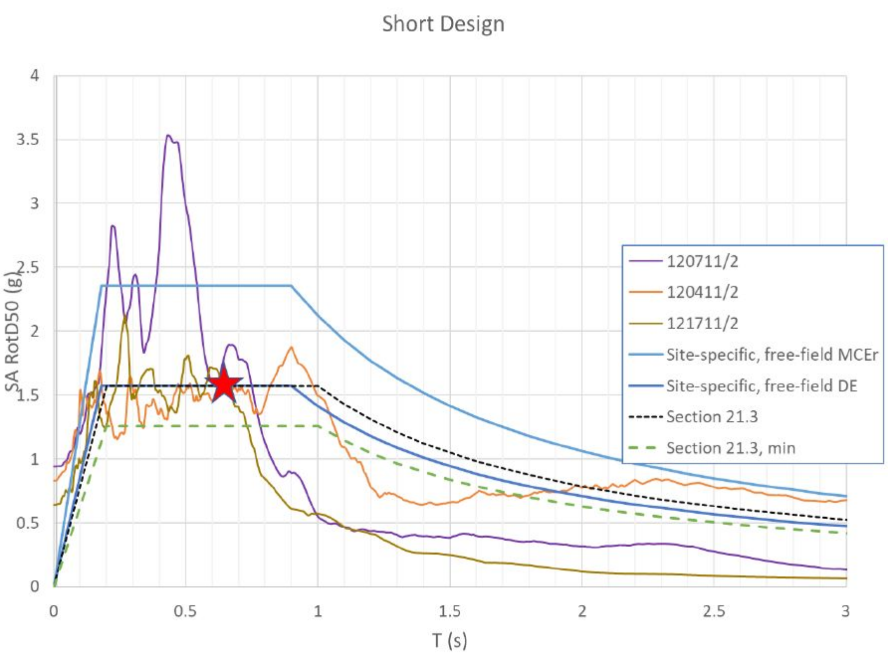

Figure 2.1: Low, steel building ground motion scaling at the DE level.

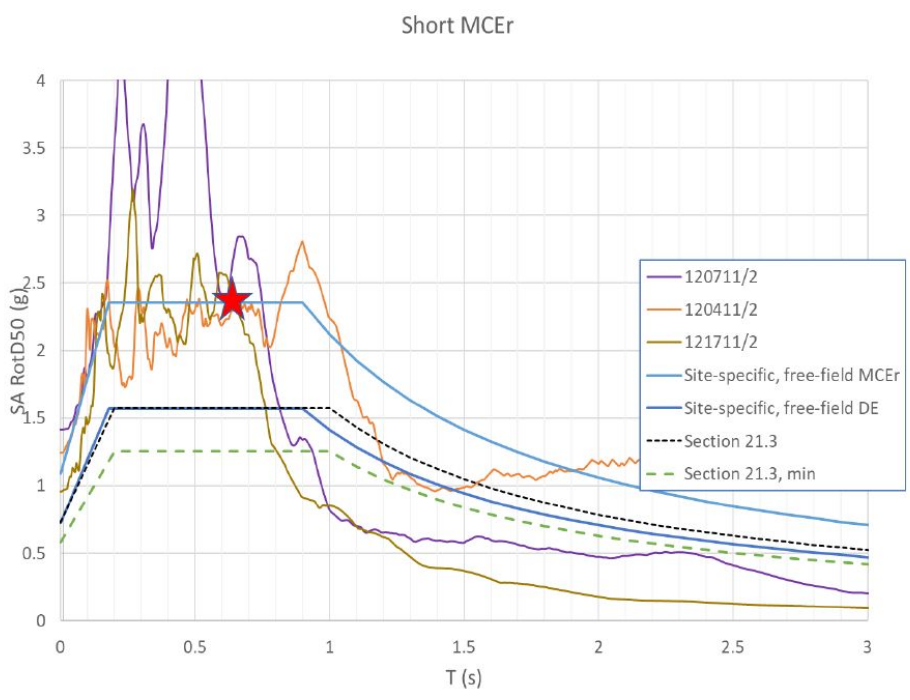

Figure 2.2: Low, steel building ground motion scaling at the MCE_R level.

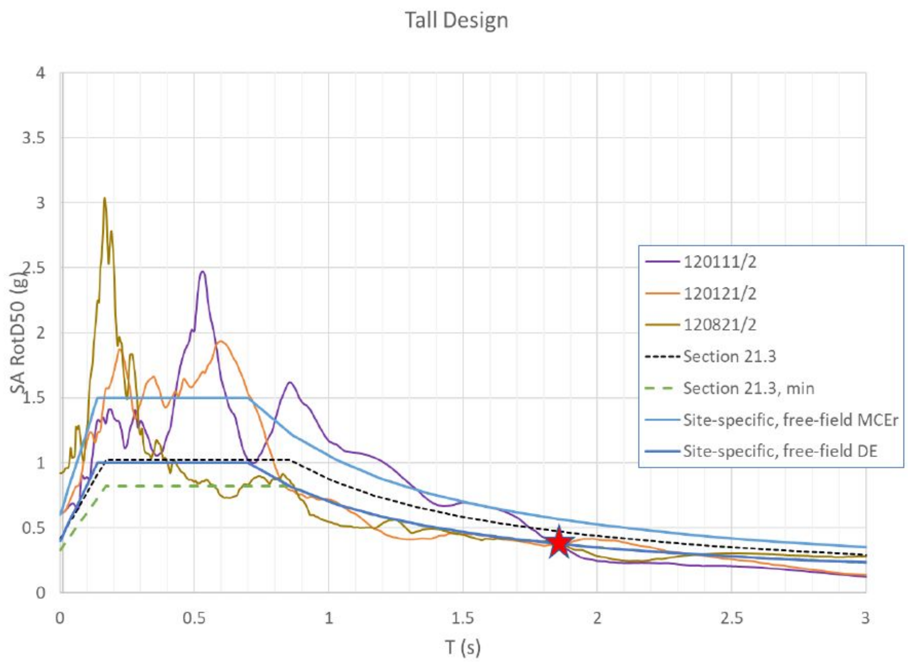

Figure 2.3: Tall, concrete building ground motion scaling at the DE level.

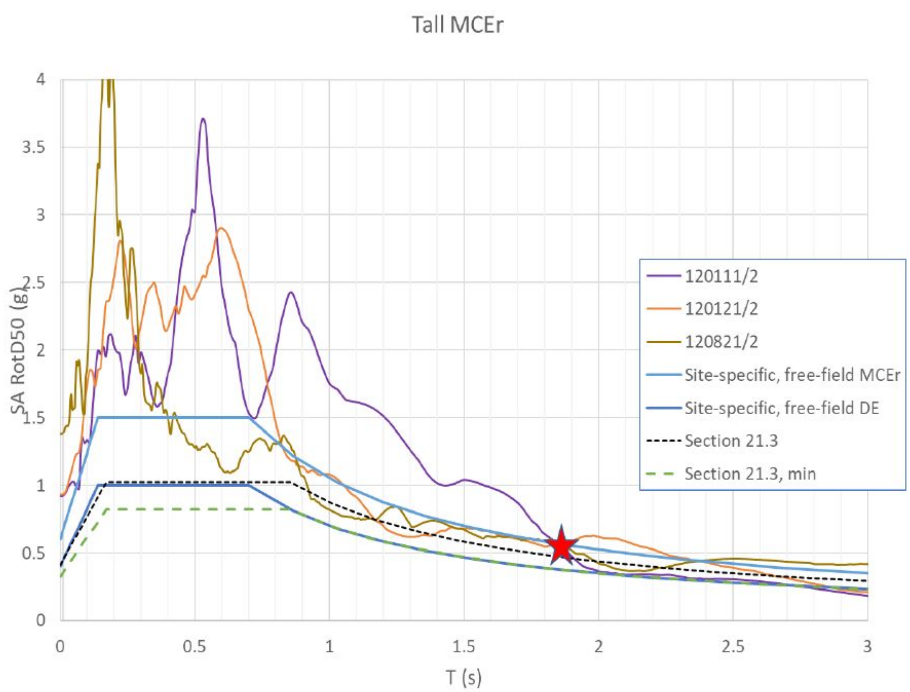

Figure 2.4: Tall, concrete building ground motion scaling at the MCE$_R$ level.

2.3 Soil Modeling

A number of elastic and inelastic, nonlinear, elastic-plastic soil models were used in analysis. Details of soil models are provided in sections below. Theoretical background, and further modeling details for each soil model used are available in Jeremić et al. (1989-2021).

2.3.1 Low, Steel Building Site

The site information for the low building, obtained from the Loma Linda Hospital site in Stewart and Stewart (1997), is shown in Figure 2.5.

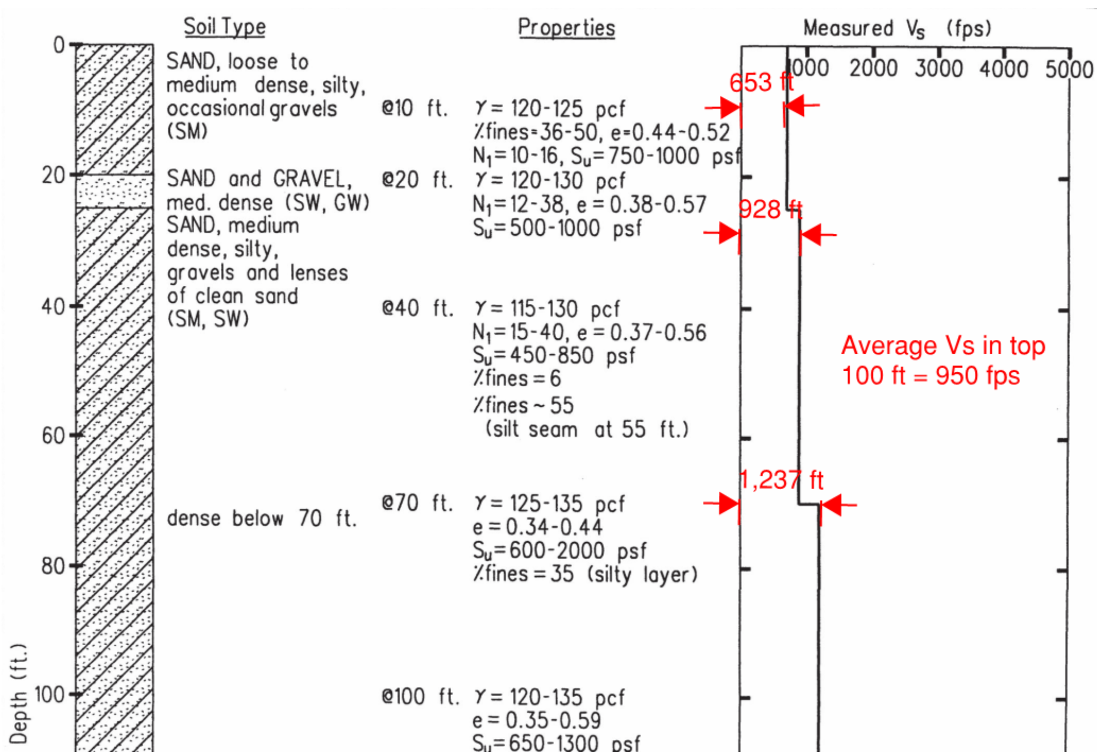

Figure 2.5: Site condition for low, steel frame building.

Soil Model - Elastic 1 (SM-EL1): Table 2.5 shows material parameters for the linear elastic model used for soil.

Table 2.5: Elastic material parameters for soil for low, steel building model.

Layer ID		1	2
Thickness [ft]		25	30
Mat. Param.	`mass_density` $[\mathrm{kg/m^3}]$	1954	1954
	`Young's modulus E [MPa]`	203.2	412.7
	`Poisson_ratio`	0.3	0.3

Soil Model - Elastic-Plastic 1 (SM-EP1) :

Tables 2.6 shows material parameters for inelastic modeling of soil: von Mises Armstrong-Frederick kinematic hardening with vanishing elastic region (SM-EP1).

Table 2.6: Inelastic, elastic-plastic material parameters for soil with vanishing elastic region for low, steel building model (SM-EP1).

Layer ID		1	2
Thickness [ft]		25	30
Mat. Param.	mass_density $[\mathrm{kg/m^3}]$	1954	1954
	Young's modulus E [MPa]	203.2	412.7
	Poisson_ratio	0.3	0.3
	von_Mises_radius [Pa]	1000	1000
	armstrong_frederick_ha [Pa]	3×10^6	3×10^6
	armstrong_frederick_cr	37.5	52.0
	Initial elastic shear stiffness G [MPa/ksi]	78.2/11.3	158.7/ 23.0
	1% secant shear stiffness [MPa/ksi]	1.3/0.2	1.3/0.2
	Initial yielding stiffness [MPa/ksi]	1.1/0.2	1.1/0.2
	Ultimate shear strength [kPa/psi]	40/5.8	45/6.5

Figure 2.6 shows the cyclic behavior of top layer soil at low building engineering site modeled with vanishing elastic region (SM-EP1).

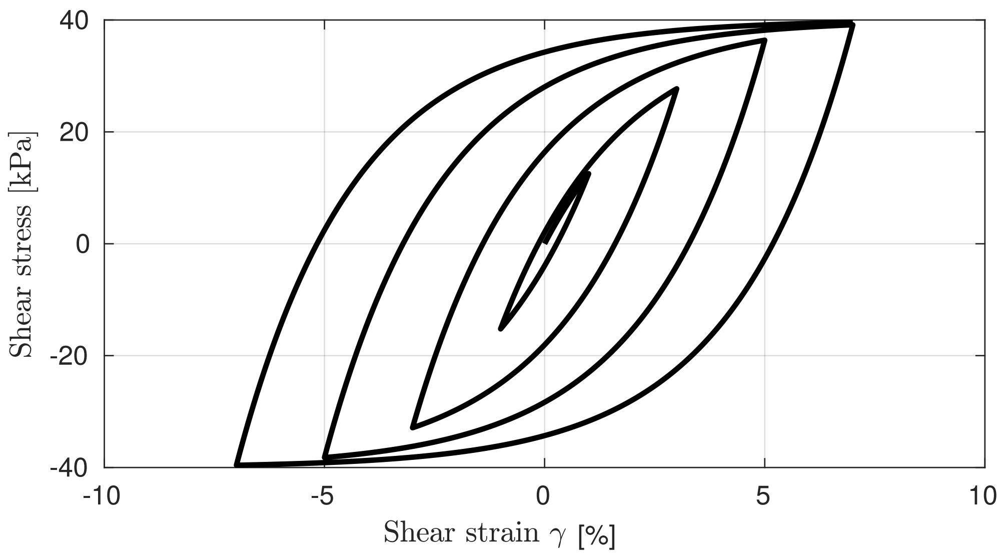

Figure 2.6: Cyclic behavior of top layer soil with vanishing elastic region at the low building engineering site with undrained shear strength 40kPa, approx. 850psf (SM-EP1).

Soil Model - Elastic-Plastic 2 (SM-EP2): The elastoplastic model can also have non-vanishing elastic region. The model parameters for the low, steel building site (SM-EP2) is given in Table 2.7.

Table 2.7: Inelastic, elastic-plastic material parameters for soil with non-vanishing elastic region for the low, steel building model (SM-EP2).

Layer ID		1	2
Thickness [ft]		25	30
Mat. Param.	mass_density $[\mathrm{kg/m^3}]$	1954	1954
	Young's modulus E [MPa]	203.2	412.7
	Poisson_ratio	0.3	0.3
	von_mises_radius [Pa]	10000	20000
	armstrong_frederick_ha [Pa]	3×10^6	3×10^6
	armstrong_frederick_cr	50	52.0
	Initial elastic shear stiffness G [MPa/ksi]	78.2/11.3	158.7/23.0
	1% secant shear stiffness [MPa/ksi]	2.1/0.3	2.6/0.4
	Initial yielding stiffness [MPa/ksi]	1.0/0.15	1.0/0.15
	Ultimate shear strength [kPa/psi]	40/5.8	45/6.5

The stronger soil model, an elastoplastic model with non-vanishing elastic region, is shown in Figure 2.7.

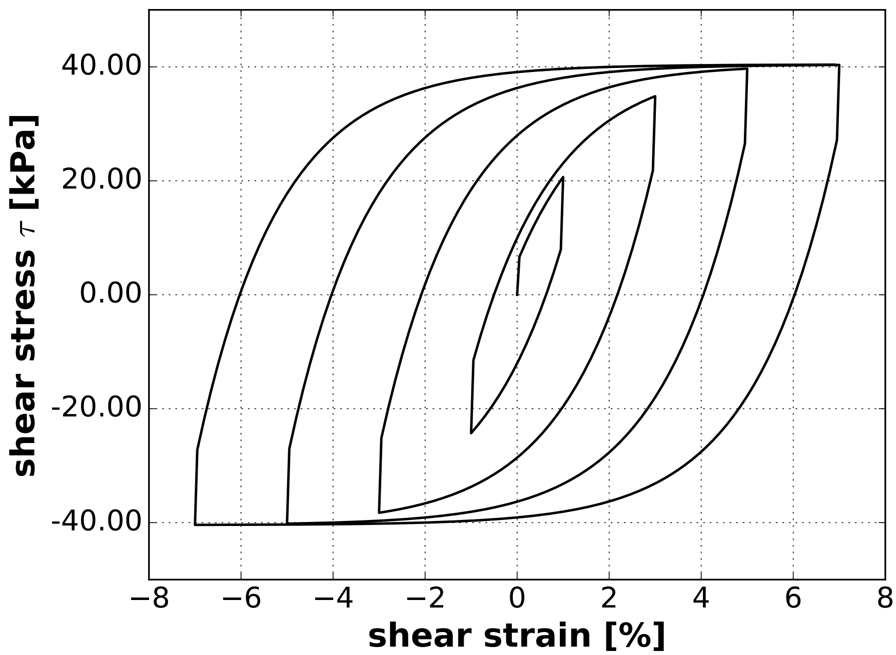

Figure 2.7: Cyclic behavior of top layer soil with non-vanishing elastic region at the low building engineering site with undrained shear strength 40kPa, approx. 850psf (SM-EP2).

Soil Model - Elastic-Plastic 3 (SM-EP3): The pressure-dependent hyperbolic Drucker Prager model with Armstrong-Frederick kinematic hardening is calibrated to have a friction angle of $\Phi = 36°$, that should model properly generic sand material. The model parameters for the low, steel building site are given in Table 2.8.

Table 2.8: Inelastic, elastic-plastic soil material parameters of hyperbolic Drucker Prager model with Armstrong-Frederick kinematic hardening for the low, steel building model (SM-EP3).

Layer ID		1	2
Thickness [ft]		25	30
Mat. Param.	`mass_density` $[\mathrm{kg/m^3}]$	1954	1954
	`Young's modulus E [MPa]`	203.2	412.7
	`Poisson_ratio`	0.3	0.3
	`Drucker-Prager_k`	0.107	0.107
	`cohesion [Pa]`	3×10^4	3×10^4
	`rounded_distance [Pa]`	5×10^4	5×10^4
	`dilatancy_angle`	0	0
	`armstrong_frederick_ha [Pa]`	5×10^6	5×10^6
	`armstrong_frederick_cr`	50	50
	`isotropic_hardening_rate [Pa]`	0	0

The cyclic behavior of pressure-dependent hyperbolic Drucker Prager material with Armstrong-Frederick kinematic hardening (SM-EP3) is shown in Figure 2.8 for soil at a depth of 10m.

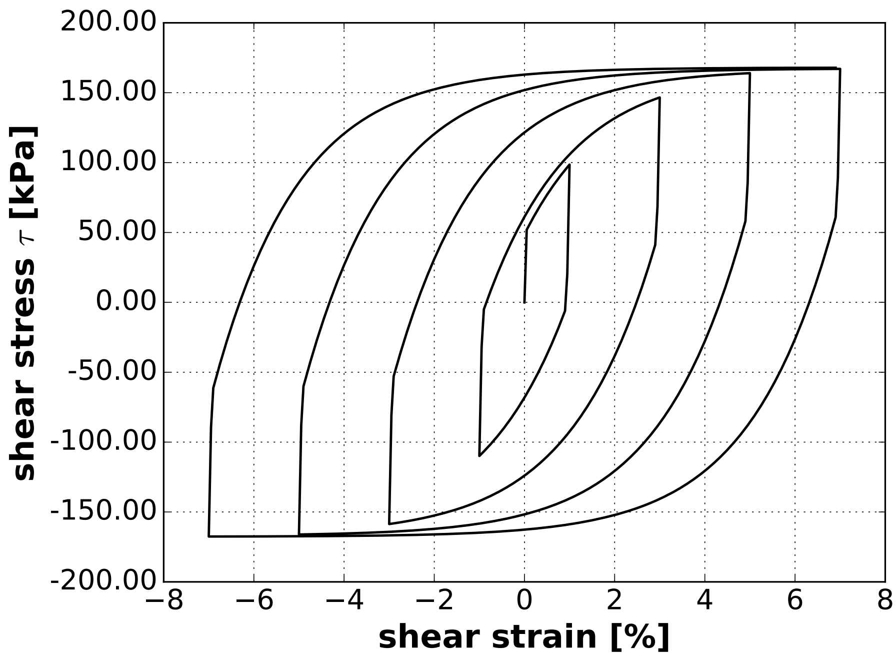

Figure 2.8: Cyclic behavior of hyperbolic Drucker Prager material with Armstrong-Frederick kinematic hardening at a depth of 10m, overburden pressure around 200 kPa (SM-EP3).

2.3.2 Tall, Reinforced Concrete Building Site

The site information for the tall reinforced concrete building is shown in Figure 2.9.

Depth	Geotechnical parameters	Nominal unit capacities
0 to 5 ft	Loose sand/fill γ= 110 pcf effective friction angle = 28 deg soil modulus parameter, k = 25 pci v_{s0} = 580 ft/s	neglect skin friction neglect end bearing
5 to 30 ft	Soft clay γ= 110 pcf undrained shear strength, s_u = 700 psf soil modulus parameter, k = 25 pci strain at 50 percent of maximum stress, ε_{50} = 0.01 v_{s0} = 700 ft/s	skin friction = 0.40 ksf neglect end bearing
30 to 100 ft	Medium dense sand γ= 120 pcf effective friction angle = 36 deg soil modulus parameter, k = 50 pci v_{s0} = 1,040 ft/s	skin friction = 3.0 ksf end bearing = 100 ksf
Pile cap resistance	300 pcf, ultimate passive pressure	

Figure 2.9: Site condition for tall, reinforced concrete frame building.

Soil Model - Elastic 2 (SM-EL2): Table 2.9 show material parameters for elastic modeling of soil for the tall, concrete building site (SM-EL2).

Table 2.9: Elastic material parameters for soil for the tall, concrete building model (SM-EL2).

Layer ID		1	2	3
Thickness [ft]		5	25	70
Mat. Param.	mass_density $[\mathrm{kg/m^3}]$	1762	1762	1762
	Young's modulus E [MPa]	148.4	208.6	502.2
	Poisson_ratio	0.3	0.3	0.3

Soil Model - Elastic-Plastic 4 (SM-EP4): Table 2.10 show material parameters for inelastic modeling of soil: von Mises Armstrong-Frederick kinematic hardening with a vanishing elastic region for the tall, concrete building site (SM-EP4).

Table 2.10: Inelastic, elastic-plastic material parameters for soil for the tall, concrete building model (SM-EP4).

Layer ID		1	2	3
Thickness [ft]		5	25	70
Mat. Param.	mass_density [$\mathrm{kg/m^3}$]	1762	1762	1762
	Young's modulus E [MPa]	148.4	208.6	502.2
	Poisson_ratio	0.3	0.3	0.3
	von_mises_radius [Pa]	1000	1000	1000
	armstrong_frederick_ha [Pa]	1.5×10^6	4.5×10^6	24×10^6
	armstrong_frederick_cr	62.5	70.0	66.5
	Initial elastic stiffness G [MPa/ksi]	57.1/8.3	80.2/11.6	193.2/28.0
	1% secant shear stiffness [MPa/ksi]	0.76/0.11	2.1/0.3	10.9/1.6
	Initial yielding stiffness [MPa/ksi]	0.5/0.07	1.5/0.22	8.0/1.16
	Ultimate shear strength [kPa/psi]	15/2.2	38/5.5	210/30.5

The cyclic behavior of second layer soil at the tall building engineering site (SM-EP4) is shown in Figure 2.10

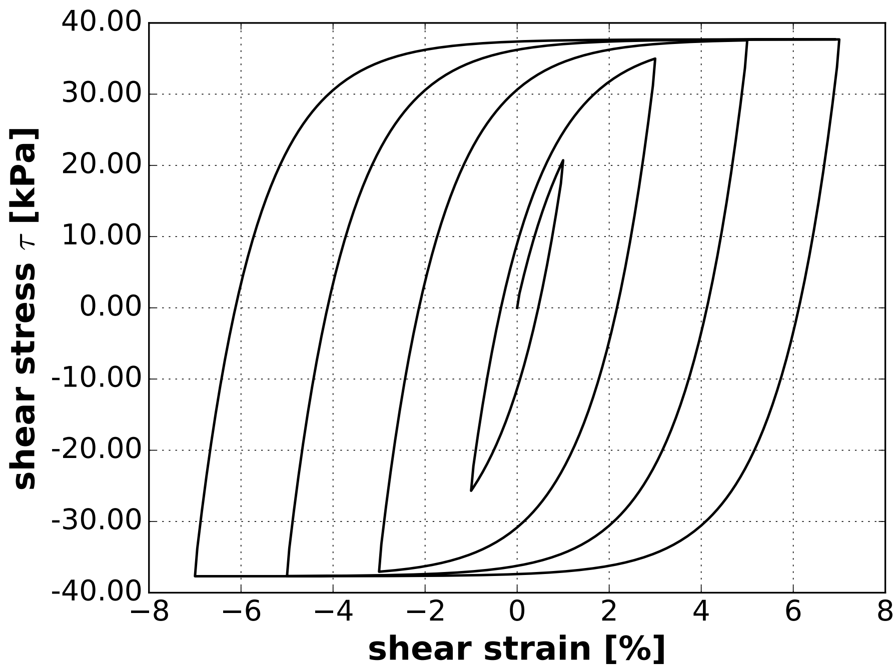

Figure 2.10: Cyclic behavior of the second layer soil at the tall building engineering site (SM-EP4).

2.3.3 Ventura Hotel Site

The Ventura site information is shown in Figure 2.11.

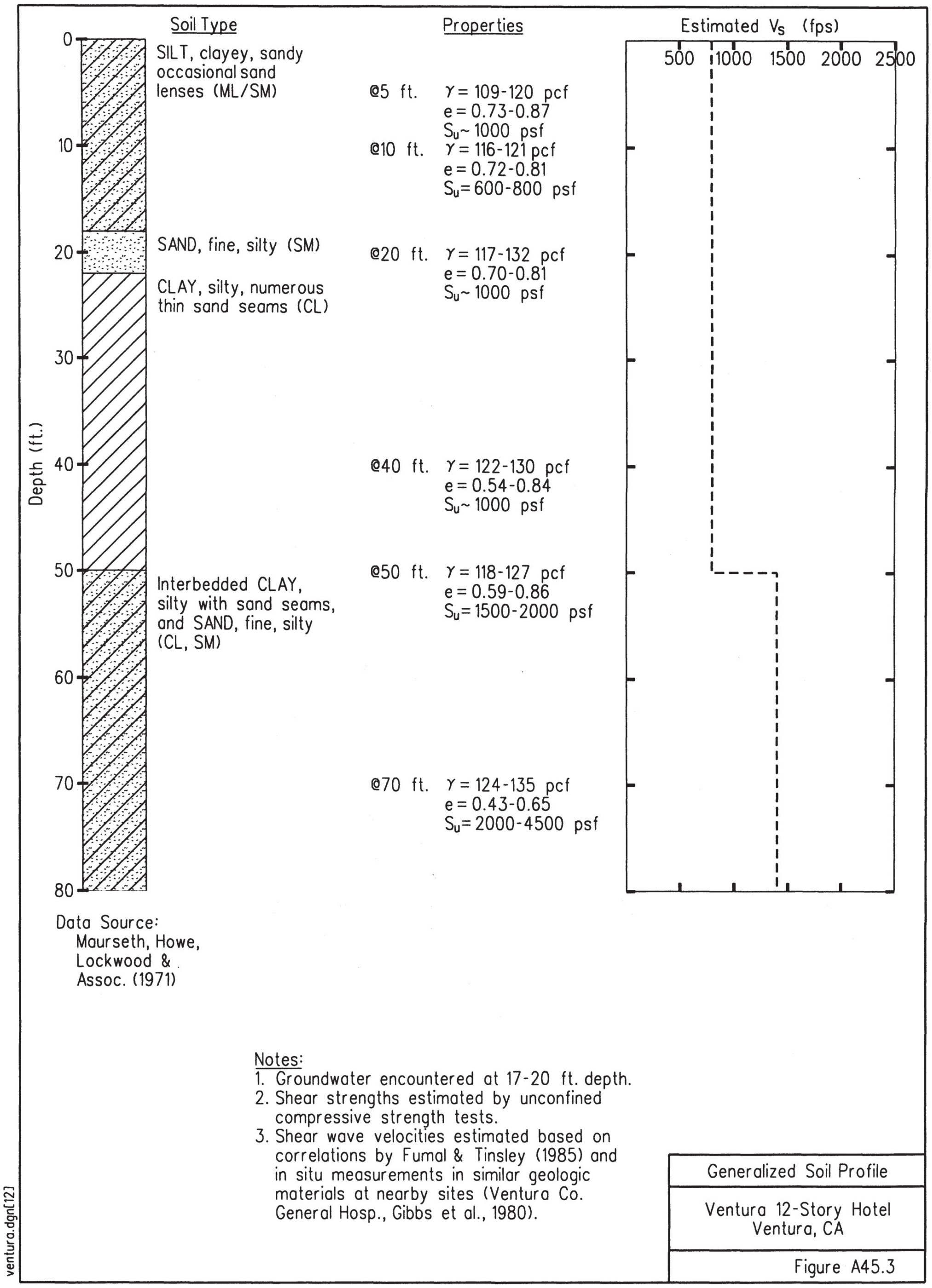

Figure 2.11: Site condition and soil profile for the 12-story Ventura Hotel.

It is noted that multiple material models were used for modeling soil for the Ventura site. A number of material models were used in order to test sensitivity of response of the Ventura Hotel soil-structure system to increasing level of modeling sophistication. Initial modeling was performed using linear elastic material model. Next, an elastic-plastic material model with no volume change was used. Lastly, an elastic-plastic material model was used that allowed for compression and dilatancy, as well as pressure dependance. Models are described in some detail on next three pages, while detailed background and further modeling details are available in Jeremić et al. (1989-2021). A number of material models were used in order to test sensitivity of response of the Ventura Hotel soil-structure system to soil material modeling.

Soil Model - Elastic 3 (SM-EL3): Table 2.11 shows malterial parameters for elastic soil material parameters for the Ventura site.

Table 2.11: Elastic soil material parameters for the Ventura site (SM-EL3).

Layer ID		1	2
Thickness [ft]		50	50
Mat. Param.	`mass_density` $[\mathrm{kg/m^3}]$	1922	1922
	`Young's modulus E [MPa]`	297.1	909.9
	`Poisson_ratio`	0.3	0.3

Soil Model - Elastic-Plastic 5 (SM-EP5): Table 2.12 shows material parameters for inelastic, von Mises soil material parameters for the Ventura site (SM-EP5).

Table 2.12: Inelastic, von Mises soil material parameters for the Ventura site (SM-EP5).

Layer ID		1	2
Thickness [ft]		50	50
Mat. Param.	`mass_density` $[\mathrm{kg/m^3}]$	1922	1922
	`Young's modulus E [MPa]`	297.1	909.9
	`Poisson_ratio`	0.3	0.3
	`von_mises_radius [Pa]`	5000	5000
	`armstrong_frederick_ha [Pa]`	4×10^6	8×10^6
	`armstrong_frederick_cr`	50	50

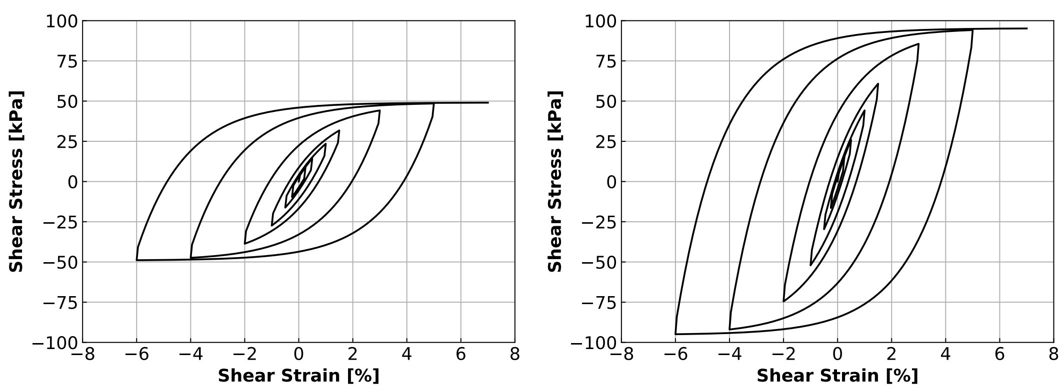

(a) Layer 1 (Depth = 10 ft) (b) Layer 2 (Depth = 50 ft)

Figure 2.12: Cyclic behavior of inelastic, von Mises soil layers at the Ventura site (SM-EP5).

Soil Model - Elastic-Plastic 6 (SM-EP6): Table 2.13 shows material parameters for inelastic, hyperbolic Drucker-Prager with Armstrong-Frederick kinematic hardening and vanishing elastic region soil material parameters for the Ventura site (SM-EP6).

Table 2.13: Inelastic, hyperbolic Drucker-Prager soil material parameters for the Ventura site (SM-EP6).

Layer ID		1	2
Thickness [ft]		50	50
Mat. Param.	`mass_density` [kg/m^3]	1922	1922
	`Young's modulus E [MPa]`	297.1	909.9
	`Poisson_ratio`	0.3	0.3
	`Drucker-Prager_k`	0.01	0.01
	`cohesion [kPa]`	30	30
	`rounded_distance [kPa]`	5	5
	`dilatancy_angle`	0	0
	`armstrong_frederick_ha [Pa]`	3×10^6	3×10^6
	`armstrong_frederick_cr`	50	50
	`isotropic_hardening_rate [Pa]`	0	0

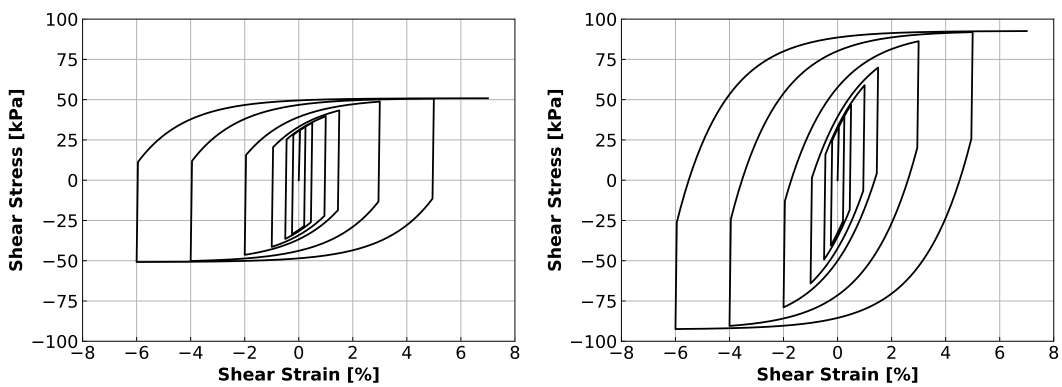

(a) Layer 1 (Depth = 10 ft) (b) Layer 2 (Depth = 50 ft)

Figure 2.13: Cyclic behavior of inelastic, hyperbolic Drucker-Prager soil layers at the Ventura site (SM-EP6).

2.4 Foundation Modeling

The Ventura Hotel model has a pile foundation.

The low, steel building features spread foundations, while there is a variant with slab foundation as well.

The tall, concrete frame building features embedded foundations with slab and foundation walls.

2.5 Structural Modeling

Structural modeling was done using a number of different finite elements and material models. The following finite elements were used:

- Beam-column finite elements for beams, columns, piles, and buckling-restrained braces (BRB)
- Wall-Plate-Shells finite elements for wall, plates, and shells

Linear elastic material was used for most structural modeling, except for the BRBs. Calibration of the buckling-restrained brace (BRB) with 1D steel-fiber truss element is shown in Figure 2.14. Calibration was performed by characterizing steel response within the BRB and optimizing steel elastic-plastic parameters.

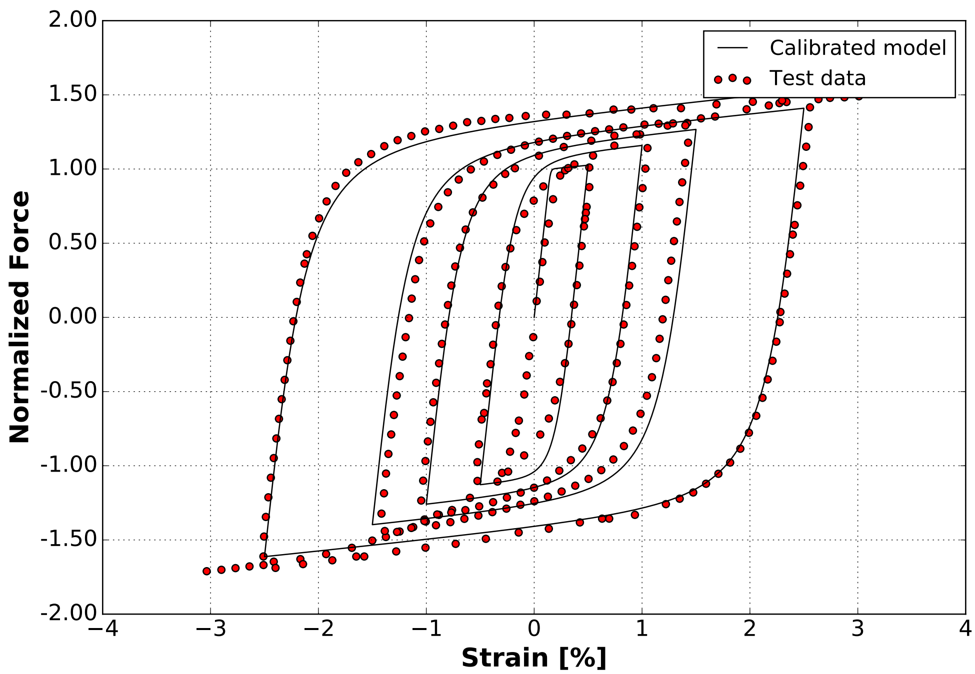

Figure 2.14: Calibration of the inelastic behavior of buckling restrained brace (BRB)

Theoretical background, formulation and details of used finite elements as well as details about material models used are available in Jeremić et al. (1989-2021).

Chapter 3

Building Models

Four building models were developed, namely:

- Ventura Hotel model
- Loma Linda Hospital model
- The low, steel building model
- The tall concrete building model

Models were developed with significant attention to detail, for both structural, foundation and soil components. All developed models feature both soil and structure components. In addition, the Domain Reduction Method (DRM) Bielak et al. (2003); Yoshimura et al. (2003) is used for seismic motion input. Visualization of model finite element meshes is provided in next sections. Structural elements, beam-columns and walls-plates-shells elements are clearly visible. Foundation slabs and walls as well as piles are visualized as well, with an addition of pile-soil interface elements as well for Ventura Hotel. It is noted that the DRM layers are clearly visible as layers of soil-solid part of models.

Model input files that describe finite elements, material properties, coherent and incoherent input motions, used for all soil-structure system models for for Real-ESSI Simulator System (Jeremić et al., 1988-2020), are available in a human readable text format, at the Real-ESSI web site `http://real-essi.us/` with specific input file language described by Jeremić et al. (1989-2021). Interested user can use provided models to perform all the analysis described in this report using Real-ESSI Simulator. Finite element models were developed from source documents provided by California Geological Survey (CGS).

3.1 Ventura Hotel

Visualization of the finite element model is provided in next Figures. It is noted that all the details of models, including finite elements used, material properties for structural and soil materials, as well as coherent and incoherent input motions are available at the Real-ESSI web site http://real-essi.us/ while the specific input file language described by Jeremić et al. (1989-2021).

3.1.1 Finite Element Model

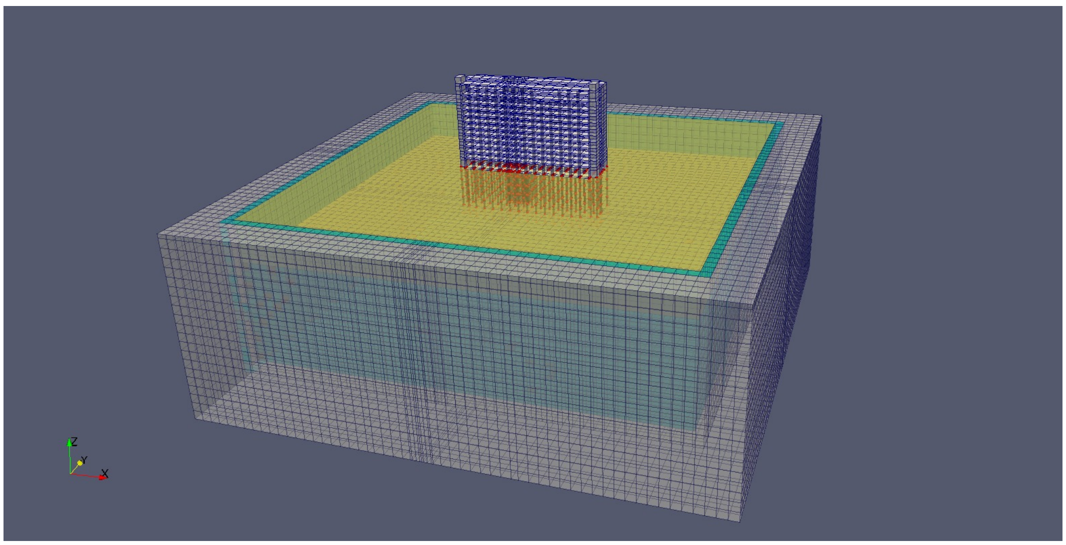

Figure 3.1: Ventura Hotel model. Structural model is founded on piles, and is located within a soil model, with DRM layer visible on model edges.

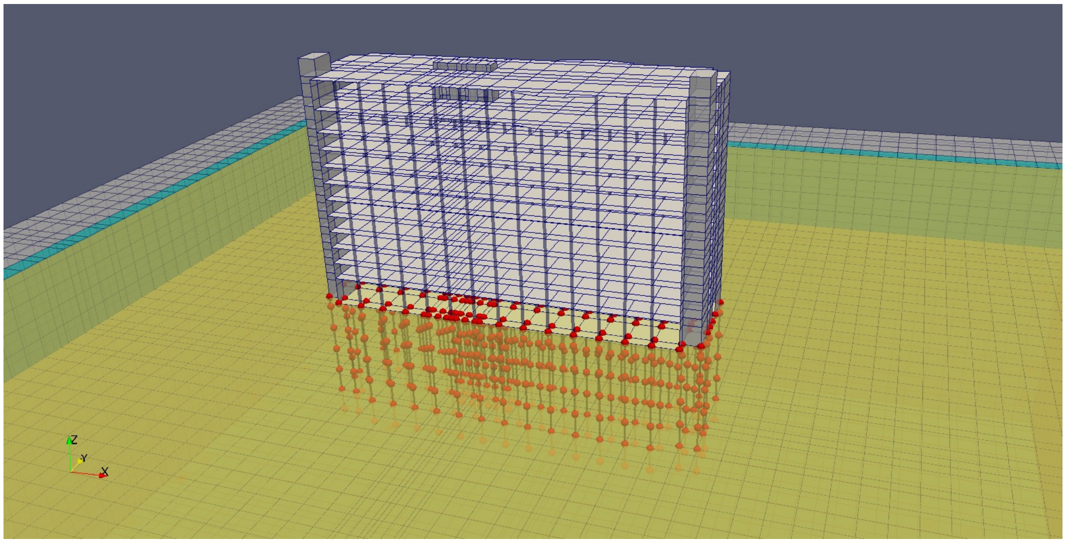

Figure 3.2: Ventura Hotel model. Structural model is founded on piles, and is located within a soil model, with DRM layer visible on model edges.

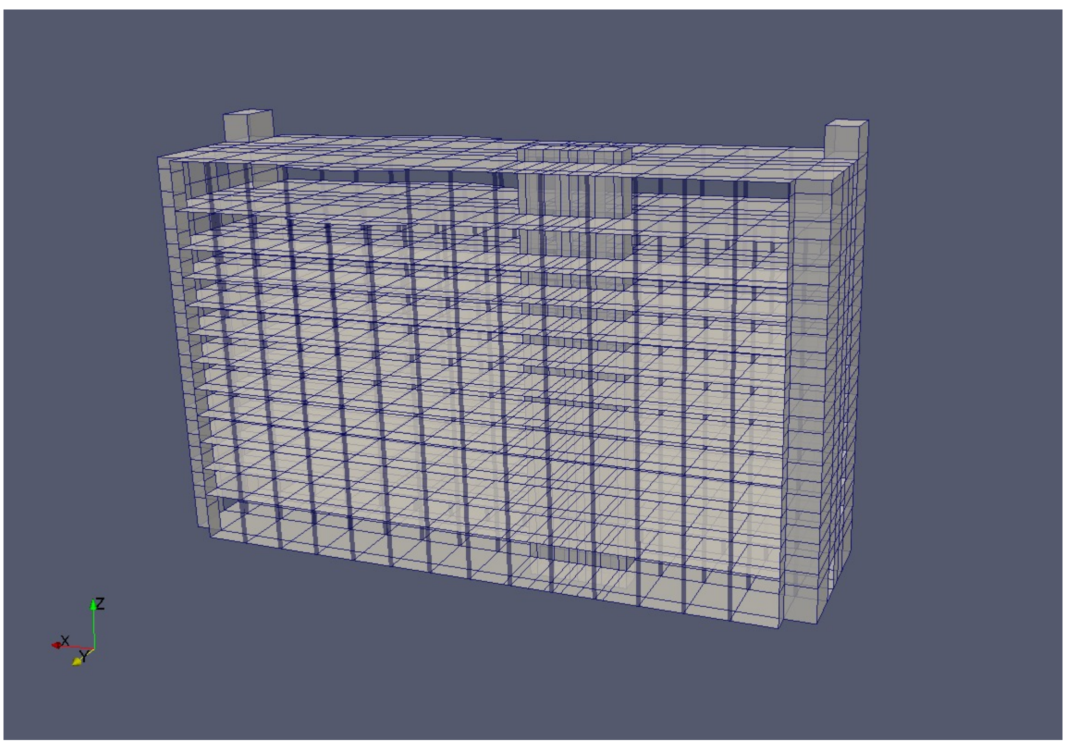

Figure 3.3: Ventura Hotel model.

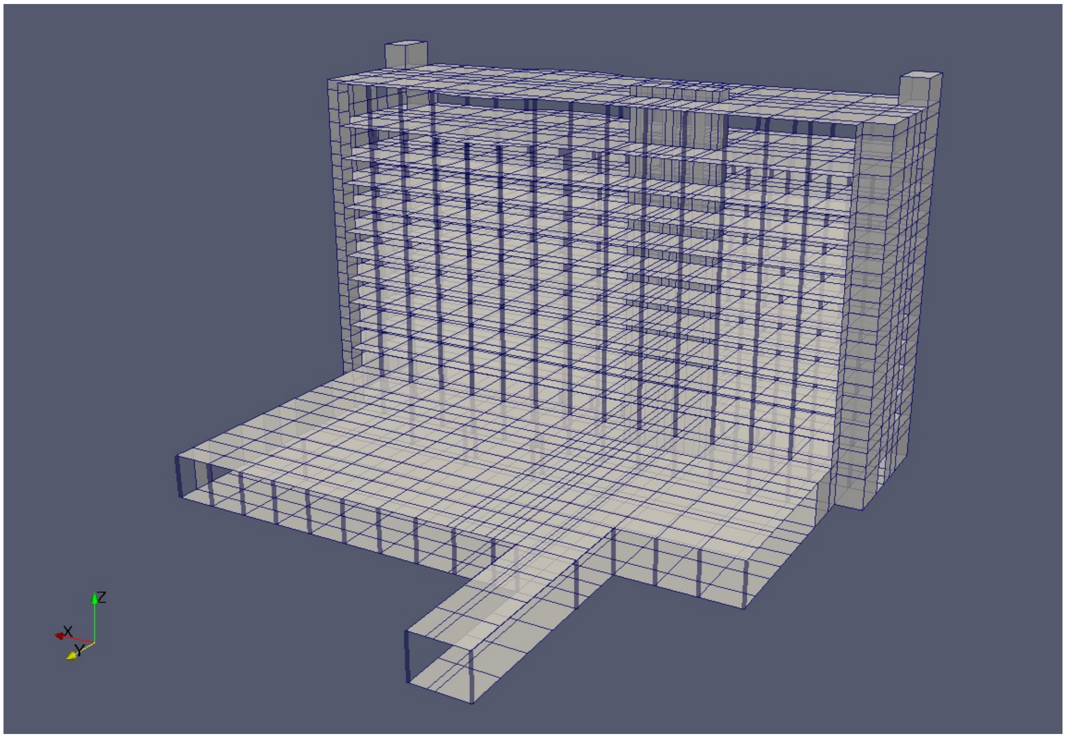

Figure 3.4: Ventura Hotel model.

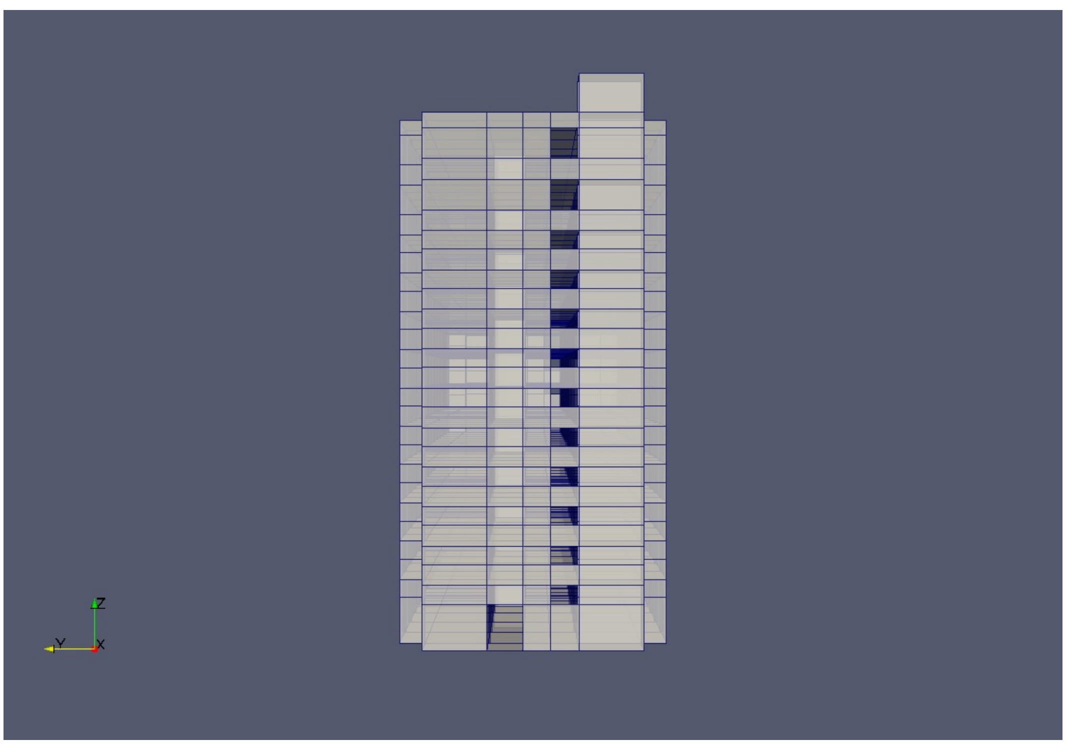

Figure 3.5: Ventura Hotel model, view in X direction.

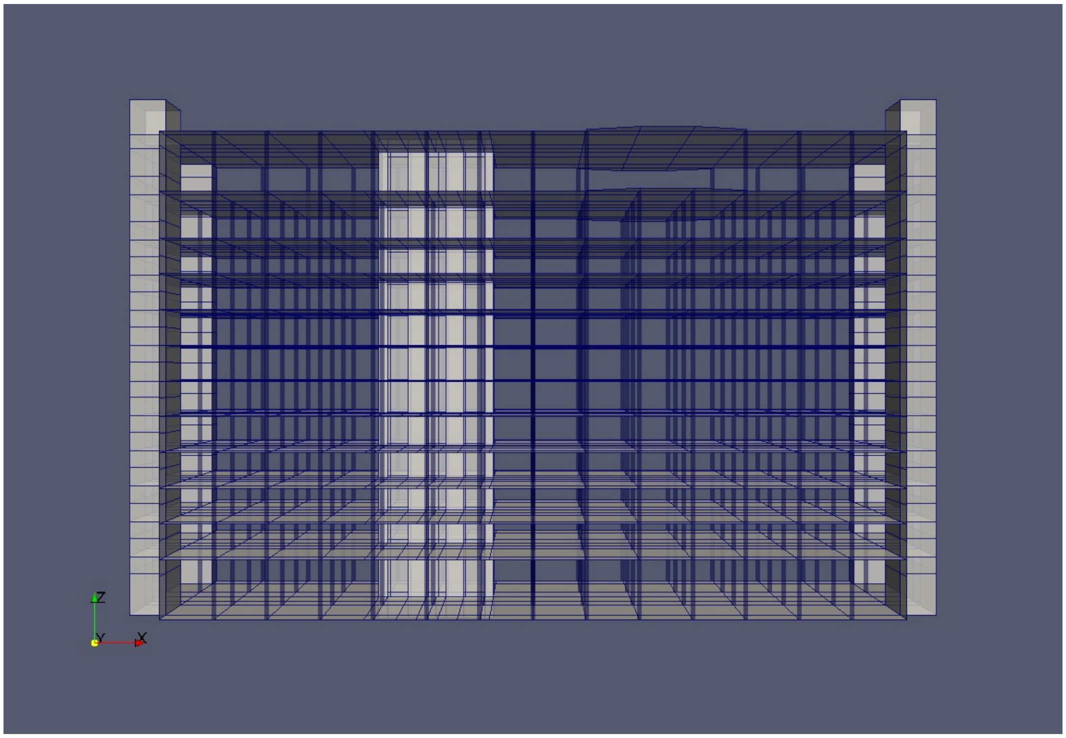

Figure 3.6: Ventura Hotel model, view in Y direction.

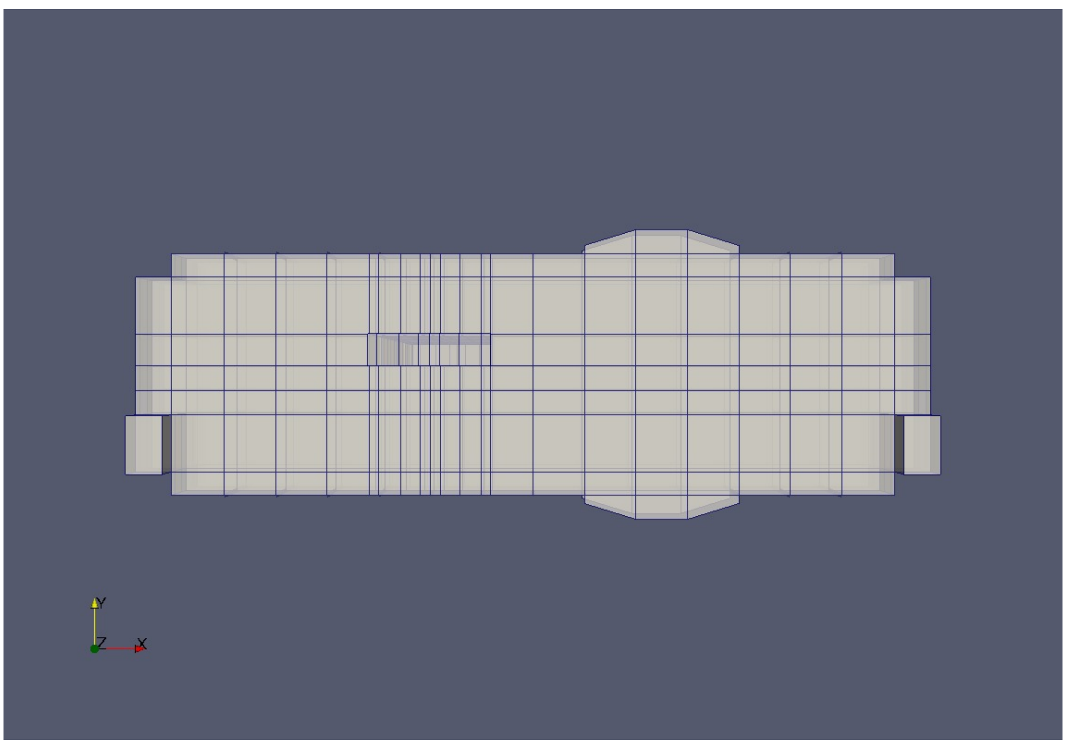

Figure 3.7: Ventura Hotel model, view in Z direction.

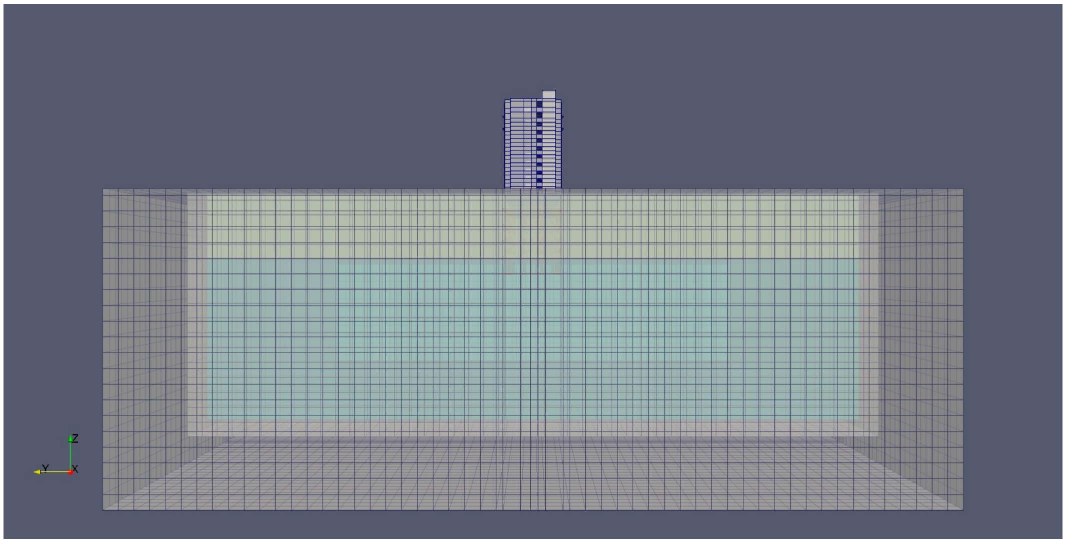

Figure 3.8: Ventura Hotel model, view along X direction. Structural model is founded on piles, and is located within a soil model, with DRM layer visible on model edges.

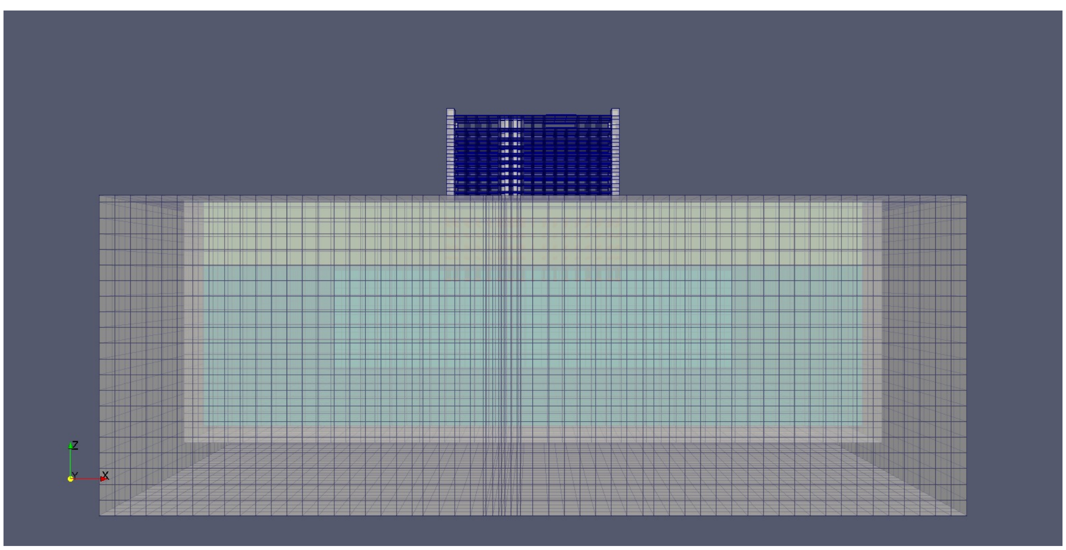

Figure 3.9: Ventura Hotel model, view along Y direction. Structural model is founded on piles, and is located within a soil model, with DRM layer visible on model edges.

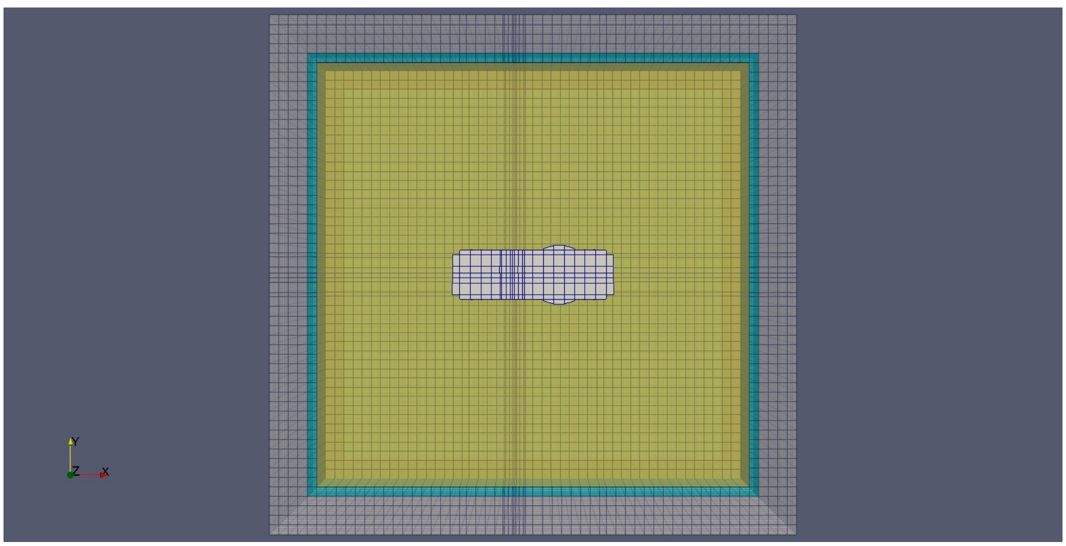

Figure 3.10: Ventura Hotel model, view along Z direction. Structural model is founded on piles, and is located within a soil model, with DRM layer visible on model edges.

3.2 Loma Linda Hospital

Visualization of the finite element model is provided in next Figures. It is noted that all the details of models, including finite elements used, material properties for structural materials are available at the Real-ESSI web site http://real-essi.us/ while the specific input file language described by Jeremić et al. (1989-2021).

3.2.1 Finite Element Model

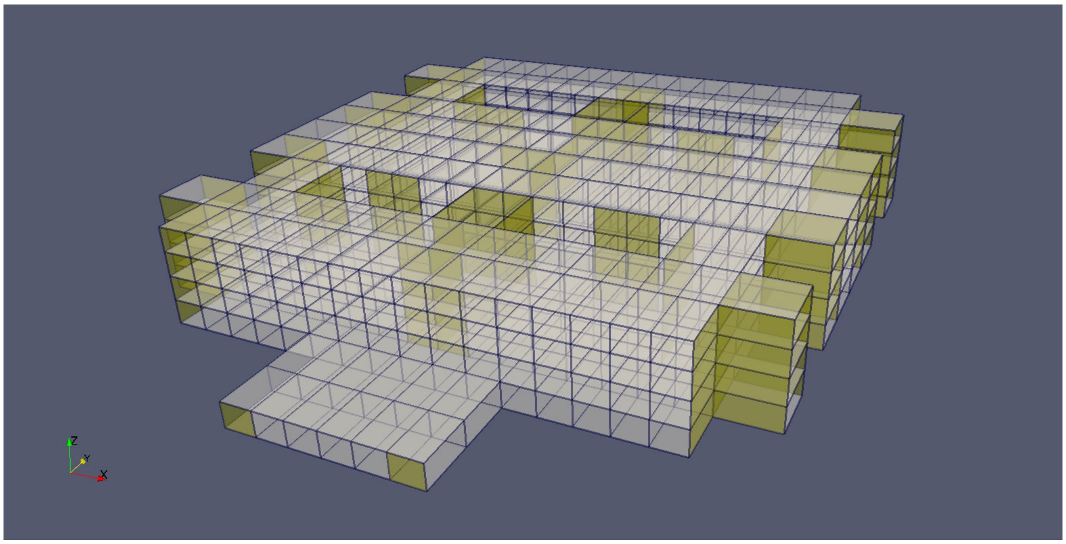

Figure 3.11: Loma Linda Hospital 3D view.

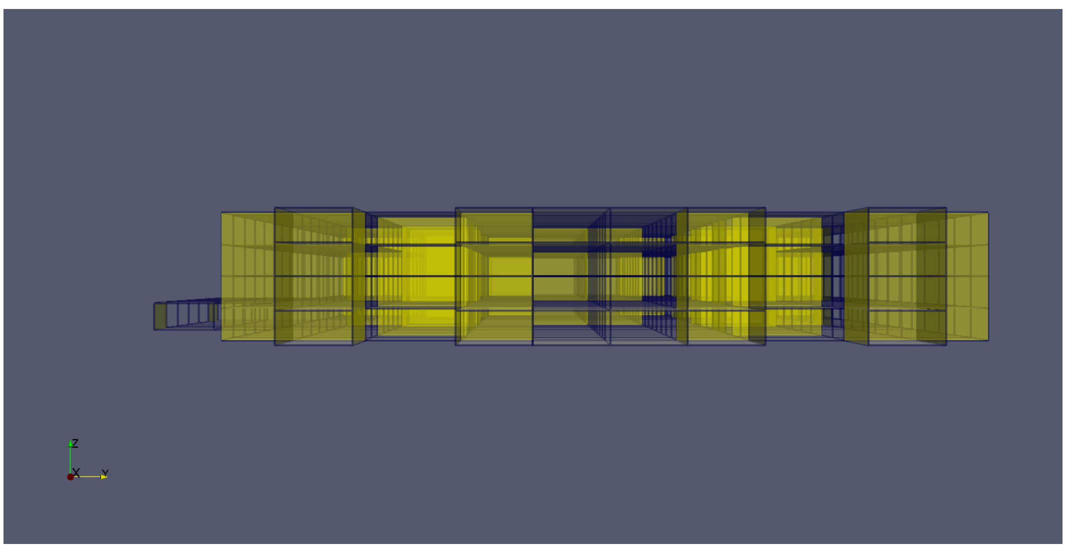

Figure 3.12: Loma Linda Hospital view in X direction.

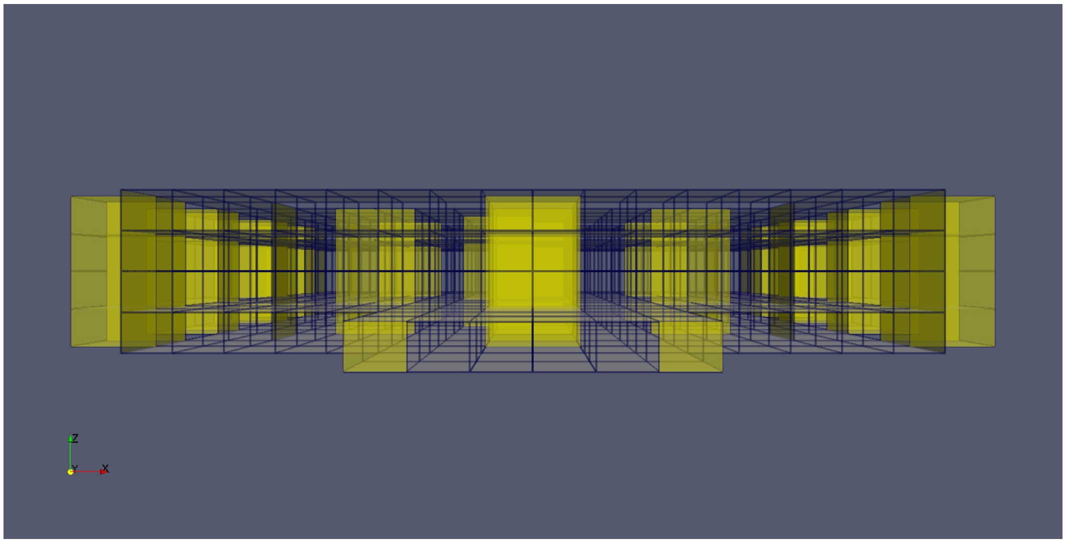

Figure 3.13: Loma Linda Hospital view in Y direction.

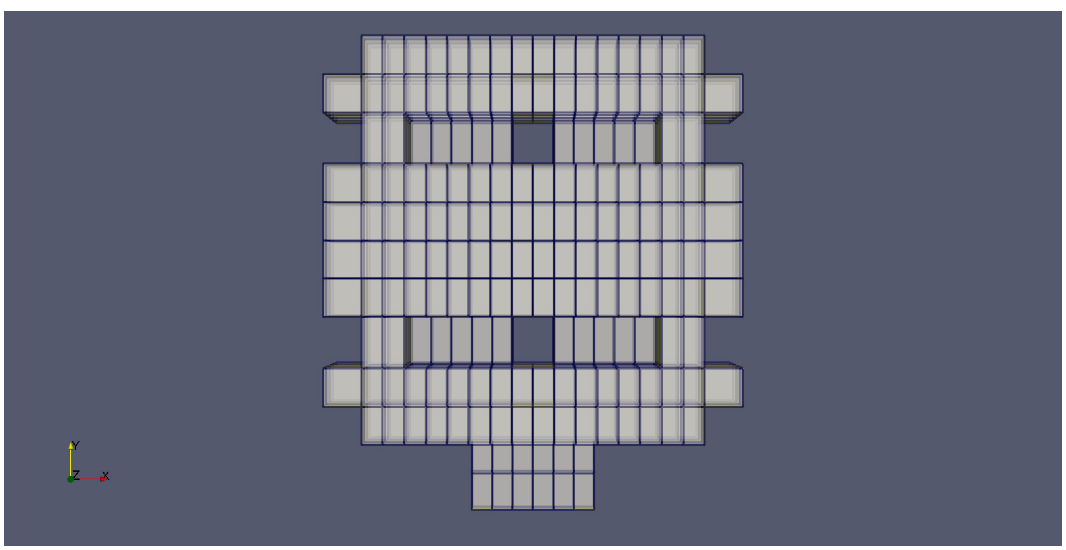

Figure 3.14: Loma Linda Hospital view in Z direction.

3.3 Low, Steel Building

Visualization of the finite element model is provided in next Figures. It is noted that all the details of models, including finite elements used, material properties for structural and soil materials, as well as coherent and incoherent input motions are available at the Real-ESSI web site http://real-essi.us/ while the specific input file language described by Jeremić et al. (1989-2021).

3.3.1 Finite Element Model

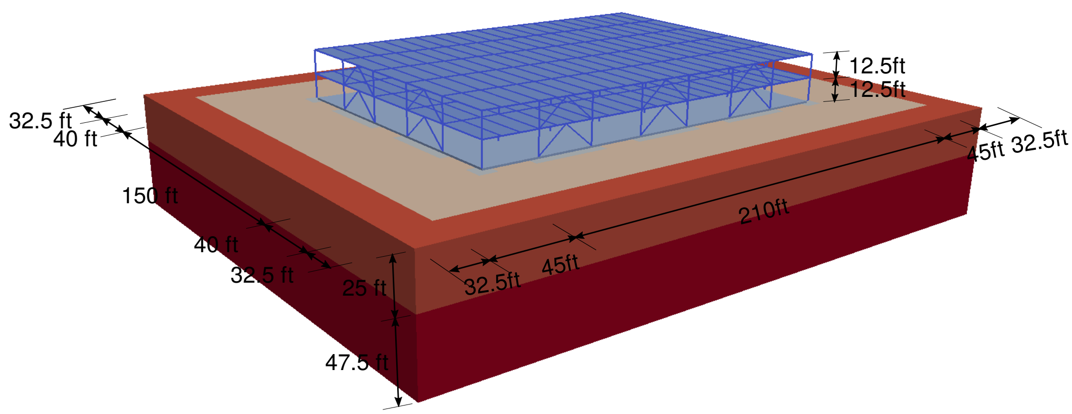

Figure 3.15: Low steel building model, 3D view.

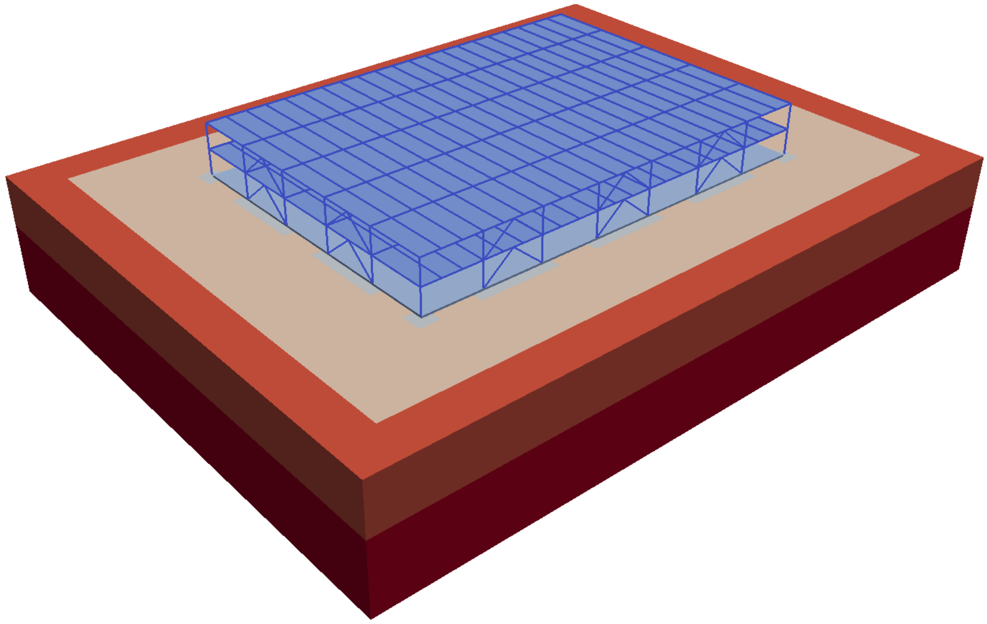

Figure 3.16: Low steel building model, 3D view.

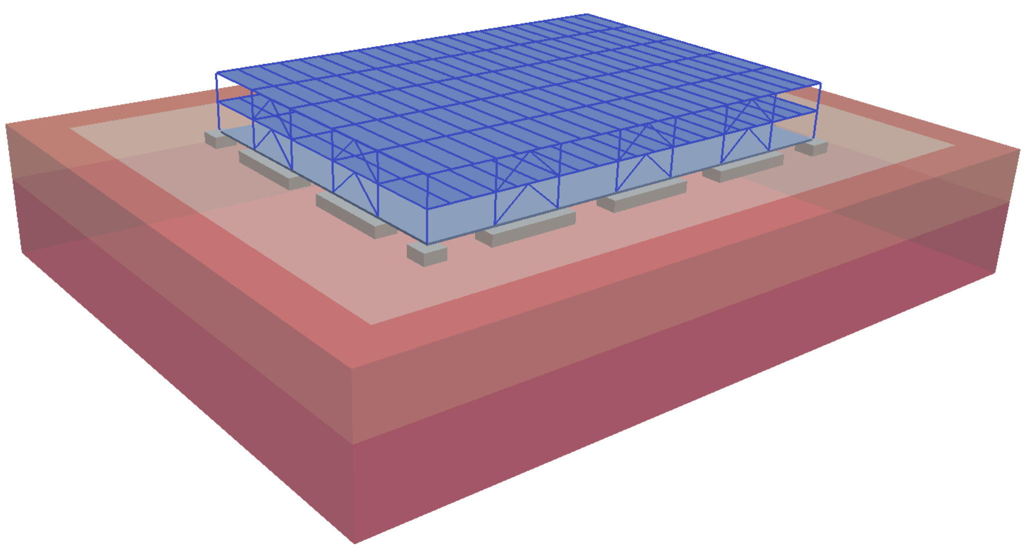

Figure 3.17: Low steel building model, 3D view.

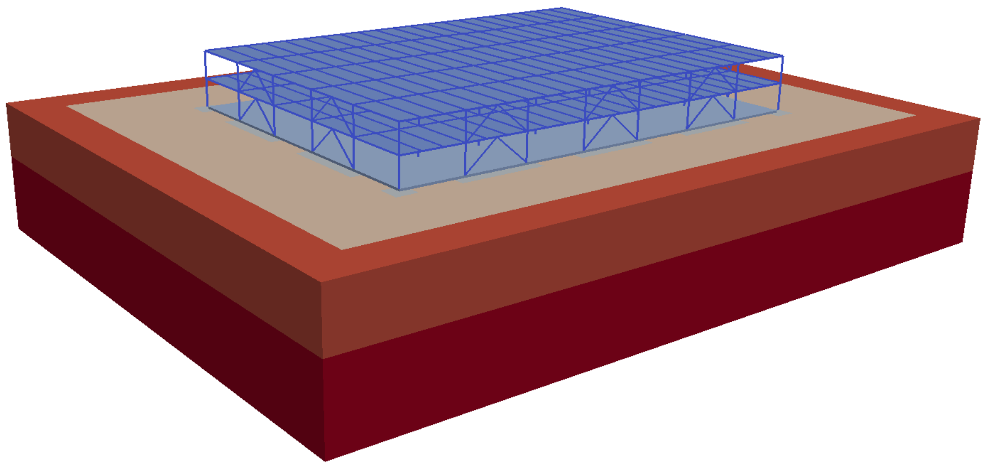

Figure 3.18: Low steel building model, 3D view.

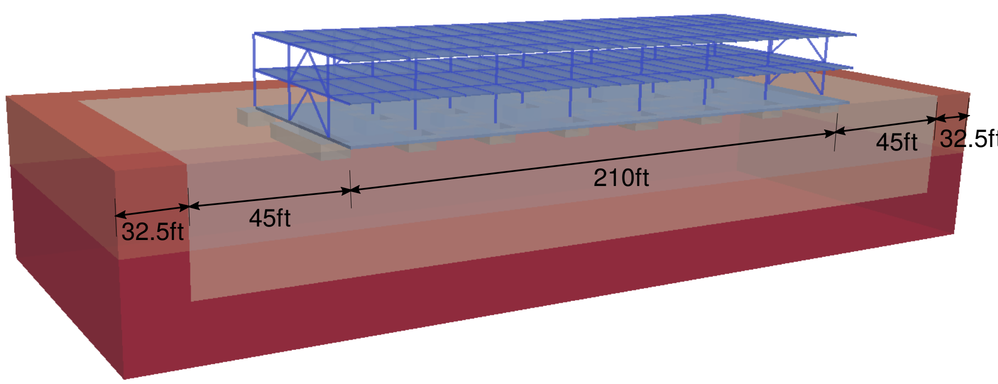

Figure 3.19: Low steel building model, 3D view.

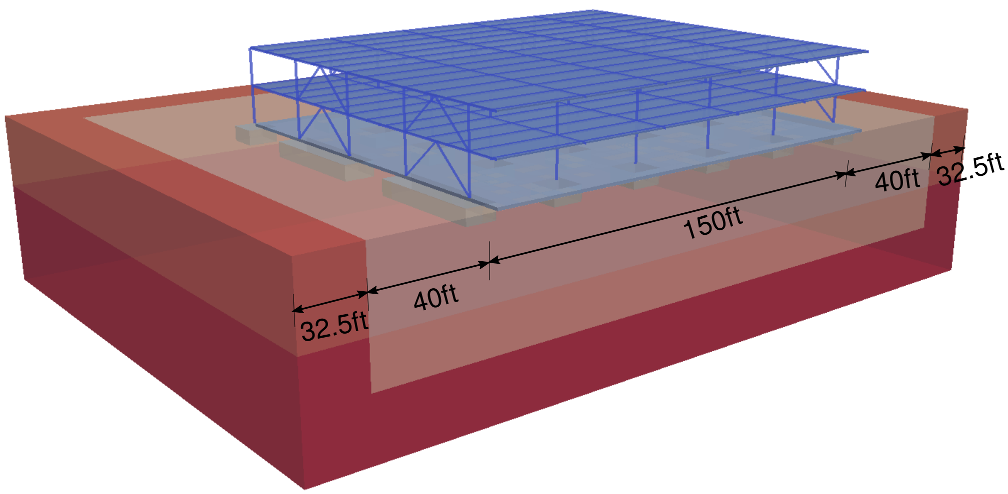

Figure 3.20: Low steel building model, 3D view.

3.4 Tall, Concrete Building

Visualization of the finite element model is provided in next Figures. It is noted that all the details of models, including finite elements used, material properties for structural and soil materials, as well as coherent and incoherent input motions are available at the Real-ESSI web site http://real-essi.us/ while the specific input file language described by Jeremić et al. (1989-2021).

3.4.1 Finite Element Model

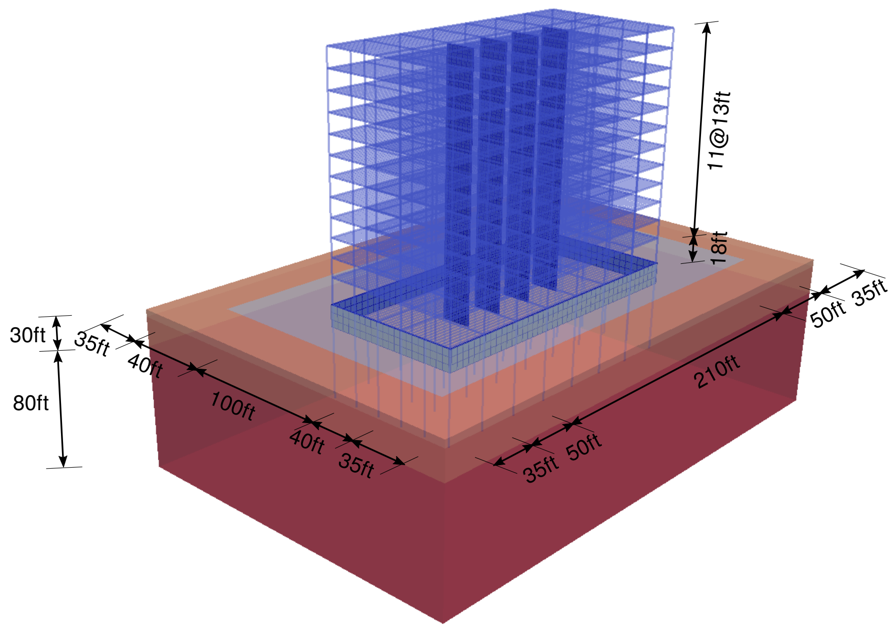

Figure 3.21: Tall concrete building model, 3D view.

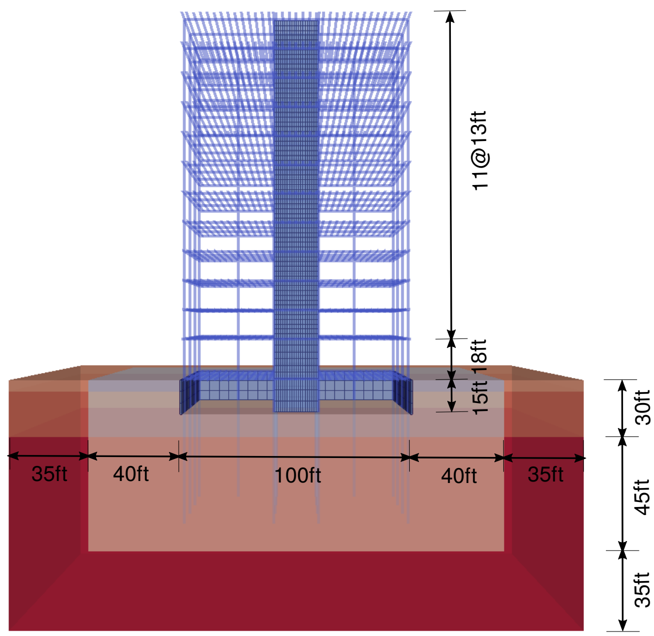

Figure 3.22: Tall concrete building model, XZ plane view.

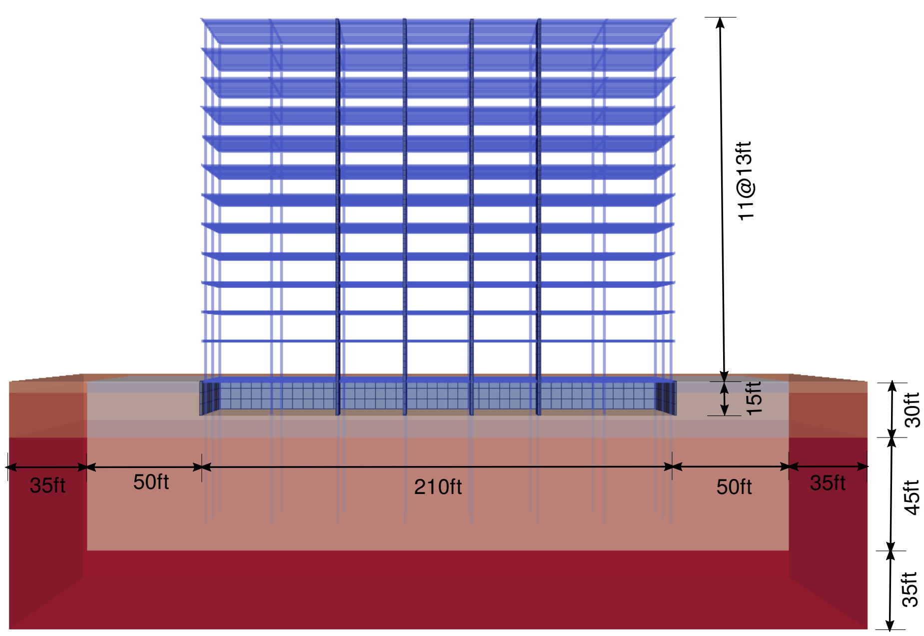

Figure 3.23: Tall concrete building model, YZ plane view.

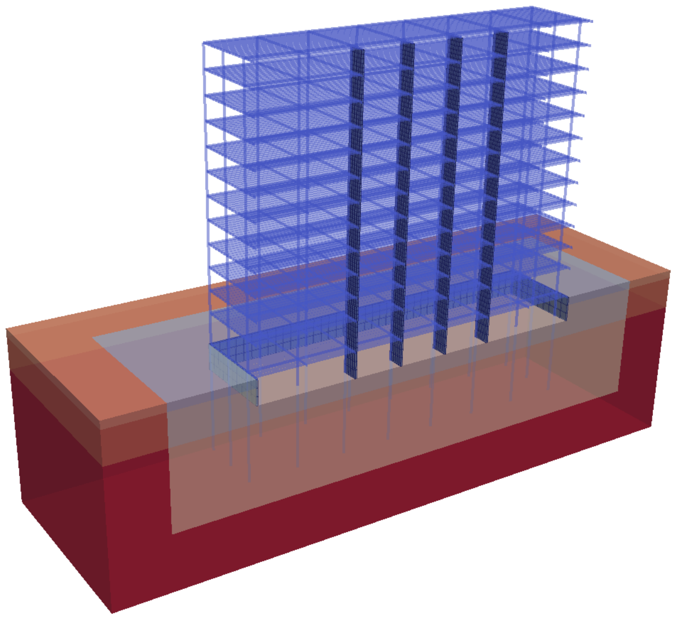

Figure 3.24: Tall concrete building model, cut through model view.

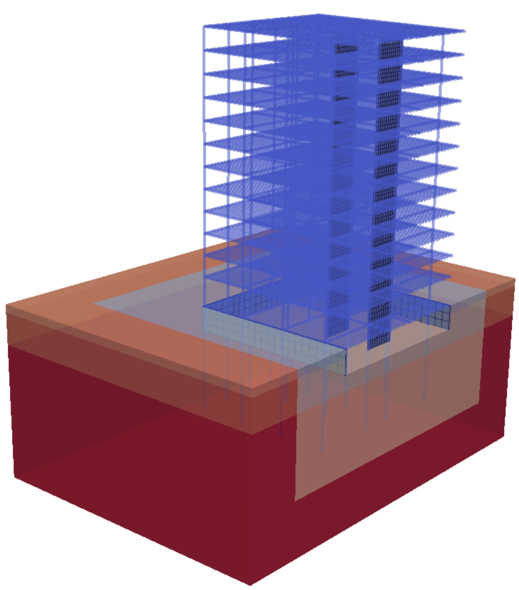

Figure 3.25: Tall concrete building model, cut through model view.

Chapter 4

Simulation Results

4.1 Seismic Excitations

Seismic motions were developed based on prescribed design spectra by Professor Lisa Star (Star, 2019, 2020).

4.1.1 Earthquake Excitation for the Low, Steel Building

Two horizontal components (2C), Earthquake Records 120711 and 120712, have been scaled to matched the design spectrum. The un-scaled seismogram is shown in Figure 4.1. Using deconvolution with elastic material model SM-EL1, a scale factor of 1.82 was chosen to match the design spectrum. Earthquake Records 120711 and 120712 scaled by 1.82 are noted as the baseline input surface motion (Star, 2019, 2020) in Section 4.2 and Section 4.5.

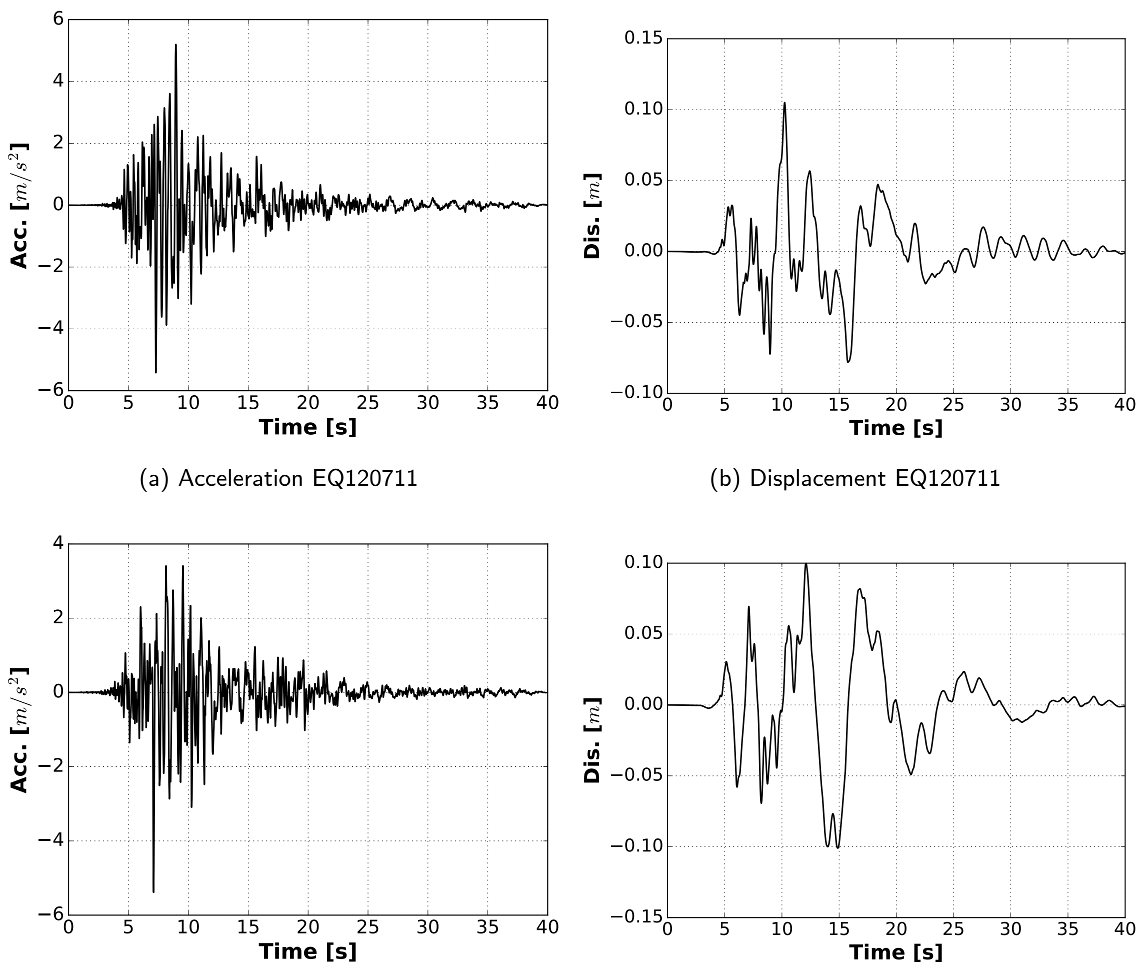

(a) Acceleration EQ120711

(b) Displacement EQ120711

(c) Acceleration EQ120712

(d) Displacement EQ120712

Figure 4.1: Two horizontal components (2×1C) of the un-scaled seismogram from Earthquake Record 120711 and Earthquake Record 120712.

4.1.2 Earthquake Excitation for Tall Concrete Building

Two horizontal components (2C), Earthquake Records 120111 and 120112, have been used and scaled to matched the design spectrum. The un-scaled seismogram is shown in Figure 4.2. Using deconvolution with elastic material model SM-EL2, a scale factor of 3.65 was chosen to match the design spectrum. In addition, a scale factor of 1.94 was also used for a different material models for soils. Results for both scaling factors are provided in results section. Earthquake Records 120111 and 120112 scaled by 3.65 are noted as the baseline input surface motion in Section 4.6.

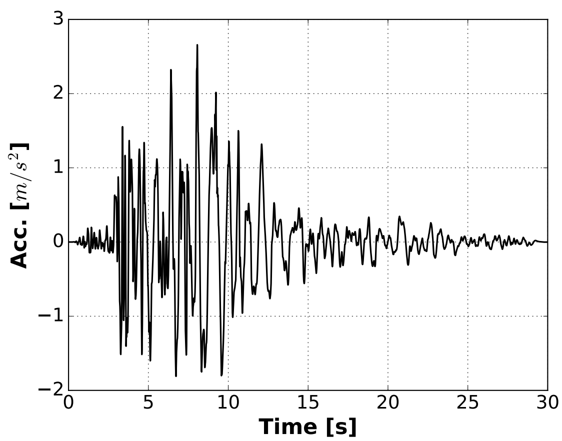

(a) Acceleration EQ120111

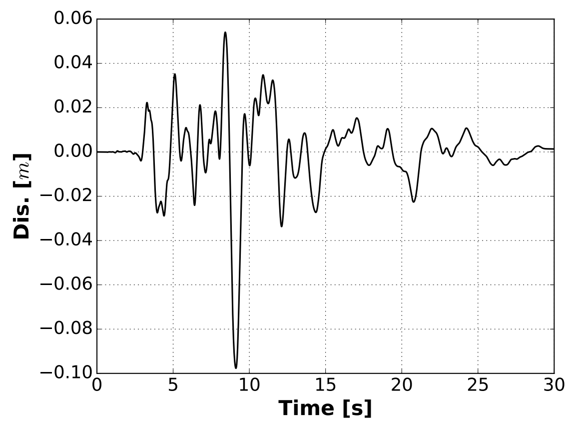

(b) Displacement EQ120111

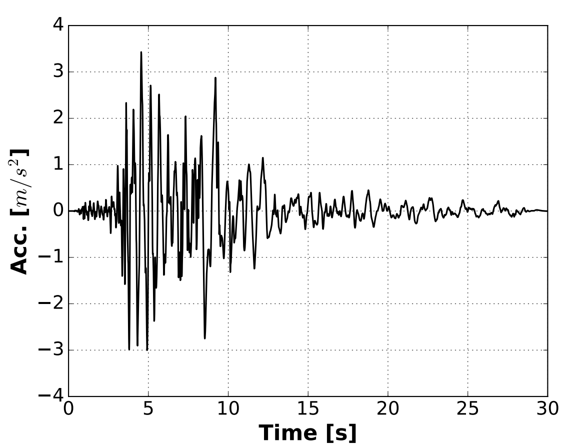

(c) Acceleration EQ120112

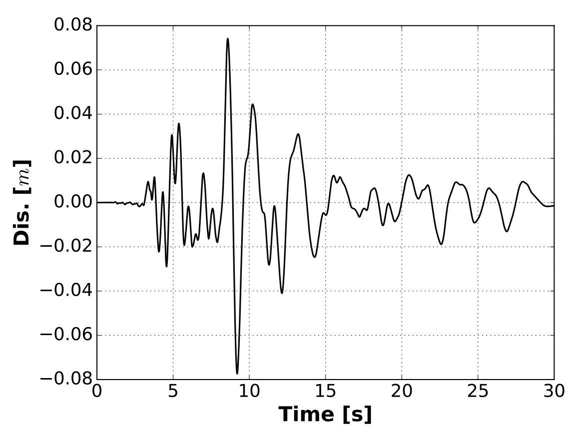

(d) Displacement EQ120112

Figure 4.2: Two horizontal components (2×1C) of the un-scaled seismogram from Earthquake Record 120111 and Earthquake Record 120112.

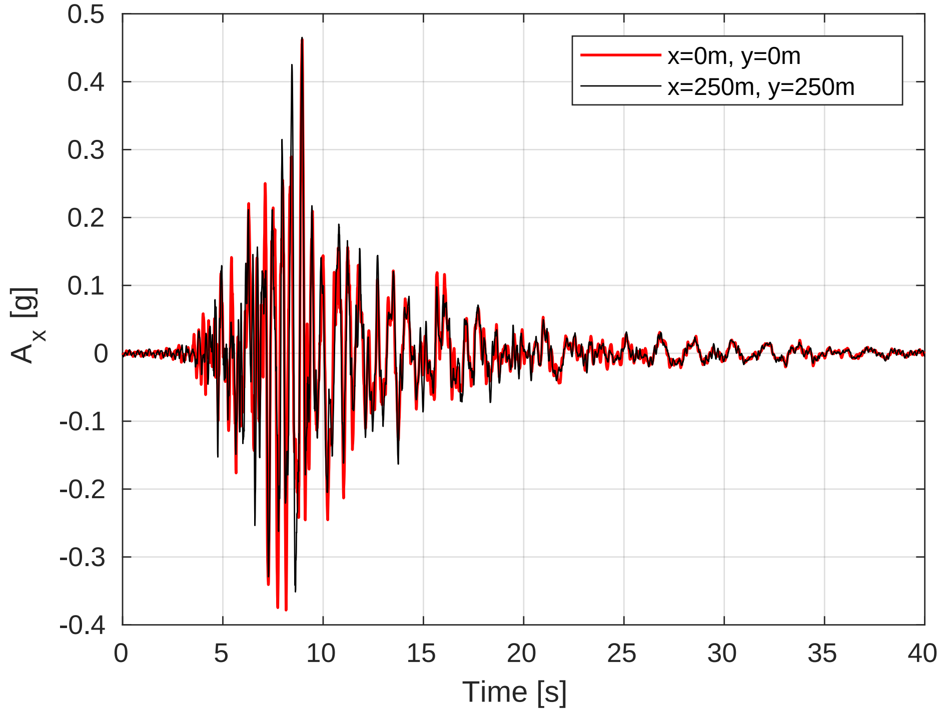

Figure 4.3: Incoherent motions for two corner points on $250m \times 250m$ with the largest separate distance.

4.1.3 Incoherent Surface Motion

Incoherent motions have been developed by Dr. Tim Ancheta.

Using scaled coherent motion as seed motion, incoherent, spatially varying, surface motions in both horizontal directions are simulated on the 2D grid with statistical Fourier amplitude and phase variability (Ancheta, 2010; Ancheta et al., 2012, 2011). The 2D grid has a dimension of 250 m $\times$ 250 m, with grid spacing of 10 m. The incoherent motions corresponding to coherent motion from scaled Earthquake Record 120711. Figure 4.3 shows seed and incoherent motions at two corner points with the largest separation distance. Figure 4.1.5 shows plan view of free field model and locations of largest separation corner points.

4.1.4 Incoherent Motion Input into to ESSI System Using Domain Reduction Method (DRM)

Development of incoherent motions for input into 3D finite element models using DRM is briefly described. Nodal displacements and accelerations for all nodes located at the surface, with coordinates $(X_i, Y_i), i = 1, 2, ..., n$, are developed on a regular grid. Surface motion at locations of DRM nodes at the surface or projections of DRM nodes from depth to surface are interpolated from incoherent motions from a previously developed grid, using four nearest grid points. Interpolation for motions in plan view is done using shape functions of a quadrilateral finite element (Bathe, 1996). For DRM nodes at depth, a $1C$ deconvolution analysis is performed for primary, compressional (P) waves and for secondary, shear (S) waves in order to develop time-series of accelerations and displacement at DRM node locations, (X_i, Y_i, Z_i) from the surface interpolated motions. Thus, developed DRM motions are then used to input spatially variable ground motions into the finite element model.

4.1.5 Free-Field versus Far-Field versus Foundation-Level Seismic Motions

This section sets locations for free-field, far-field, and foundation surface points for results presentation.

- Free field response is a seismic response at soil surface when no structure is present. This is shown in figure 3.15(left). Since modeling in this project relies on 1 component (1C) seismic wave propagation (SV wave, see more in Kramer (1996)), all points on the surface will have the same motions. This is illustrated in Figure 4.4(left).
- Far-field response is a seismic response at the soil surface as far away from the structure as the finite element model would allow, in the far corner of the model, for models that feature a soil-structure system, This is illustrated in Figure 4.4(right). For a steel building, for example, this corner is approximately 60 feet away from the corner of the structure ($\sqrt{40^2 + 45^2} \approx 60$, see figure 3.15 on page 64).
- Foundation surface response is a seismic response in a soil-structure model, in the middle of the model, at the top of the foundation surface. This is illustrated in Figure 4.4(right).

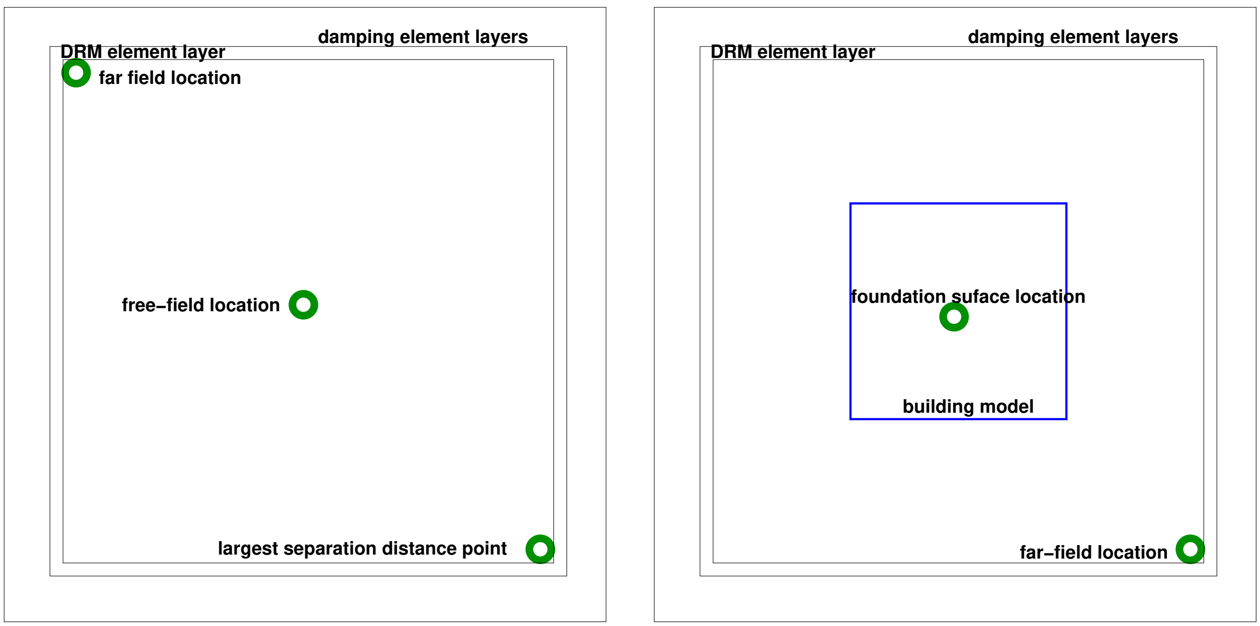

Figure 4.4: Plan view of the building soil-structure model. Illustration of soil/foundation surface point locations for seismic response. (left) Free field model is a model with no structure present; hence the response of any location on the surface for 1C wave propagation is the same. (right) Far-field location is a location on the soil surface as far away from the structure as possible. On the other hand, the Foundation surface location is at the surface of the foundation, the spread of slab, in the middle of the building model.

4.2 Nonlinear Free-Field Response at the Low Building Site

Surface defined seismic motions are usually propagated back in time, de-convoluted, using linear elastic wave propagation methodology (Kramer, 1996). This methodology works well. Those same motions are to be propagated from depth back to surface using methods, based on an equivalent elastic assumption for soil, even when mildly nonlinear, inelastic response of soil is present. When soil deformation during seismic shaking is nonlinear, inelastic, then it is not appropriate to use linear elastic deconvolution. This is because deconvolution is based on elastic material assumption. In contrast, the actual soil behavior is fully nonlinear, inelastic. However, such deconvolution can be sometimes made to work with careful choices and tuning of modeling parameters. However, it is noted that the primary purpose of such modeling is to fit the data, and the predictive capabilities of such models are questionable.

Presented below is a sensitivity analysis of the free-field response due to variations in material and seismic motion parameters. Earthquake Record 120711, shown in Figure 4.1, is used for all simulations shown in this section. As mentioned in Section 4.1.1, the scale factor for baseline input motion is 1.82.

4.2.1 Varying Intensity of Input Motion

- PGA $= 0.9g$ (baseline input motion, scale factor 1.82), stiffness baseline, baseline strength

  Figure 4.5 (a) compares the surface input motion for deconvolution and inelastic propagated surface motion. Figure 4.5 (b) presents nonlinear free-field site response at different depths.

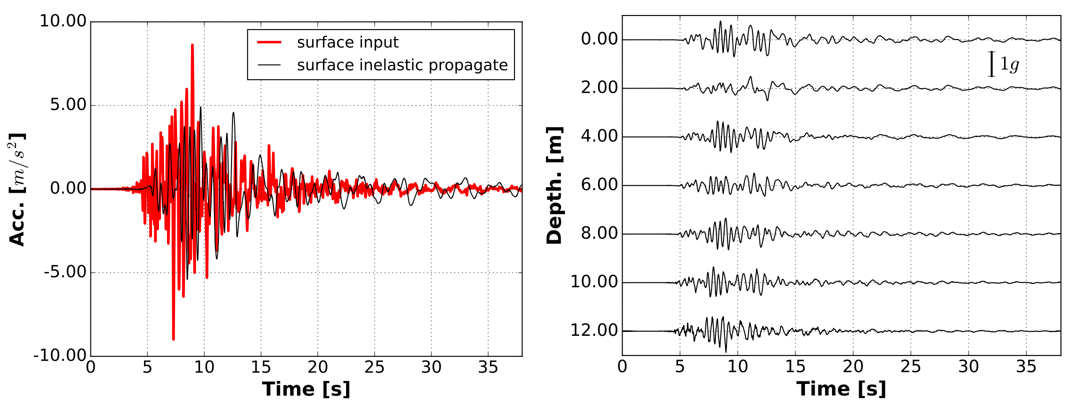

(a) Surface input and nonlinear surface site response

(b) Nonlinear site response

Figure 4.5: Inelastic site response using motions developed from surface input PGA $0.9g$ (baseline input motion, scale factor 1.82), baseline stiffness, baseline strength, Soil Material Model SM-EP1.

- PGA $= 0.5g$ (scale factor 1.011), stiffness baseline, baseline strength

Figure 4.6 (a) compares the surface input motion for deconvolution and inelastic propagated surface motion. Figure 4.6 (b) presents nonlinear free-field site response at different depths.

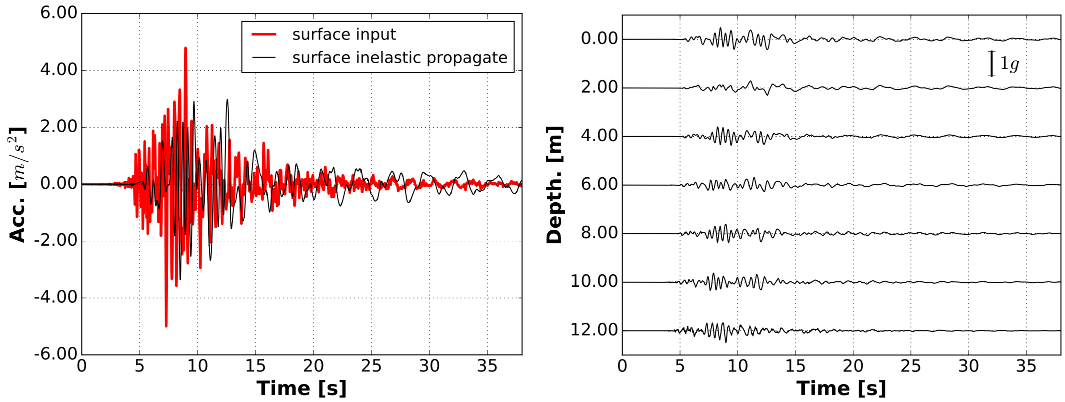

(a) Surface input and nonlinear surface site response

(b) Nonlinear site response

Figure 4.6: Inelastic site response with surface input PGA $0.5g$ (scale factor 1.011), baseline stiffness, baseline strength, Soil Material Model SM-EP1.

- PGA $= 0.2g$ (scale factor 0.404), stiffness baseline, baseline strength

  Figure 4.7 (a) compares the surface input motion for deconvolution and inelastic propagated surface motion. Figure 4.7 (b) presents nonlinear free-field site response at different depths.

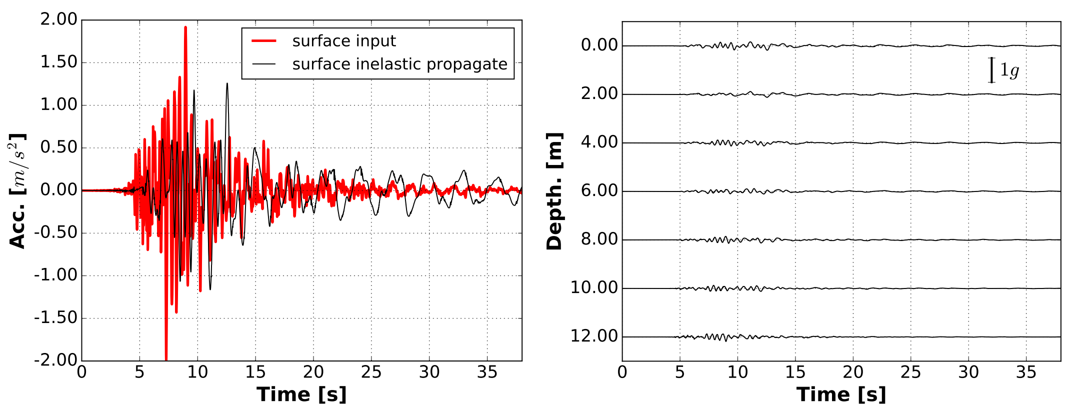

(a) Surface input and nonlinear surface site response

(b) Nonlinear site response

Figure 4.7: Inelastic site response with surface input PGA $0.2g$ (scale factor 0.404), baseline stiffness, baseline strength, Soil Material Model SM-EP1.

- PGA $= 2g$ (scale factor 4.044), stiffness baseline, baseline strength

Figure 4.8 (a) compares the surface input motion for deconvolution and inelastic propagated surface motion. Figure 4.8 (b) presents nonlinear free-field site response at different depths.

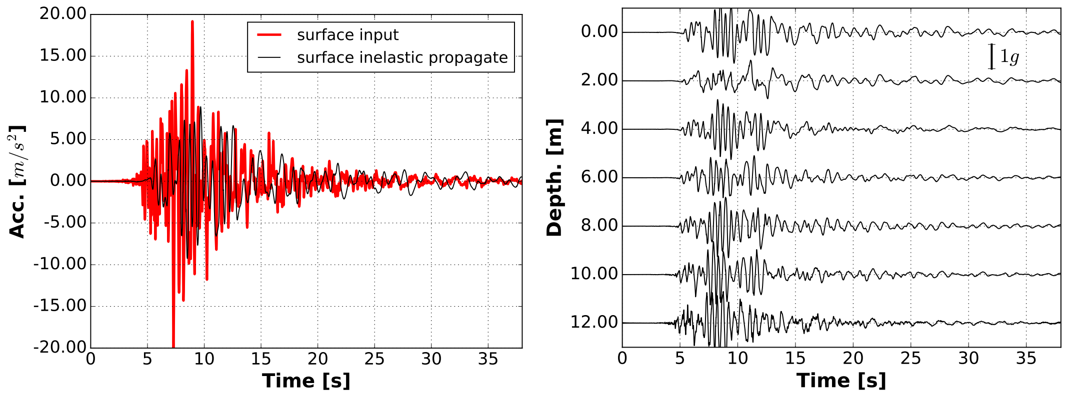

(a) Surface input and nonlinear surface site response

(b) Nonlinear site response

Figure 4.8: Inelastic site response with surface input PGA $2g$ (scale factor 4.044), baseline stiffness, baseline strength, Soil Material Model SM-EP1.

Table 4.1 presents comparison of PGA results, for nonlinear free-field site response at the low building site with varying scaling of input motions at depth. It is noted that scaling of input motions at depth was used in order to fit required surface motions that are obtained after nonlinear wave propagation from depth. In other words, for target surface PGA, in this case $\approx 9\,\mathrm{m/s}$, and for a case of wave propagation through nonlinear soil, seismic wave at the bottom needs to have PGA of $20\,\mathrm{m/s}$.

Table 4.1: Nonlinear free-field site response of low building site, no building, with varying input PGA, Soil Material Model SM-EP1.

Input PGA $[m/s^2]$	9	2	5	20
Stiffness	baseline	baseline	baseline	baseline
Strength	baseline	baseline	baseline	baseline
Depth z [m]	PGA(z) along depth $[m/s^2]$			
0	5.41	1.26	3.36	9.25
2	3.57	0.86	2.11	5.96
4	4.61	0.92	2.77	8.74
6	3.57	0.82	2.19	6.33
8	4.57	1.04	2.74	9.14
10	4.57	0.91	2.64	9.56
12	6.12	1.32	3.43	13.42
Depth [m]	Ratio PGA(z)/Input PGA			
0	0.60	0.63	0.67	0.46
2	0.40	0.43	0.42	0.30
4	0.51	0.46	0.55	0.44
6	0.40	0.41	0.44	0.32
8	0.51	0.52	0.55	0.46
10	0.51	0.45	0.53	0.48
12	0.68	0.66	0.69	0.67

4.2.2 Varying Strength of Soil

In Soil Material Model SM-EP1, material strength is controlled by the ratio of parameter armstrong_frederick_ha over parameter armstrong_frederick_cr. In this section, parameter armstrong_frederick_cr is changed to achieve target strength. Example cases are shown below.

- PGA $= 0.9g$ (baseline input motion, scale factor 1.82), stiffness baseline, strength 150% of baseline

  Figure 4.9 (a) compares the surface input motion for deconvolution and inelastic propagated surface motion. Figure 4.9 (b) presents nonlinear free-field site response at different depths

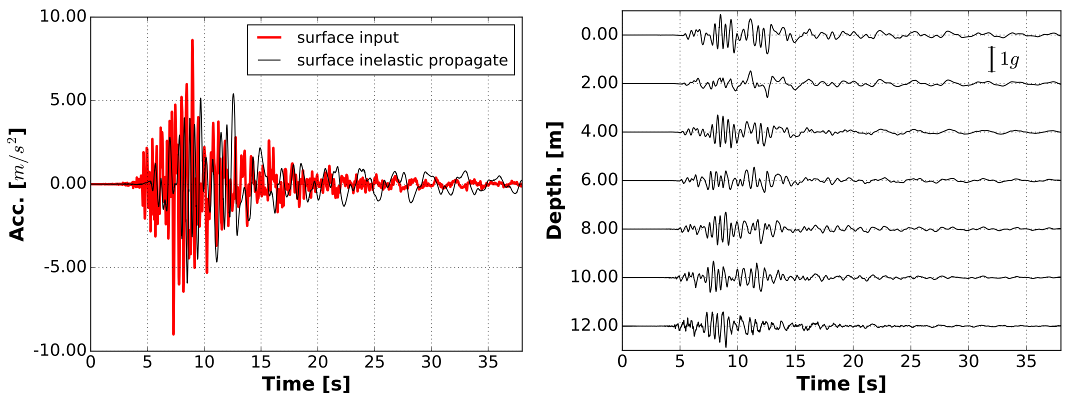

(a) Surface input and nonlinear surface site response (b) Nonlinear site response

Figure 4.9: Inelastic site response with surface input PGA $0.9g$ (baseline input motion, scale factor 1.82), baseline stiffness, 150% baseline strength, Soil Material Model SM-EP1.

- PGA $= 0.9g$ (baseline input motion, scale factor 1.82), stiffness baseline, strength 80% of baseline

  Figure 4.10 (a) compares the surface input motion for deconvolution and inelastic propagated surface motion. Figure 4.10 (b) presents nonlinear free-field site response at different depths.

- PGA $= 0.9g$ (baseline input motion, scale factor 1.82), stiffness baseline, strength 50% of baseline

  Figure 4.11 (a) compares the surface input motion for deconvolution and inelastic propagated surface motion. Figure 4.11 (b) presents nonlinear free-field site response at different depths.

Table 4.2 presents comparison results of nonlinear free-field site response of the low building site with varying soil strength. Results present soil response at the same location as shown in Table 4.1.

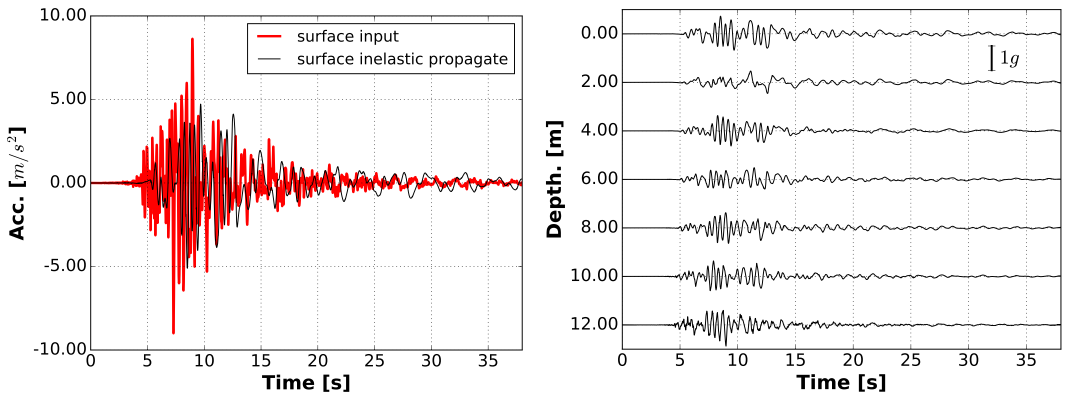

(a) Surface input and nonlinear surface site response (b) Nonlinear site response

Figure 4.10: Inelastic site response with surface input PGA $0.9g$ (baseline input motion, scale factor 1.82), baseline stiffness, 80% baseline strength, Soil Material Model SM-EP1.

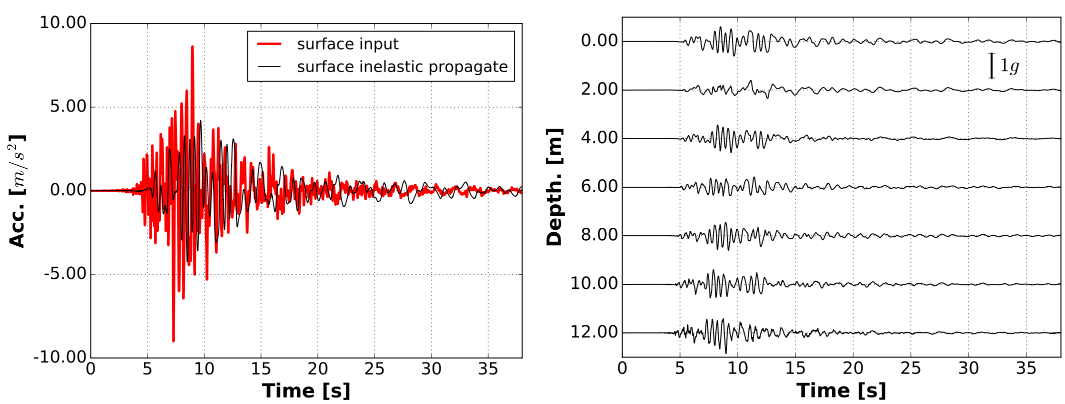

(a) Surface input and nonlinear surface site response (b) Nonlinear site response

Figure 4.11: Inelastic site response with surface input PGA $0.9g$ (baseline input motion, scale factor 1.82), baseline stiffness, 50% baseline strength, Soil Material Model SM-EP1.

Table 4.2: Nonlinear free-field site response of the low building site with varying soil strength, Soil Material Model SM-EP1.

Input PGA $[m/s^2]$	9	9	9	9
Stiffness	baseline	baseline	baseline	baseline
Strength	baseline	150% baseline	80% baseline	50% baseline
Depth z [m]	PGA(z) along depth $[m/s^2]$			
0	5.41	5.92	5.11	4.25
2	3.57	4.03	3.27	2.82
4	4.61	4.93	4.43	4.07
6	3.57	3.85	3.39	2.96
8	4.57	4.86	4.46	4.20
10	4.57	4.75	4.49	4.21
12	6.12	6.18	6.11	6.03
Depth [m]	Ratio PGA(z)/Input PGA			
0	0.60	0.66	0.57	0.47
2	0.40	0.45	0.36	0.31
4	0.51	0.55	0.49	0.45
6	0.40	0.43	0.38	0.33
8	0.51	0.54	0.50	0.47
10	0.51	0.53	0.50	0.47
12	0.68	0.69	0.68	0.67

4.2.3 Varying Stiffness of Soil

In Soil Material Model SM-EP1, material stiffness is controlled by parameter `Young's modulus E`. In this section, parameter `Young's modulus E` is changed to achieve target stiffness.

- PGA $= 0.9g$ (baseline input motion, scale factor 1.82), stiffness 150% of baseline, strength baseline

  Figure 4.12 (a) compares the surface input motion for deconvolution and inelastic propagated surface motion. Figure 4.12 (b) presents nonlinear free-field site response at different depths.

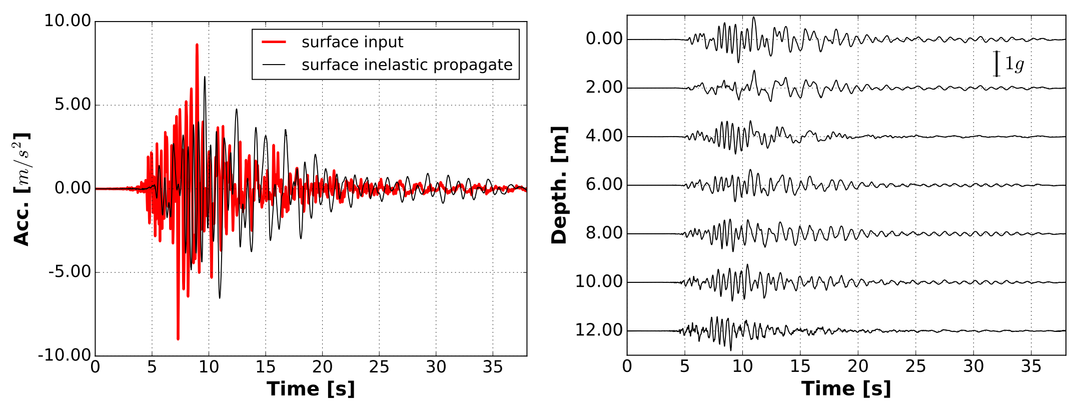

(a) Surface input and nonlinear surface site response (b) Nonlinear site response

Figure 4.12: Inelastic site response with surface input PGA $0.9g$ (baseline input motion, scale factor 1.82), 150% baseline stiffness, baseline strength, Soil Material Model SM-EP1.

- PGA $= 0.9g$ (baseline input motion, scale factor 1.82), stiffness 80% of baseline, strength baseline

  Figure 4.13 (a) compares the surface input motion for deconvolution and inelastic propagated surface motion. Figure 4.13 (b) presents nonlinear free-field site response at different depths.

- PGA $= 0.9g$ (baseline input motion, scale factor 1.82), stiffness 50% of baseline, strength baseline

  Figure 4.14 (a) compares the surface input motion for deconvolution and inelastic propagated surface motion. Figure 4.14 (b) presents nonlinear free-field site response at different depth.

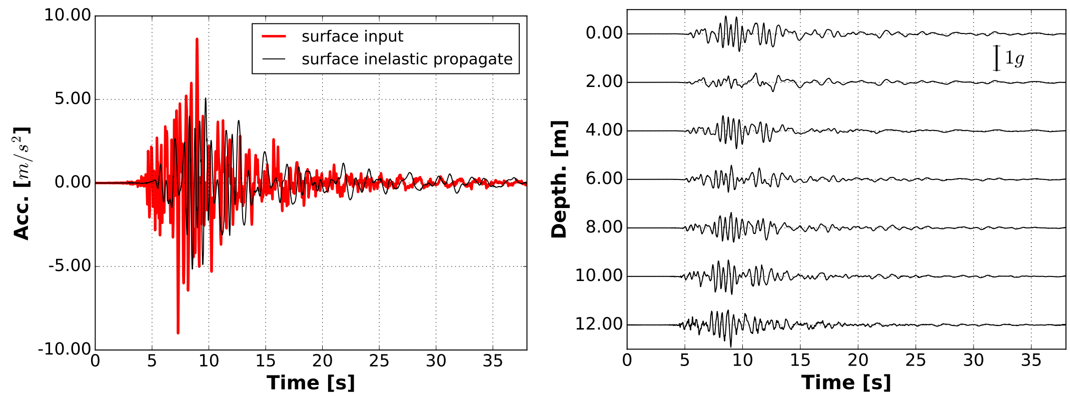

(a) Surface input and nonlinear surface site response (b) Nonlinear site response

Figure 4.13: Inelastic site response with surface input PGA $0.9g$ (baseline input motion, scale factor 1.82), 80% baseline stiffness, baseline strength, Soil Material Model SM-EP1.

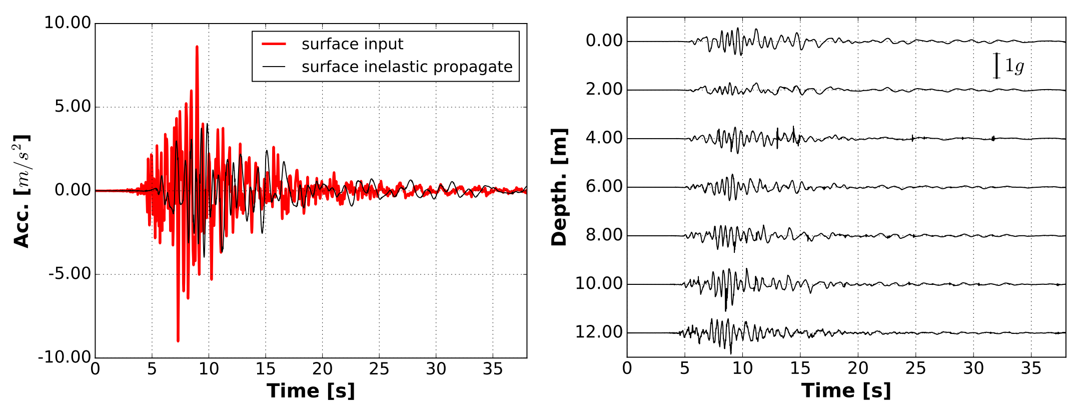

(a) Surface input and nonlinear surface site response (b) Nonlinear site response

Figure 4.14: Inelastic site response with surface input PGA $0.9g$ (baseline input motion, scale factor 1.82), 50% baseline stiffness, baseline strength, Soil Material Model SM-EP1.

Table 4.3 presents comparison results of nonlinear free-field site response of the low building site with varying soil stiffness.

Table 4.3: Nonlinear free-field site response of the low building site with varying soil stiffness, Soil Material Model SM-EP1.

Input PGA $[m/s^2]$	9	9	9	9
Stiffness	baseline	150% baseline	80% baseline	50% baseline
Strength	baseline	baseline	baseline	baseline
Depth z [m]	PGA(z) along depth $[m/s^2]$			
0	5.41	6.72	5.16	4.03
2	3.57	5.14	2.68	2.10
4	4.61	5.01	5.16	4.33
6	3.57	4.75	4.07	3.84
8	4.57	5.15	4.45	4.81
10	4.57	5.40	5.22	7.79
12	6.12	5.71	6.42	6.11
Depth [m]	Ratio PGA(z)/Input PGA			
0	0.60	0.75	0.57	0.45
2	0.40	0.57	0.30	0.23
4	0.51	0.56	0.57	0.48
6	0.40	0.53	0.45	0.43
8	0.51	0.57	0.49	0.53
10	0.51	0.60	0.58	0.87
12	0.68	0.63	0.71	0.68

4.2.4 Deconvolution and Wave Propagation with Scaled Free-Field Motion

In order to match PGA on the surface, a procedure is developed, as described below. We scale the linear elastic deconvoluted free-field motion by 2.1. This gives an overall scale factor of $2.1 \times 1.82 = 3.822$. The PGA of nonlinear inelastic wave propagation surface response can then match the surface input PGA $9\,m/s^2$.

Figure 4.15 (a) compares the surface input motion for deconvolution and inelastic propagated surface motion. Figure 4.15 (b) presents nonlinear free-field site response at different depths.

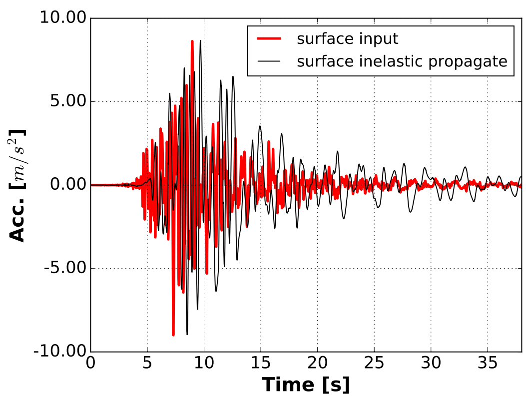

(a) Surface input and nonlinear surface site response

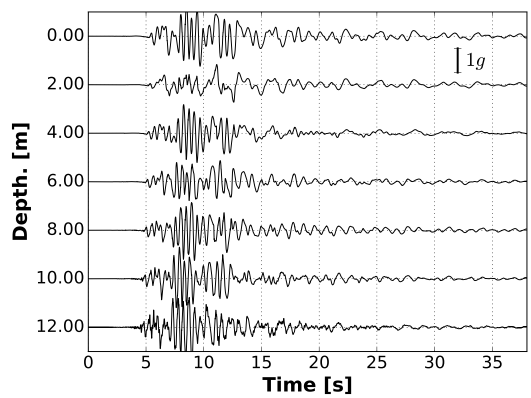

(b) Nonlinear site response

Figure 4.15: Inelastic site response, scale factor 3.822, Soil Material Model SM-EP1.

Table 4.4 presents comparison results of nonlinear free-field site response of the low building site with scaled and unscaled seismic input.

Table 4.4: Nonlinear free-field site response of the low building site with different scaled seismic input, Soil Material Model SM-EP1.

Input motion	Scaled 1.82	Scaled 3.82
Depth z [m]	PGA(z) along depth $[m/s^2]$	
0	5.41	8.97
2	3.57	5.83
4	4.61	8.46
6	3.57	6.09
8	4.57	8.73
10	4.57	9.11
12	6.12	12.70
Depth [m]	Ratio PGA(z)/Input PGA	
0	0.60	1.00
2	0.40	0.65
4	0.51	0.94
6	0.40	0.68
8	0.51	0.97
10	0.51	1.01
12	0.68	1.41

4.2.5 Seismic Wave Propagation using Alternative Material Model, Non-vanishing Elastic Region

We adopt elastoplastic material with a non-vanishing elastic region (SM-EP2) as described in Section 2.3. Surface deconvoluted free-field motion with small magnitude PGA is propagated.

- PGA $= 1m/s^2$ (scale factor 0.202)

  Figure 4.16 (a) compares the surface input motion for deconvolution and inelastic propagated surface motion. Figure 4.16 (b) presents nonlinear free-field site response at different depths.

  It can be seen that for small input motion with a non-vanishing elastic region, the free-field response can be recovered.

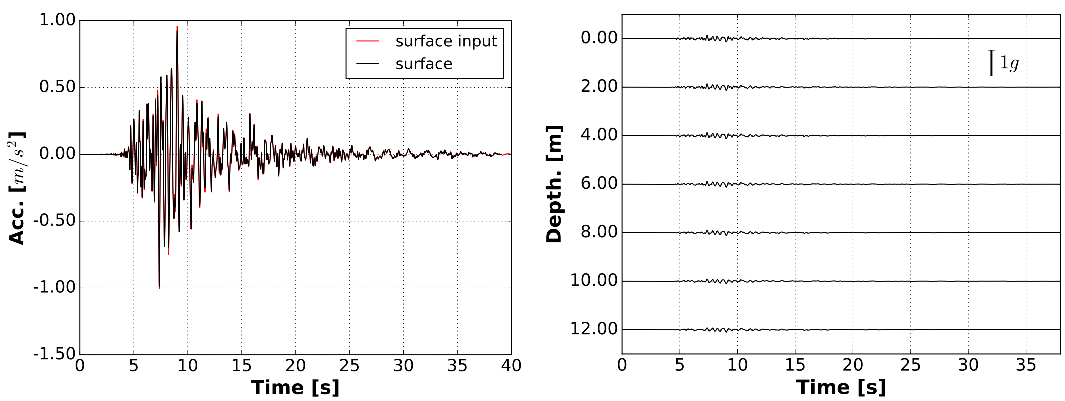

(a) Surface input and nonlinear surface site response

(b) Nonlinear site response

Figure 4.16: Inelastic site response with non-vanishing elastic region material and surface input acceleration PGA $1m/s^2$ (scale factor 0.202), Soil Material Model SM-EP2.

- PGA $= 2m/s^2$ (scale factor 0.404)

  Figure 4.17 (a) compares the surface input motion for deconvolution and inelastic propagated surface motion. Figure 4.17 (b) presents nonlinear free-field site response at different depths.

  It can be seen that around 20% reduction of PGA can be observed when PGA increases from $1\,m/s^2$ to $2\,m/s^2$.

  However, if the elastic region is large enough, for example, the size of a non-vanishing elastic region is doubled, then the free-field response can still be recovered as shown in Figure 4.18 (a) and (b).

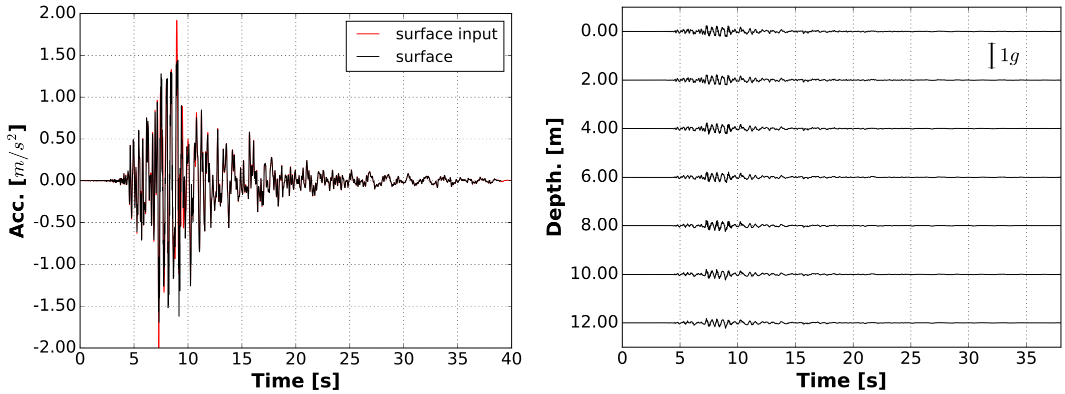

(a) Surface input and nonlinear surface site response

(b) Nonlinear site response

Figure 4.17: Inelastic site response with non-vanishing elastic region material and surface input acceleration PGA $2m/s^2$ (scale factor 0.404), Soil Material Model SM-EP2.

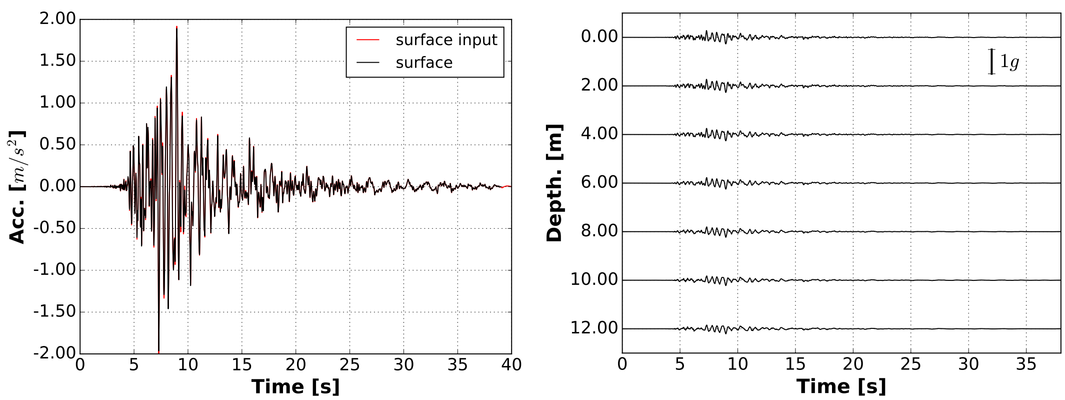

(a) Surface input and nonlinear surface site response

(b) Nonlinear site response

Figure 4.18: Inelastic site response with double sized non-vanishing elastic region material and surface input acceleration PGA $2m/s^2$ (scale factor 0.404), Soil Material Model SM-EP2.

4.2.6 Seismic Wave Propagation using Hyperbolic Drucker Prager Model with Armstrong Frederick Kinematic Hardening

- Surface Input PGA = 1 g (scale factor 2.022)

  Figure 4.19 (a) compares the surface input motion for deconvolution and inelastic propagated surface motion. Figure 4.19 (b) presents nonlinear free-field site response at different depths.

- Surface Input PGA = 1.3 g (scale factor 2.629)

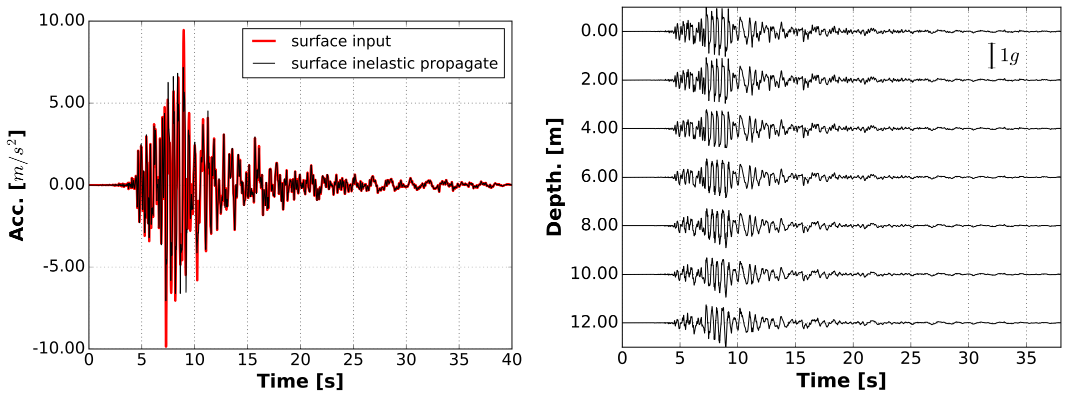

(a) Surface input and nonlinear surface site response (b) Nonlinear site response

Figure 4.19: Inelastic site response under hyperbolic Drucker Prager model with Armstrong Frederick Kinematic Hardening material and surface input acceleration PGA 1 g (scale factor 2.022), Soil Material Model SM-EP3.

Figure 4.20 (a) compares the surface input motion for deconvolution and inelastic propagated surface motion. Figure 4.20 (b) presents nonlinear free-field site response at different depth.

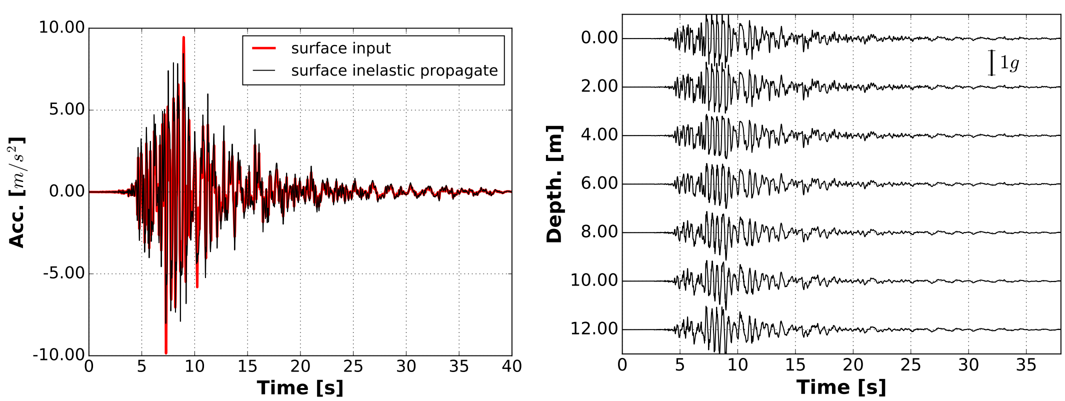

(a) Surface input and nonlinear surface site response (b) Nonlinear site response

Figure 4.20: Inelastic site response under hyperbolic Drucker Prager model with Armstrong Frederick kinematic hardening material surface input acceleration PGA 1.3 g (scale factor 2.629), Soil Material Model SM-EP3.

4.3 Ventura Hotel ESSI Results

4.3.1 Eigen Analysis

The variations of the structural model of the Ventura Hotel were investigated. Addition of mass was done based on recommendations by advisory board, in order to take ionto account non-structural, facade elements, approximately 20% extra.

- Table 4.5: Original model, without additional mass and without stiffness reduction due to plasticity;
- Table 4.6: Modified model, with additional mass and without stiffness reduction due to plasticity;
- Table 4.7: Final model, with additional mass and with 20% stiffness reduction due to plasticity;

Table 4.5: Eigen analysis results for the Ventura Hotel, without additional mass and without stiffness reduction.

Mode	Eigen periods [s]	Eigen frequencies [Hz]
1	0.6689	1.4955
2	0.3786	2.6412
3	0.2334	4.2849
4	0.1642	6.0898
5	0.1572	6.3628
6	0.1433	6.9777
7	0.1358	7.3629
8	0.1341	7.4575
9	0.1240	8.0664
10	0.1185	8.4414

Table 4.6: Eigen analysis results for the Ventura Hotel, with additional mass and without stiffness reduction.

Mode	Eigen periods [s]	Eigen frequencies [Hz]
1	0.7421	1.3476
2	0.4205	2.3782
3	0.2580	3.8754
4	0.1825	5.4802
5	0.1746	5.7274
6	0.1591	6.2847
7	0.1508	6.6323
8	0.1488	6.7189
9	0.1376	7.2682
10	0.1320	7.5769

Table 4.7: Eigen analysis results for the Ventura Hotel, with additional mass and with 20% stiffness reduction.

Mode	Eigen periods [s]	Eigen frequencies [Hz]
1	0.8297	1.2053
2	0.4701	2.1271
3	0.2885	3.4662
4	0.2040	4.9017
5	0.1952	5.1227
6	0.1779	5.6212
7	0.1686	5.9321
8	0.1664	6.0095
9	0.1538	6.5009
10	0.1476	6.7769

(a) X direction

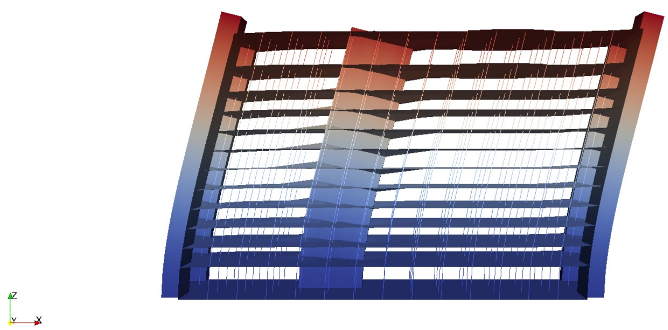

(b) Y direction

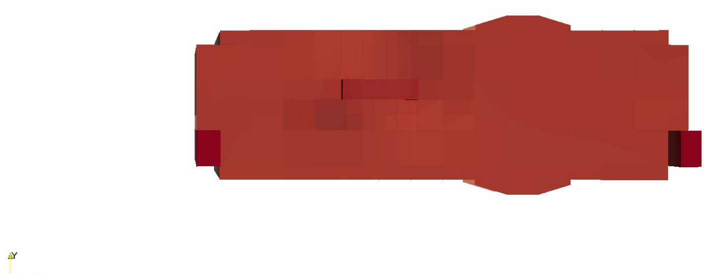

(c) Z direction

Figure 4.21: First eigen-mode of the Ventura Hotel model.

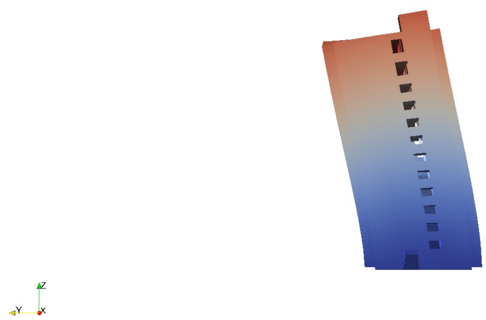

(a) X direction

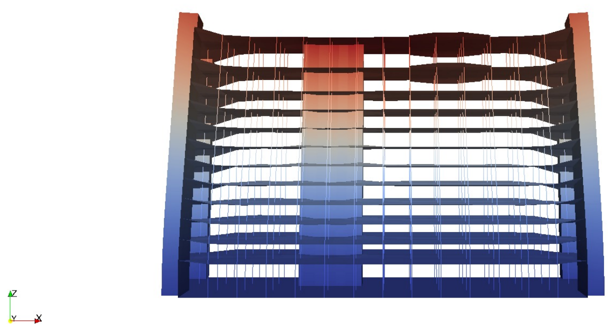

(b) Y direction

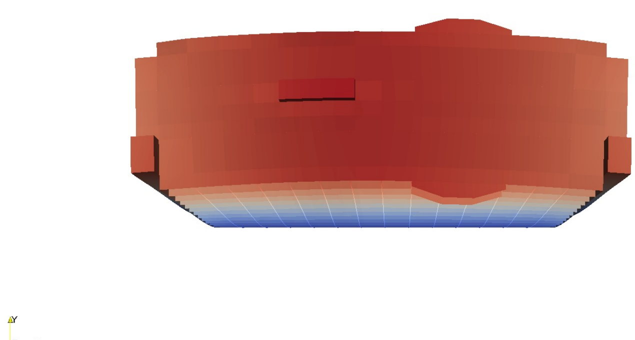

(c) Z direction

Figure 4.22: Second eigen-mode of the Ventura Hotel model.

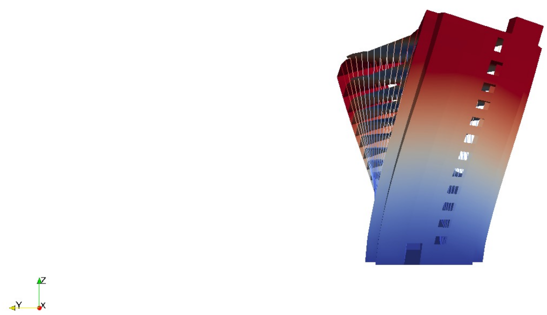

(a) X direction

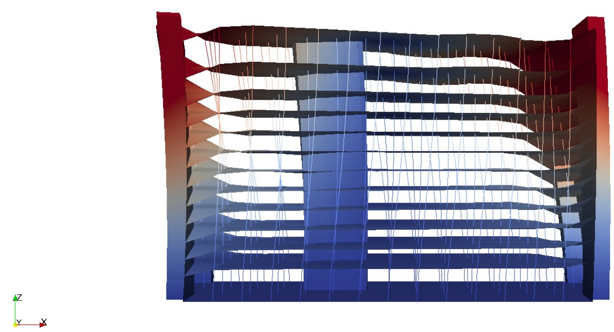

(b) Y direction

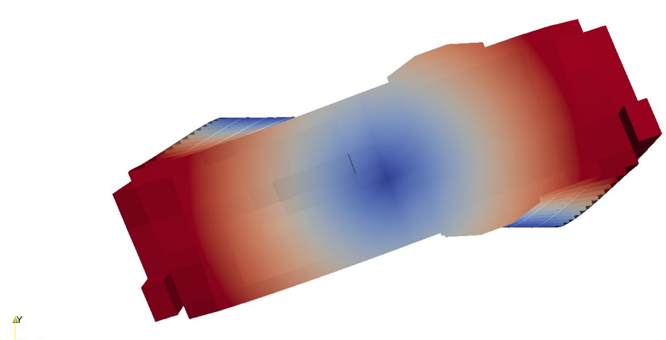

(c) Z direction

Figure 4.23: Third eigen-mode of the Ventura Hotel model.

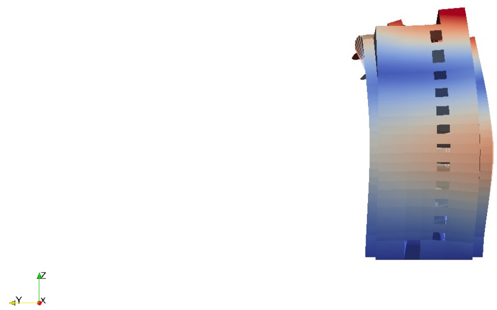

(a) X direction

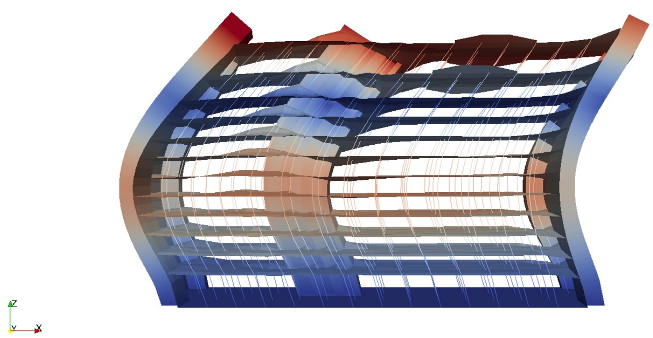

(b) Y direction

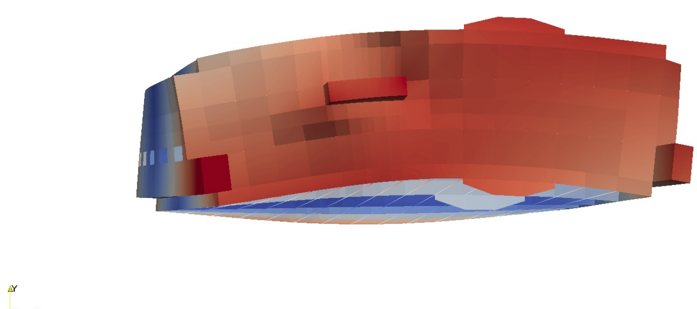

(c) Z direction

Figure 4.24: Fourth eigen-mode of the Ventura Hotel model.

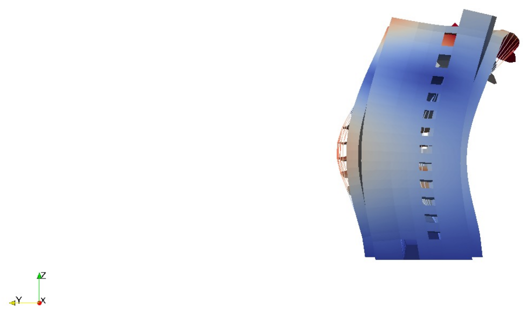

(a) X direction

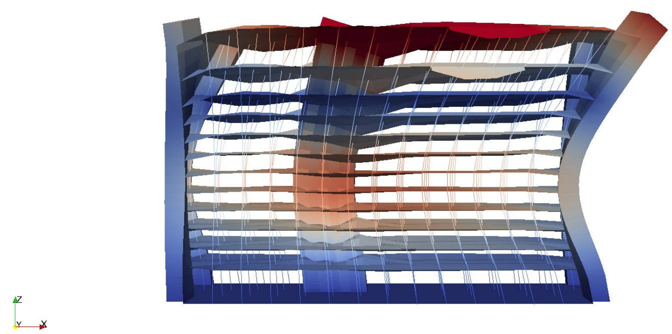

(b) Y direction

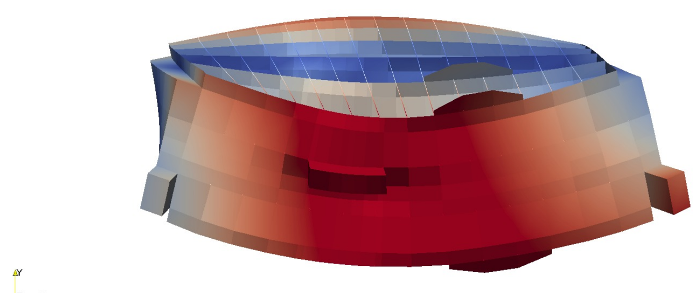

(c) Z direction

Figure 4.25: Fifth eigen-mode of the Ventura Hotel model.

4.3.2 Ventura Hotel, Location of Accelerometers

The locations of accelerometers for the Ventura Hotel are shown in Figure 4.26, taken from the CSMIP website documentation for the building.

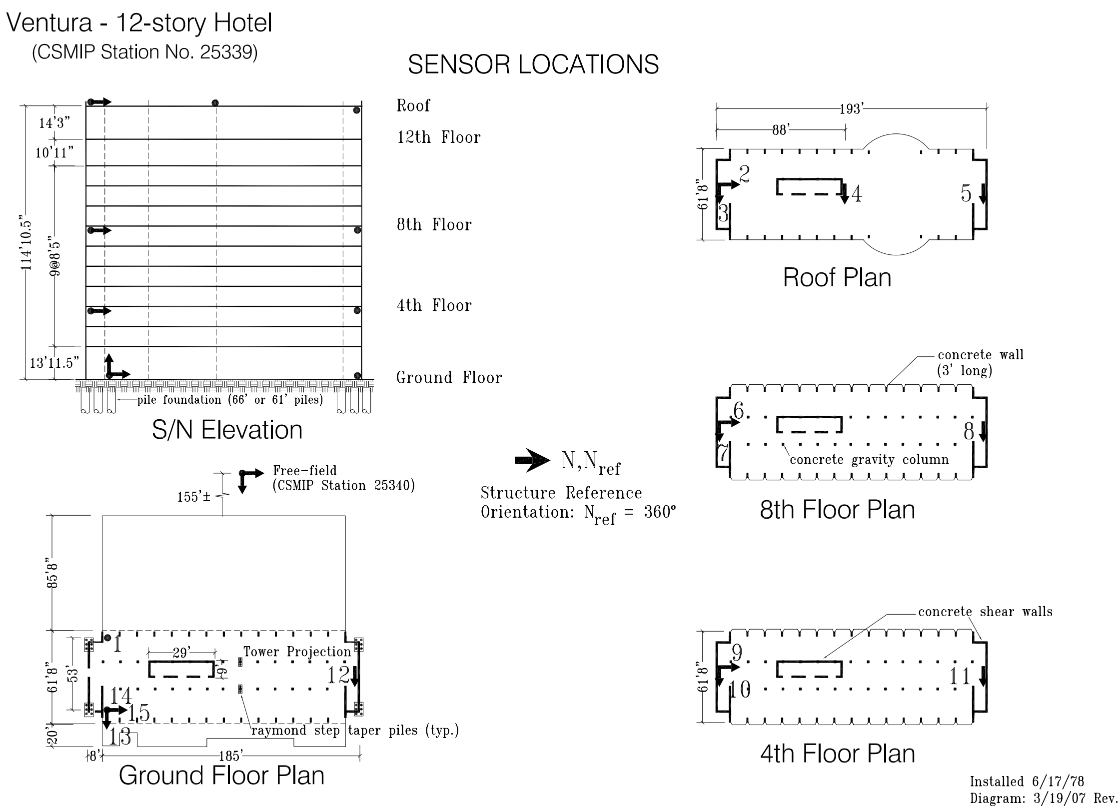

Figure 4.26: Locations of accelerometers for Ventura Hotel.

4.3.3 Rayleigh Damping

Rayleigh damping is used to simulate energy dissipation due to viscous coupling between solids and fluids. As pointed out by Hall (2006) and Yang et al. (2019c), classic Rayleigh damping must be used with appropriate damping coefficients, which should give a near-constant value of damping for all modes with frequencies that are of interest. For the modes outside the prescribed frequency range, the damping ratios can be unrealistically high.

For linear viscous damping of the Rayleigh type, the damping matrix is expressed as

$$C_{ij} = a_M M_{ij} + a_K K_{ij} \tag{4.1}$$

where C_{ij} is the damping matrix, M_{ij} is the mass matrix, K_{ij} is the stiffness matrix, a_M and a_K are damping constants with units of s^{-1} and s, respectively.

After calibration, the damping coefficients are chosen as $a_M = 1.0$, $a_K = 0.006$ for soil (10% damping ratio) and $a_M = 0.3$, $a_K = 0.0018$ for structure (3% damping ratio). Figure 4.27 shows damping ratio vs. frequency for the soil elements in this model.

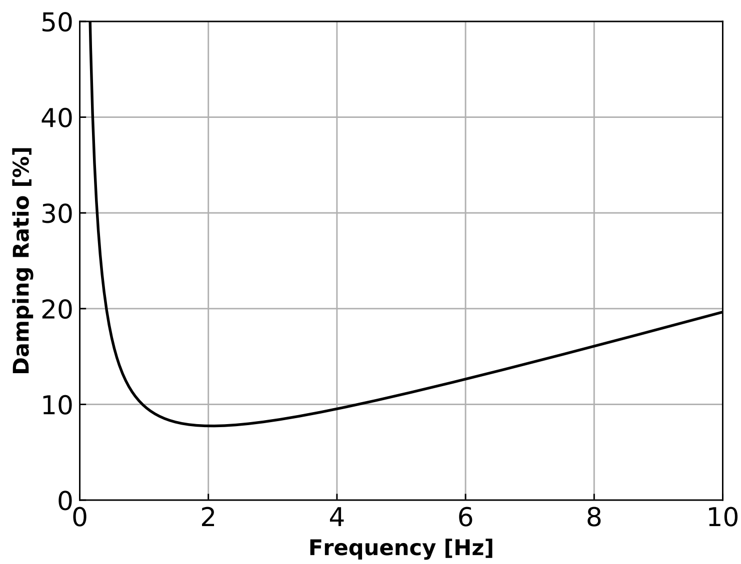

Figure 4.27: Damping ratio vs frequency for soil in the Ventura Hotel model.

4.3.4 Free-Field Results

The record of the 1994 Northridge earthquake at CSMIP Station No. 25340, which is very close to the Ventura Hotel site, was evaluated. Displacement and acceleration time series at ground surface are deconvoluted to generate the input seismic motions. It is noted that this is a free field model, with not building present.

The soil profile of this site consists of two main layers. The first 50 ft is a silt and clay layer with a shear wave velocity of 800 ft/s. The second layer is inter-bedded clay and sand with a shear wave velocity of 1400 ft/s. A mass density of 120 pcf is used for both layers. As mentioned in the previous section, 10% damping is assumed for the soil layers.

In order to verify the deconvolution results, a free-field model under seismic motion is simulated. Ideally, the simulation results at the ground surface should match the given records. Figure 4.28 shows the comparison between Real-ESSI free-field simulation and CSMIP records in X direction.

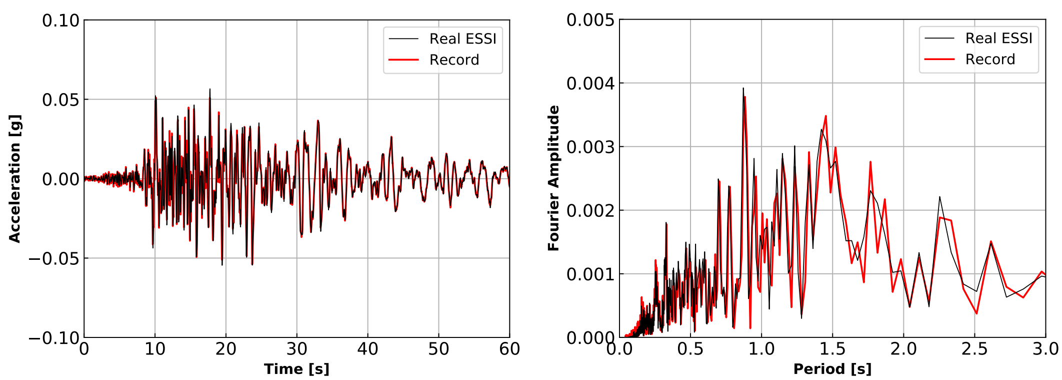

(a) Acceleration

(b) FFT Acceleration

Figure 4.28: Comparison between Real-ESSI free-field simulation and CSMIP records for Ventura Hotel under Northridge Earthquake, coherent motion, in X direction, Soil Material Model SM-EL3 (elastic, shown in Table 2.11), 10% soil damping.

According to Figure 4.28, Real-ESSI simulation results match well with records. Thus, the generated input motion is verified and can be used in later ESSI simulations.

4.3.5 1994 Northridge Earthquake

Ventura Hotel is well-instrumented with seismometers (CSMIP Station No. 25339). This section presents the comparison between actual records during the Northridge earthquake and the corresponding Real-ESSI simulation results. The simulation results are from the final version of the model, which has additional structure mass and 20% stiffness reduction due to material plasticity.

Note that all plots are set to have the same scale for direct comparison.

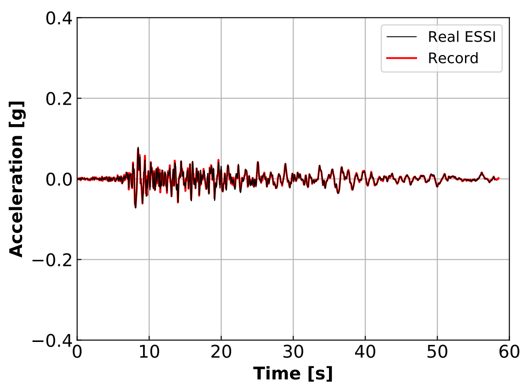

(a) Acceleration

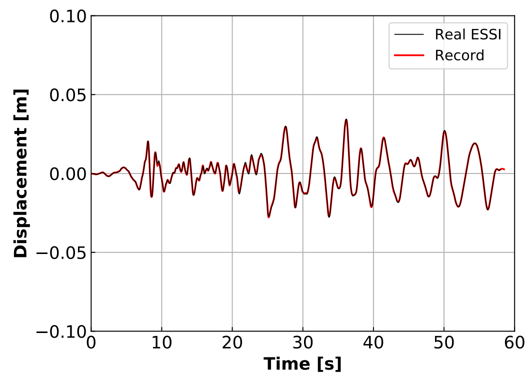

(b) Displacement

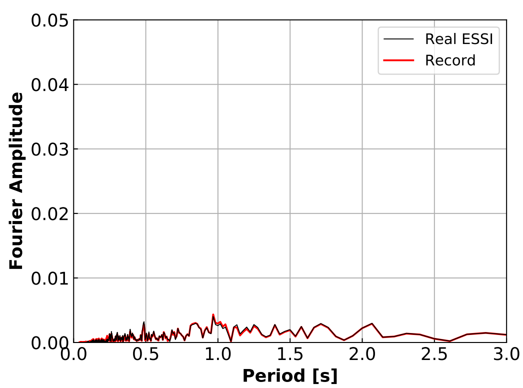

(c) FFT Acceleration

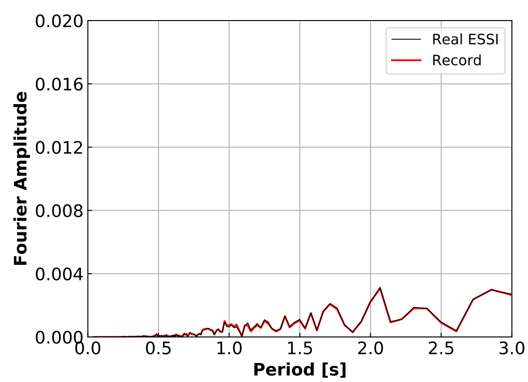

(d) FFT Displacement

Figure 4.29: Dynamic response of Ventura Hotel under Northridge earthquake at the ground floor in X direction (CHAN15), with additional structural mass, 20% structural stiffness reduction, Soil Material Model SM-EL3 (elastic, shown in Table 2.11), 3% structural damping and 10% soil damping, coherent motion.

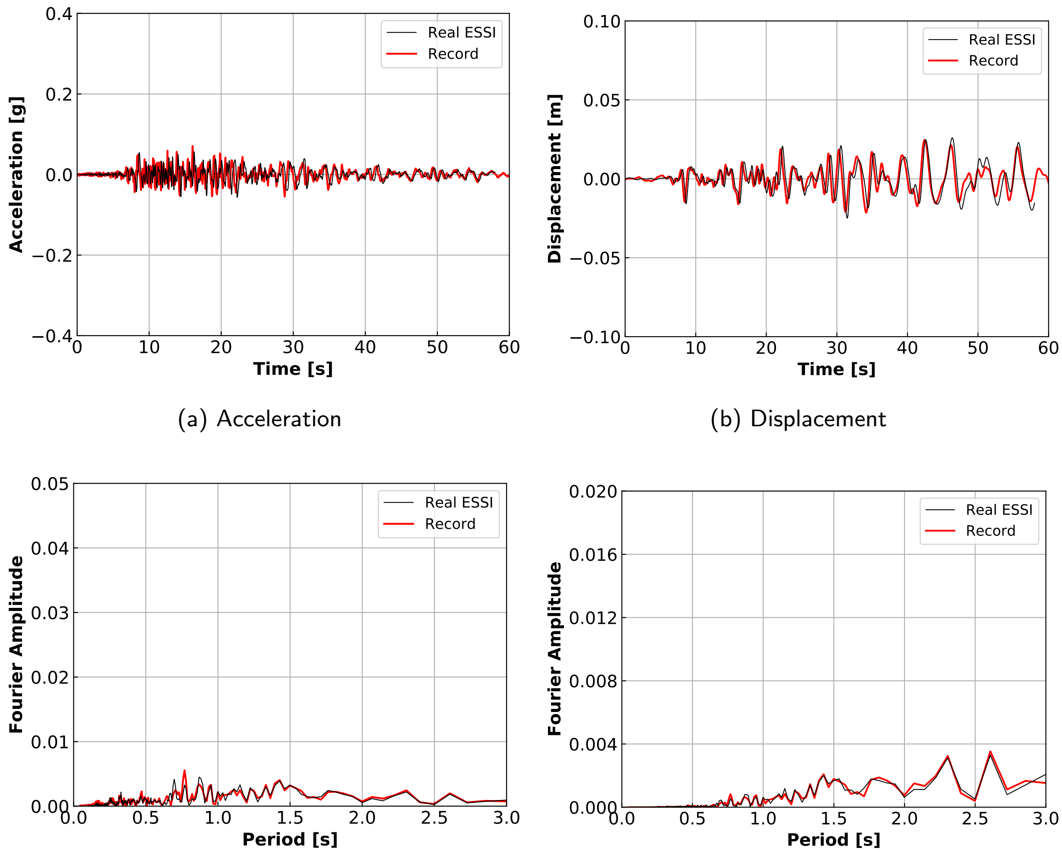

(a) Acceleration (b) Displacement

(c) FFT Acceleration (d) FFT Displacement

Figure 4.30: Dynamic response of Ventura Hotel under Northridge earthquake at the ground floor in Y direction (CHAN12), with additional structural mass, 20% structural stiffness reduction, Soil Material Model SM-EL3 (elastic, shown in Table 2.11), 3% structural damping and 10% soil damping, coherent motion.

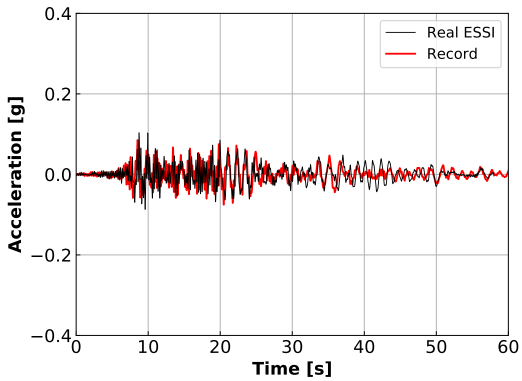

(a) Acceleration

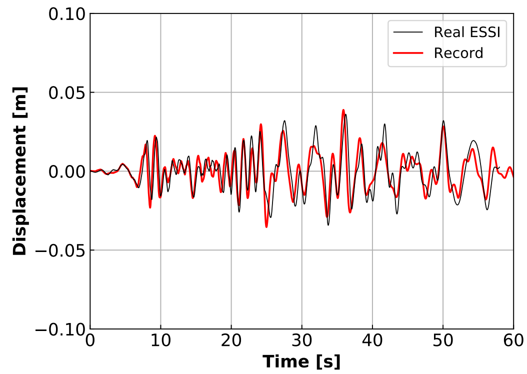

(b) Displacement

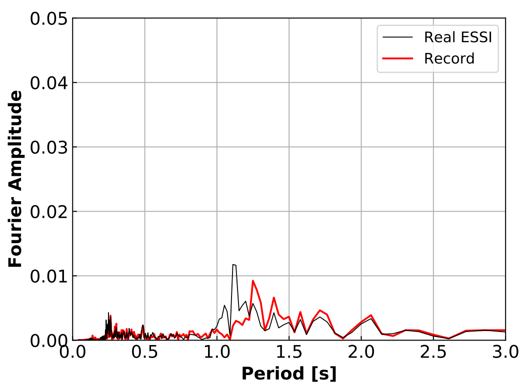

(c) FFT Acceleration

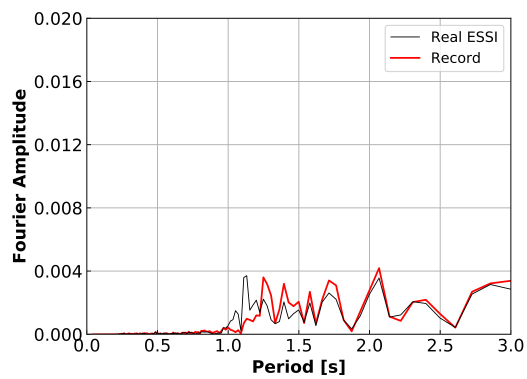

(d) FFT Displacement

Figure 4.31: Dynamic response of Ventura Hotel under Northridge earthquake at the 4th floor in X direction (CHAN09), with additional structural mass, 20% structural stiffness reduction, Soil Material Model SM-EL3 (elastic, shown in Table 2.11), 3% structural damping and 10% soil damping, coherent motion.

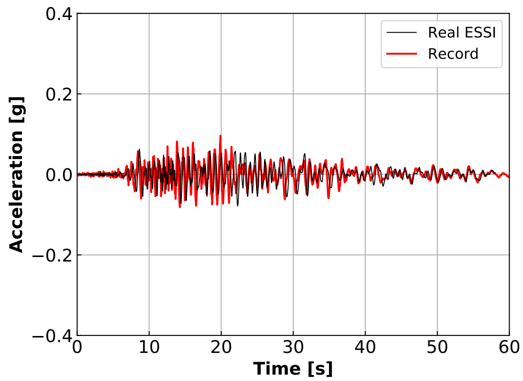

(a) Acceleration

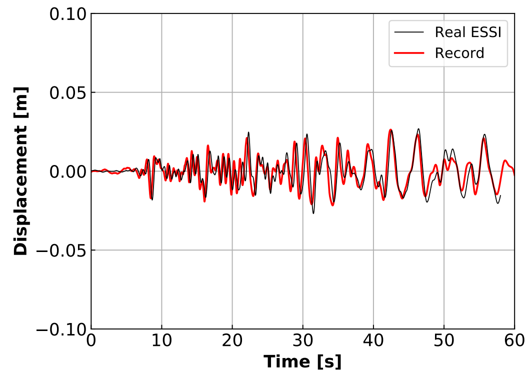

(b) Displacement

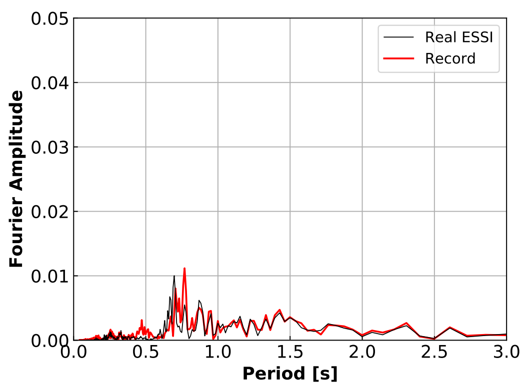

(c) FFT Acceleration

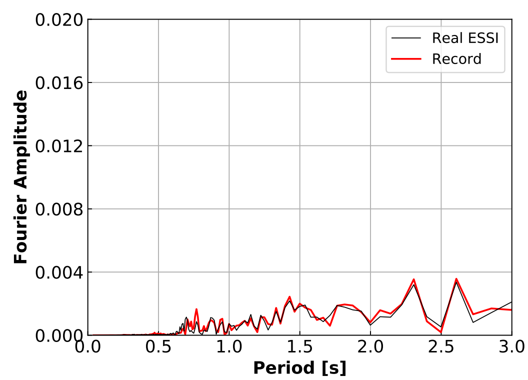

(d) FFT Displacement

Figure 4.32: Dynamic response of Ventura Hotel under Northridge earthquake at the 4th floor in Y direction (CHAN11), with additional structural mass, 20% structural stiffness reduction, Soil Material Model SM-EL3 (elastic, shown in Table 2.11), 3% structural damping and 10% soil damping, coherent motion.

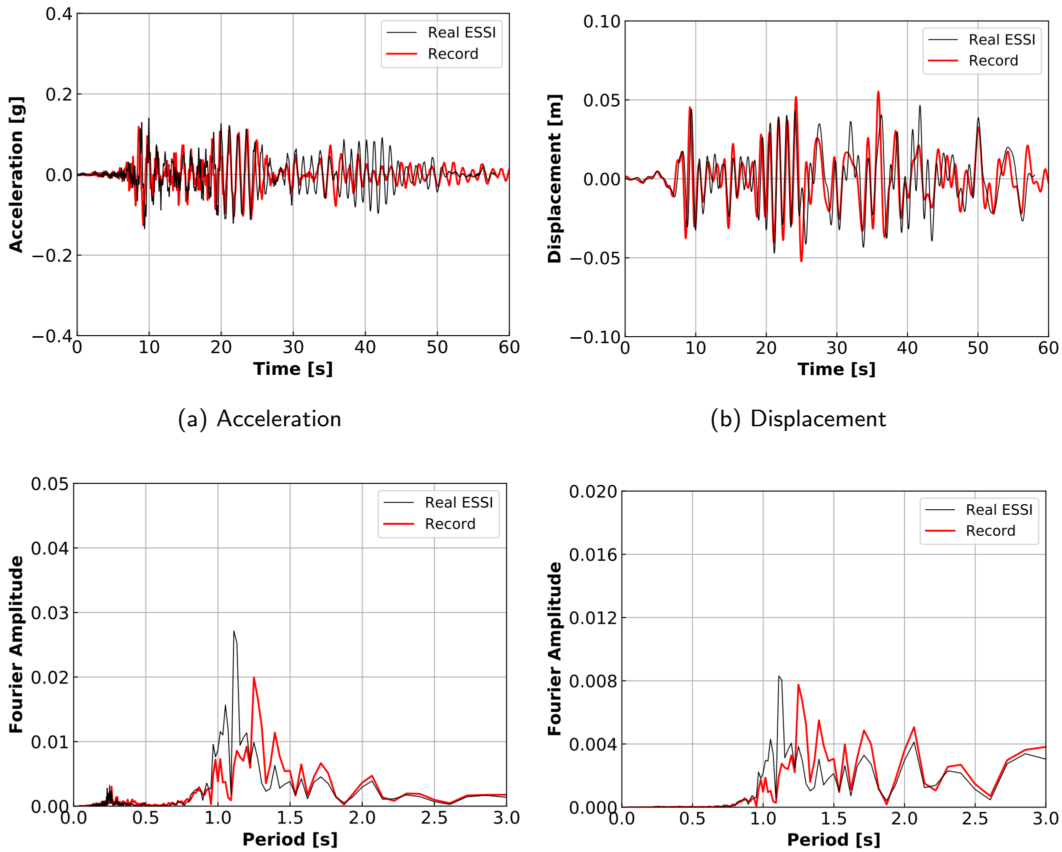

(a) Acceleration (b) Displacement

(c) FFT Acceleration (d) FFT Displacement

Figure 4.33: Dynamic response of Ventura Hotel under Northridge earthquake at the 8th floor in X direction (CHAN06), with additional structural mass, 20% structural stiffness reduction, Soil Material Model SM-EL3 (elastic, shown in Table 2.11), 3% structural damping and 10% soil damping, coherent motion.

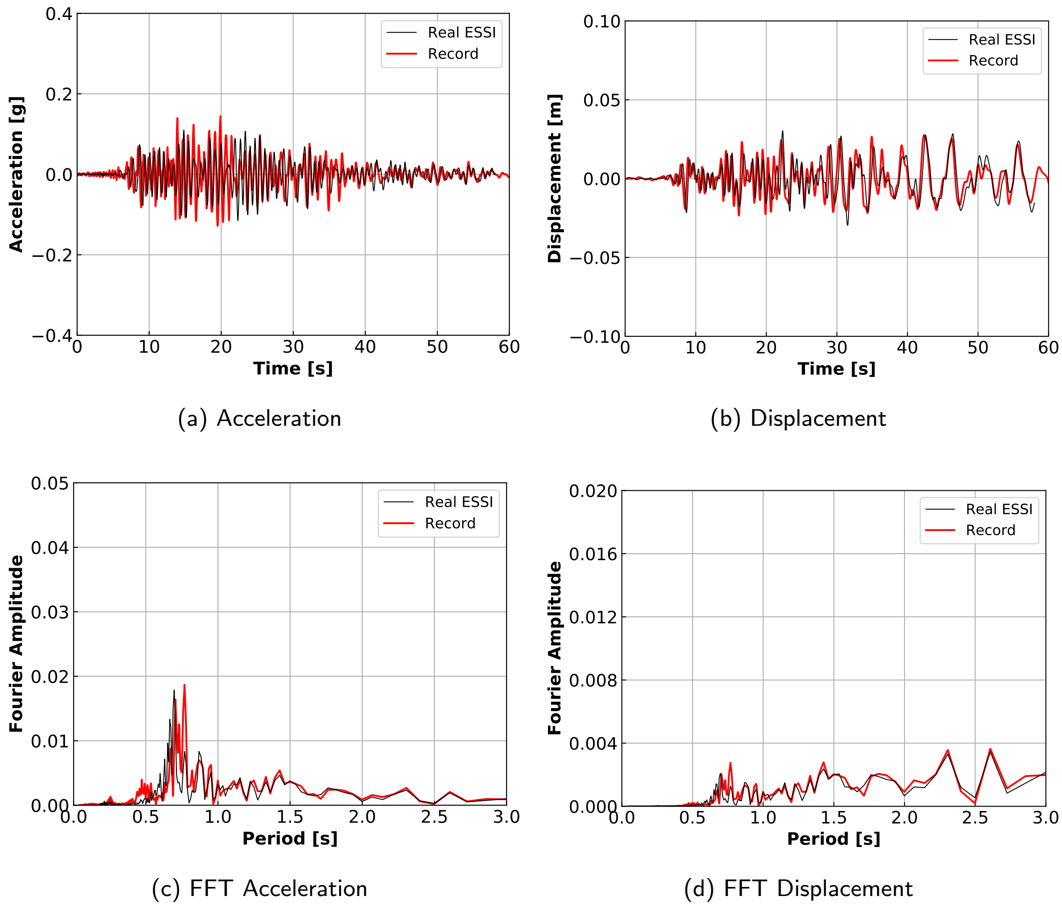

Figure 4.34: Dynamic response of Ventura Hotel under Northridge earthquake at the 8th floor in Y direction (CHAN08), with additional structural mass, 20% structural stiffness reduction, Soil Material Model SM-EL3 (elastic, shown in Table 2.11), 3% structural damping and 10% soil damping, coherent motion.

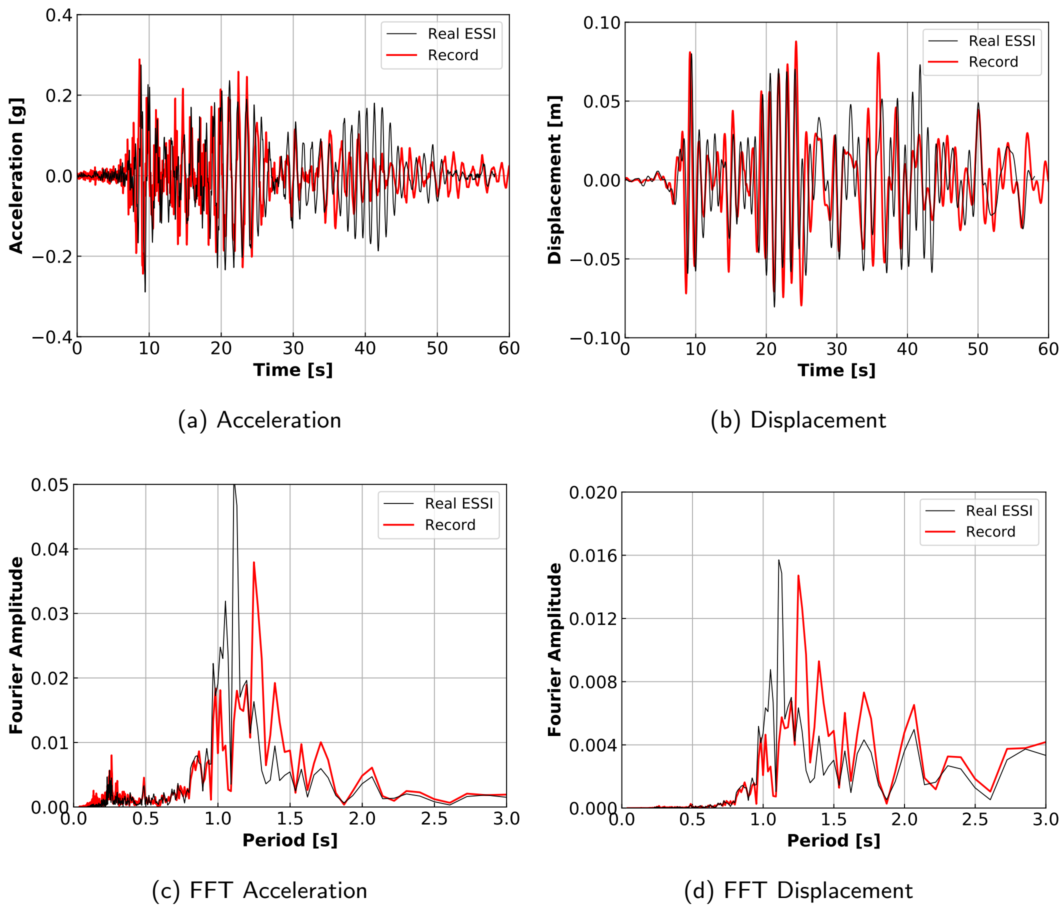

Figure 4.35: Dynamic response of Ventura Hotel under Northridge earthquake at the roof in X direction (CHAN02), with additional structural mass, 20% structural stiffness reduction, Soil Material Model SM-EL3 (elastic, shown in Table 2.11), 3% structural damping and 10% soil damping, coherent motion.

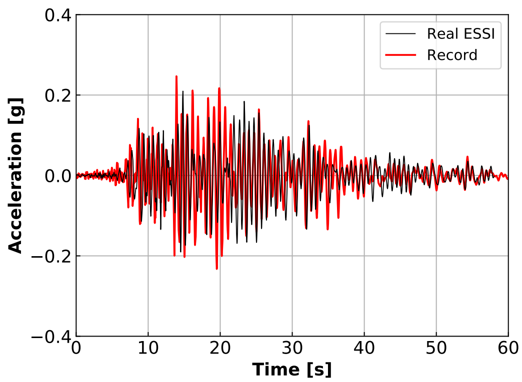

(a) Acceleration

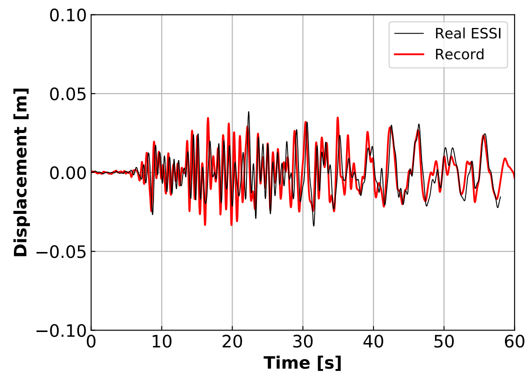

(b) Displacement

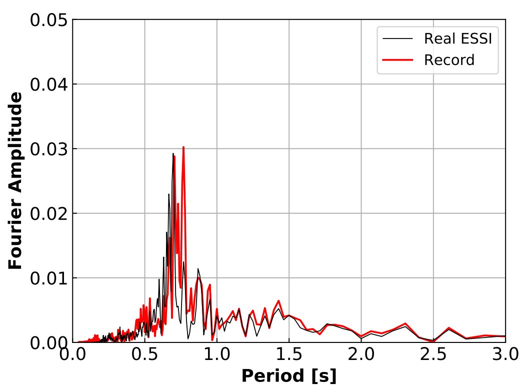

(c) FFT Acceleration

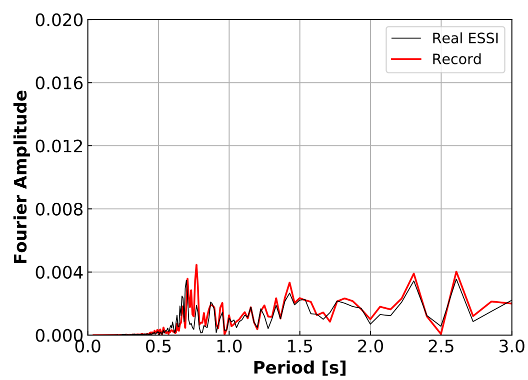

(d) FFT Displacement

Figure 4.36: Dynamic response of Ventura Hotel under Northridge earthquake at the roof in Y direction (CHAN05), with additional structural mass, 20% structural stiffness reduction, Soil Material Model SM-EL3 (elastic, shown in Table 2.11), 3% structural damping and 10% soil damping, coherent motion.

Comparison of SSI and non-SSI Responses

On the ground floor, CHAN15 and CHAN12, full SSI and non-SSI, only structure simulations have precisely the same response.

However, at higher elevations, the results diverge. Only structure, non-SSI behavior shows unrealistically large acceleration responses. Interestingly, in the x-direction, the displacement result of non-SSI becomes unrealistically large, especially during the first 20 seconds. In the y-direction, the displacement results for non-SSI response are smaller.

Overall, full SSI results match much better with recorded seismic responses at corresponding floors.

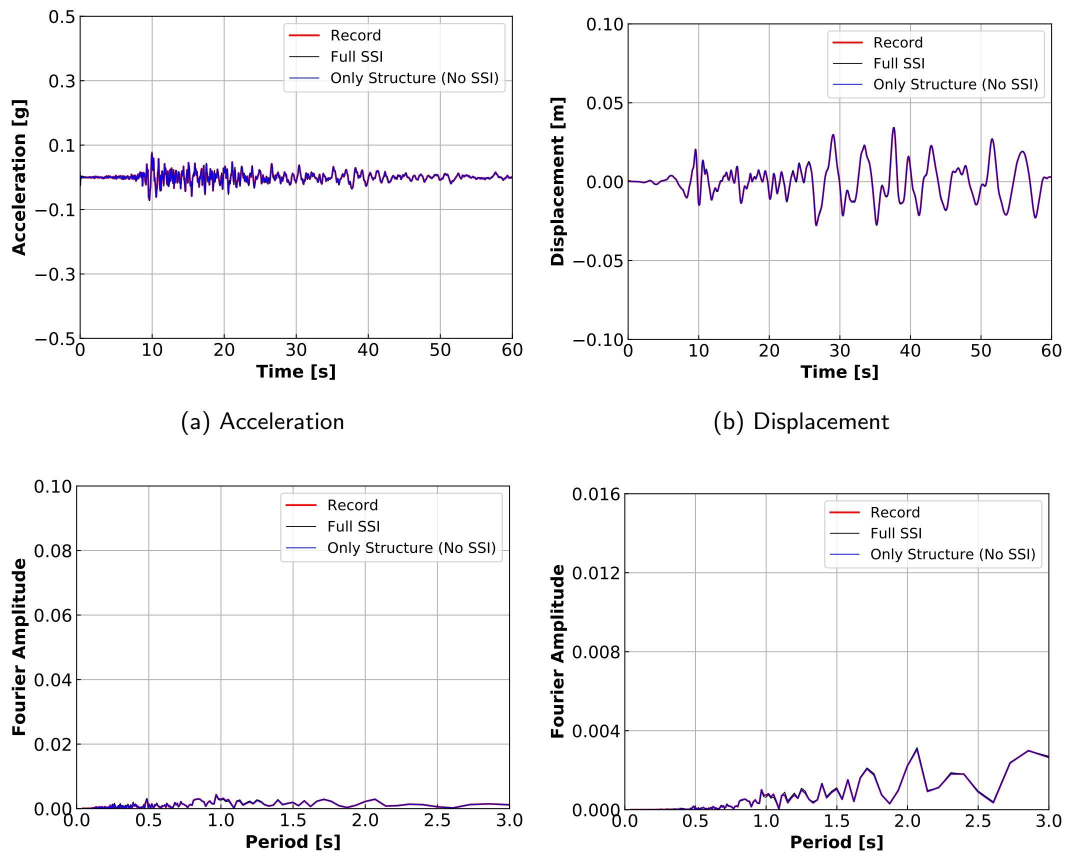

(a) Acceleration (b) Displacement

(c) FFT Acceleration (d) FFT Displacement

Figure 4.37: Dynamic response of Ventura Hotel under Northridge earthquake at the ground floor in X direction (CHAN15), compare SSI and non-SSI response, with additional structural mass, 20% structural stiffness reduction, Soil Material Model SM-EL3 (elastic, shown in Table 2.11), 3% structural damping and 10% soil damping, coherent motion.

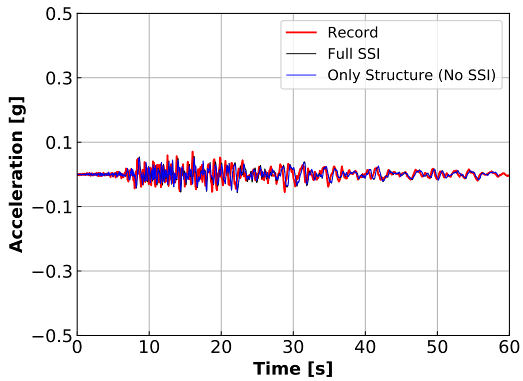

(a) Acceleration

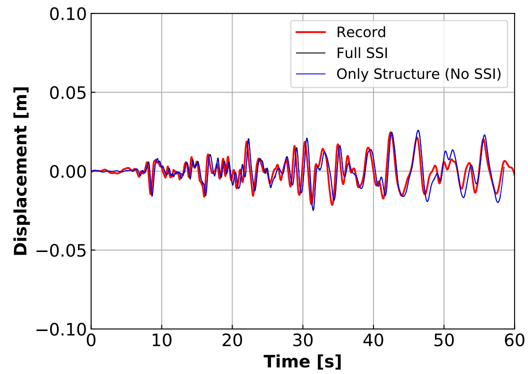

(b) Displacement

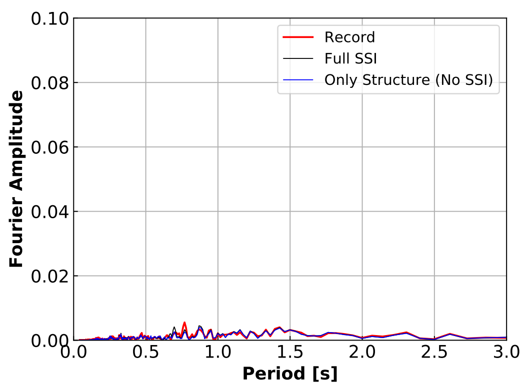

(c) FFT Acceleration

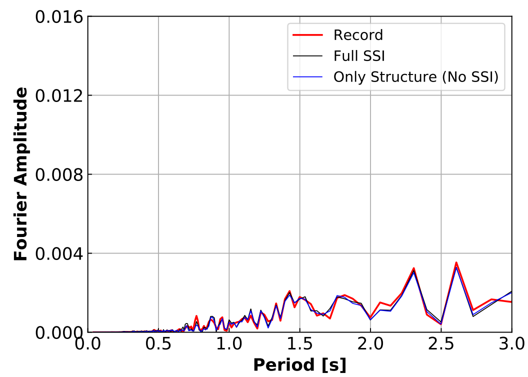

(d) FFT Displacement

Figure 4.38: Dynamic response of Ventura Hotel under Northridge earthquake at the ground floor in Y direction (CHAN12), compare SSI and non-SSI response, with additional structural mass, 20% structural stiffness reduction, Soil Material Model SM-EL3 (elastic, shown in Table 2.11), 3% structural damping and 10% soil damping, coherent motion.

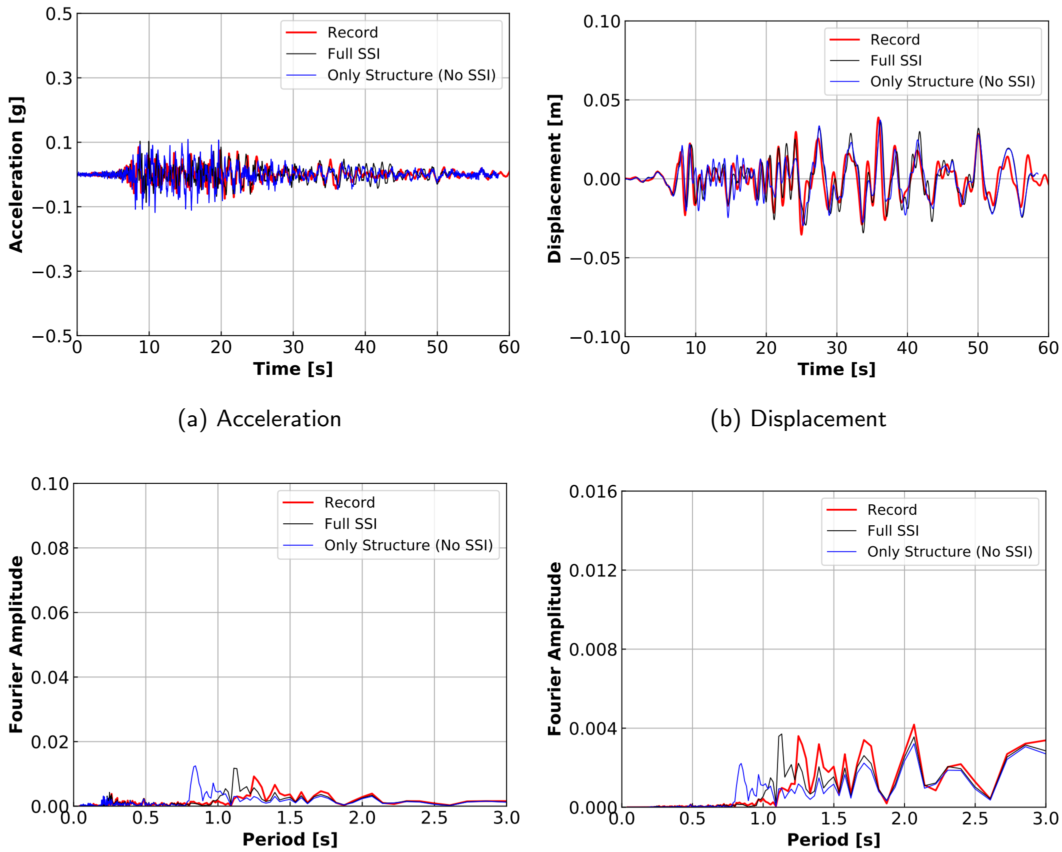

(a) Acceleration (b) Displacement

(c) FFT Acceleration (d) FFT Displacement

Figure 4.39: Dynamic response of Ventura Hotel under Northridge earthquake at the 4th floor in X direction (CHAN09), compare SSI and non-SSI response, with additional structural mass, 20% structural stiffness reduction, Soil Material Model SM-EL3 (elastic, shown in Table 2.11), 3% structural damping and 10% soil damping, coherent motion.

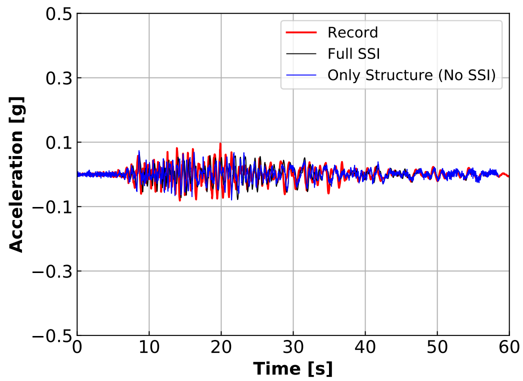

(a) Acceleration

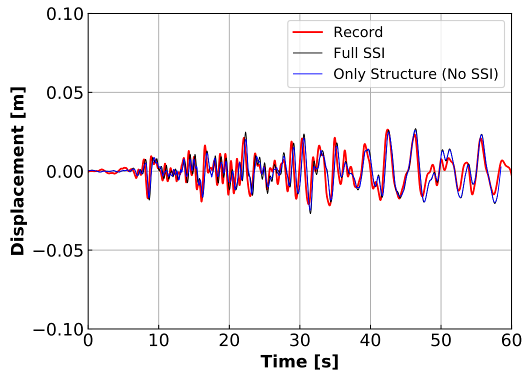

(b) Displacement

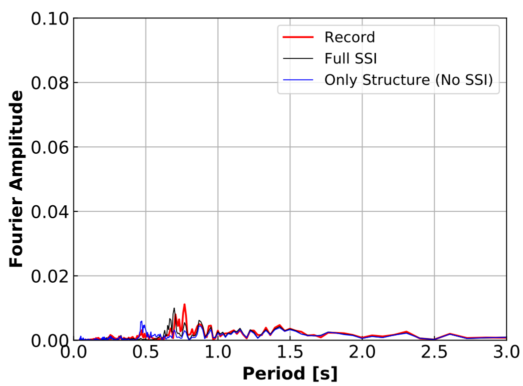

(c) FFT Acceleration

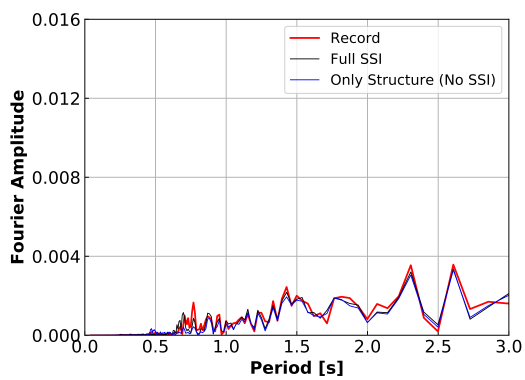

(d) FFT Displacement

Figure 4.40: Dynamic response of Ventura Hotel under Northridge earthquake at the 4th floor in Y direction (CHAN11), compare SSI and non-SSI response, with additional structural mass, 20% structural stiffness reduction, Soil Material Model SM-EL3 (elastic, shown in Table 2.11), 3% structural damping and 10% soil damping, coherent motion.

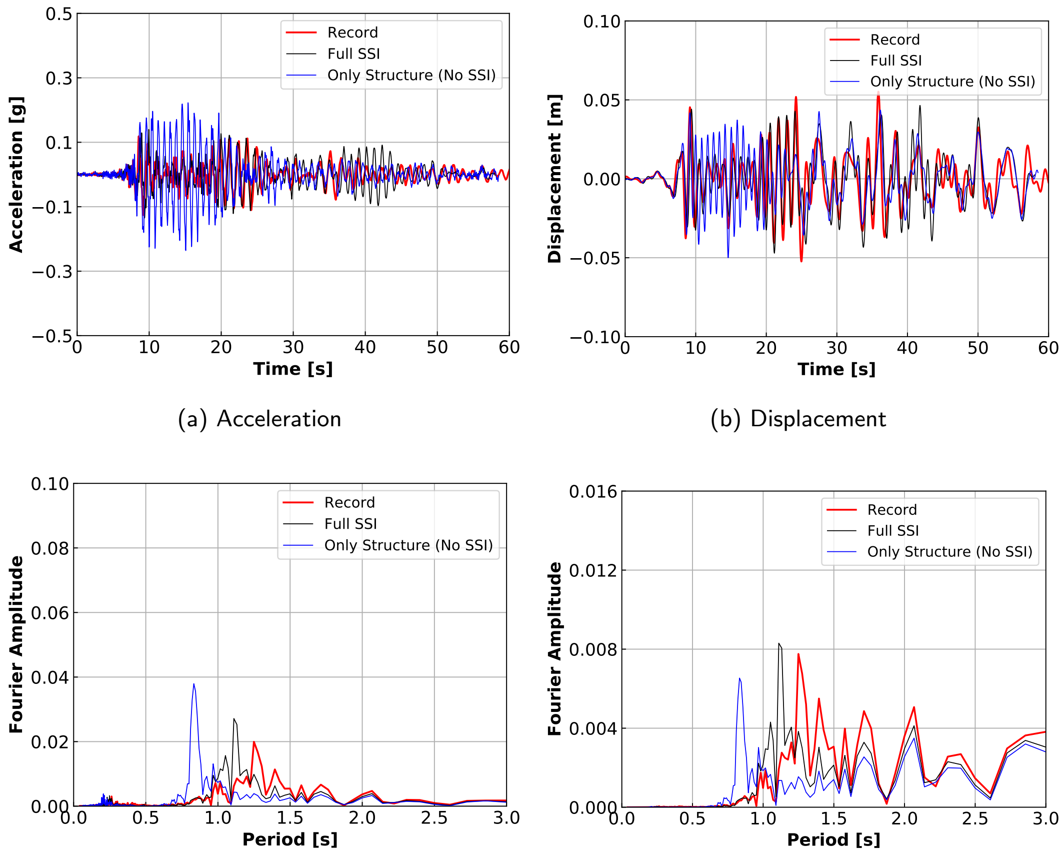

(a) Acceleration

(b) Displacement

(c) FFT Acceleration

(d) FFT Displacement

Figure 4.41: Dynamic response of Ventura Hotel under Northridge earthquake at the 8th floor in X direction (CHAN06), compare SSI and non-SSI response, with additional structural mass, 20% structural stiffness reduction, Soil Material Model SM-EL3 (elastic, shown in Table 2.11), 3% structural damping and 10% soil damping, coherent motion.

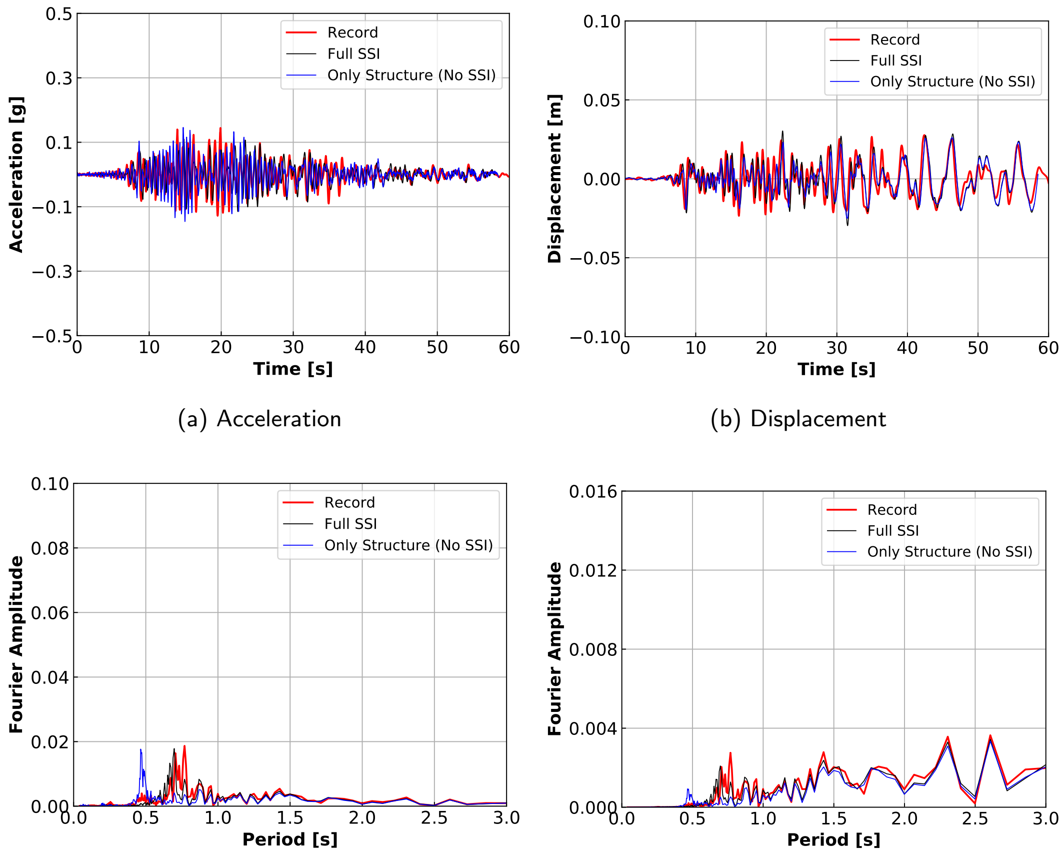

(a) Acceleration

(b) Displacement

(c) FFT Acceleration

(d) FFT Displacement

Figure 4.42: Dynamic response of Ventura Hotel under Northridge earthquake at the 8th floor in Y direction (CHAN08), compare SSI and non-SSI response, with additional structural mass, 20% structural stiffness reduction, Soil Material Model SM-EL3 (elastic, shown in Table 2.11), 3% structural damping and 10% soil damping, coherent motion.

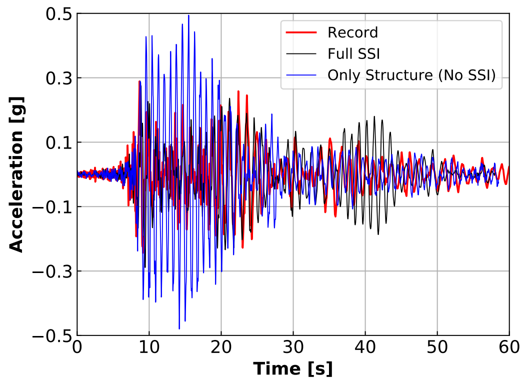

(a) Acceleration

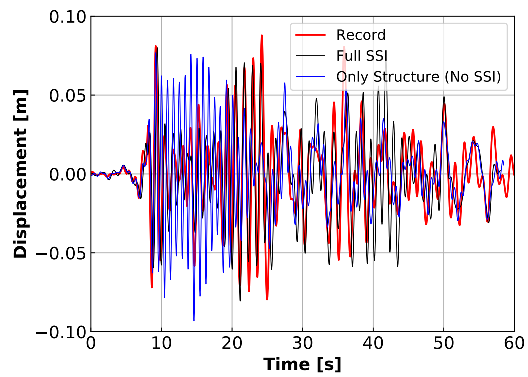

(b) Displacement

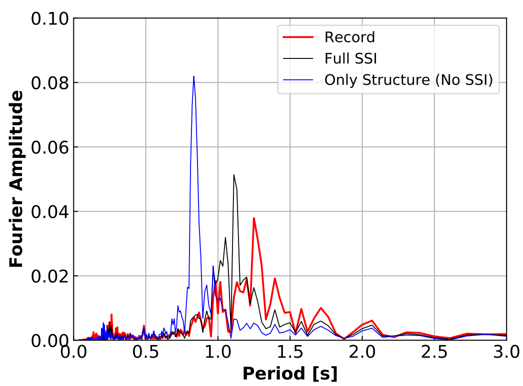

(c) FFT Acceleration

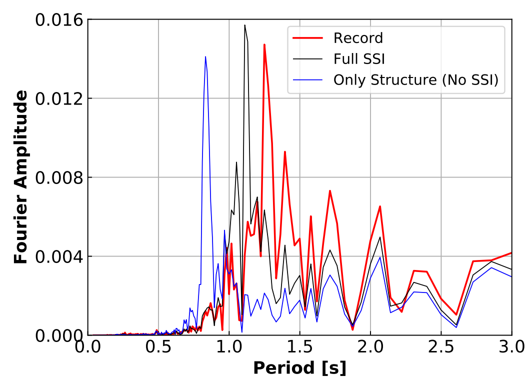

(d) FFT Displacement

Figure 4.43: Dynamic response of Ventura Hotel under Northridge earthquake at the roof in X direction (CHAN02), compare SSI and non-SSI response, with additional structural mass, 20% structural stiffness reduction, Soil Material Model SM-EL3 (elastic, shown in Table 2.11), 3% structural damping and 10% soil damping, coherent motion.

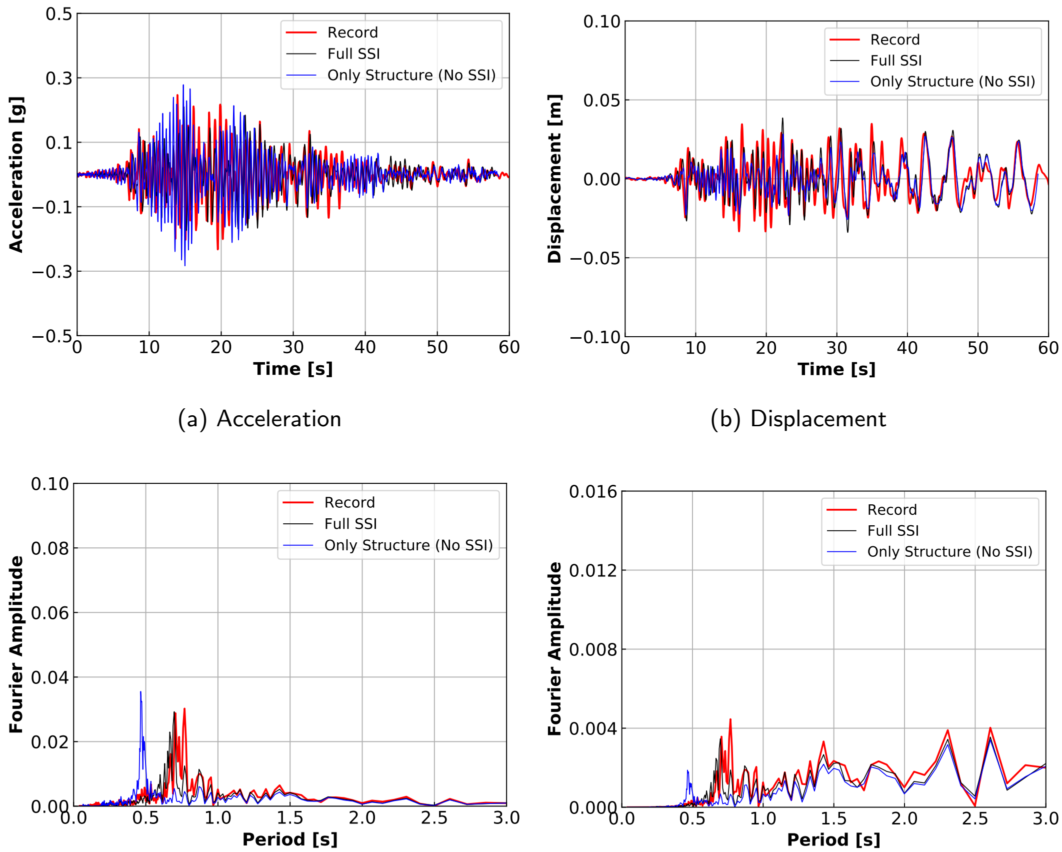

(a) Acceleration

(b) Displacement

(c) FFT Acceleration

(d) FFT Displacement

Figure 4.44: Dynamic response of Ventura Hotel under Northridge earthquake at the roof in Y direction (CHAN05), compare SSI and non-SSI response, with additional structural mass, 20% structural stiffness reduction, Soil Material Model SM-EL3 (elastic, shown in Table 2.11), 3% structural damping and 10% soil damping, coherent motion.

Influence of Structural Damping Ratio

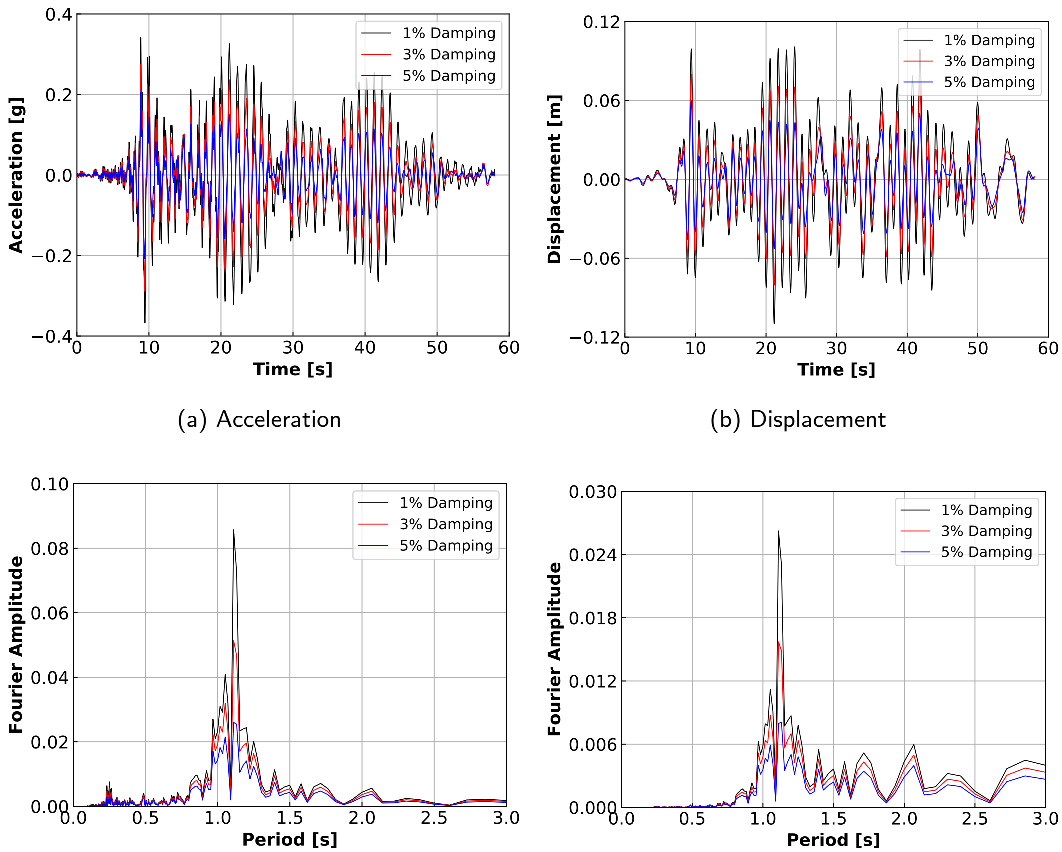

(a) Acceleration (b) Displacement

(c) FFT Acceleration (d) FFT Displacement

Figure 4.45: Dynamic response of Ventura Hotel under Northridge earthquake at the roof in X direction (CHAN02), compare different structural damping ratio (1%, 3%, 5%), with additional structural mass, 20% structural stiffness reduction, Soil Material Model SM-EL3 (elastic, shown in Table 2.11), coherent motion.

Influence of Structural Stiffness Reduction

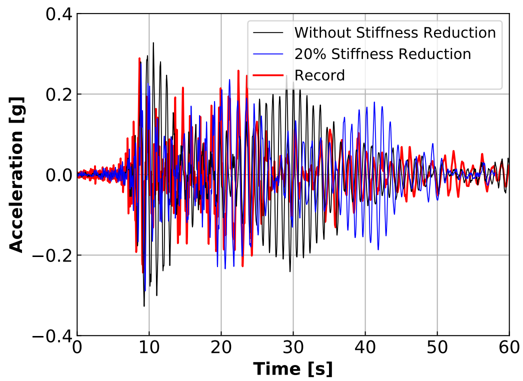

(a) Acceleration

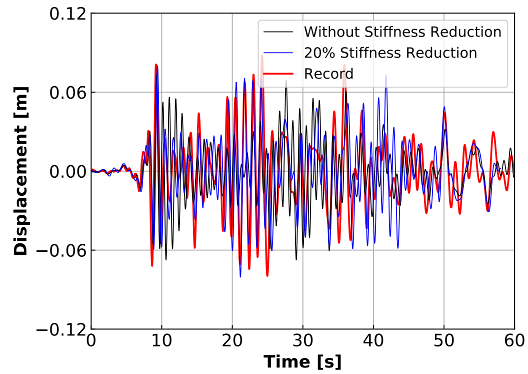

(b) Displacement

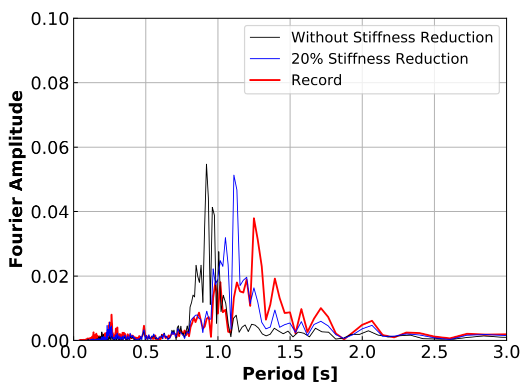

(c) FFT Acceleration

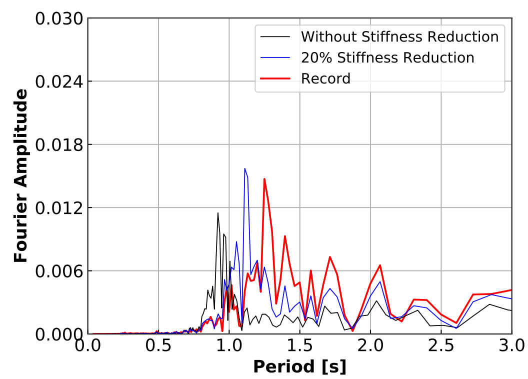

(d) FFT Displacement

Figure 4.46: Dynamic response of Ventura Hotel under Northridge earthquake at the roof in X direction (CHAN02), compare different structural stiffness reduction (no reduction, 20% reduction, record), with additional structural mass, Soil Material Model SM-EL3 (elastic, shown in Table 2.11), 3% structural damping and 10% soil damping, coherent motion.

Coherent Motion vs. Incoherent Motion

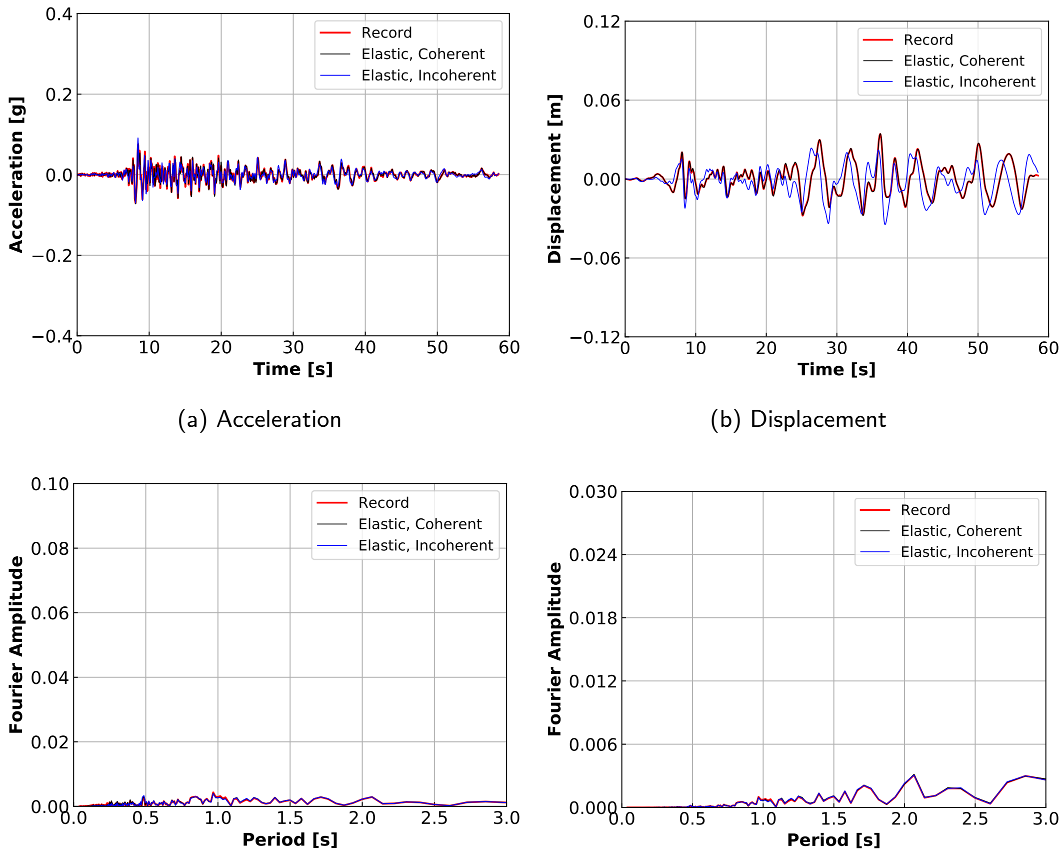

(a) Acceleration

(b) Displacement

(c) FFT Acceleration

(d) FFT Displacement

Figure 4.47: Dynamic response of Ventura Hotel under Northridge earthquake, coherent motion vs incoherent motion, at the ground floor in X direction (CHAN15), with additional structural mass, 20% structural stiffness reduction, Soil Material Model SM-EL3 (elastic, shown in Table 2.11), 3% structural damping and 10% soil damping.

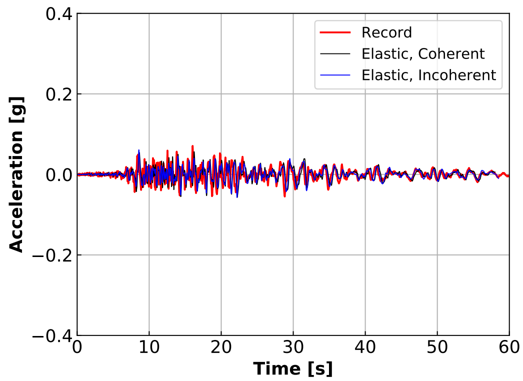

(a) Acceleration

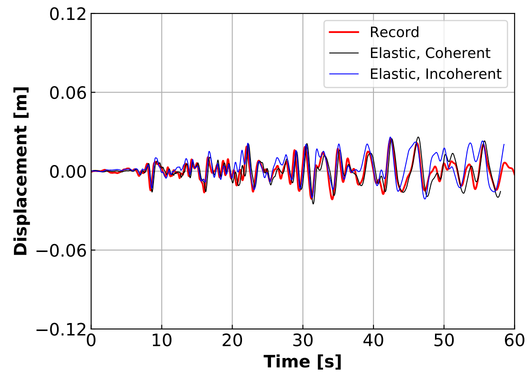

(b) Displacement

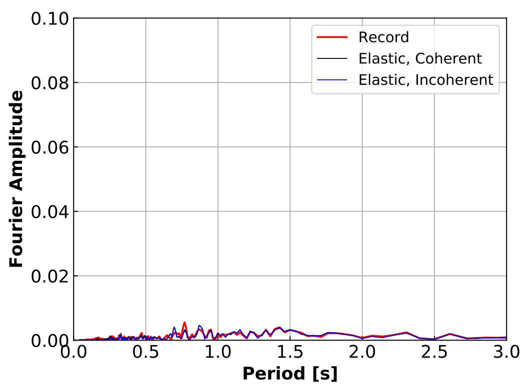

(c) FFT Acceleration

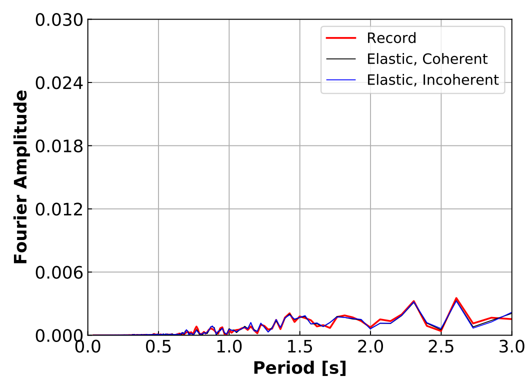

(d) FFT Displacement

Figure 4.48: Dynamic response of Ventura Hotel under Northridge earthquake, coherent motion vs incoherent motion, at the ground floor in Y direction (CHAN12), with additional structural mass, 20% structural stiffness reduction, Soil Material Model SM-EL3 (elastic, shown in Table 2.11), 3% structural damping and 10% soil damping.

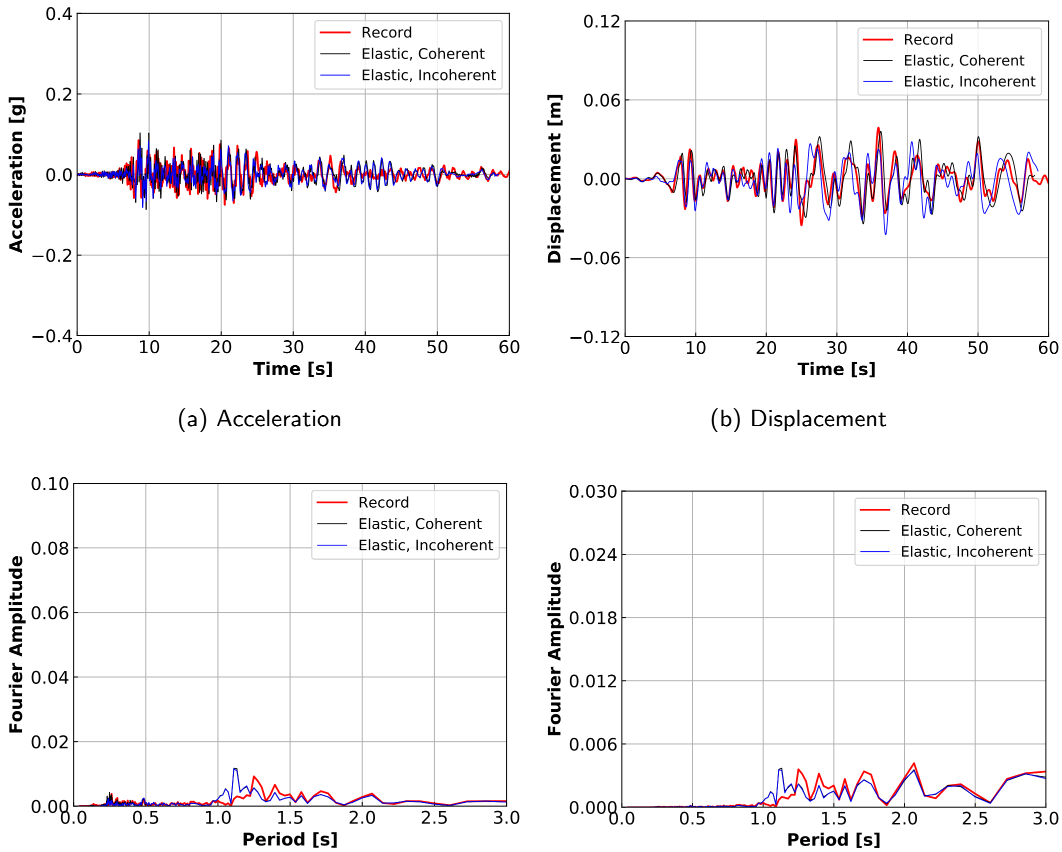

(a) Acceleration

(b) Displacement

(c) FFT Acceleration

(d) FFT Displacement

Figure 4.49: Dynamic response of Ventura Hotel under Northridge earthquake, coherent motion vs incoherent motion, at the 4th floor in X direction (CHAN09), with additional structural mass, 20% structural stiffness reduction, Soil Material Model SM-EL3 (elastic, shown in Table 2.11), 3% structural damping and 10% soil damping.

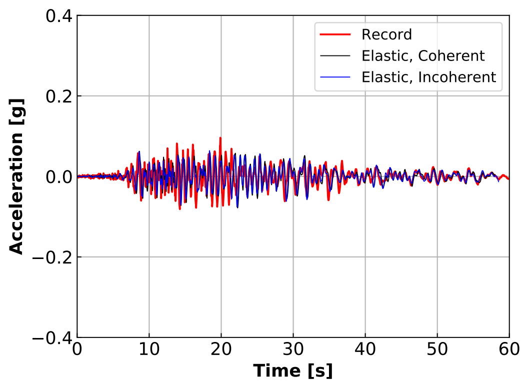

(a) Acceleration

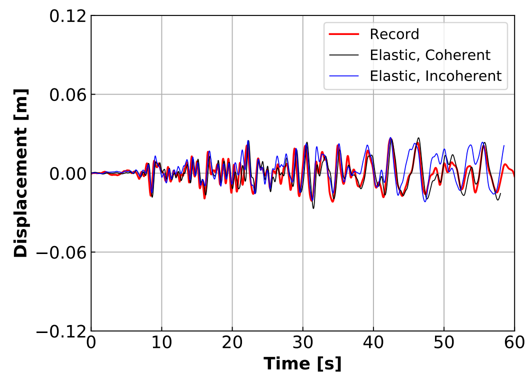

(b) Displacement

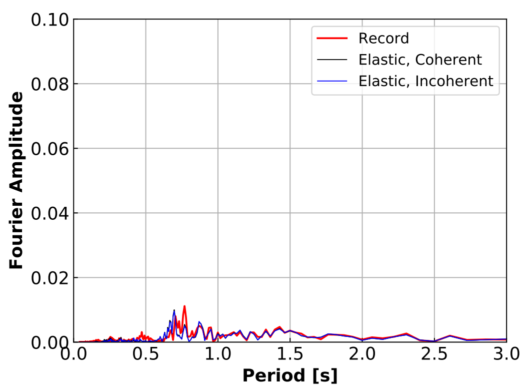

(c) FFT Acceleration

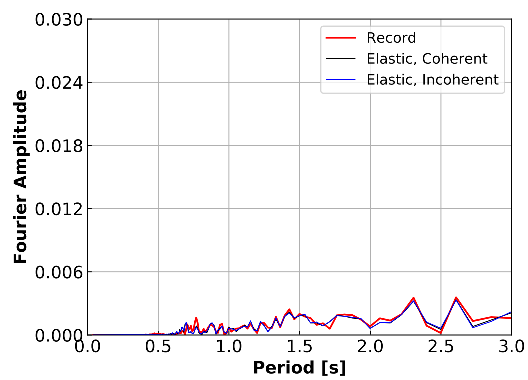

(d) FFT Displacement

Figure 4.50: Dynamic response of Ventura Hotel under Northridge earthquake, coherent motion vs incoherent motion, at the 4th floor in Y direction (CHAN11), with additional structural mass, 20% structural stiffness reduction, Soil Material Model SM-EL3 (elastic, shown in Table 2.11), 3% structural damping and 10% soil damping.

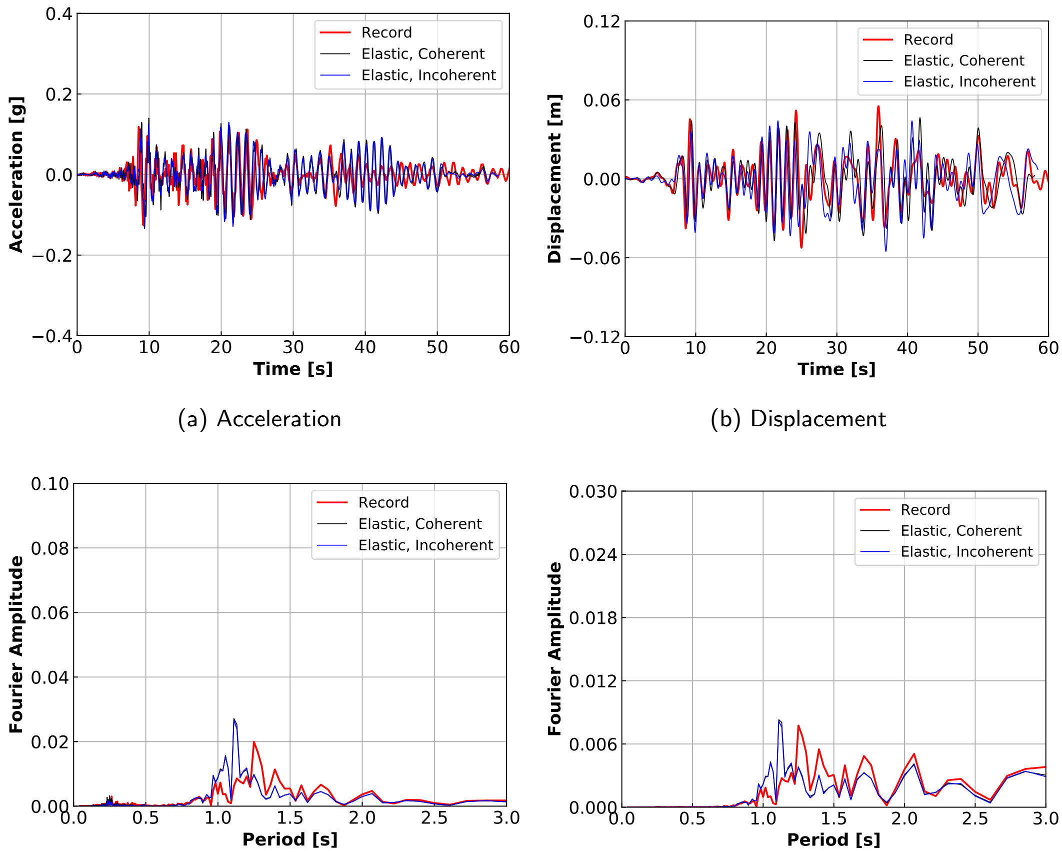

(a) Acceleration

(b) Displacement

(c) FFT Acceleration

(d) FFT Displacement

Figure 4.51: Dynamic response of Ventura Hotel under Northridge earthquake, coherent motion vs incoherent motion, at the 8th floor in X direction (CHAN06), with additional structural mass, 20% structural stiffness reduction, Soil Material Model SM-EL3 (elastic, shown in Table 2.11), 3% structural damping and 10% soil damping.

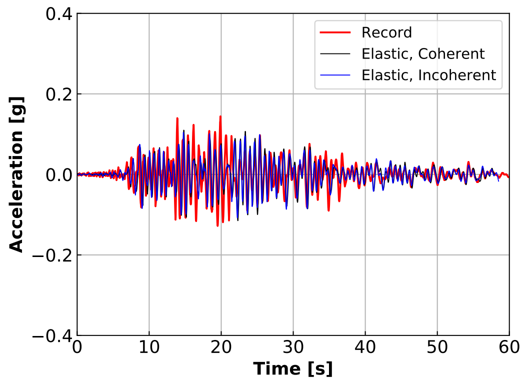

(a) Acceleration

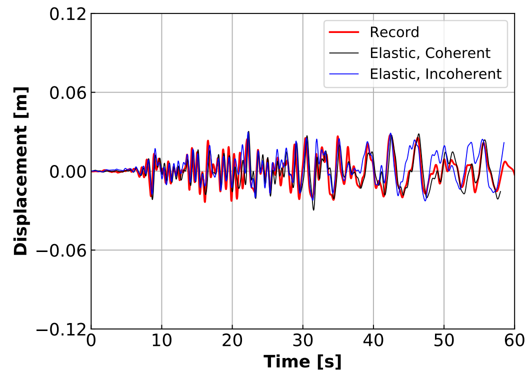

(b) Displacement

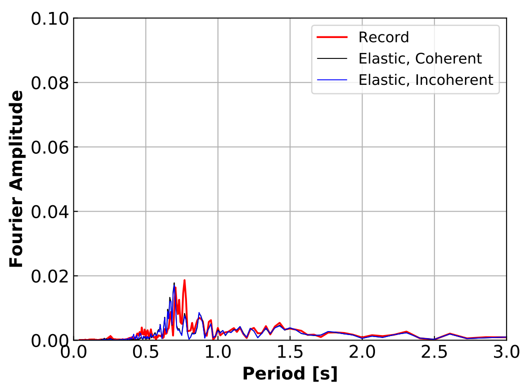

(c) FFT Acceleration

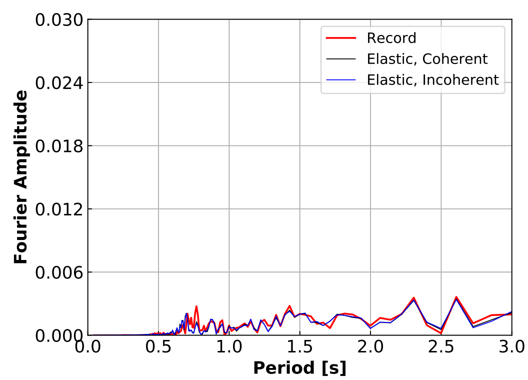

(d) FFT Displacement

Figure 4.52: Dynamic response of Ventura Hotel under Northridge earthquake, coherent motion vs incoherent motion, at the 8th floor in Y direction (CHAN08), with additional structural mass, 20% structural stiffness reduction, Soil Material Model SM-EL3 (elastic, shown in Table 2.11), 3% structural damping and 10% soil damping.

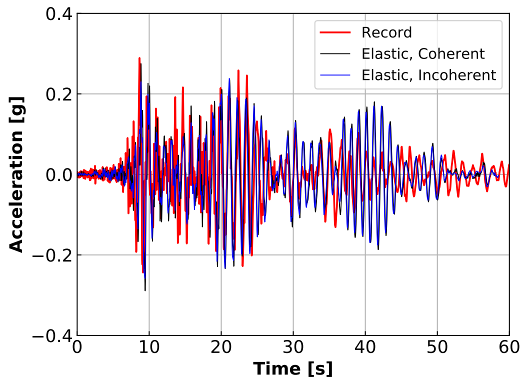

(a) Acceleration

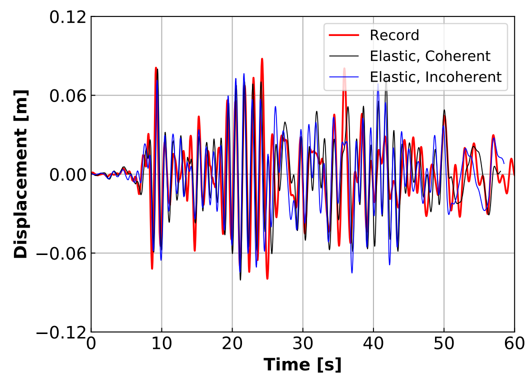

(b) Displacement

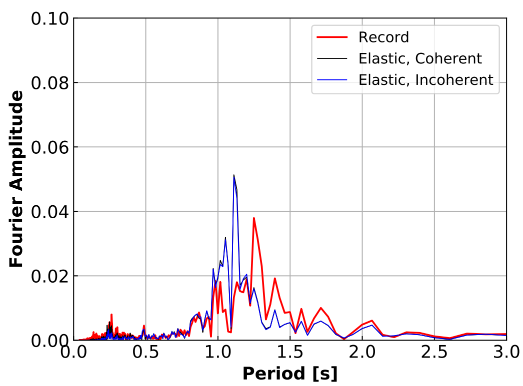

(c) FFT Acceleration

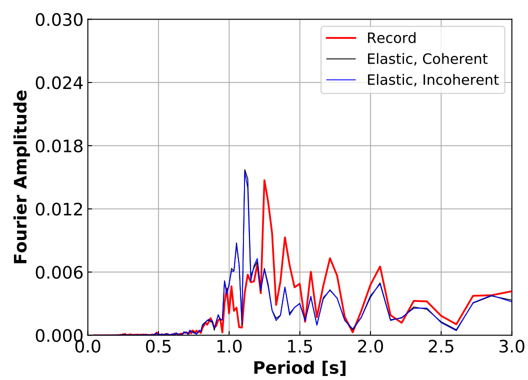

(d) FFT Displacement

Figure 4.53: Dynamic response of Ventura Hotel under Northridge earthquake, coherent motion vs incoherent motion, at the roof in X direction (CHAN02), with additional structural mass, 20% structural stiffness reduction, Soil Material Model SM-EL3 (elastic, shown in Table 2.11), 3% structural damping and 10% soil damping.

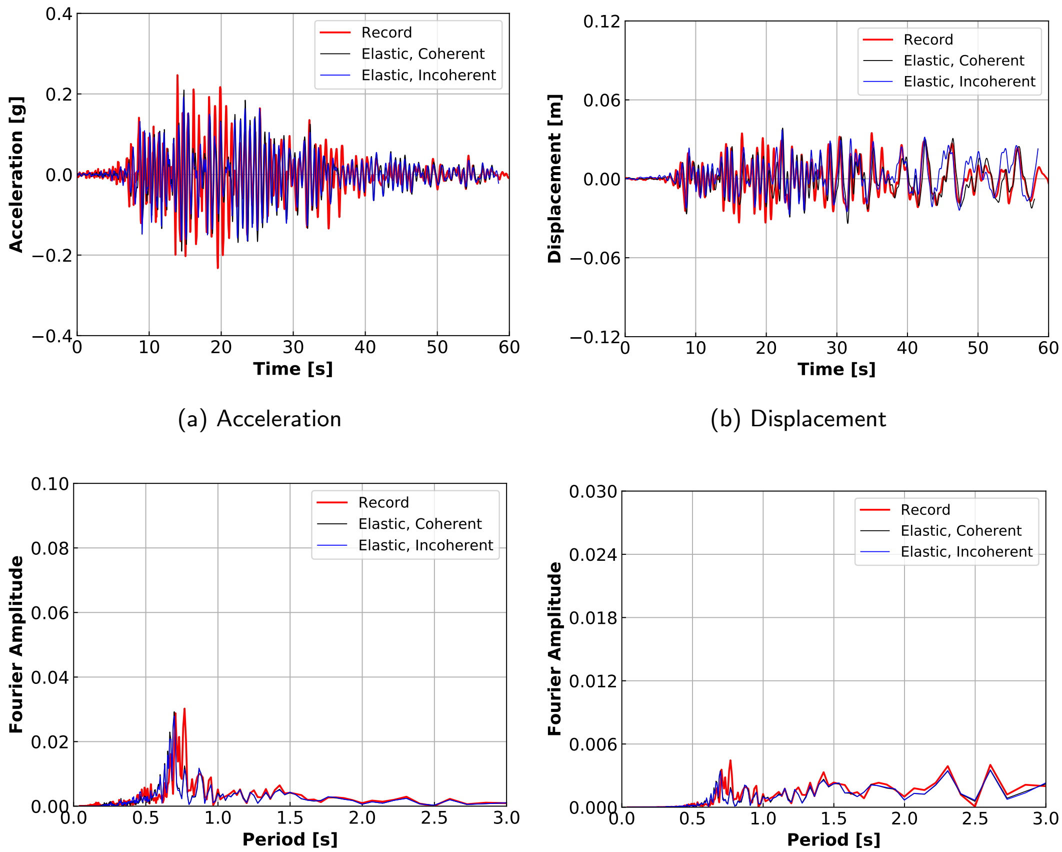

(a) Acceleration

(b) Displacement

(c) FFT Acceleration

(d) FFT Displacement

Figure 4.54: Dynamic response of Ventura Hotel under Northridge earthquake, coherent motion vs incoherent motion, at the roof in Y direction (CHAN05), with additional structural mass, 20% structural stiffness reduction, Soil Material Model SM-EL3 (elastic, shown in Table 2.11), 3% structural damping and 10% soil damping.

Elastic Soil vs. Pressure-Dependent Inelastic Soil

Hyperbolic Drucker-Prager model with Armstrong-Frederick nonlinear kinematic hardening, shown in Table 2.13, is used for soil in this section.

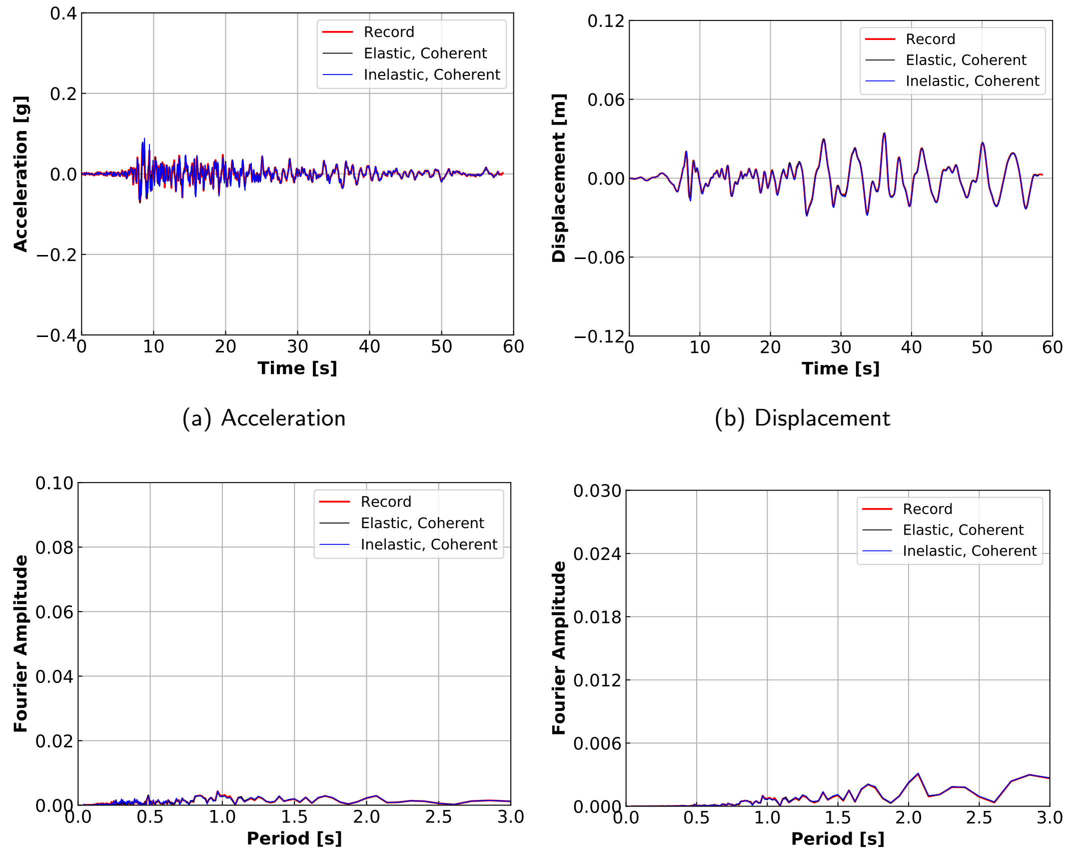

(a) Acceleration (b) Displacement

(c) FFT Acceleration (d) FFT Displacement

Figure 4.55: Dynamic response of Ventura Hotel under Northridge earthquake, elastic soil (SM-EL3 shown in Table 2.11) vs pressure-dependent inelastic soil (SM-EP6 shown in Table 2.13), at the ground floor in X direction (CHAN15), with additional structural mass, 20% structural stiffness reduction, 3% structural damping and 10% soil damping, coherent motion.

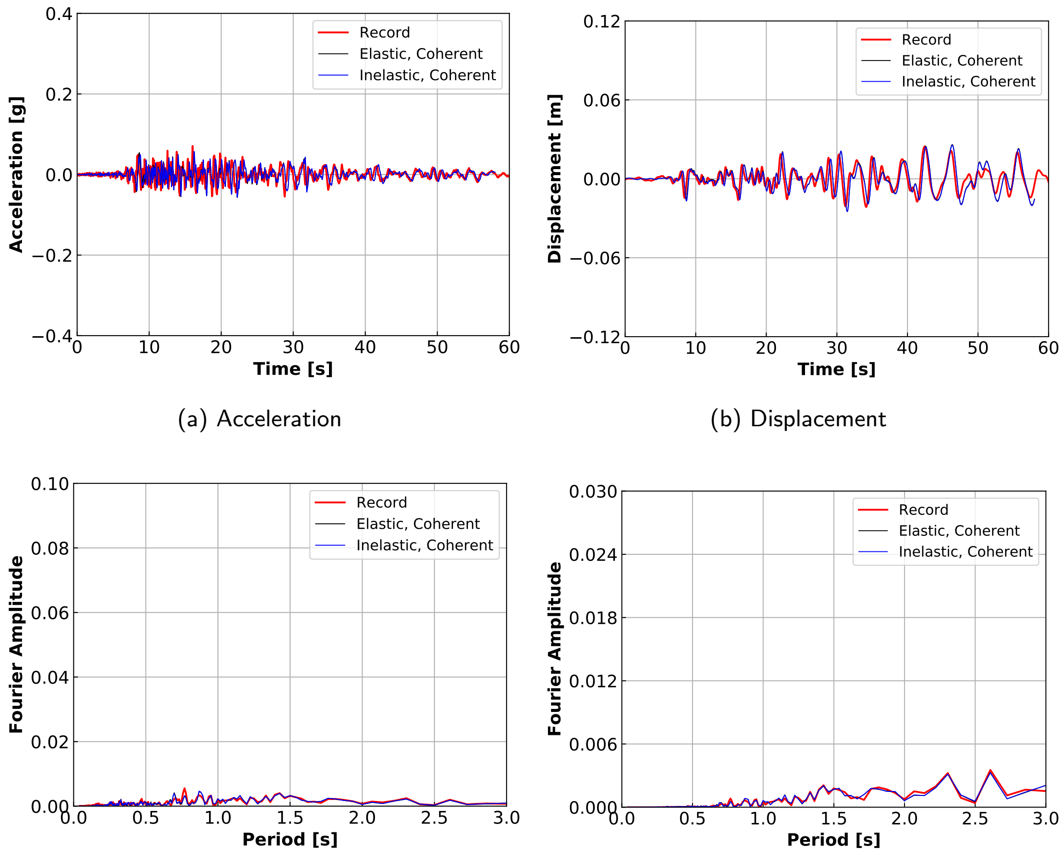

(a) Acceleration

(b) Displacement

(c) FFT Acceleration

(d) FFT Displacement

Figure 4.56: Dynamic response of Ventura Hotel under Northridge earthquake, elastic soil (SM-EL3 shown in Table 2.11) vs pressure-dependent inelastic soil (SM-EP6 shown in Table 2.13), at the ground floor in Y direction (CHAN12), with additional structural mass, 20% structural stiffness reduction, 3% structural damping and 10% soil damping, coherent motion.

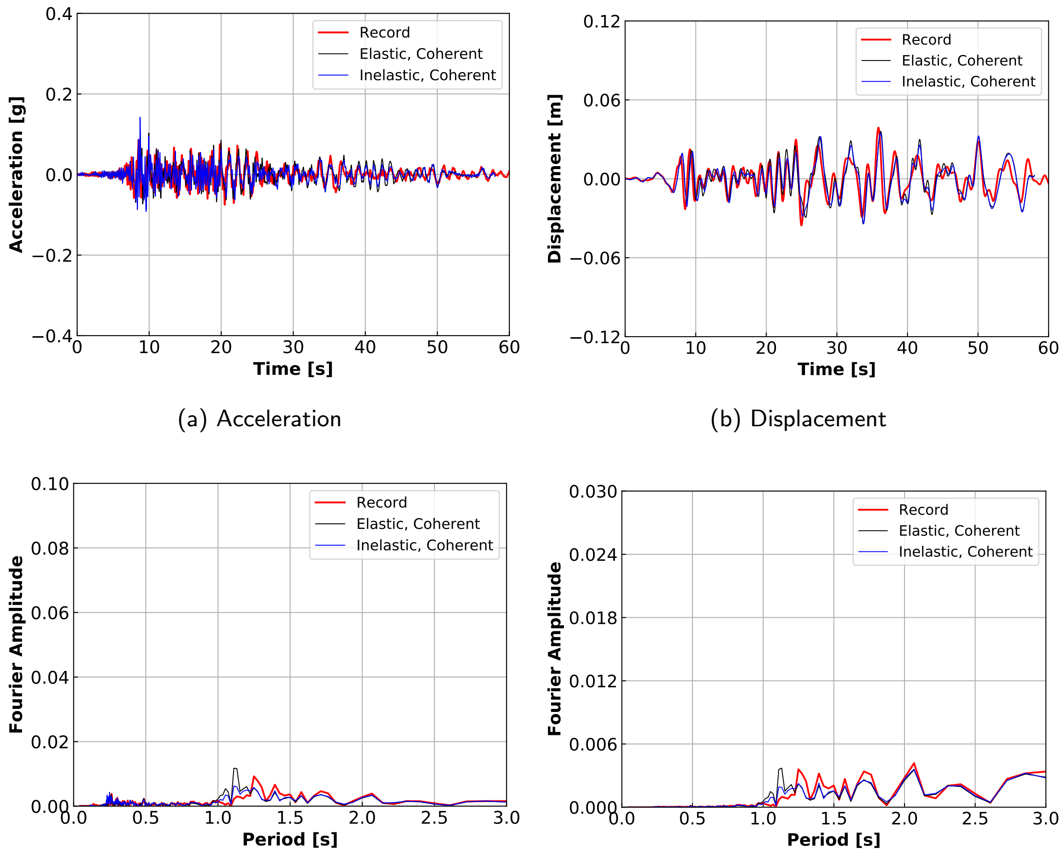

(a) Acceleration

(b) Displacement

(c) FFT Acceleration

(d) FFT Displacement

Figure 4.57: Dynamic response of Ventura Hotel under Northridge earthquake, elastic soil (SM-EL3 shown in Table 2.11) vs pressure-dependent inelastic soil (SM-EP6 shown in Table 2.13), at the 4th floor in X direction (CHAN09), with additional structural mass, 20% structural stiffness reduction, 3% structural damping and 10% soil damping, coherent motion.

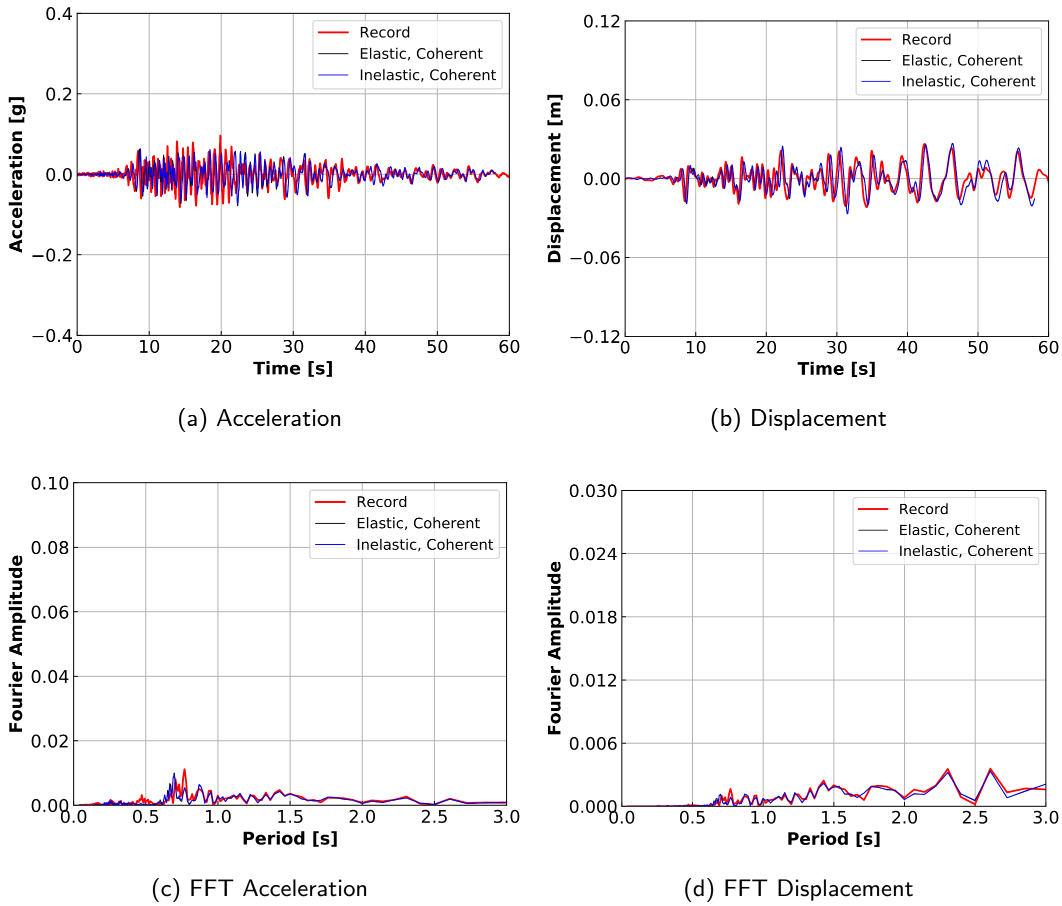

(a) Acceleration

(b) Displacement

(c) FFT Acceleration

(d) FFT Displacement

Figure 4.58: Dynamic response of Ventura Hotel under Northridge earthquake, elastic soil (SM-EL3 shown in Table 2.11) vs pressure-dependent inelastic soil (SM-EP6 shown in Table 2.13), at the 4th floor in Y direction (CHAN11), with additional structural mass, 20% structural stiffness reduction, 3% structural damping and 10% soil damping, coherent motion.

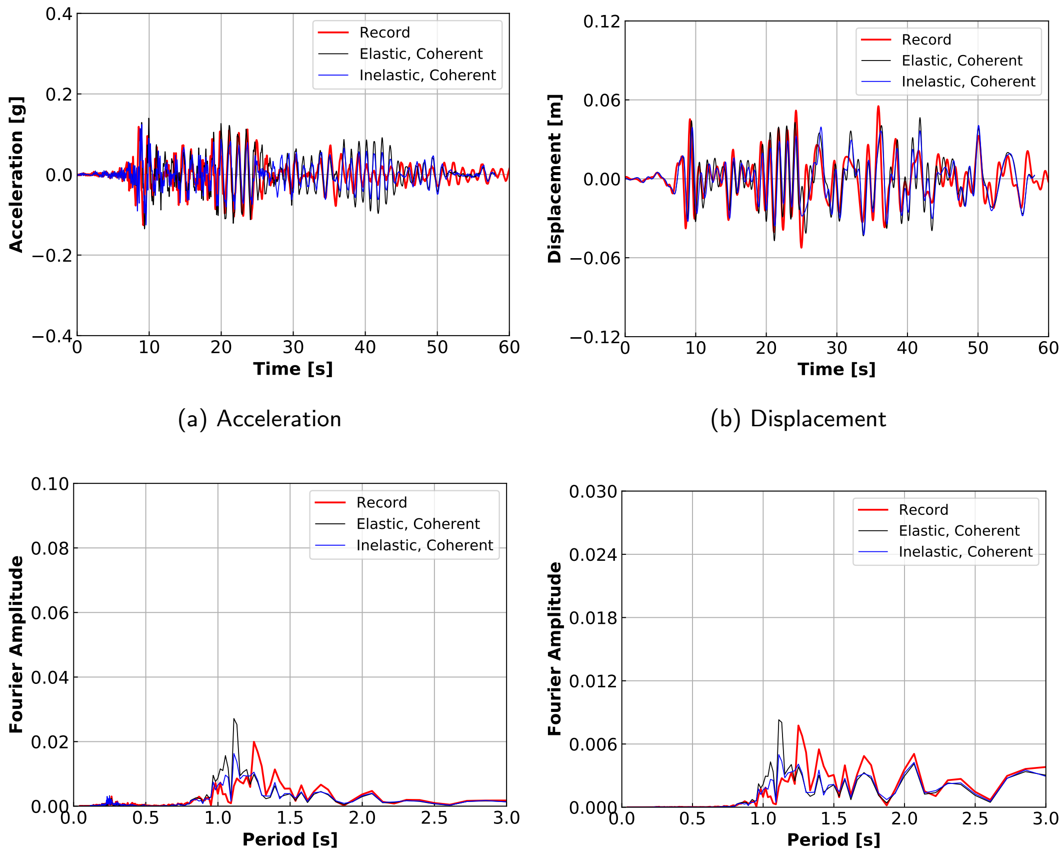

(a) Acceleration

(b) Displacement

(c) FFT Acceleration

(d) FFT Displacement

Figure 4.59: Dynamic response of Ventura Hotel under Northridge earthquake, elastic soil (SM-EL3 shown in Table 2.11) vs pressure-dependent inelastic soil (SM-EP6 shown in Table 2.13), at the 8th floor in X direction (CHAN06), with additional structural mass, 20% structural stiffness reduction, 3% structural damping and 10% soil damping, coherent motion.

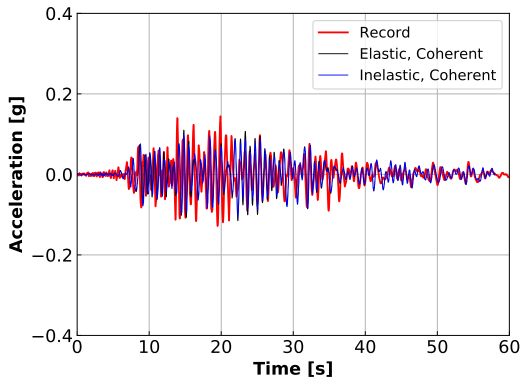

(a) Acceleration

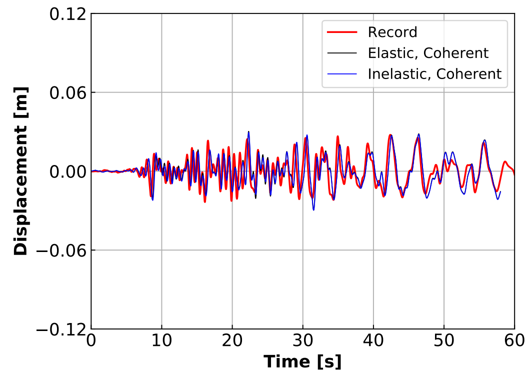

(b) Displacement

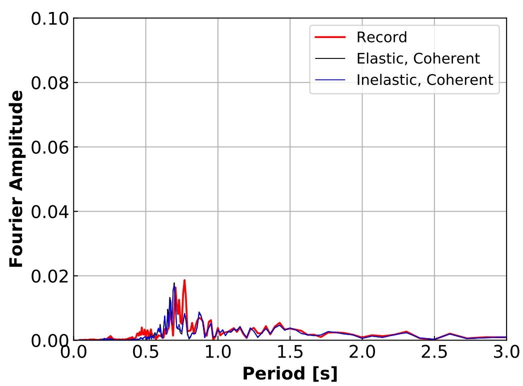

(c) FFT Acceleration

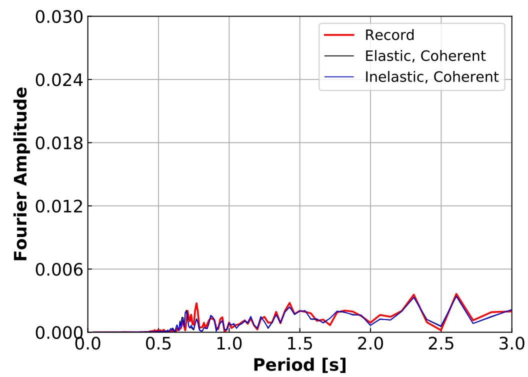

(d) FFT Displacement

Figure 4.60: Dynamic response of Ventura Hotel under Northridge earthquake, elastic soil (SM-EL3 shown in Table 2.11) vs pressure-dependent inelastic soil (SM-EP6 shown in Table 2.13), at the 8th floor in Y direction (CHAN08), with additional structural mass, 20% structural stiffness reduction, 3% structural damping and 10% soil damping, coherent motion.

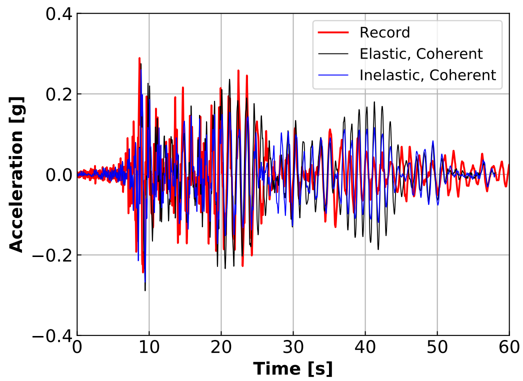

(a) Acceleration

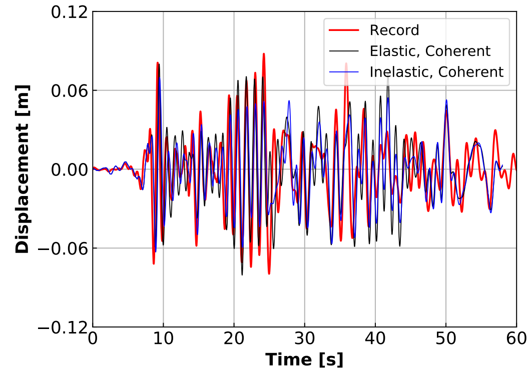

(b) Displacement

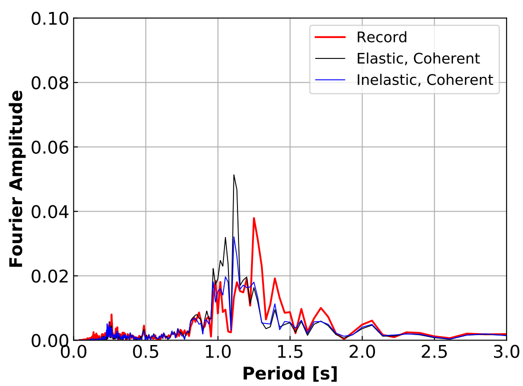

(c) FFT Acceleration

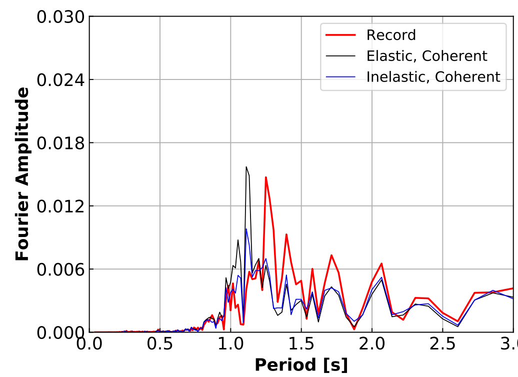

(d) FFT Displacement

Figure 4.61: Dynamic response of Ventura Hotel under Northridge earthquake, elastic soil (SM-EL3 shown in Table 2.11) vs pressure-dependent inelastic soil (SM-EP6 shown in Table 2.13), at the roof in X direction (CHAN02), with additional structural mass, 20% structural stiffness reduction, 3% structural damping and 10% soil damping, coherent motion.

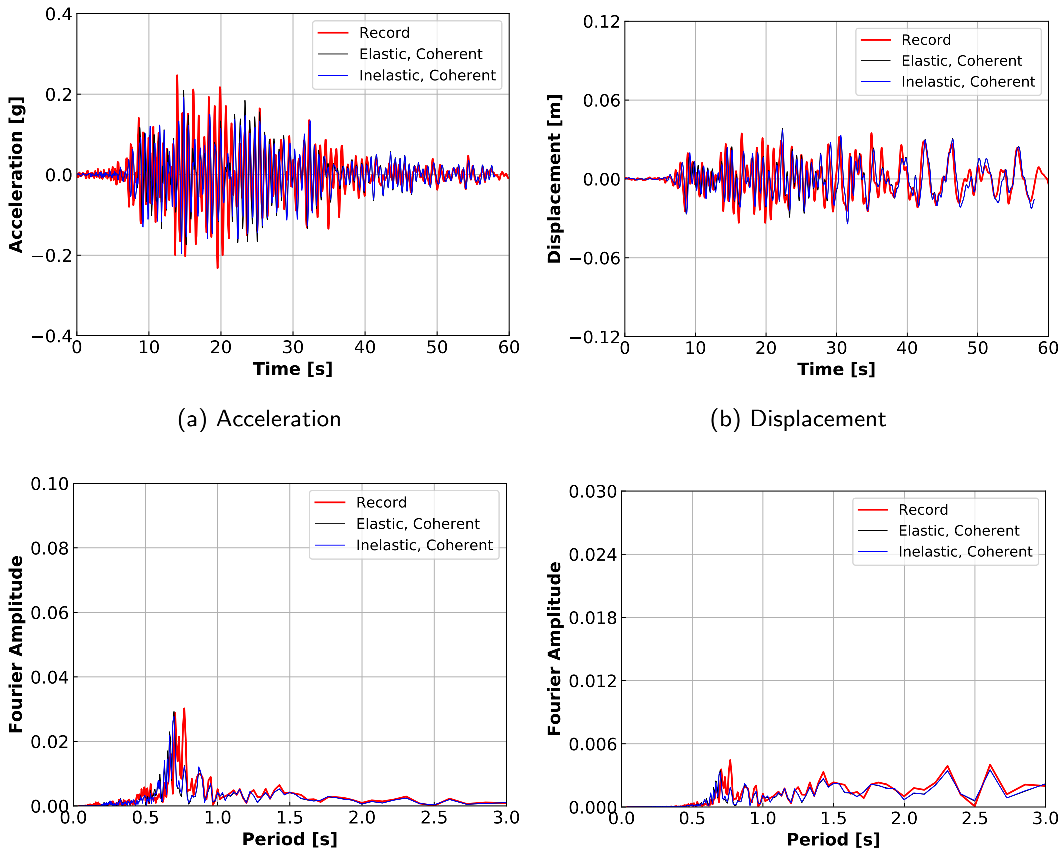

(a) Acceleration

(b) Displacement

(c) FFT Acceleration

(d) FFT Displacement

Figure 4.62: Dynamic response of Ventura Hotel under Northridge earthquake, elastic soil (SM-EL3 shown in Table 2.11) vs pressure-dependent inelastic soil (SM-EP6 shown in Table 2.13), at the roof in Y direction (CHAN05), with additional structural mass, 20% structural stiffness reduction, 3% structural damping and 10% soil damping, coherent motion.

Pressure-Dependent Inelastic Soil vs. Pressure-Independent Inelastic Soil

Hyperbolic Drucker-Prager model with Armstrong-Frederick nonlinear kinematic hardening is used for pressure-dependent soil, SM-EP6 shown in Table 2.13. von Mises model with Armstrong-Frederick nonlinear kinematic hardening is used for pressure-independent soil, SM-EP5 shown in Table 2.12.

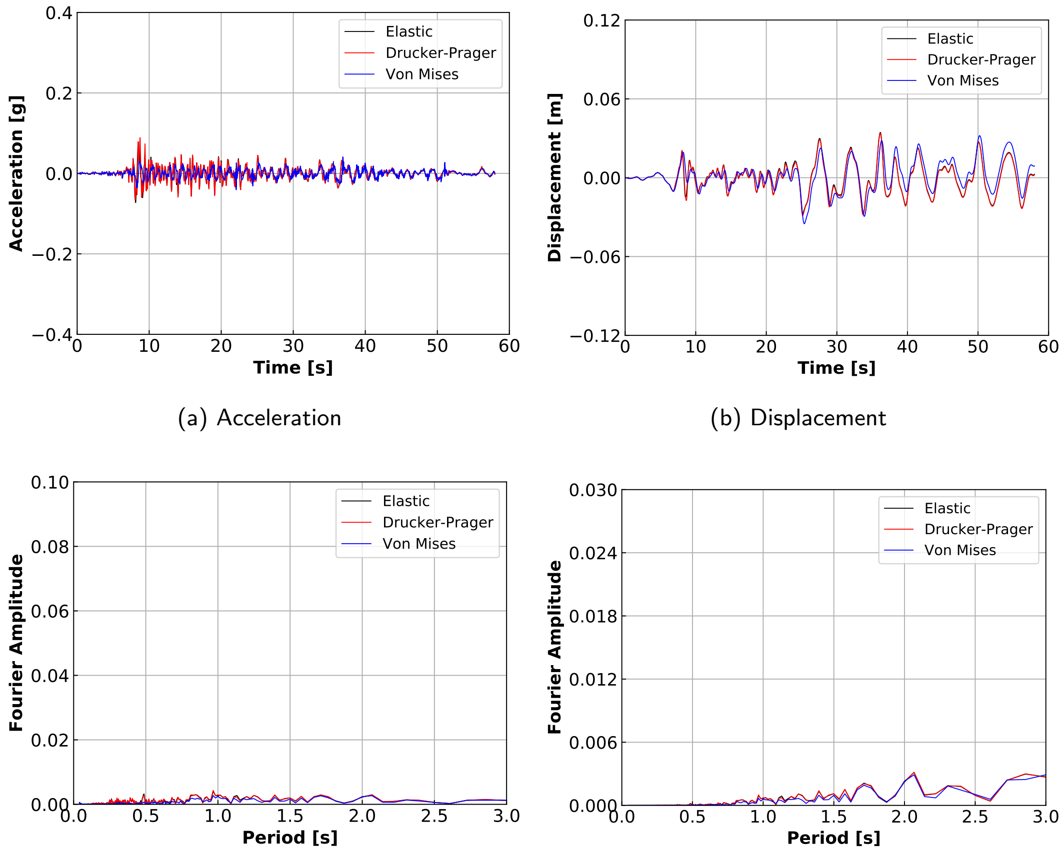

(a) Acceleration (b) Displacement

(c) FFT Acceleration (d) FFT Displacement

Figure 4.63: Dynamic response of Ventura Hotel under Northridge earthquake, pressure-dependent inelastic soil (SM-EP6 shown in Table 2.13) vs pressure-independent inelastic soil (SM-EP5 shown in Table 2.12), at the ground floor in X direction (CHAN15), with additional structural mass, 20% structural stiffness reduction, 3% structural damping and 10% soil damping, coherent motion.

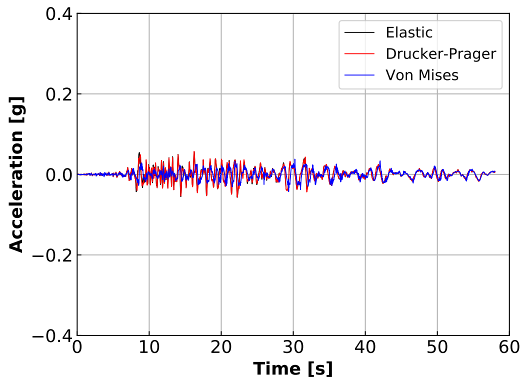

(a) Acceleration

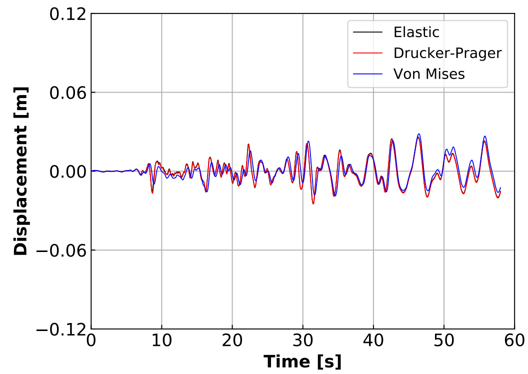

(b) Displacement

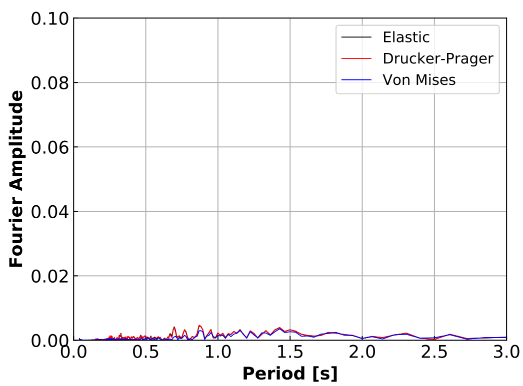

(c) FFT Acceleration

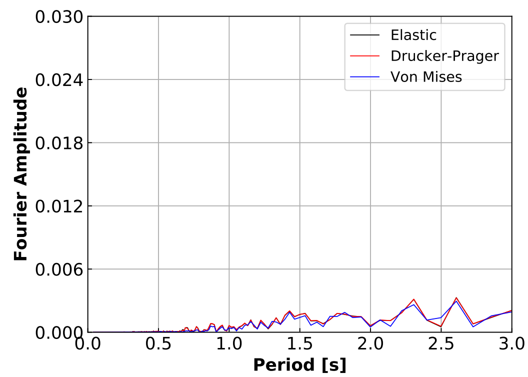

(d) FFT Displacement

Figure 4.64: Dynamic response of Ventura Hotel under Northridge earthquake, pressure-dependent inelastic soil (SM-EP6 shown in Table 2.13) vs pressure-independent inelastic soil (SM-EP5 shown in Table 2.12), at the ground floor in Y direction (CHAN12), with additional structural mass, 20% structural stiffness reduction, 3% structural damping and 10% soil damping, coherent motion.

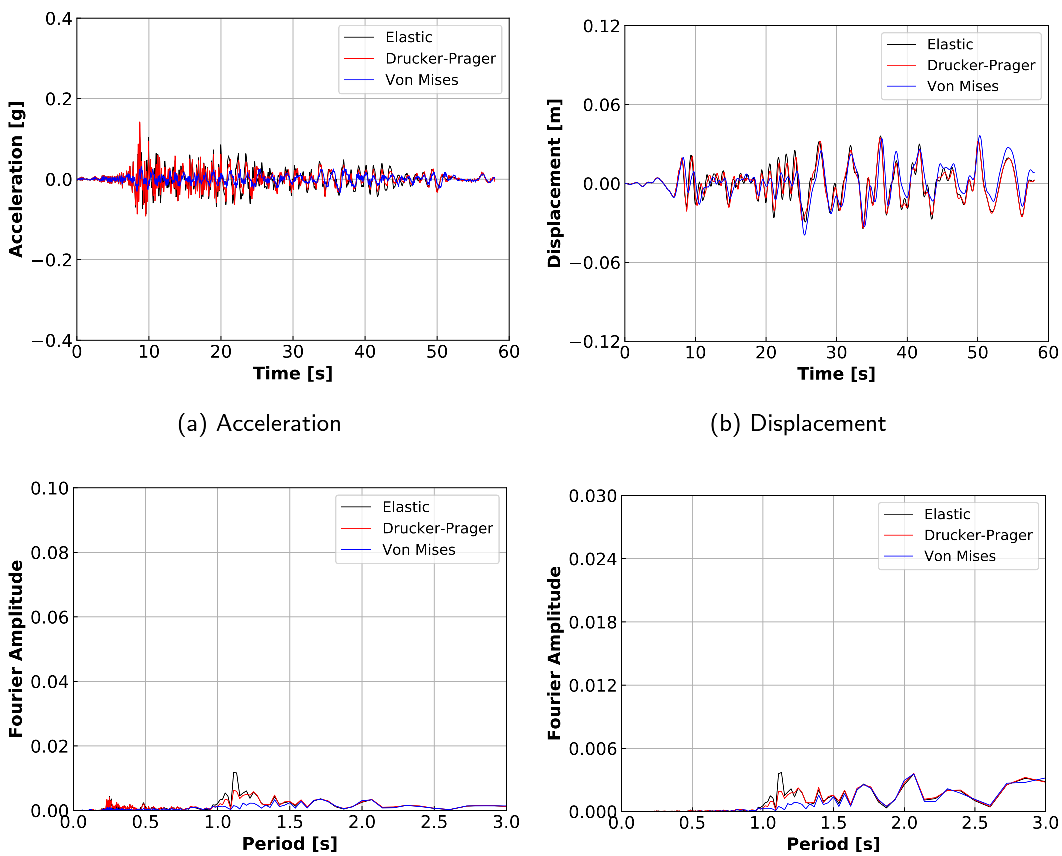

(a) Acceleration

(b) Displacement

(c) FFT Acceleration

(d) FFT Displacement

Figure 4.65: Dynamic response of Ventura Hotel under Northridge earthquake, pressure-dependent inelastic soil (SM-EP6 shown in Table 2.13) vs pressure-independent inelastic soil (SM-EP5 shown in Table 2.12), at the 4th floor in X direction (CHAN09), with additional structural mass, 20% structural stiffness reduction, 3% structural damping and 10% soil damping, coherent motion.

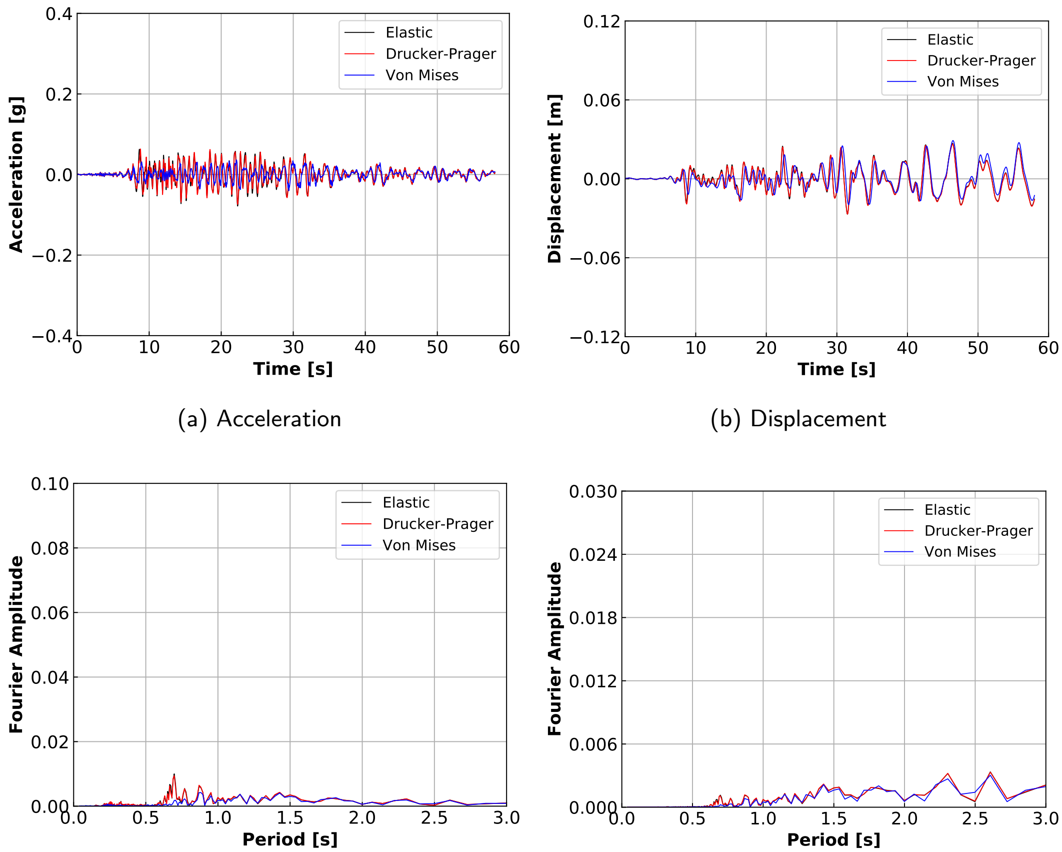

(a) Acceleration

(b) Displacement

(c) FFT Acceleration

(d) FFT Displacement

Figure 4.66: Dynamic response of Ventura Hotel under Northridge earthquake, pressure-dependent inelastic soil (SM-EP6 shown in Table 2.13) vs pressure-independent inelastic soil (SM-EP5 shown in Table 2.12), at the 4th floor in Y direction (CHAN11), with additional structural mass, 20% structural stiffness reduction, 3% structural damping and 10% soil damping, coherent motion.

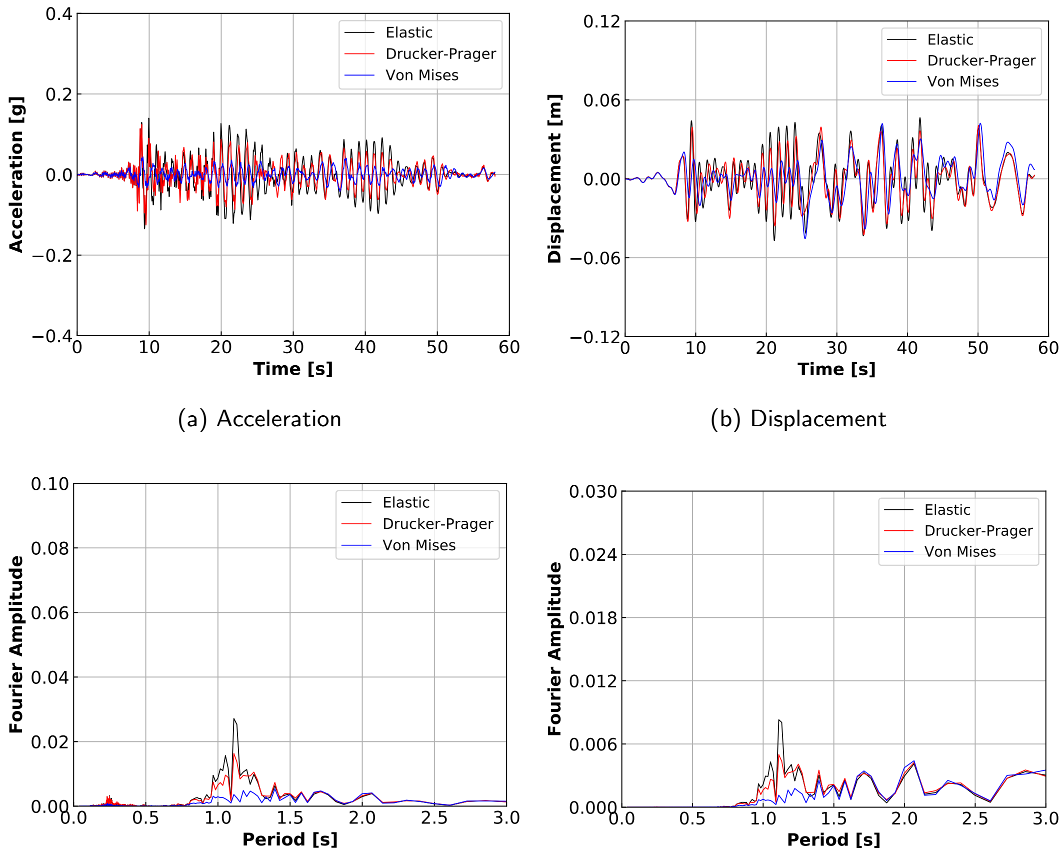

(a) Acceleration (b) Displacement

(c) FFT Acceleration (d) FFT Displacement

Figure 4.67: Dynamic response of Ventura Hotel under Northridge earthquake, pressure-dependent inelastic soil (SM-EP6 shown in Table 2.13) vs pressure-independent inelastic soil (SM-EP5 shown in Table 2.12), at the 8th floor in X direction (CHAN06), with additional structural mass, 20% structural stiffness reduction, 3% structural damping and 10% soil damping, coherent motion.

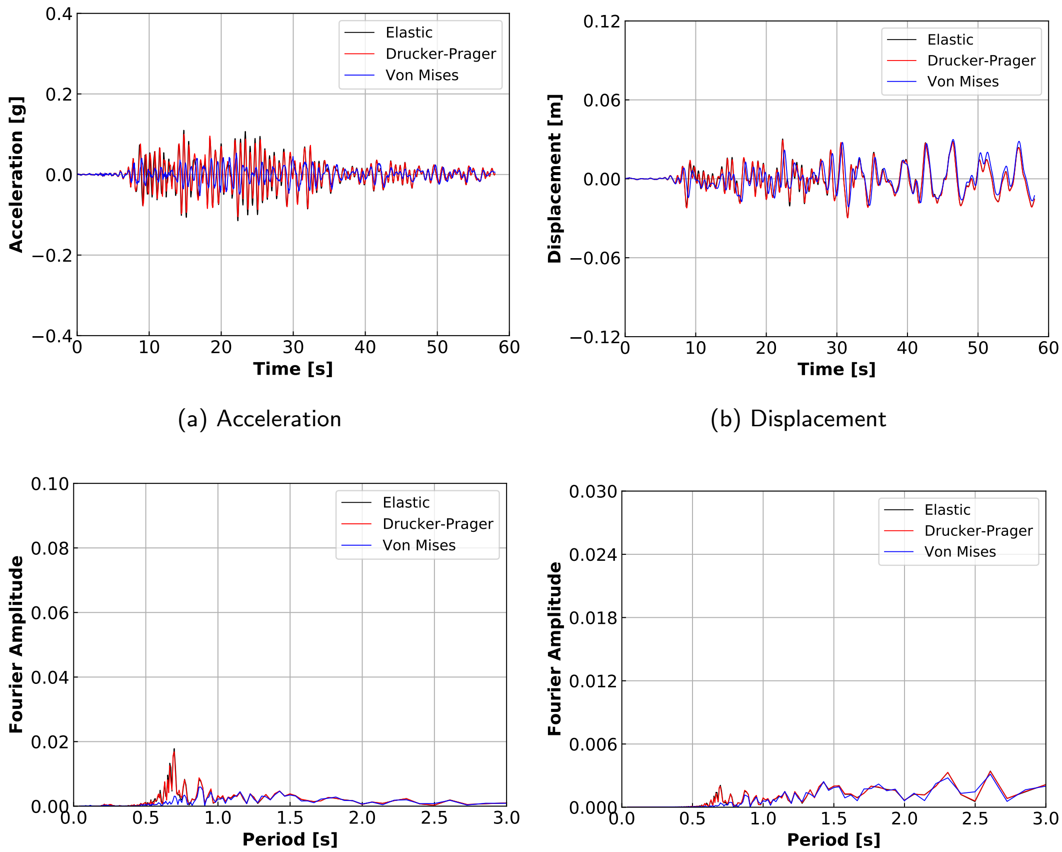

(a) Acceleration

(b) Displacement

(c) FFT Acceleration

(d) FFT Displacement

Figure 4.68: Dynamic response of Ventura Hotel under Northridge earthquake, pressure-dependent inelastic soil (SM-EP6 shown in Table 2.13) vs pressure-independent inelastic soil (SM-EP5 shown in Table 2.12), at the 8th floor in Y direction (CHAN08), with additional structural mass, 20% structural stiffness reduction, 3% structural damping and 10% soil damping, coherent motion.

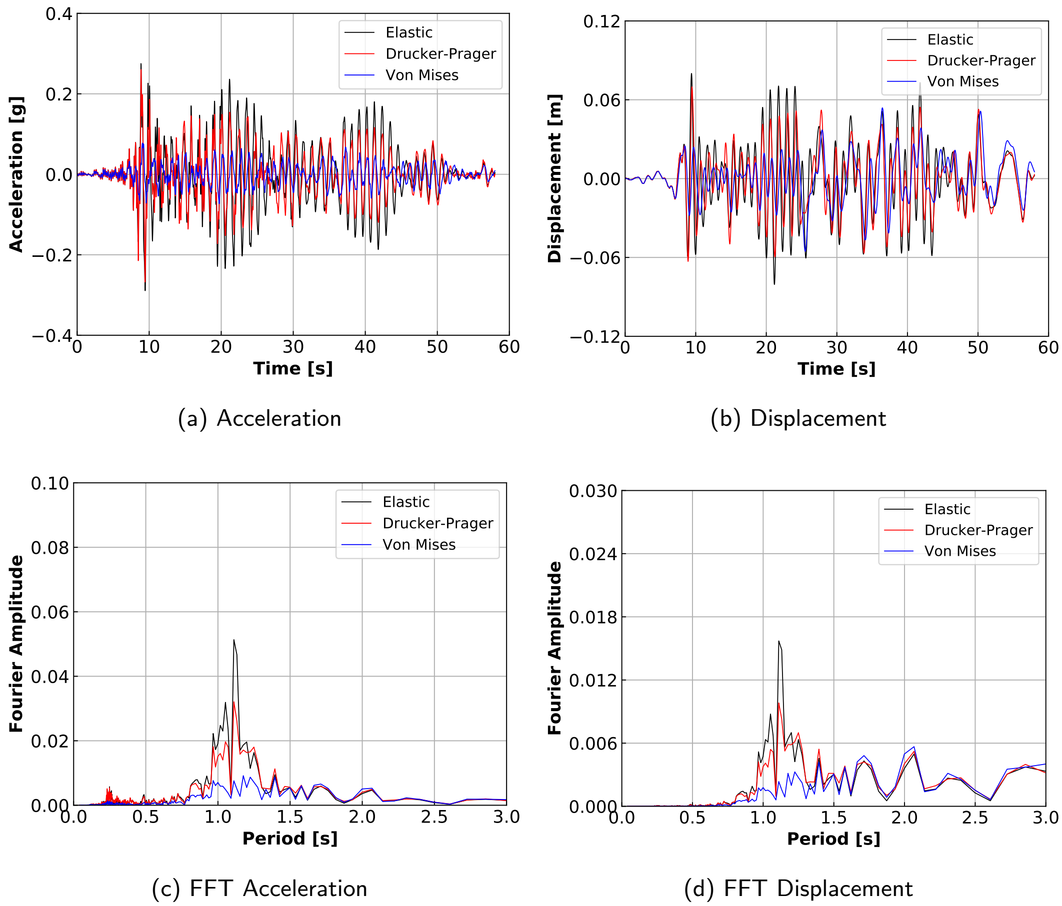

(a) Acceleration

(b) Displacement

(c) FFT Acceleration

(d) FFT Displacement

Figure 4.69: Dynamic response of Ventura Hotel under Northridge earthquake, pressure-dependent inelastic soil (SM-EP6 shown in Table 2.13) vs pressure-independent inelastic soil (SM-EP5 shown in Table 2.12), at the roof in X direction (CHAN02), with additional structural mass, 20% structural stiffness reduction, 3% structural damping and 10% soil damping, coherent motion.

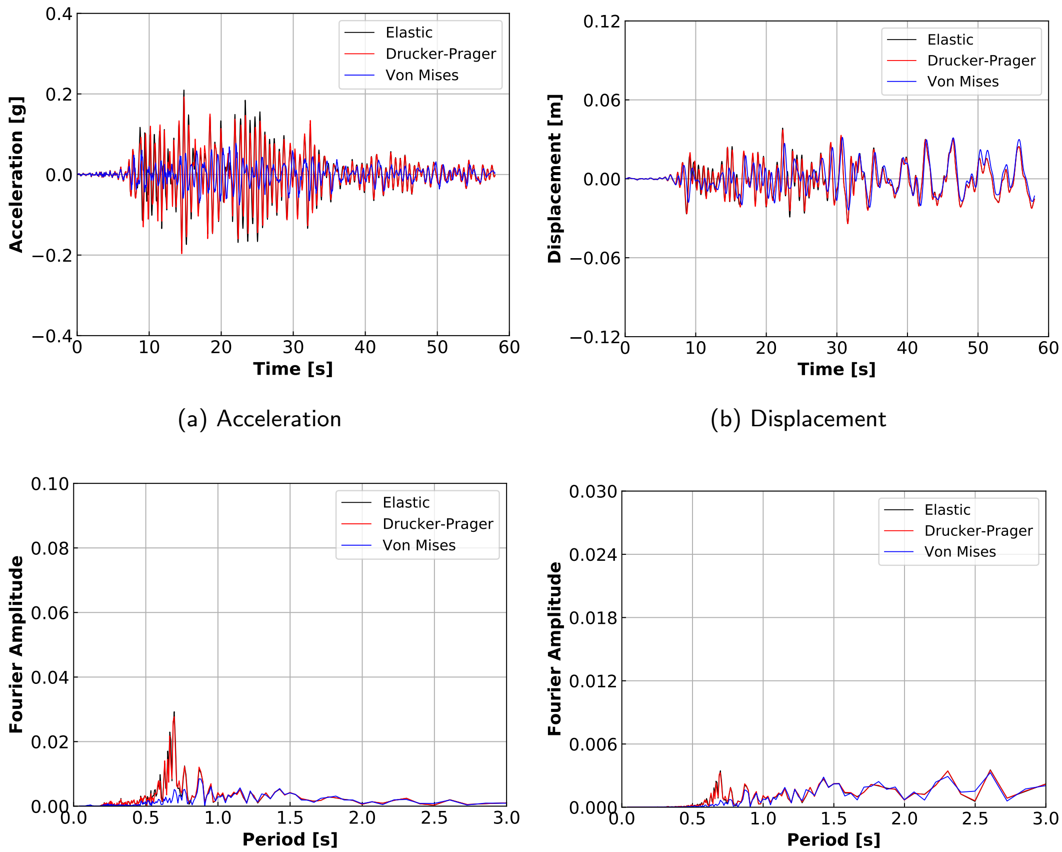

(a) Acceleration (b) Displacement

(c) FFT Acceleration (d) FFT Displacement

Figure 4.70: Dynamic response of Ventura Hotel under Northridge earthquake, pressure-dependent inelastic soil (SM-EP6 shown in Table 2.13) vs pressure-independent inelastic soil (SM-EP5 shown in Table 2.12), at the roof in Y direction (CHAN05), with additional structural mass, 20% structural stiffness reduction, 3% structural damping and 10% soil damping, coherent motion.

4.3.6 2016 Ojai Earthquake

All material parameters, damping coefficients, and other simulation parameters are the same as in the previous cases. The only change is the input motion. Another motion is the Ojai earthquake, which happened on March 12, 2016, recorded at Ventura Hotel (CSMIP Station No. 25339). The figures below show the comparison between recorded motions and Real-ESSI simulation results.

Comparing the records at the ground surface is shown in Figure 4.72 and 4.73, it is seen that the two recorded motions, from CHAN012 and CHAN013, are noticeably different. This difference indicates that the Ojai motion is highly incoherent. However, there is not enough information to construct a full, 3C motion field. Input seismic motion is generated from the deconvolution of surface motion in the two horizontal directions. In other words, the input motion is 2×1C. Therefore, due to the incoherency of Ojai motion, the simulation results are expected to have some differences when compared with records.

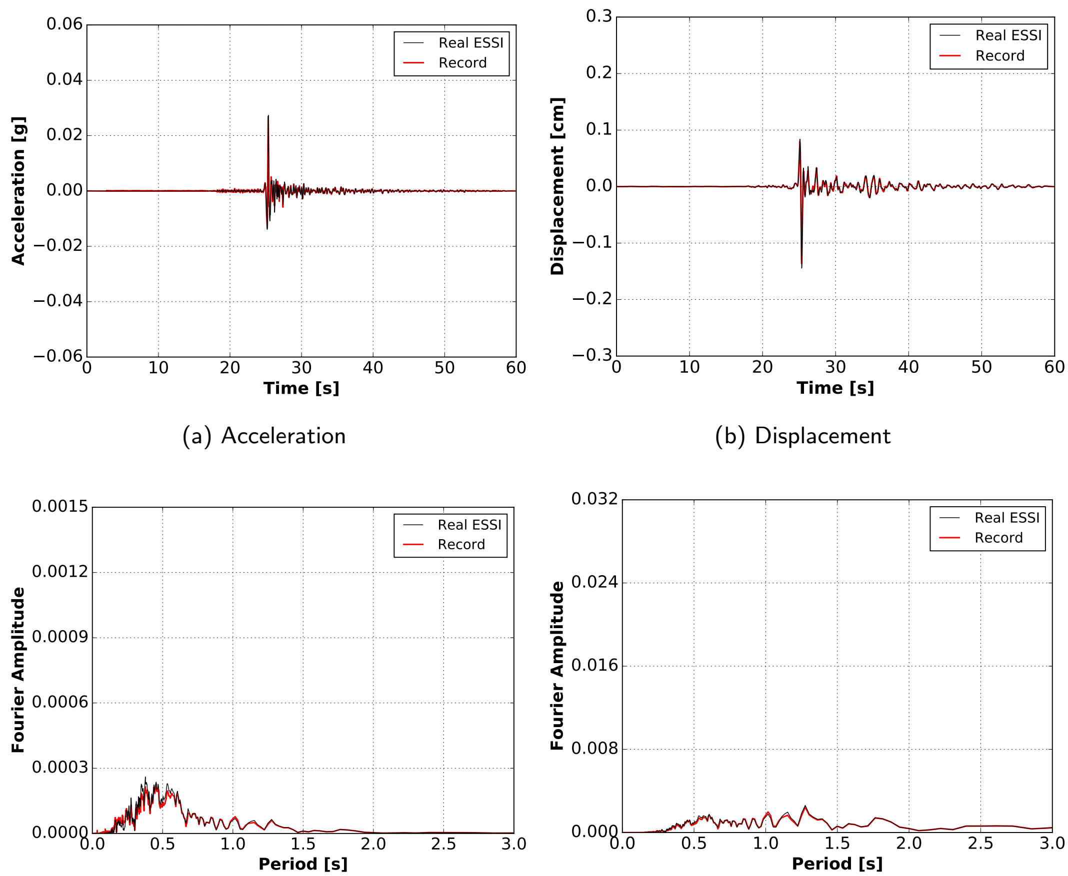

(a) Acceleration

(b) Displacement

(c) FFT Acceleration

(d) FFT Displacement

Figure 4.71: Dynamic response of Ventura Hotel under Ojai earthquake at the ground floor in X direction (CHAN15), with additional structural mass, 20% structural stiffness reduction, Soil Material Model SM-EL3 (elastic, shown in Table 2.11), 3% structural damping and 10% soil damping, coherent motion.

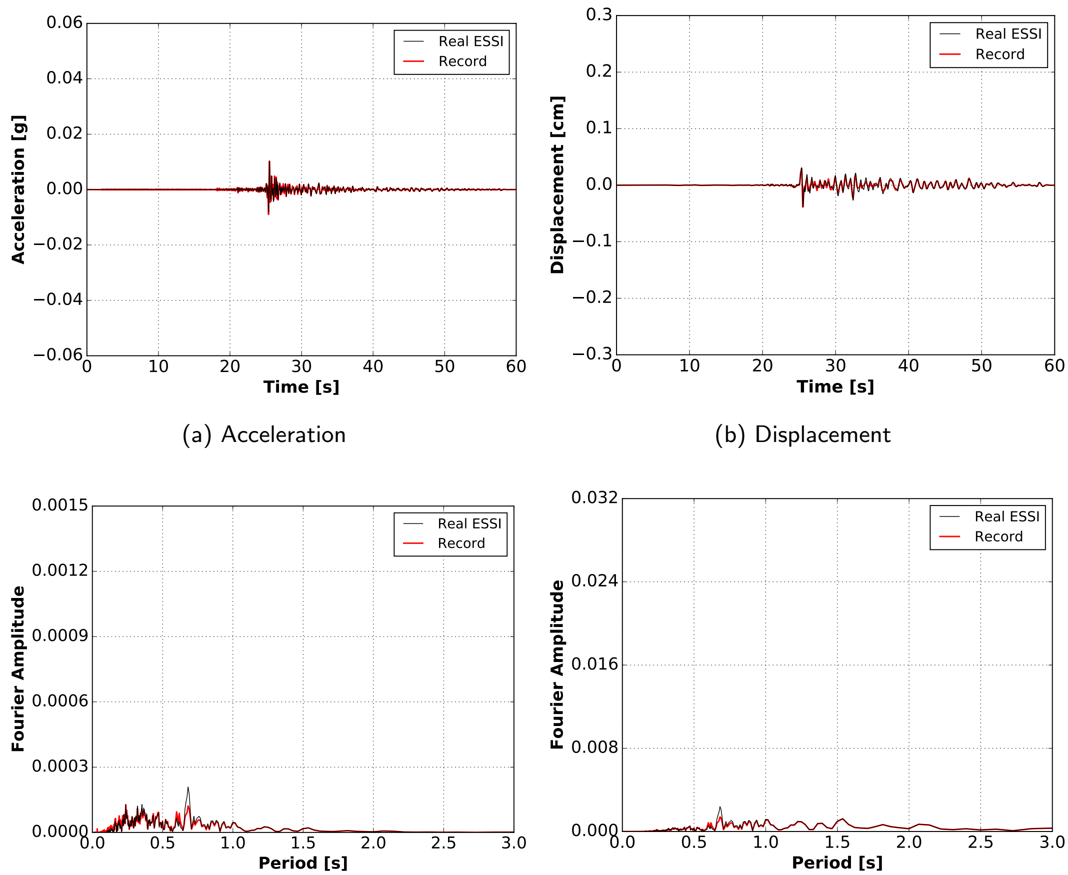

(a) Acceleration (b) Displacement

(c) FFT Acceleration (d) FFT Displacement

Figure 4.72: Dynamic response of Ventura Hotel under Ojai earthquake at the ground floor in Y direction (CHAN13), with additional structural mass, 20% structural stiffness reduction, Soil Material Model SM-EL3 (elastic, shown in Table 2.11), 3% structural damping and 10% soil damping, coherent motion.

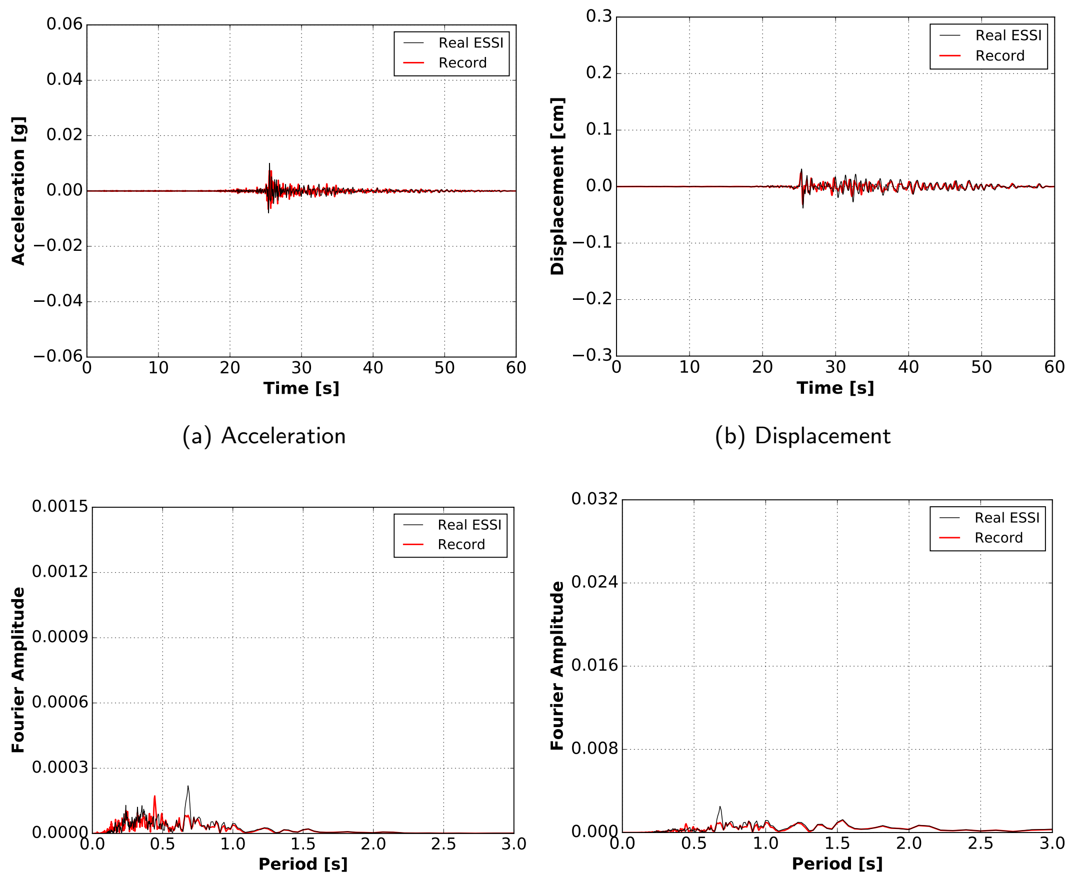

(a) Acceleration (b) Displacement

(c) FFT Acceleration (d) FFT Displacement

Figure 4.73: Dynamic response of Ventura Hotel under Ojai earthquake at the ground floor in Y direction (CHAN12), with additional structural mass, 20% structural stiffness reduction, Soil Material Model SM-EL3 (elastic, shown in Table 2.11), 3% structural damping and 10% soil damping, coherent motion.

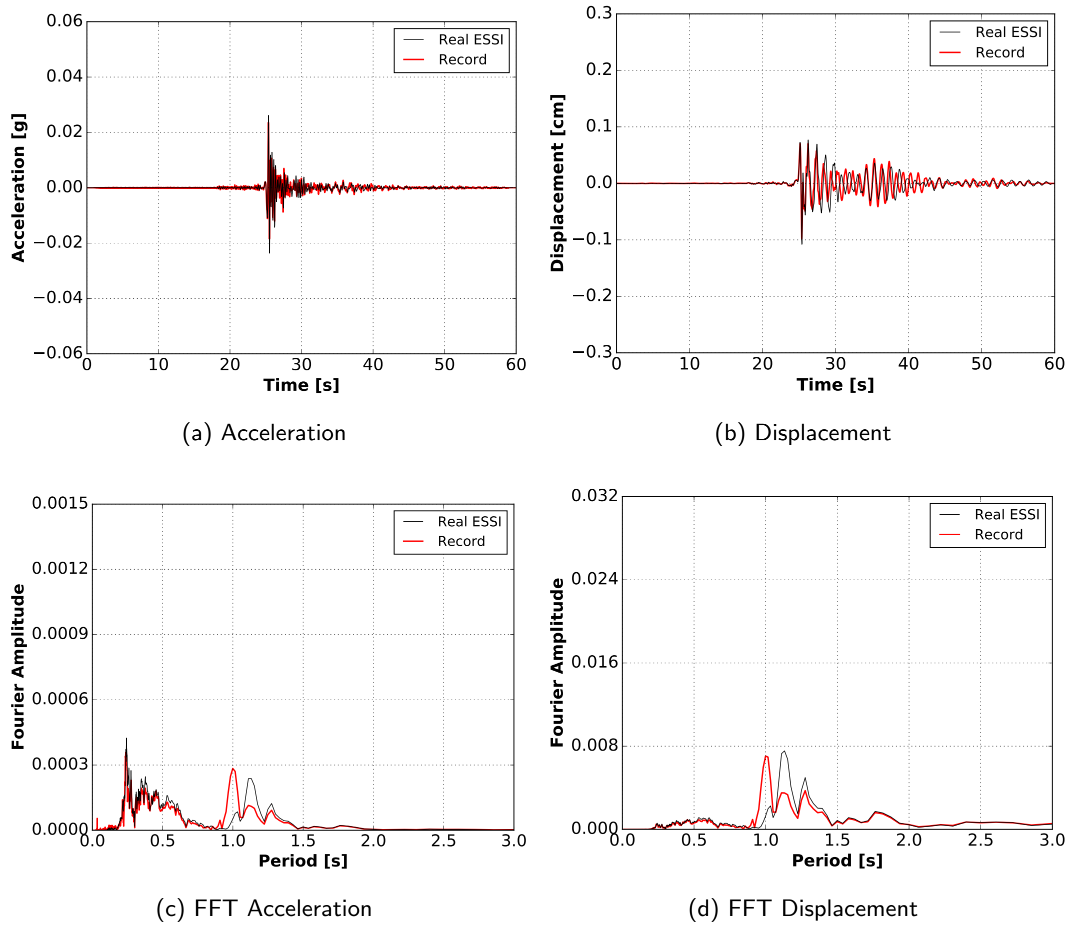

(a) Acceleration

(b) Displacement

(c) FFT Acceleration

(d) FFT Displacement

Figure 4.74: Dynamic response of Ventura Hotel under Ojai earthquake at the 4th floor in X direction (CHAN09), with additional structural mass, 20% structural stiffness reduction, Soil Material Model SM-EL3 (elastic, shown in Table 2.11), 3% structural damping and 10% soil damping, coherent motion.

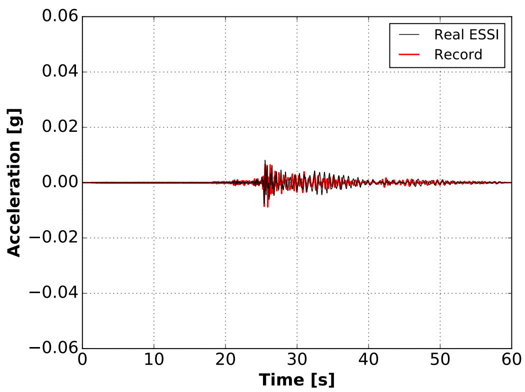

(a) Acceleration

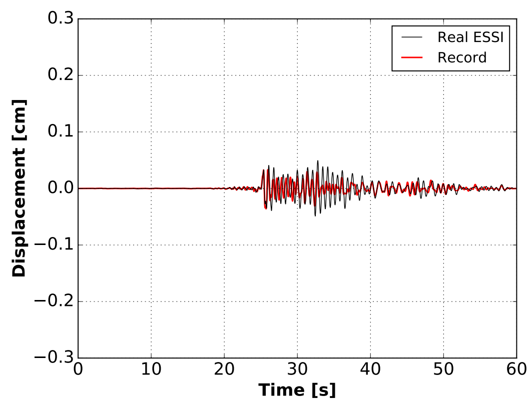

(b) Displacement

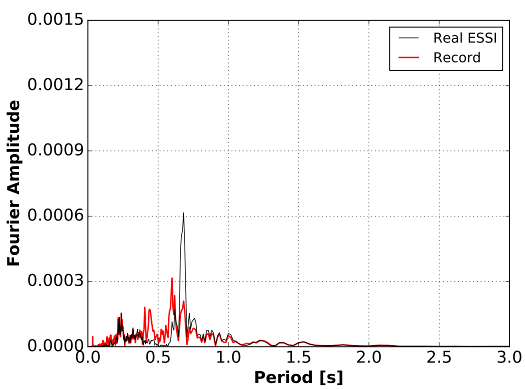

(c) FFT Acceleration

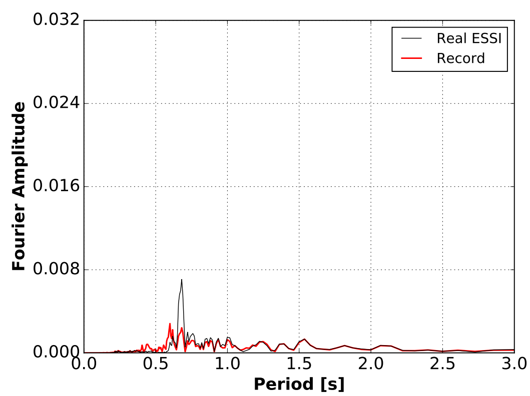

(d) FFT Displacement

Figure 4.75: Dynamic response of Ventura Hotel under Ojai earthquake at the 4th floor in Y direction (CHAN10), with additional structural mass, 20% structural stiffness reduction, Soil Material Model SM-EL3 (elastic, shown in Table 2.11), 3% structural damping and 10% soil damping, coherent motion.

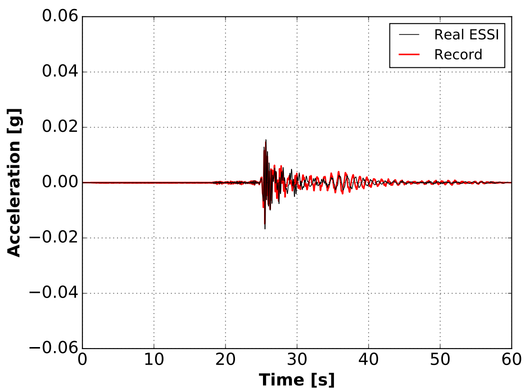

(a) Acceleration

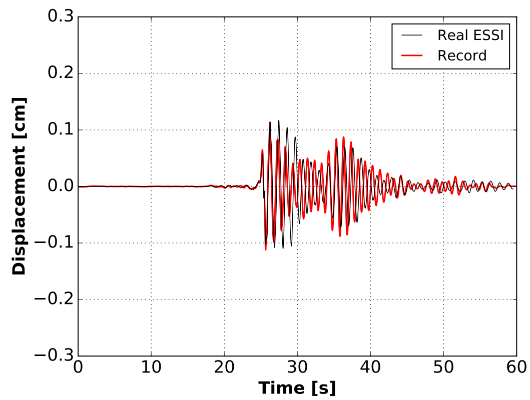

(b) Displacement

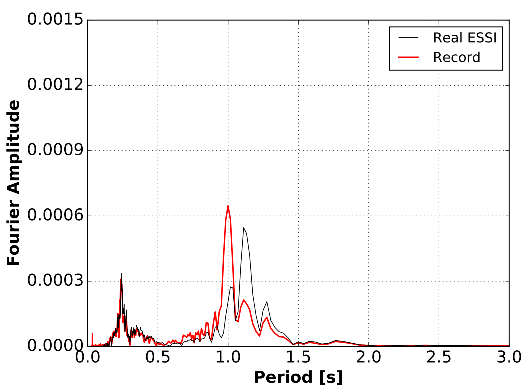

(c) FFT Acceleration

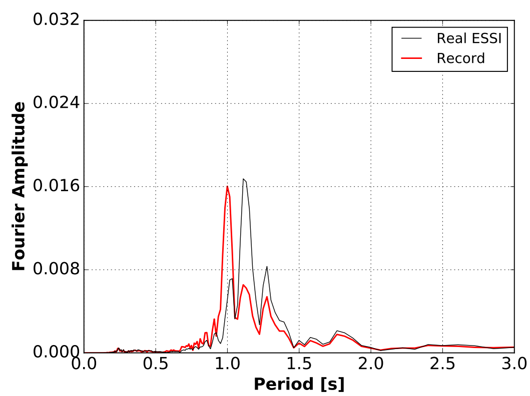

(d) FFT Displacement

Figure 4.76: Dynamic response of Ventura Hotel under Ojai earthquake at the 8th floor in X direction (CHAN06), with additional structural mass, 20% structural stiffness reduction, Soil Material Model SM-EL3 (elastic, shown in Table 2.11), 3% structural damping and 10% soil damping, coherent motion.

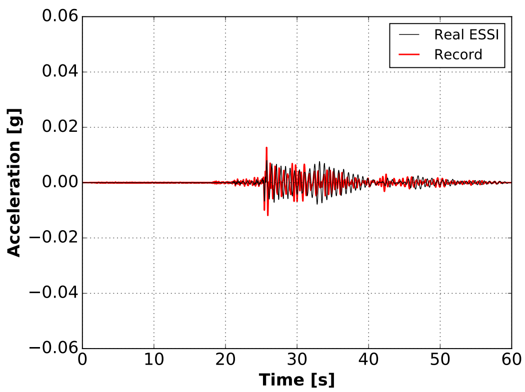

(a) Acceleration

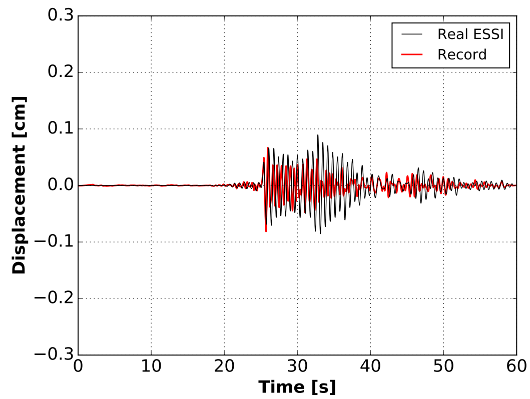

(b) Displacement

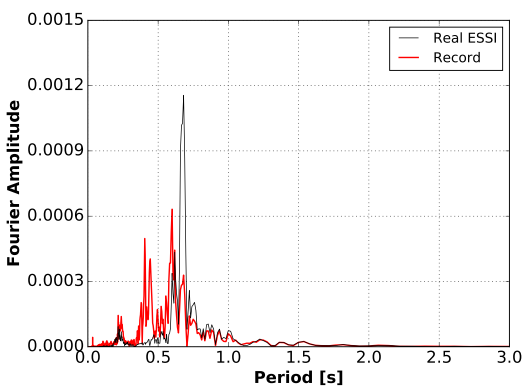

(c) FFT Acceleration

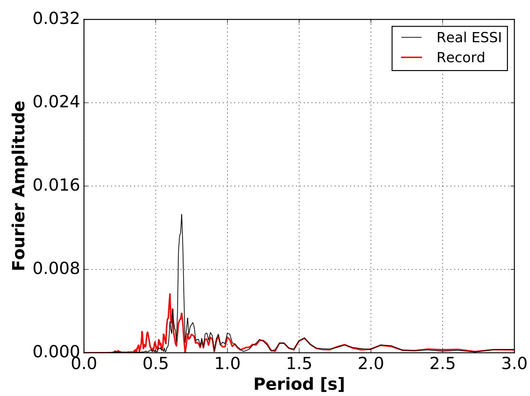

(d) FFT Displacement

Figure 4.77: Dynamic response of Ventura Hotel under Ojai earthquake at the 8th floor in Y direction (CHAN07), with additional structural mass, 20% structural stiffness reduction, Soil Material Model SM-EL3 (elastic, shown in Table 2.11), 3% structural damping and 10% soil damping, coherent motion.

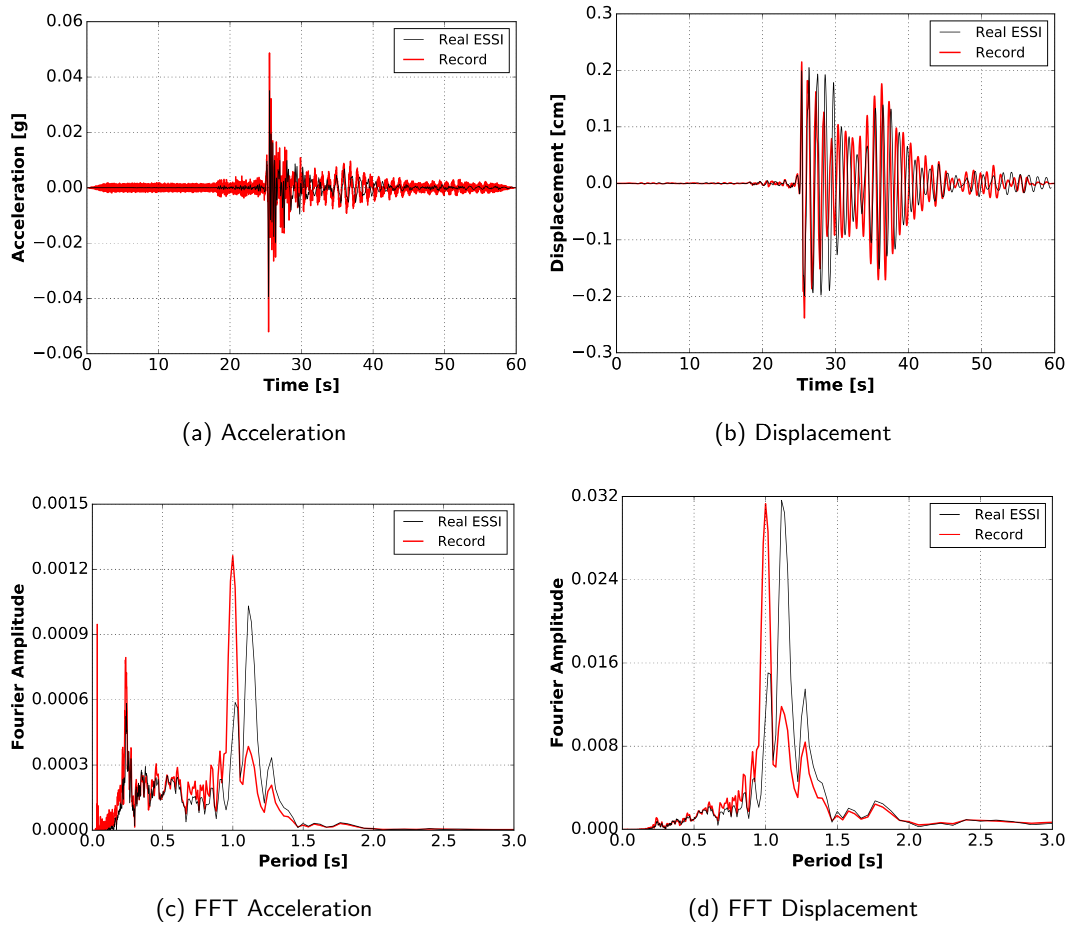

Figure 4.78: Dynamic response of Ventura Hotel under Ojai earthquake at the roof in X direction (CHAN02), with additional structural mass, 20% structural stiffness reduction, Soil Material Model SM-EL3 (elastic, shown in Table 2.11), 3% structural damping and 10% soil damping, coherent motion.

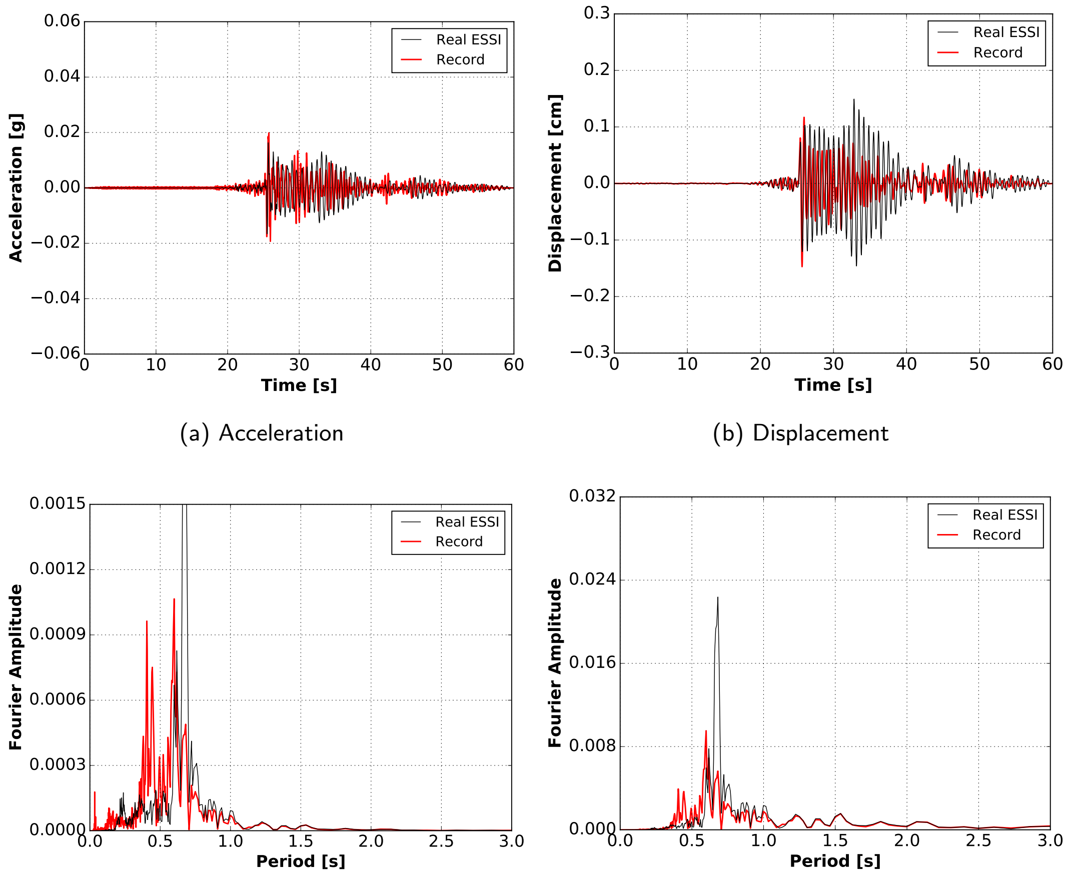

(a) Acceleration

(b) Displacement

(c) FFT Acceleration

(d) FFT Displacement

Figure 4.79: Dynamic response of Ventura Hotel under Ojai earthquake at the roof in Y direction (CHAN03), with additional structural mass, 20% structural stiffness reduction, Soil Material Model SM-EL3 (elastic, shown in Table 2.11), 3% structural damping and 10% soil damping, coherent motion.

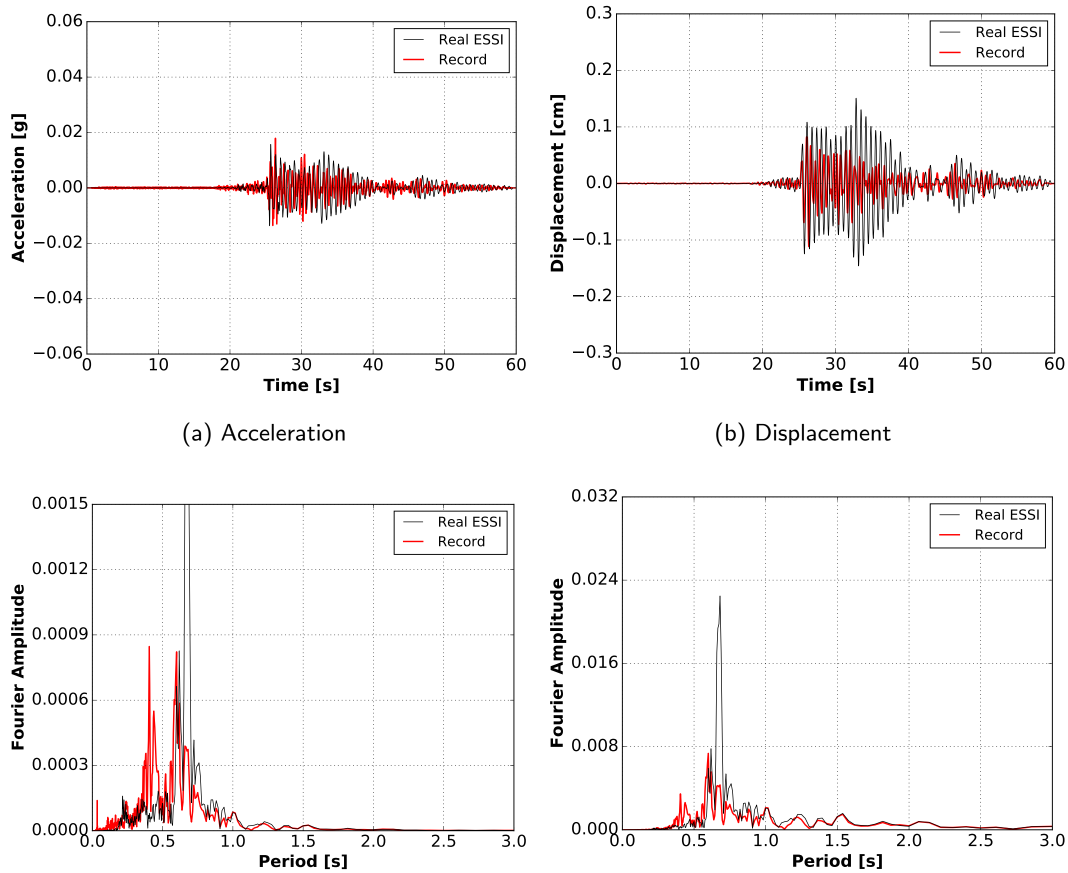

(a) Acceleration (b) Displacement

(c) FFT Acceleration (d) FFT Displacement

Figure 4.80: Dynamic response of Ventura Hotel under Ojai earthquake at the roof in Y direction (CHAN05), with additional structural mass, 20% structural stiffness reduction, Soil Material Model SM-EL3 (elastic, shown in Table 2.11), 3% structural damping and 10% soil damping, coherent motion.

Transfer Functions of Foundation/Free-Field Motion

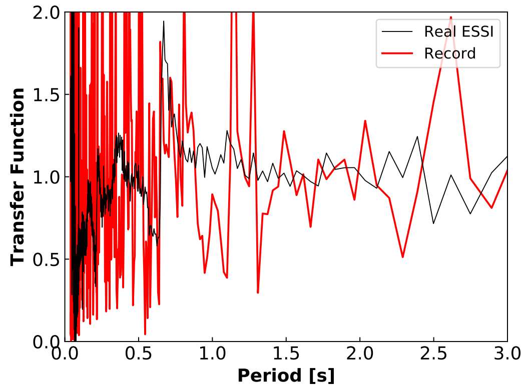

(a) CHAN12

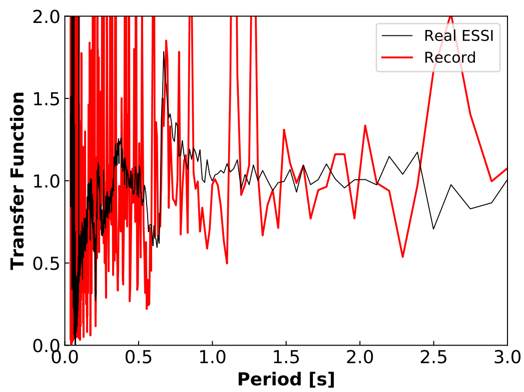

(b) CHAN13

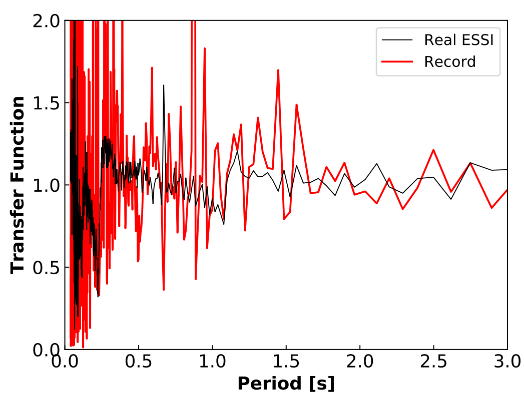

(c) CHAN15

Figure 4.81: Transfer functions of foundation/free-field motion for Ventura Hotel under Ojai earthquake, with additional structural mass, 20% structural stiffness reduction, Soil Material Model SM-EL3 (elastic, shown in Table 2.11), 3% structural damping and 10% soil damping, coherent motion.

Spectral Acceleration and RRS

The Required Response Spectrum, RRS, is defined in the ASCE/SEI 7-16, as $RRS = Sa_{fndn}/Sa_{ff}$.

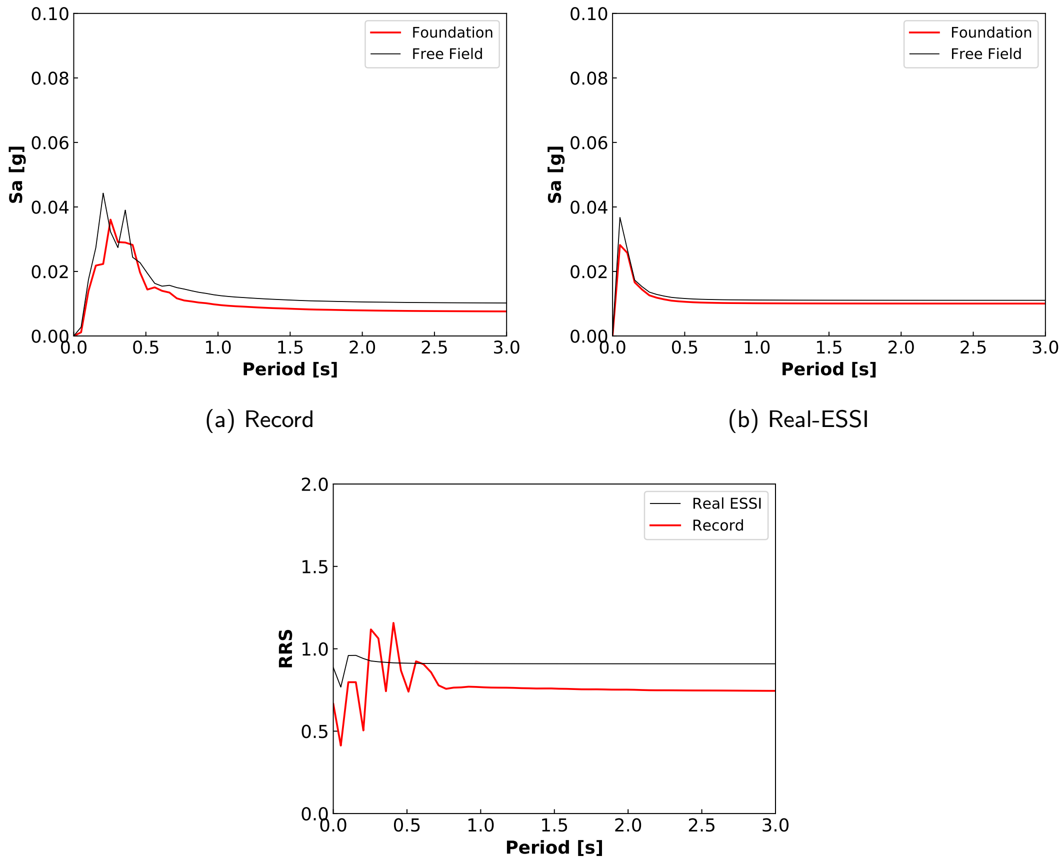

(a) Record

(b) Real-ESSI

(c) RRS Comparison

Figure 4.82: Spectral acceleration and RRS for Ventura Hotel under Ojai earthquake, CHAN12, with additional structural mass, 20% structural stiffness reduction, Soil Material Model SM-EL3 (elastic, shown in Table 2.11), 3% structural damping and 10% soil damping, coherent motion.

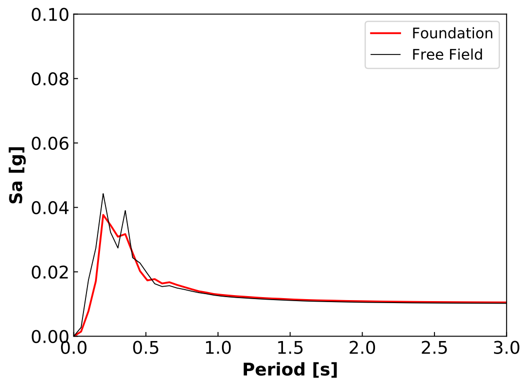

(a) Record

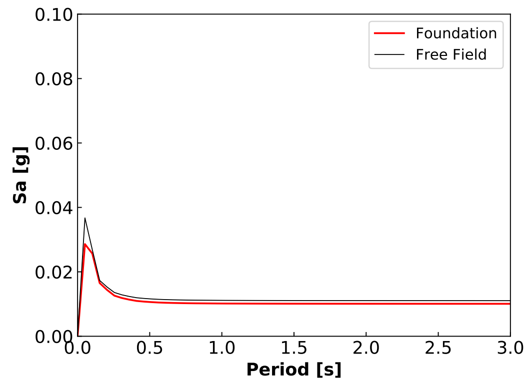

(b) Real-ESSI

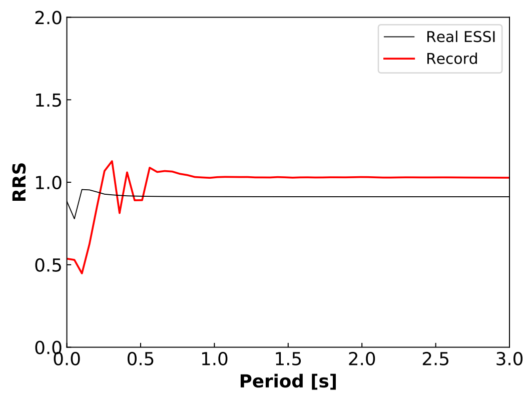

(c) RRS Comparison

Figure 4.83: Spectral acceleration and RRS for Ventura Hotel under Ojai earthquake, CHAN13, with additional structural mass, 20% structural stiffness reduction, Soil Material Model SM-EL3 (elastic, shown in Table 2.11), 3% structural damping and 10% soil damping, coherent motion.

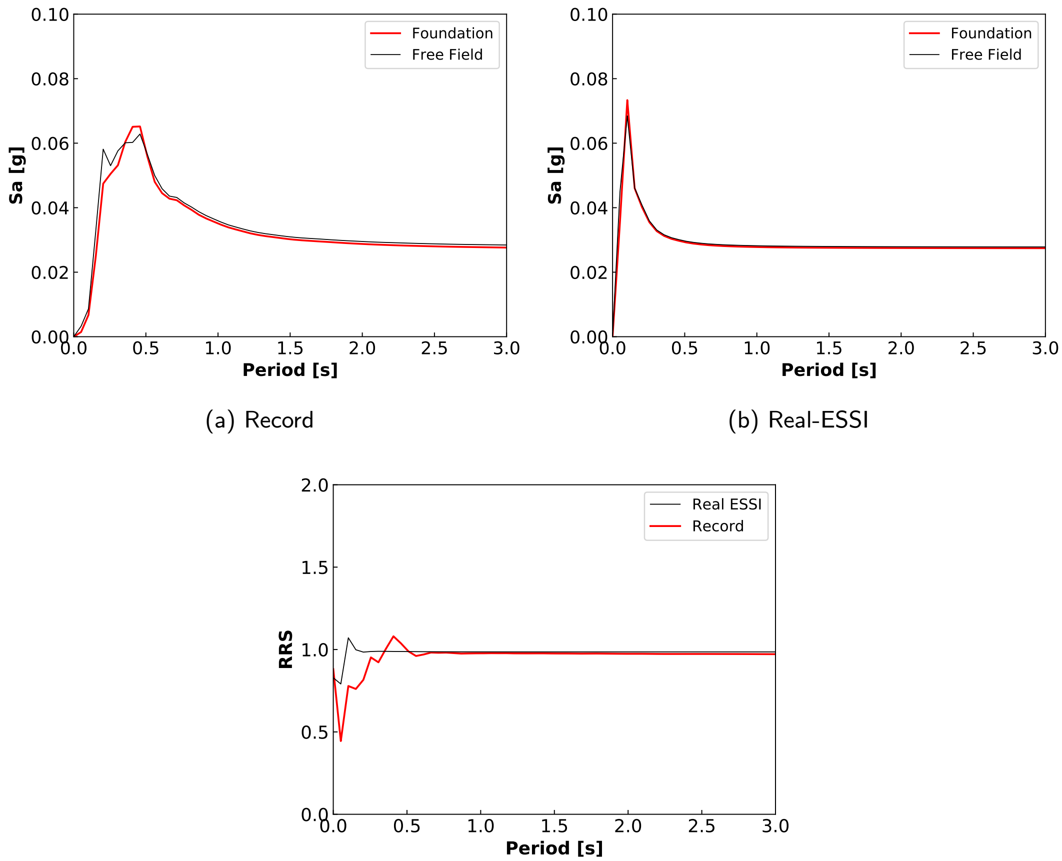

(a) Record

(b) Real-ESSI

(c) RRS Comparison

Figure 4.84: Spectral acceleration and RRS for Ventura Hotel under Ojai earthquake, CHAN15, with additional structural mass, 20% structural stiffness reduction, Soil Material Model SM-EL3 (elastic, shown in Table 2.11), 3% structural damping and 10% soil damping, coherent motion.

Coherent Motion vs. Incoherent Motion

Presented in this section are results that compare response of the Ventura Hotel, for coherent and incoherent motions. According to the simulation results, the provided incoherent motion seems incorrect. The magnitude of the (input) incoherent motion is much larger than the coherent one. Also, the displacement history of the incoherent motion might need to be baseline-corrected, however this is left for future work.

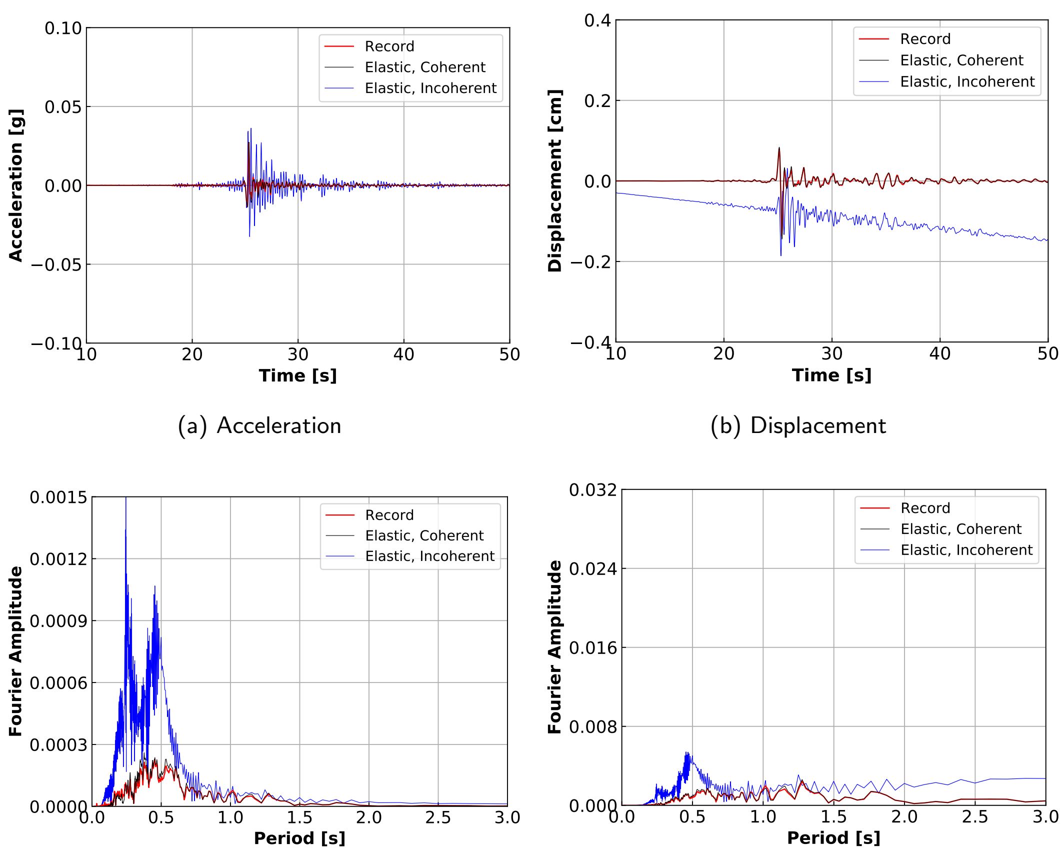

(a) Acceleration (b) Displacement

(c) FFT Acceleration (d) FFT Displacement

Figure 4.85: Dynamic response of Ventura Hotel under Ojai earthquake, coherent motion vs incoherent motion, at the ground floor in X direction (CHAN15), with additional structural mass, 20% structural stiffness reduction, Soil Material Model SM-EL3 (elastic, shown in Table 2.11), 3% structural damping and 10% soil damping.

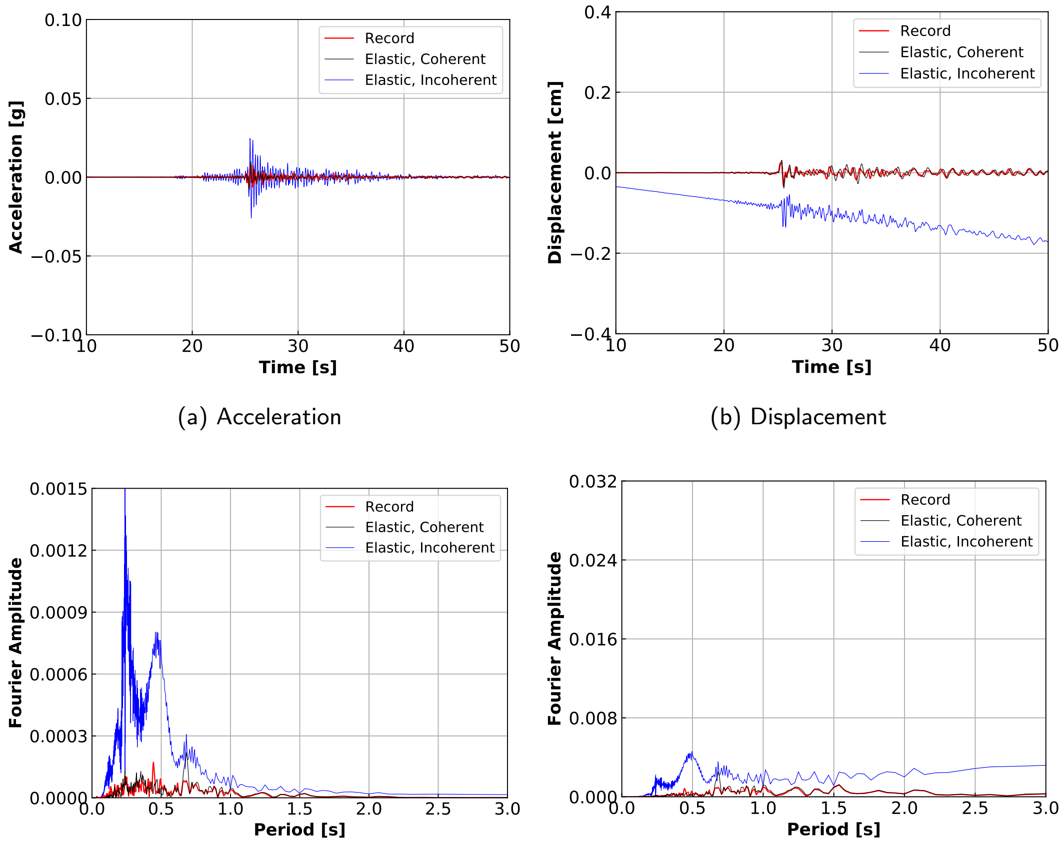

(a) Acceleration

(b) Displacement

(c) FFT Acceleration

(d) FFT Displacement

Figure 4.86: Dynamic response of Ventura Hotel under Ojai earthquake, coherent motion vs incoherent motion, at the ground floor in Y direction (CHAN12), with additional structural mass, 20% structural stiffness reduction, Soil Material Model SM-EL3 (elastic, shown in Table 2.11), 3% structural damping and 10% soil damping.

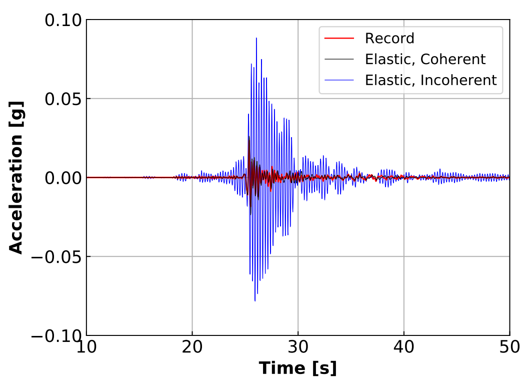

(a) Acceleration

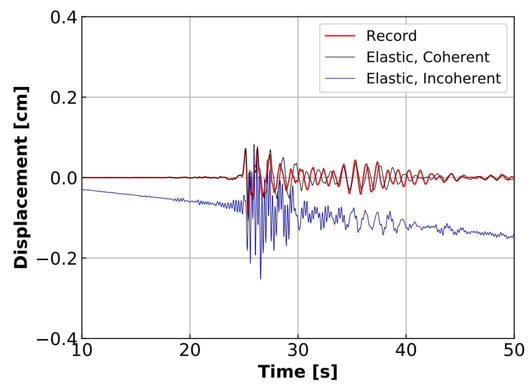

(b) Displacement

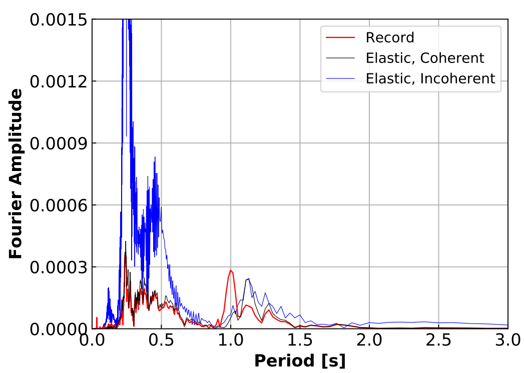

(c) FFT Acceleration

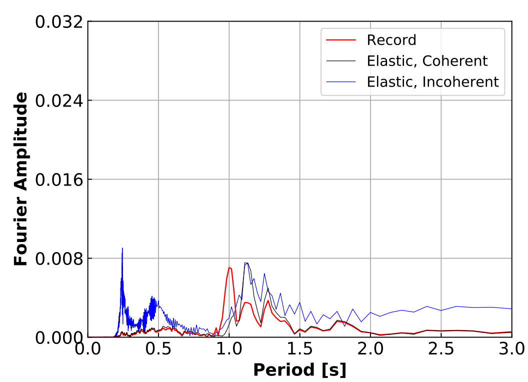

(d) FFT Displacement

Figure 4.87: Dynamic response of Ventura Hotel under Ojai earthquake, coherent motion vs incoherent motion, at the 4th floor in X direction (CHAN09), with additional structural mass, 20% structural stiffness reduction, Soil Material Model SM-EL3 (elastic, shown in Table 2.11), 3% structural damping and 10% soil damping.

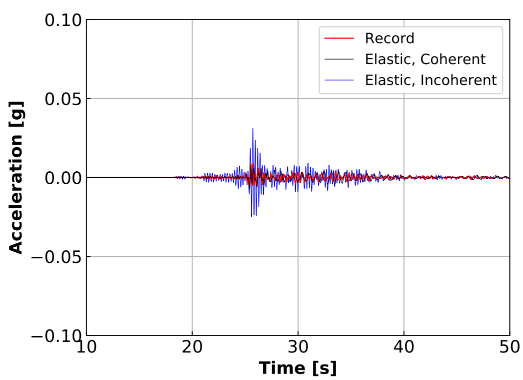

(a) Acceleration

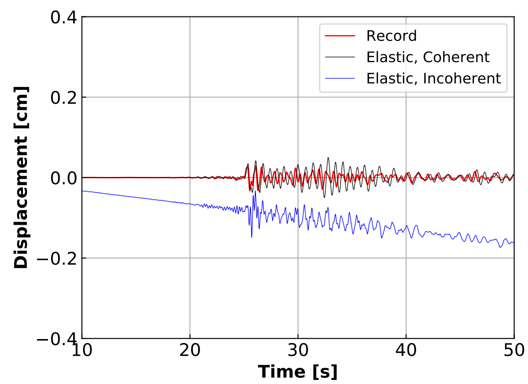

(b) Displacement

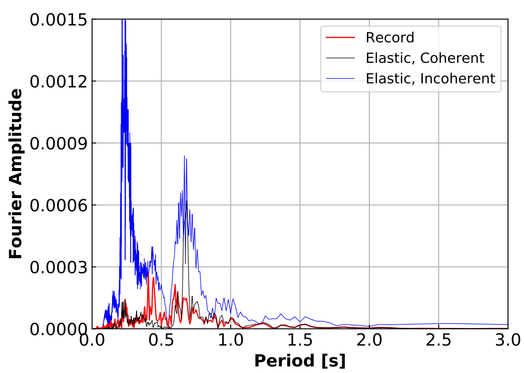

(c) FFT Acceleration

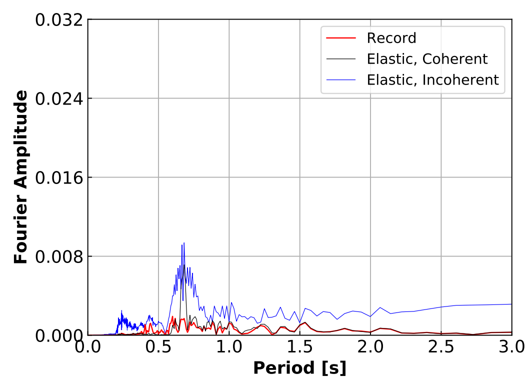

(d) FFT Displacement

Figure 4.88: Dynamic response of Ventura Hotel under Ojai earthquake, coherent motion vs incoherent motion, at the 4th floor in Y direction (CHAN11), with additional structural mass, 20% structural stiffness reduction, Soil Material Model SM-EL3 (elastic, shown in Table 2.11), 3% structural damping and 10% soil damping.

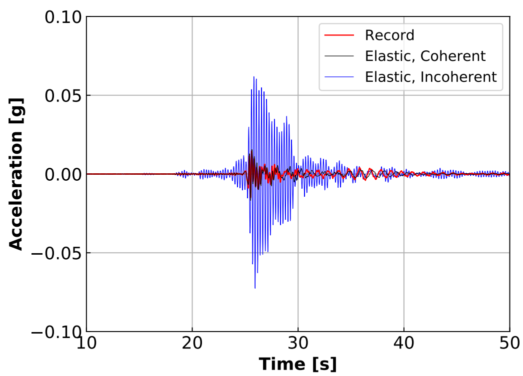

(a) Acceleration

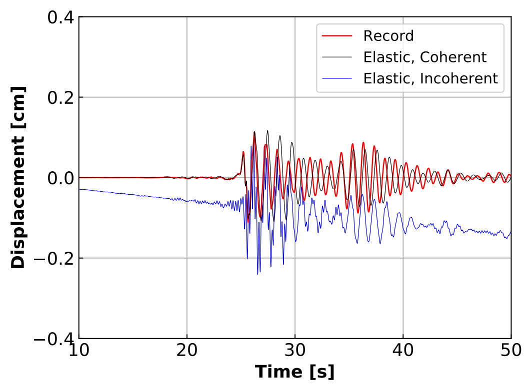

(b) Displacement

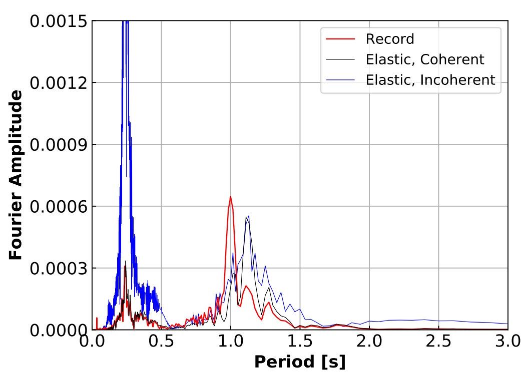

(c) FFT Acceleration

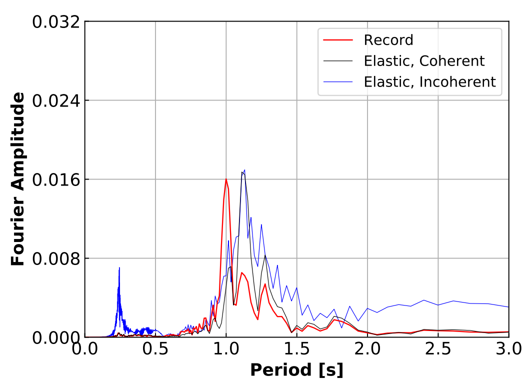

(d) FFT Displacement

Figure 4.89: Dynamic response of Ventura Hotel under Ojai earthquake, coherent motion vs incoherent motion, at the 8th floor in X direction (CHAN06), with additional structural mass, 20% structural stiffness reduction, Soil Material Model SM-EL3 (elastic, shown in Table 2.11), 3% structural damping and 10% soil damping.

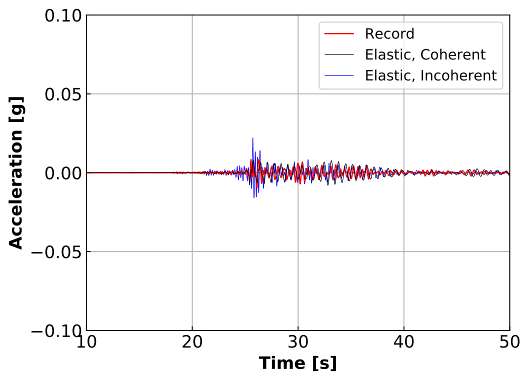

(a) Acceleration

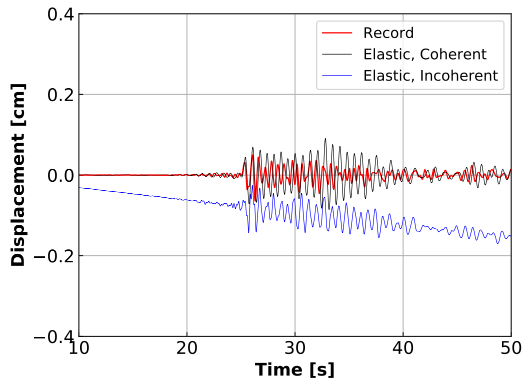

(b) Displacement

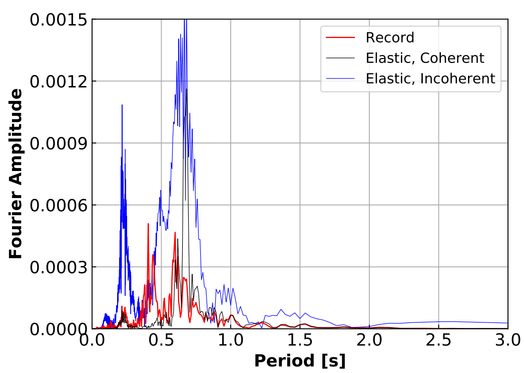

(c) FFT Acceleration

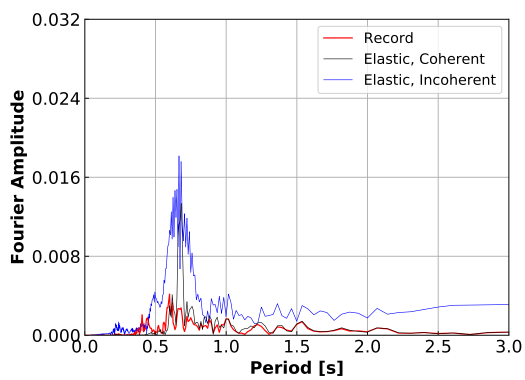

(d) FFT Displacement

Figure 4.90: Dynamic response of Ventura Hotel under Ojai earthquake, coherent motion vs incoherent motion, at the 8th floor in Y direction (CHAN08), with additional structural mass, 20% structural stiffness reduction, Soil Material Model SM-EL3 (elastic, shown in Table 2.11), 3% structural damping and 10% soil damping.

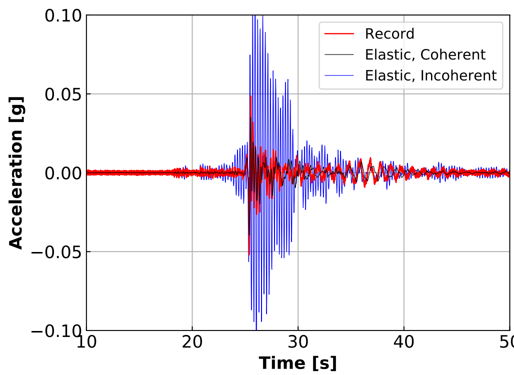

(a) Acceleration

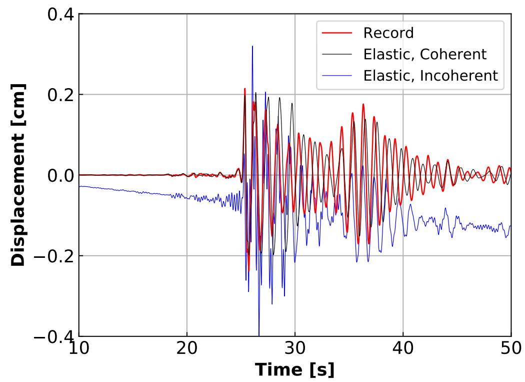

(b) Displacement

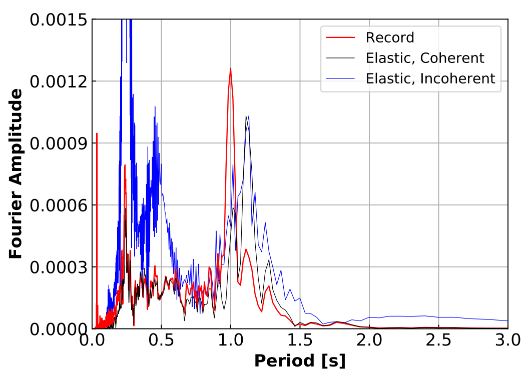

(c) FFT Acceleration

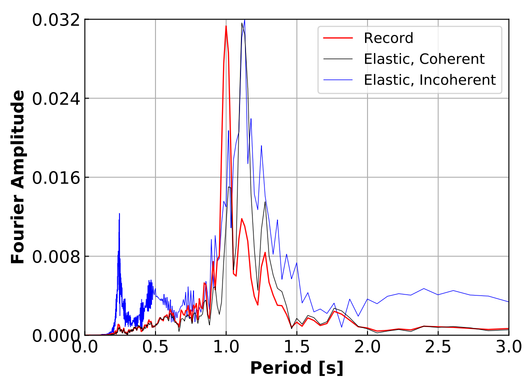

(d) FFT Displacement

Figure 4.91: Dynamic response of Ventura Hotel under Ojai earthquake, coherent motion vs incoherent motion, at the roof in X direction (CHAN02), with additional structural mass, 20% structural stiffness reduction, Soil Material Model SM-EL3 (elastic, shown in Table 2.11), 3% structural damping and 10% soil damping.

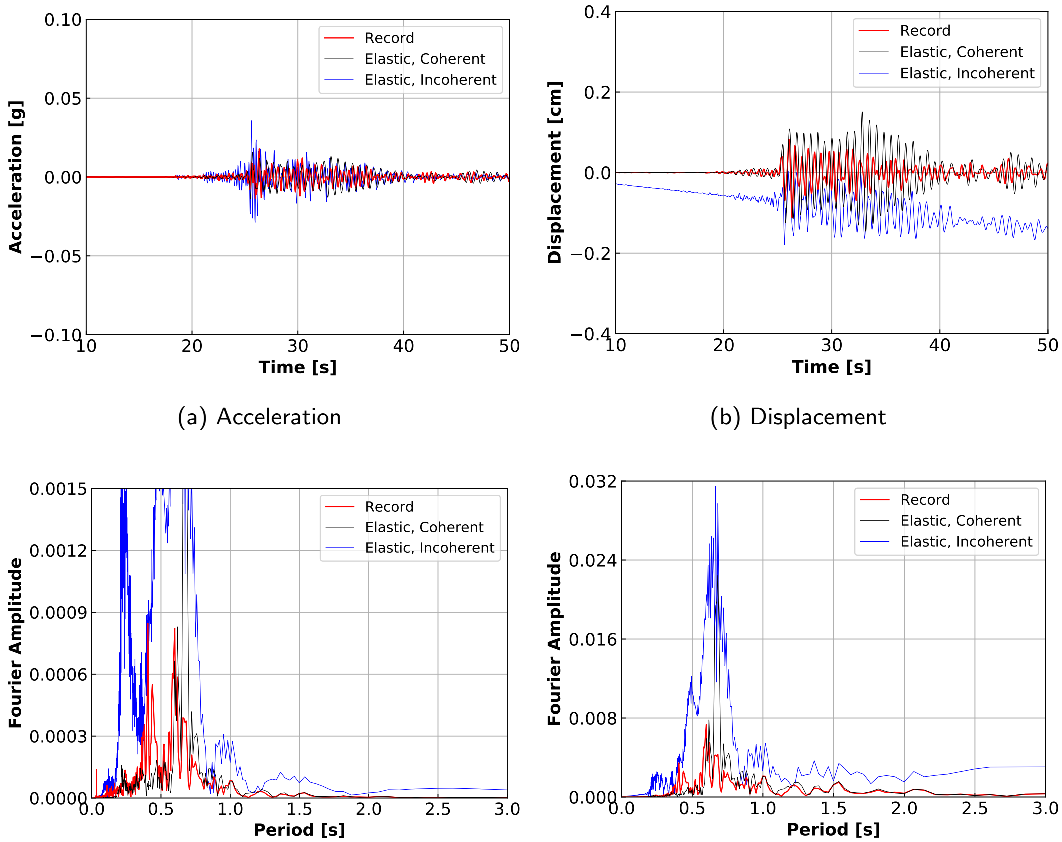

(a) Acceleration

(b) Displacement

(c) FFT Acceleration

(d) FFT Displacement

Figure 4.92: Dynamic response of Ventura Hotel under Ojai earthquake, coherent motion vs incoherent motion, at the roof in Y direction (CHAN05), with additional structural mass, 20% structural stiffness reduction, Soil Material Model SM-EL3 (elastic, shown in Table 2.11), 3% structural damping and 10% soil damping.

Elastic Soil vs. Inelastic Soil

When inelastic soil is used, reductions in both acceleration and displacement are observed. Permanent, inelastic deformation/displacement in the soil is observed It is noted that the same axes for all plots, in order to facilitate visual comparison of results.

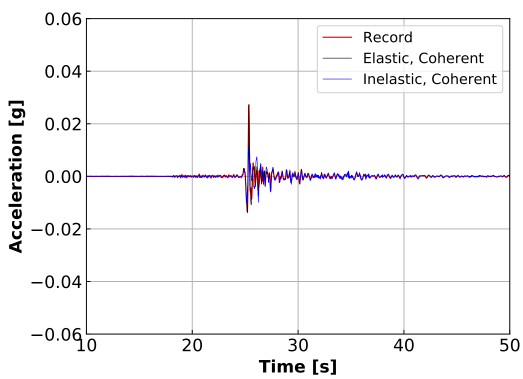

(a) Acceleration

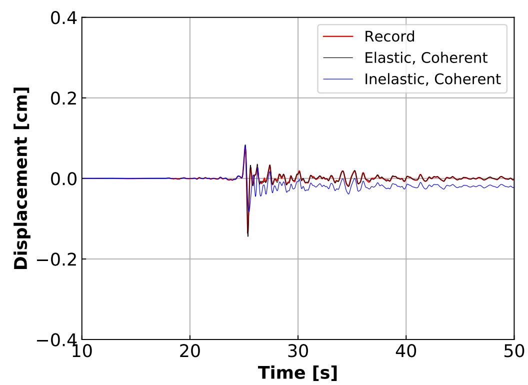

(b) Displacement

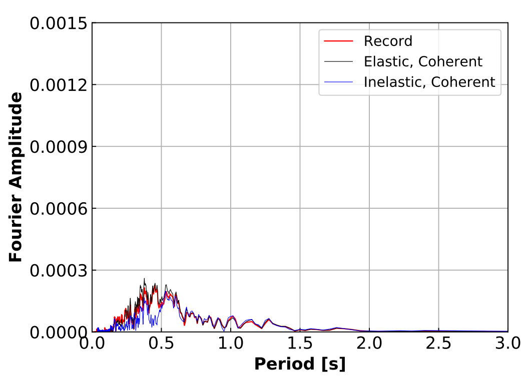

(c) FFT Acceleration

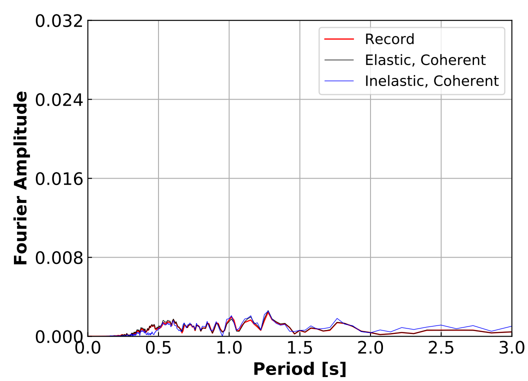

(d) FFT Displacement

Figure 4.93: Dynamic response of Ventura Hotel under Ojai earthquake, elastic soil (SM-EL3 shown in Table 2.11) vs inelastic soil (von Mises, SM-EP5 shown in Table 2.12), at the ground floor in X direction (CHAN15), with additional structural mass, 20% structural stiffness reduction, 3% structural damping and 10% soil damping.

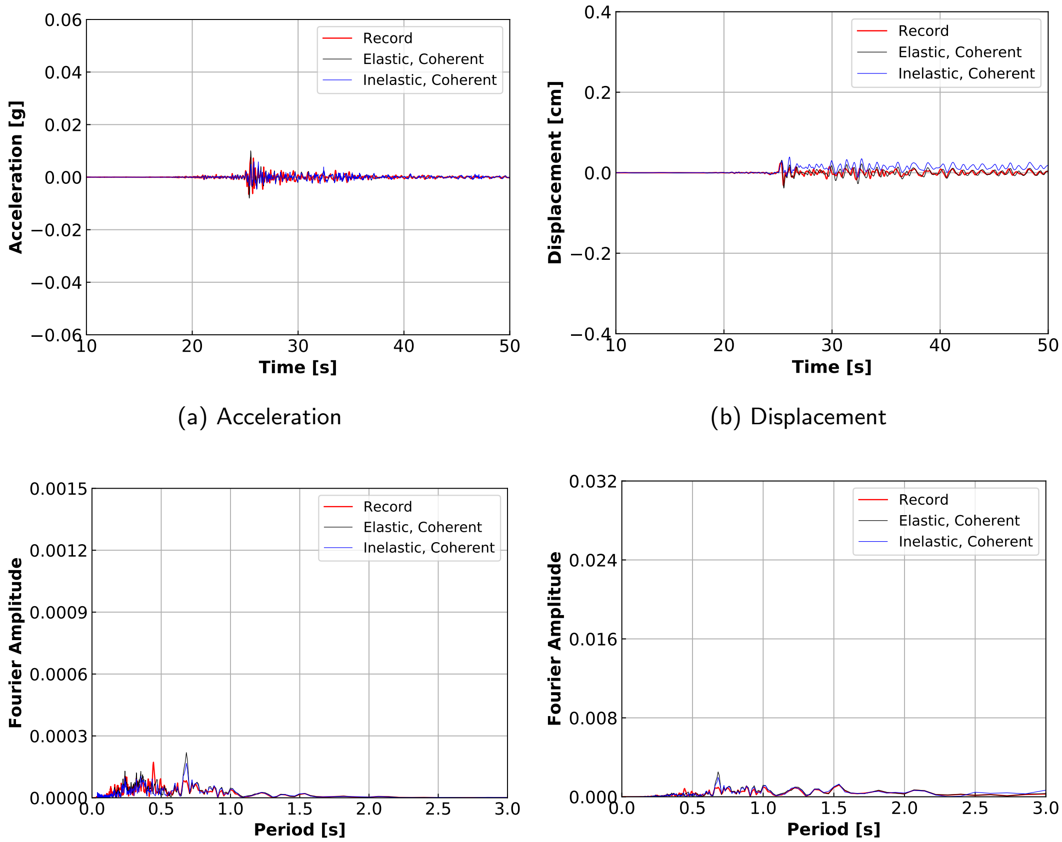

(a) Acceleration (b) Displacement

(c) FFT Acceleration (d) FFT Displacement

Figure 4.94: Dynamic response of Ventura Hotel under Ojai earthquake, elastic soil (SM-EL3 shown in Table 2.11) vs inelastic soil (von Mises, SM-EP5 shown in Table 2.12), at the ground floor in Y direction (CHAN12), with additional structural mass, 20% structural stiffness reduction, 3% structural damping and 10% soil damping.

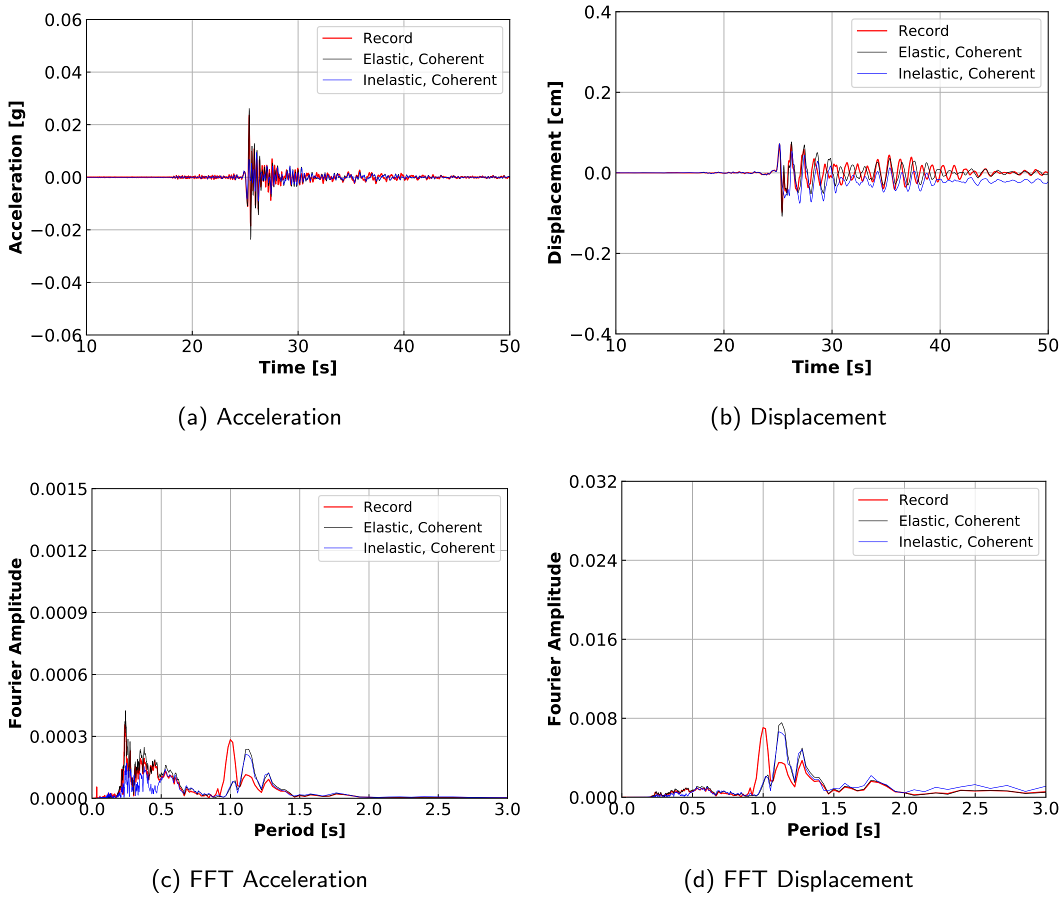

Figure 4.95: Dynamic response of Ventura Hotel under Ojai earthquake, elastic soil (SM-EL3 shown in Table 2.11) vs inelastic soil (von Mises, SM-EP5 shown in Table 2.12), at the 4th floor in X direction (CHAN09), with additional structural mass, 20% structural stiffness reduction, 3% structural damping and 10% soil damping.

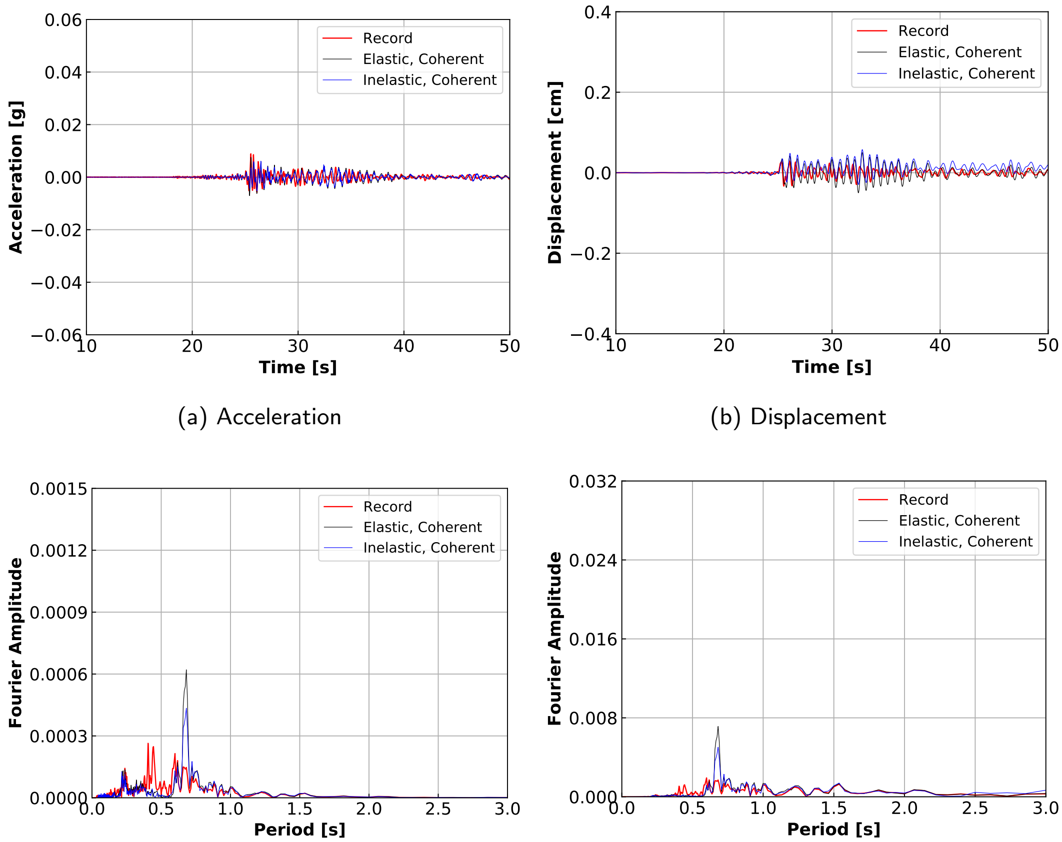

(a) Acceleration

(b) Displacement

(c) FFT Acceleration

(d) FFT Displacement

Figure 4.96: Dynamic response of Ventura Hotel under Ojai earthquake, elastic soil (SM-EL3 shown in Table 2.11) vs inelastic soil (von Mises, SM-EP5 shown in Table 2.12), at the 4th floor in Y direction (CHAN11), with additional structural mass, 20% structural stiffness reduction, 3% structural damping and 10% soil damping.

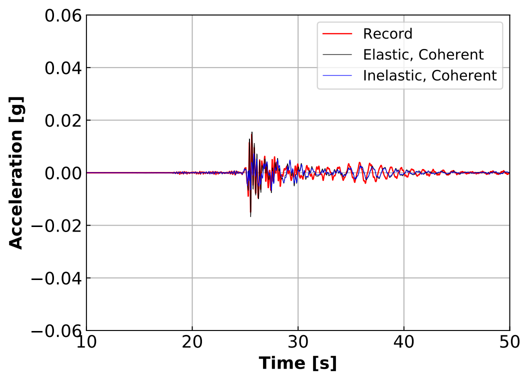

(a) Acceleration

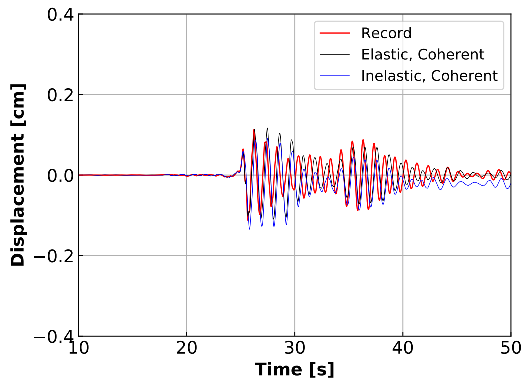

(b) Displacement

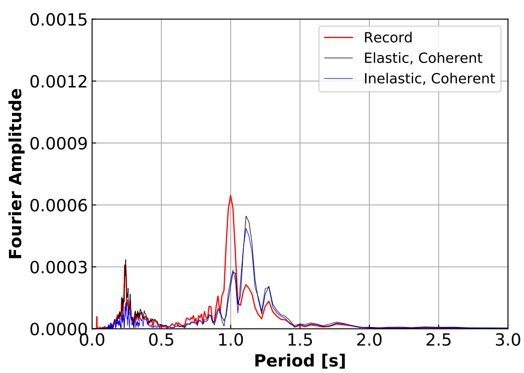

(c) FFT Acceleration

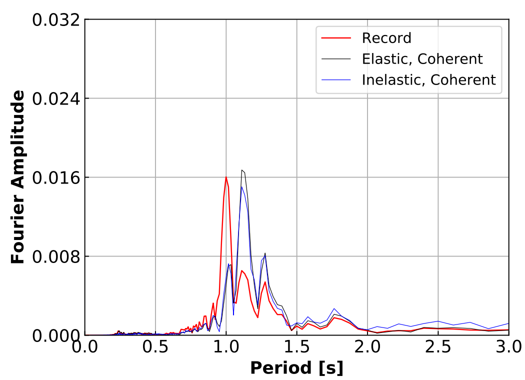

(d) FFT Displacement

Figure 4.97: Dynamic response of Ventura Hotel under Ojai earthquake, elastic soil (SM-EL3 shown in Table 2.11) vs inelastic soil (von Mises, SM-EP5 shown in Table 2.12), at the 8th floor in X direction (CHAN06), with additional structural mass, 20% structural stiffness reduction, 3% structural damping and 10% soil damping.

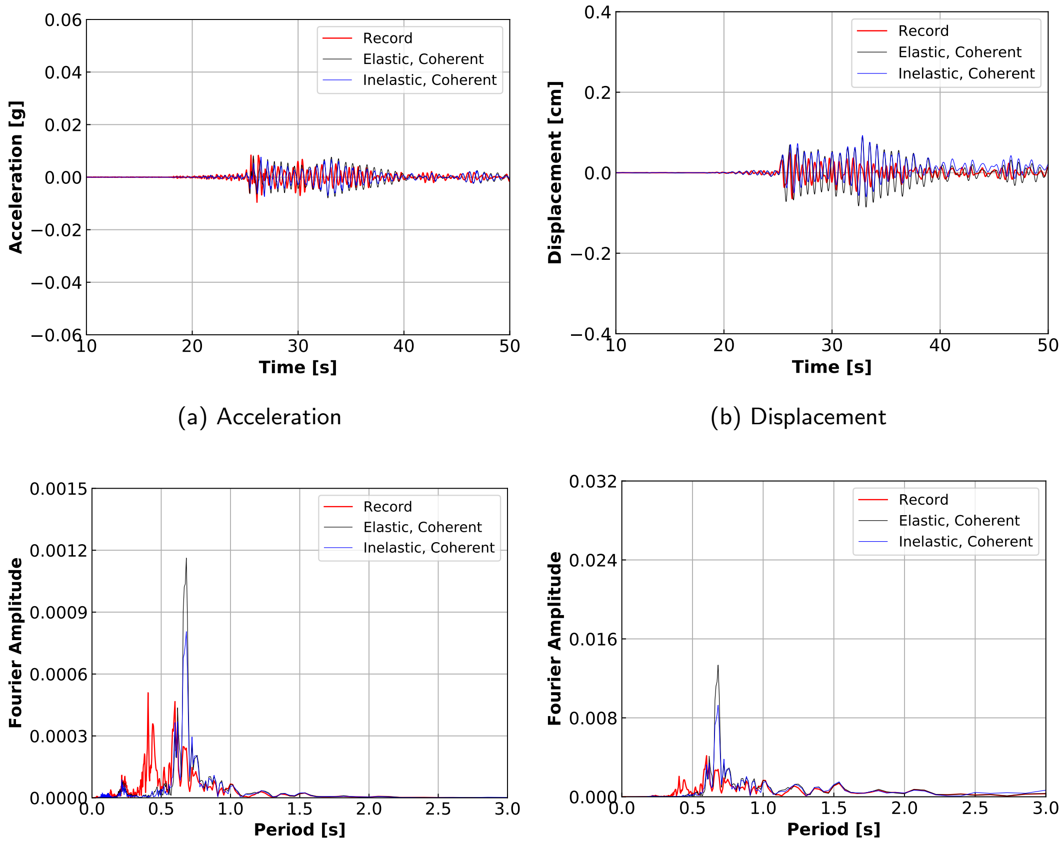

(a) Acceleration (b) Displacement

(c) FFT Acceleration (d) FFT Displacement

Figure 4.98: Dynamic response of Ventura Hotel under Ojai earthquake, elastic soil (SM-EL3 shown in Table 2.11) vs inelastic soil (von Mises, SM-EP5 shown in Table 2.12), at the 8th floor in Y direction (CHAN08), with additional structural mass, 20% structural stiffness reduction, 3% structural damping and 10% soil damping.

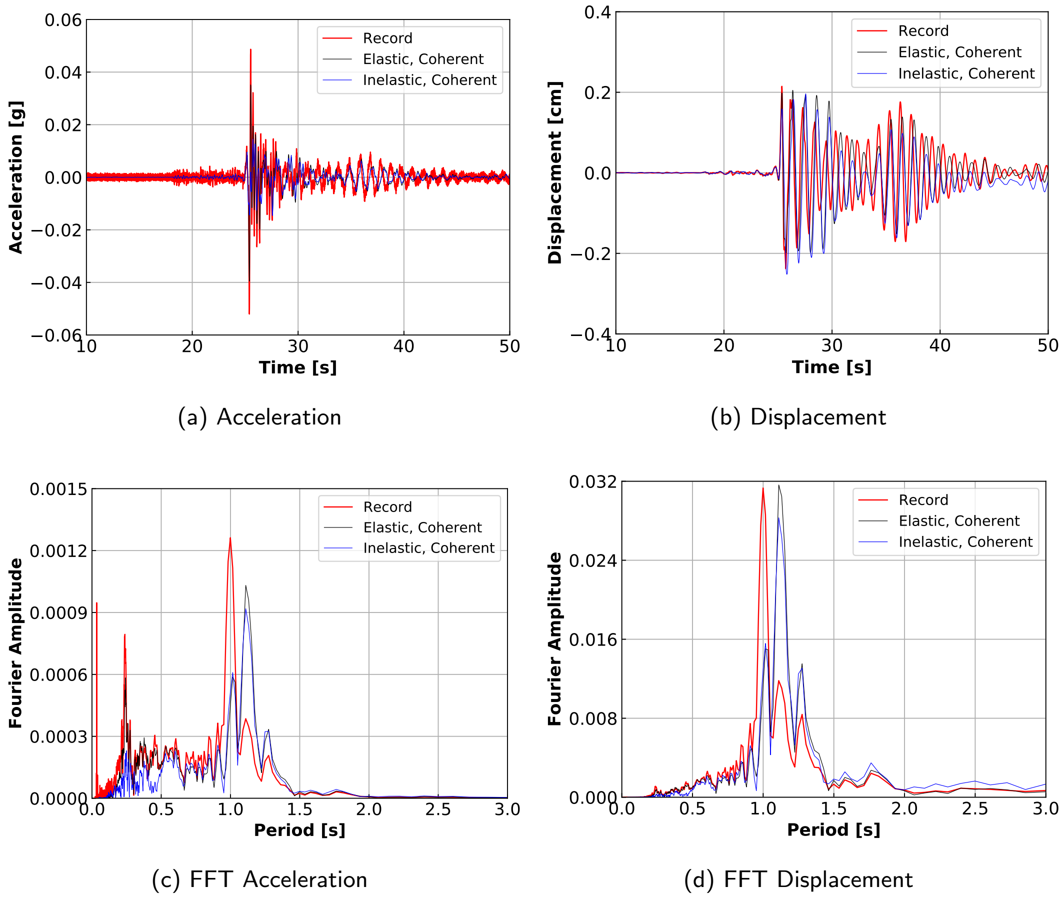

(a) Acceleration (b) Displacement

(c) FFT Acceleration (d) FFT Displacement

Figure 4.99: Dynamic response of Ventura Hotel under Ojai earthquake, elastic soil (SM-EL3 shown in Table 2.11) vs inelastic soil (von Mises, SM-EP5 shown in Table 2.12), at the roof in X direction (CHAN02), with additional structural mass, 20% structural stiffness reduction, 3% structural damping and 10% soil damping.

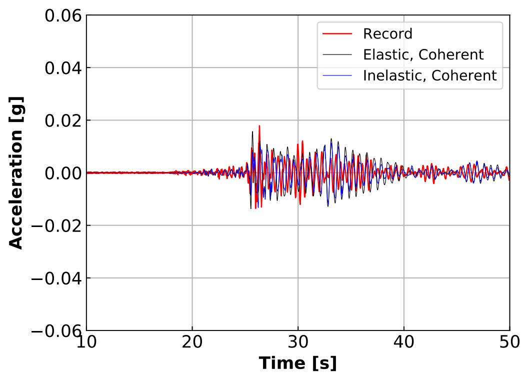

(a) Acceleration

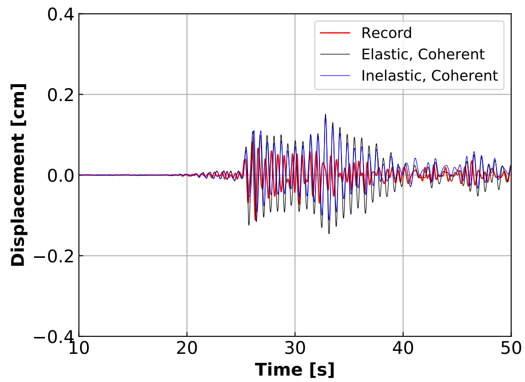

(b) Displacement

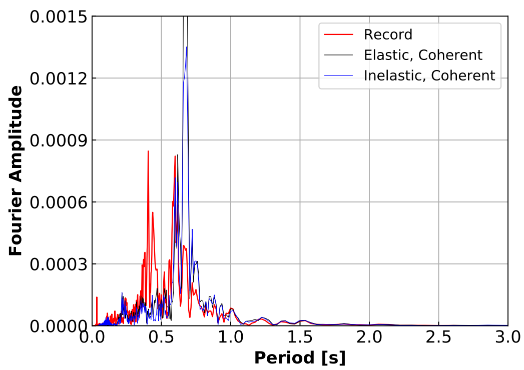

(c) FFT Acceleration

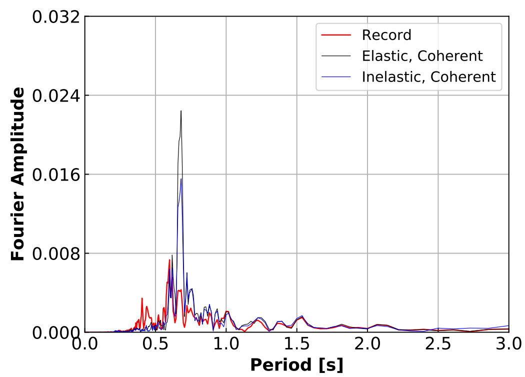

(d) FFT Displacement

Figure 4.100: Dynamic response of Ventura Hotel under Ojai earthquake, elastic soil (SM-EL3 shown in Table 2.11) vs inelastic soil (von Mises, SM-EP5 shown in Table 2.12), at the roof in Y direction (CHAN05), with additional structural mass, 20% structural stiffness reduction, 3% structural damping and 10% soil damping.

4.3.7 2019 Ridgecrest Earthquake

Another motion is the Ridgecrest earthquake, which occurred on July 4, 2019, recorded at Ventura Hotel (CSMIP Station No. 25339). All material parameters, damping coefficients, and other simulation parameters are the same as in the previous cases. The only change is the input motion. The figures below show the comparison between recorded motions and Real-ESSI simulation results.

The Ridgecrest motion shows minimal incoherency, as the records shown in Figure 4.102 and 4.103 are almost identical. This means 2×1C surface motion deconvolution is suitable for generating input seismic motion in this case. Therefore, the simulation results match better with the earthquake records.

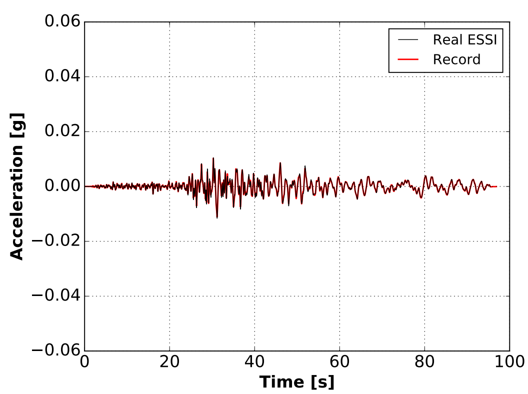

(a) Acceleration

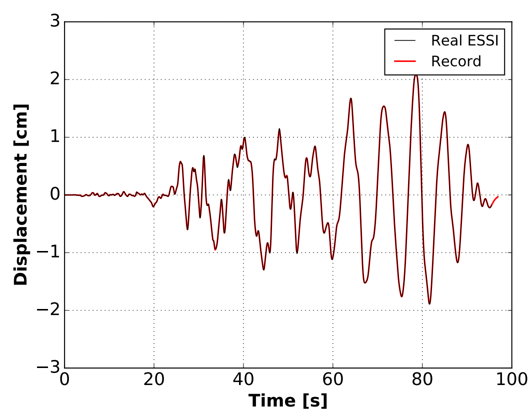

(b) Displacement

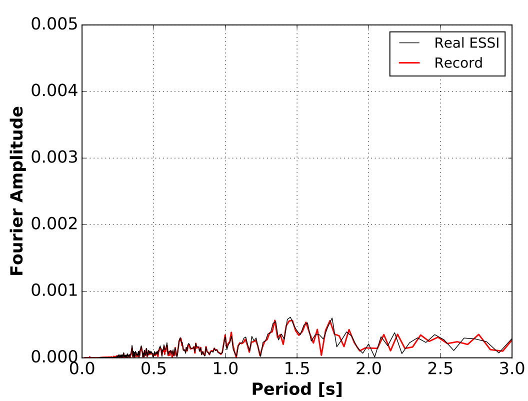

(c) FFT Acceleration

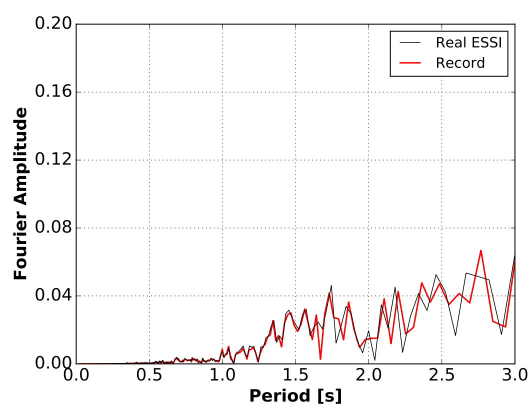

(d) FFT Displacement

Figure 4.101: Dynamic response of Ventura Hotel under Ridgecrest earthquake at the ground floor in X direction (CHAN015), with additional structural mass, 20% structural stiffness reduction, Soil Material Model SM-EL3 (elastic, shown in Table 2.11), 3% structural damping and 10% soil damping, coherent motion.

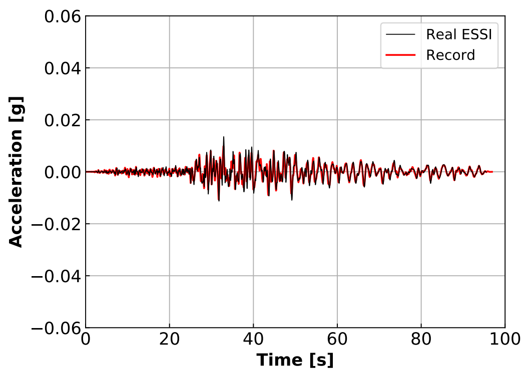

(a) Acceleration

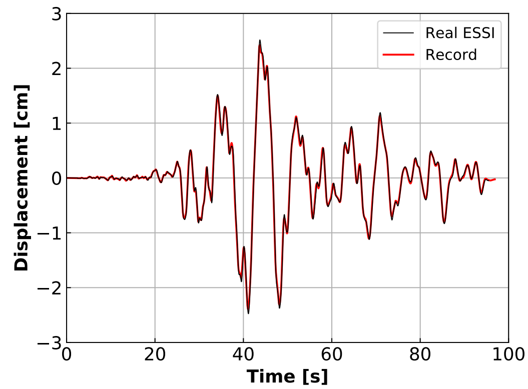

(b) Displacement

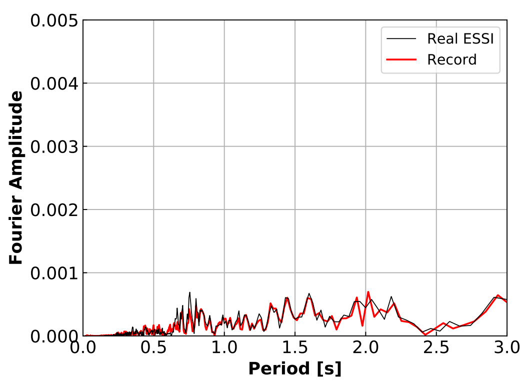

(c) FFT Acceleration

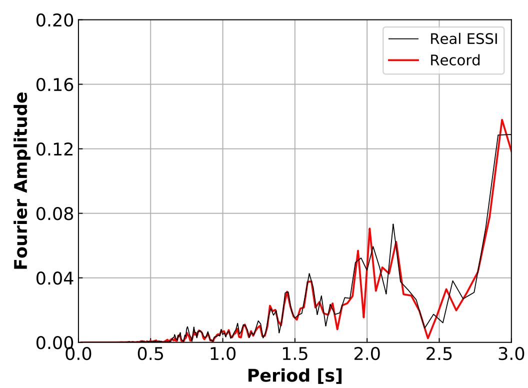

(d) FFT Displacement

Figure 4.102: Dynamic response of Ventura Hotel under Ridgecrest earthquake at the ground floor in Y direction (CHAN012), with additional structural mass, 20% structural stiffness reduction, Soil Material Model SM-EL3 (elastic, shown in Table 2.11), 3% structural damping and 10% soil damping, coherent motion.

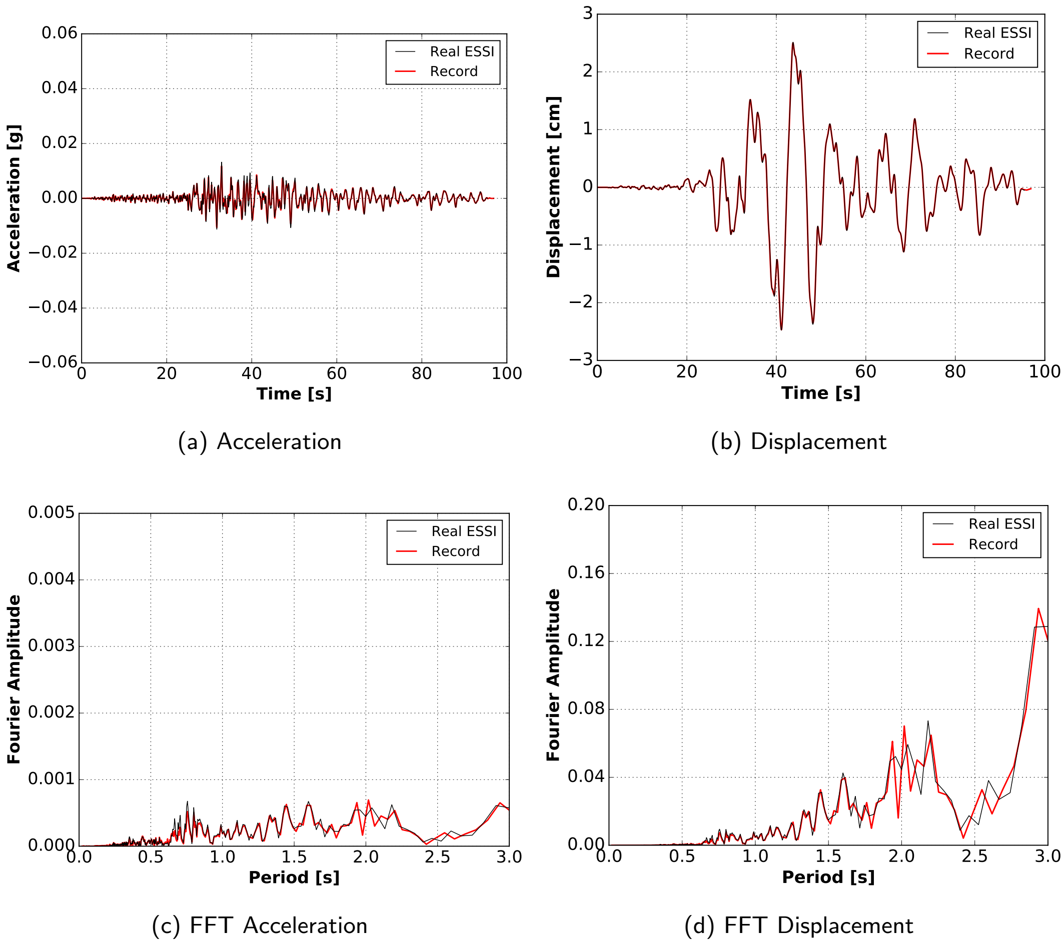

Figure 4.103: Dynamic response of Ventura Hotel under Ridgecrest earthquake at the ground floor in Y direction (CHAN013), with additional structural mass, 20% structural stiffness reduction, Soil Material Model SM-EL3 (elastic, shown in Table 2.11), 3% structural damping and 10% soil damping, coherent motion.

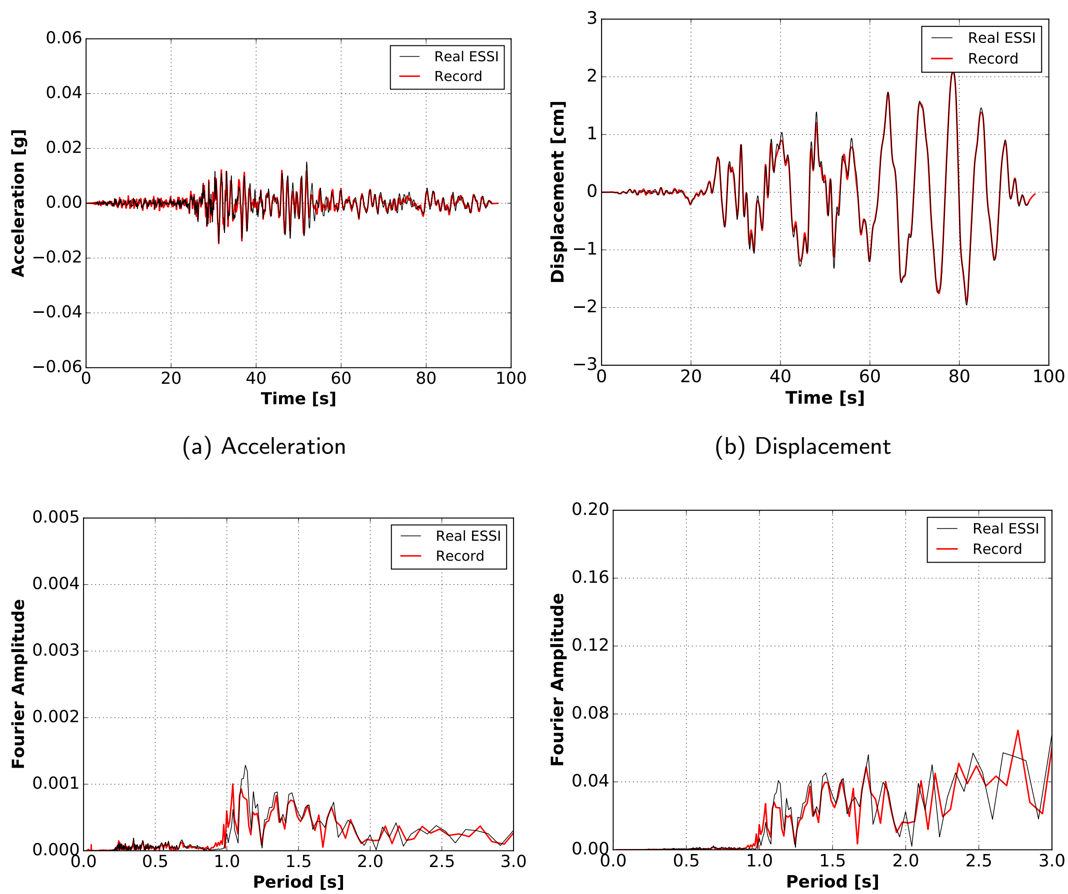

(a) Acceleration (b) Displacement

(c) FFT Acceleration (d) FFT Displacement

Figure 4.104: Dynamic response of Ventura Hotel under Ridgecrest earthquake at the 4th floor in X direction (CHAN009), with additional structural mass, 20% structural stiffness reduction, Soil Material Model SM-EL3 (elastic, shown in Table 2.11), 3% structural damping and 10% soil damping, coherent motion.

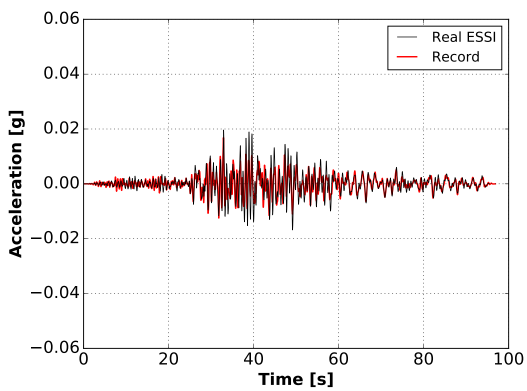

(a) Acceleration

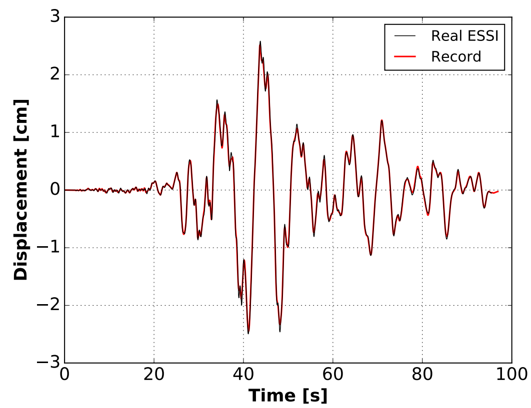

(b) Displacement

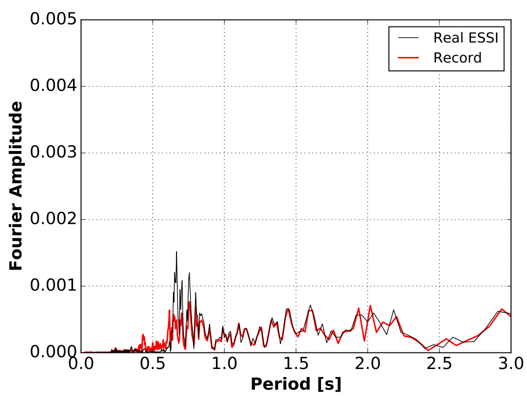

(c) FFT Acceleration

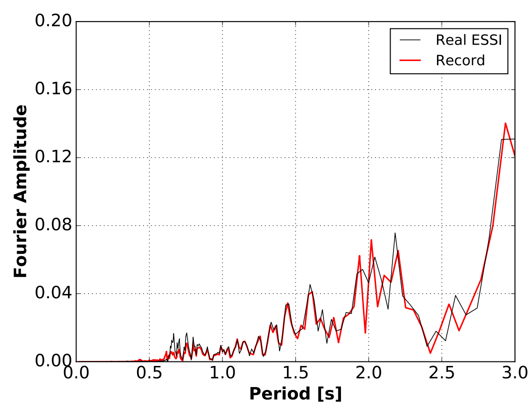

(d) FFT Displacement

Figure 4.105: Dynamic response of Ventura Hotel under Ridgecrest earthquake at the 4th floor in Y direction (CHAN010), with additional structural mass, 20% structural stiffness reduction, Soil Material Model SM-EL3 (elastic, shown in Table 2.11), 3% structural damping and 10% soil damping, coherent motion.

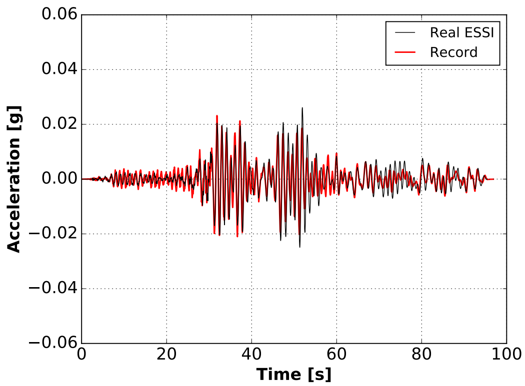

(a) Acceleration

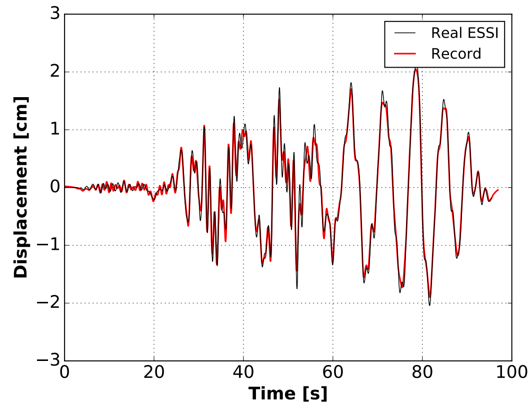

(b) Displacement

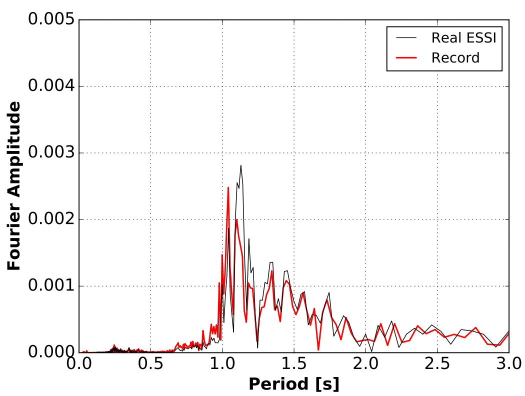

(c) FFT Acceleration

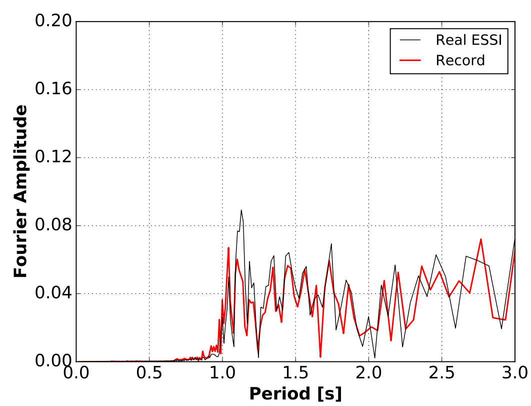

(d) FFT Displacement

Figure 4.106: Dynamic response of Ventura Hotel under Ridgecrest earthquake at the 8th floor in X direction (CHAN006), with additional structural mass, 20% structural stiffness reduction, Soil Material Model SM-EL3 (elastic, shown in Table 2.11), 3% structural damping and 10% soil damping, coherent motion.

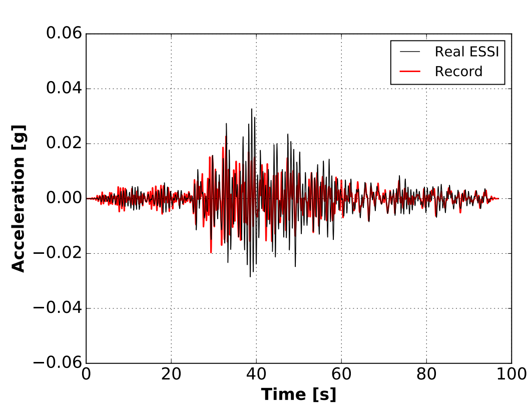

(a) Acceleration

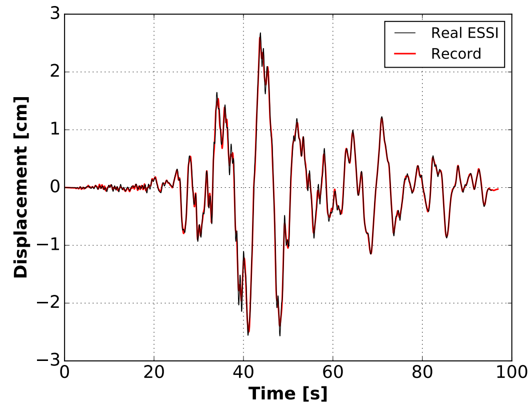

(b) Displacement

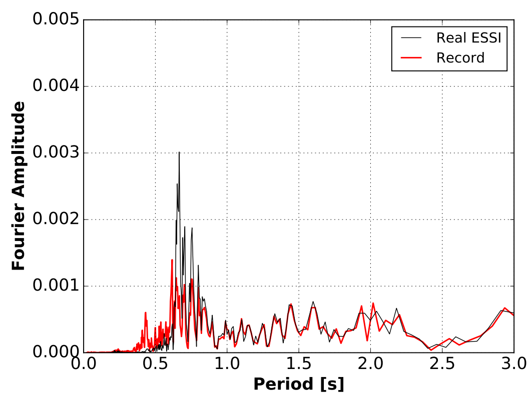

(c) FFT Acceleration

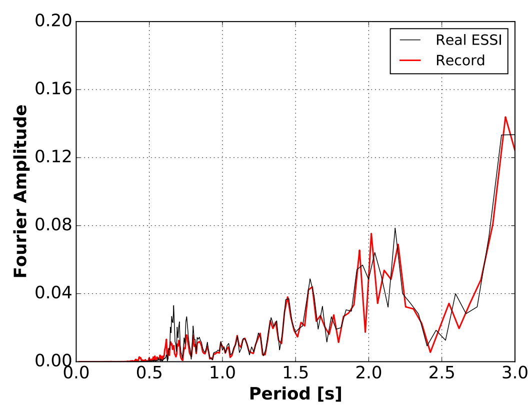

(d) FFT Displacement

Figure 4.107: Dynamic response of Ventura Hotel under Ridgecrest earthquake at the 8th floor in Y direction (CHAN007), with additional structural mass, 20% structural stiffness reduction, Soil Material Model SM-EL3 (elastic, shown in Table 2.11), 3% structural damping and 10% soil damping, coherent motion.

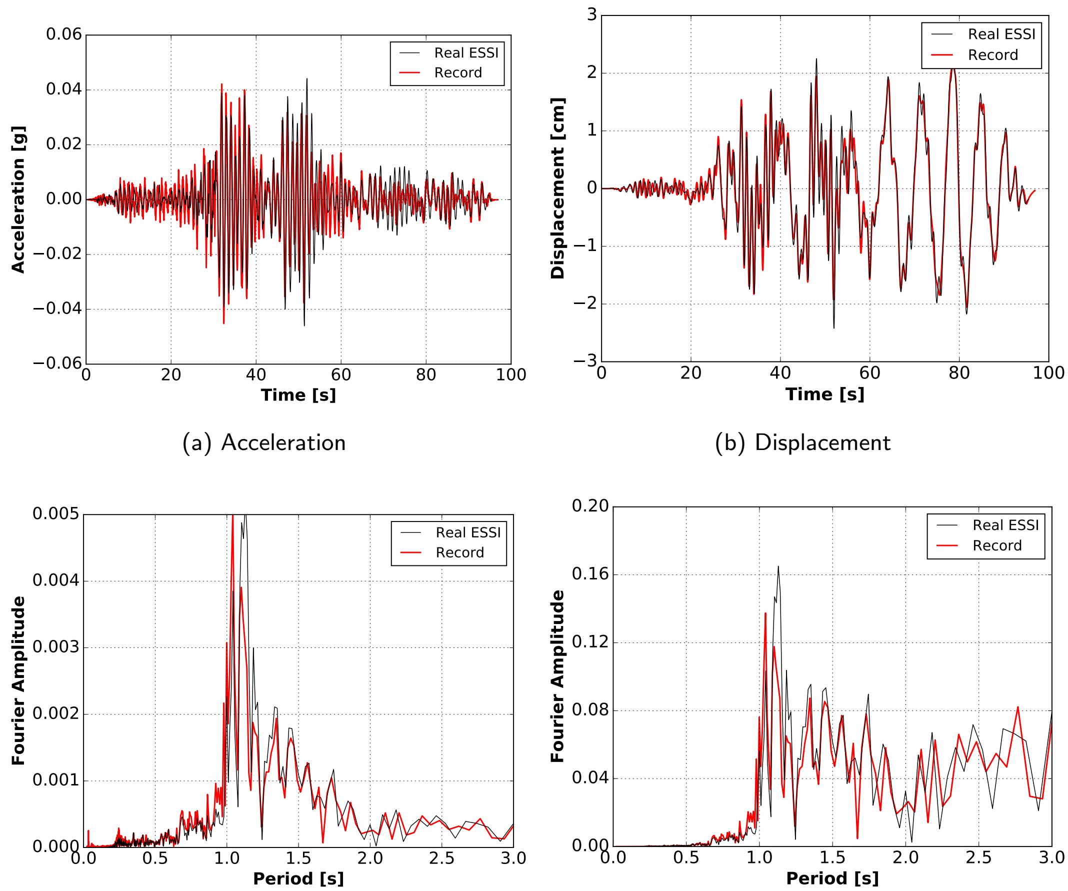

(a) Acceleration (b) Displacement

(c) FFT Acceleration (d) FFT Displacement

Figure 4.108: Dynamic response of Ventura Hotel under Ridgecrest earthquake at the roof in X direction (CHAN002), with additional structural mass, 20% structural stiffness reduction, Soil Material Model SM-EL3 (elastic, shown in Table 2.11), 3% structural damping and 10% soil damping, coherent motion.

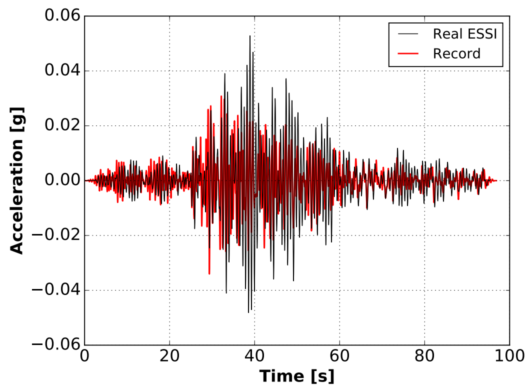

(a) Acceleration

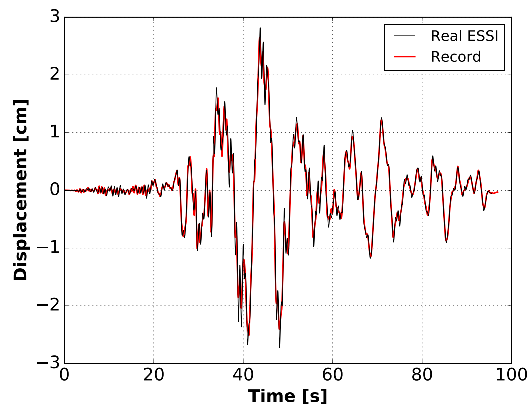

(b) Displacement

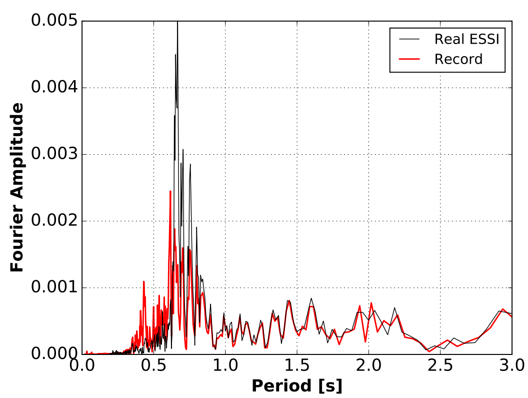

(c) FFT Acceleration

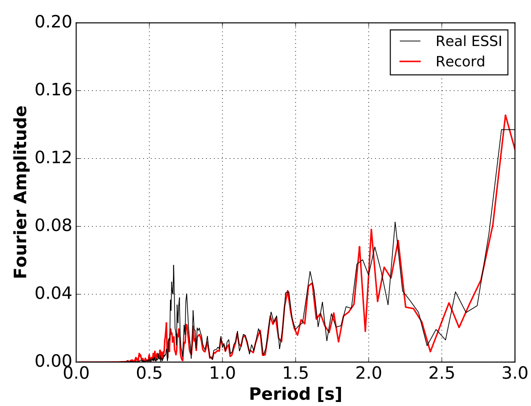

(d) FFT Displacement

Figure 4.109: Dynamic response of Ventura Hotel under Ridgecrest earthquake at the roof in Y direction (CHAN003), with additional structural mass, 20% structural stiffness reduction, Soil Material Model SM-EL3 (elastic, shown in Table 2.11), 3% structural damping and 10% soil damping, coherent motion.

4.4 Loma Linda Hospital

4.4.1 Eigen Analysis

Loma Linda hospital model is very stiff, and first 50 eigen-modes are oscillations of inter-story plates, while the full structural model does not show eigen-modes in transversal direction.

4.5 Low, Steel Building

Unless otherwise specified, a scale factor of 1.82 is used for the ESSI simulations present in this section. Seismic Records 120711 and 120712, scaled by 1.82, are noted as the baseline surface input motion in the figure captions shown in this section. It is noted Baseline Motion represent scaled records.

4.5.1 Eigen analysis, Low, Steel Building

Table 4.8 presents first 20 eigen periods and frequencies for the short, steel building.

Table 4.8: Eigen analysis results for the low, steel building.

	Eigen periods [s]	Eigen frequencies [Hz]
1	0.6917	1.4456
2	0.5752	1.7386
3	0.5076	1.9700
4	0.3251	3.0762
5	0.3251	3.0763
6	0.3243	3.0835
7	0.3243	3.0835
8	0.2744	3.6441
9	0.2743	3.6453
10	0.2721	3.6750
11	0.2721	3.6750
12	0.2661	3.7577
13	0.2652	3.7713
14	0.2649	3.7750
15	0.2649	3.7753
16	0.2643	3.7837
17	0.2643	3.7842
18	0.2630	3.8023
19	0.2366	4.2272
20	0.2241	4.4619

Figure 4.110 presents first 4 eigen modes for the low steel building.

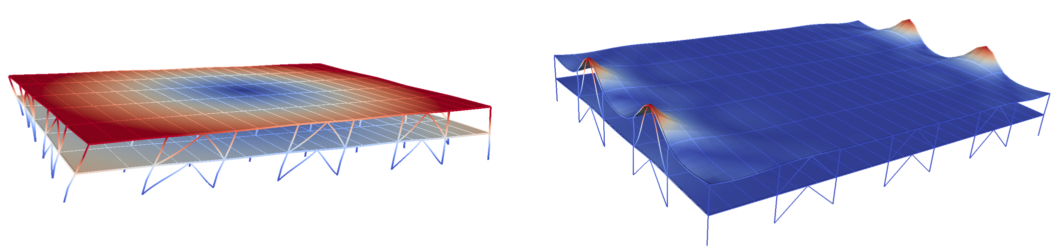

(a) 1st mode

(b) 2nd mode

(c) 3rd mode

(d) 4th mode

Figure 4.110: First 4 eigen modes for the low steel building.

4.5.2 Elastic and Inelastic Free-Field Response

The 1D elastic and inelastic free-field response is investigated: Bottom DRM excitation is first developed through 1D wave field deconvolution. Then 1D elastic and inelastic wave propagation are analyzed. Figure 4.111 compares the 1D elastic and inelastic free-field response.

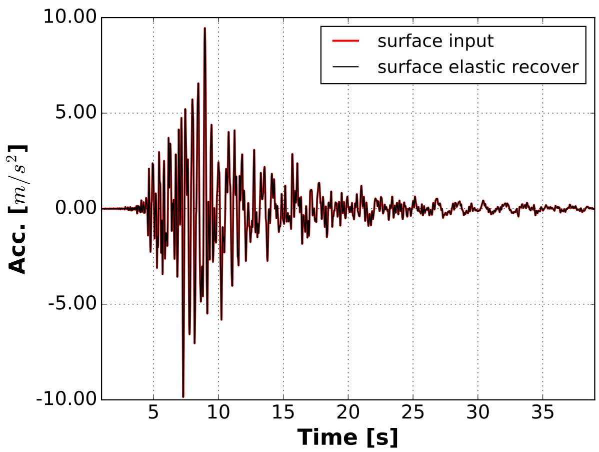

(a) Elastic free-field

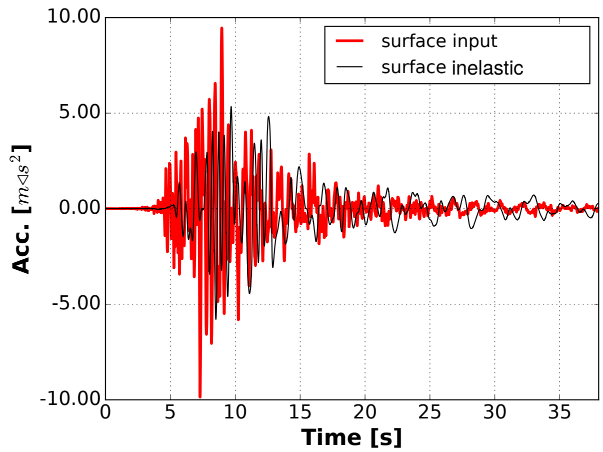

(b) Inelastic free-field

Figure 4.111: Elastic and inelastic free-field response, Baseline Motion 120711 (scale factor 1.82), Soil Material Model SM-EL1 for elastic and SM-EP1 for inelastic modeling.

4.5.3 Earthquake Soil-Structure Interaction Results - $2 \times 1C$ Coherent and Incoherent Motion

Elastic vs. Inelastic and Coherent vs. Incoherent

Simulation results from four cases are compared: elastic soil with coherent motion (denoted as elastic, coherent), inelastic soil with coherent motion (denoted as inelastic, coherent), elastic soil with incoherent motion (denoted as elastic, incoherent), and inelastic soil with incoherent motion.

Figure 4.112 to 4.117 show the dynamic response of the 2-story steel frame building subjected to $2 \times 1C$ coherent and incoherent motion from medium seismic Records 120711 and 120712. It is noted that the foundation of a low steel building is shown in Figure 3.17 in gray color.

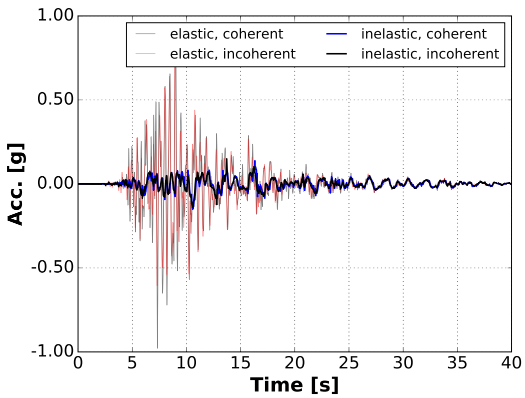

(a) Acceleration at foundation surface

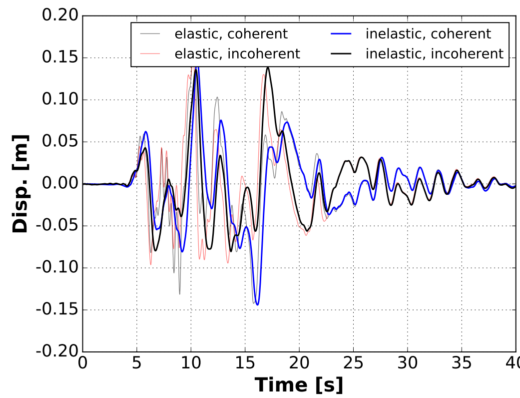

(b) Displacement at foundation surface

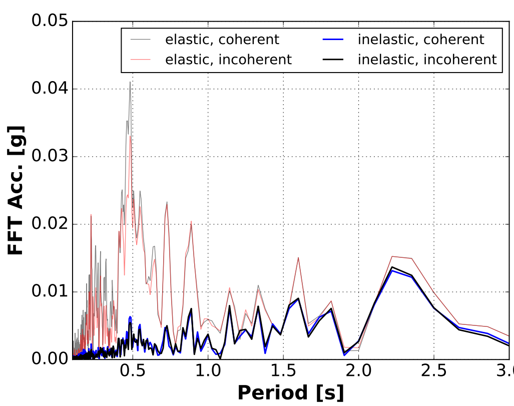

(c) FFT Acceleration at foundation surface

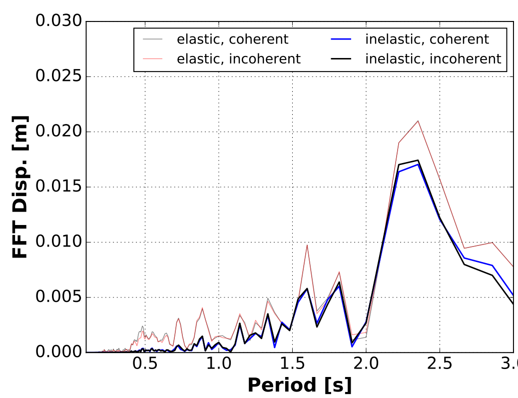

(d) FFT Displacement at foundation surface

Figure 4.112: Foundation surface, low steel building, Baseline Motion 120711 and 120712, elastic Soil Material Model SM-EL1 and inelastic Soil Material Model SM-EP1, X direction. PGA: elastic coherent 0.95g, elastic incoherent 0.88g, inelastic coherent 0.15g and inelastic incoherent 0.15g.

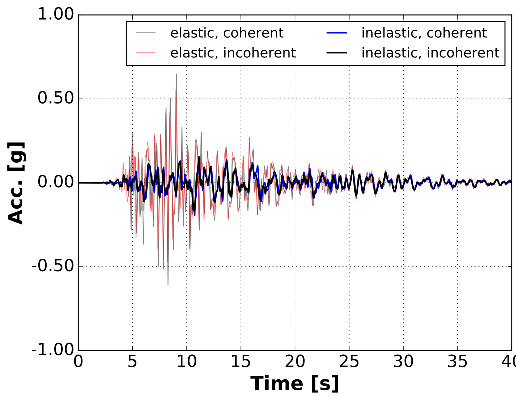

(a) Acceleration at the 1st floor

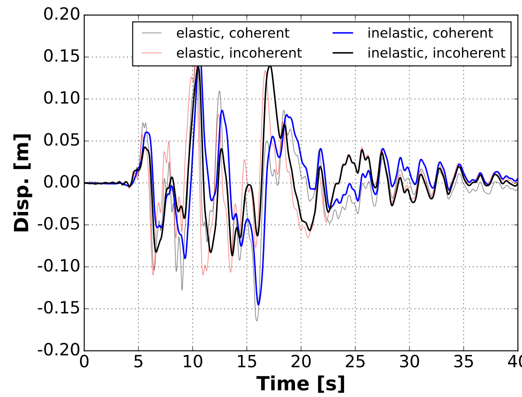

(b) Displacement at the 1st floor

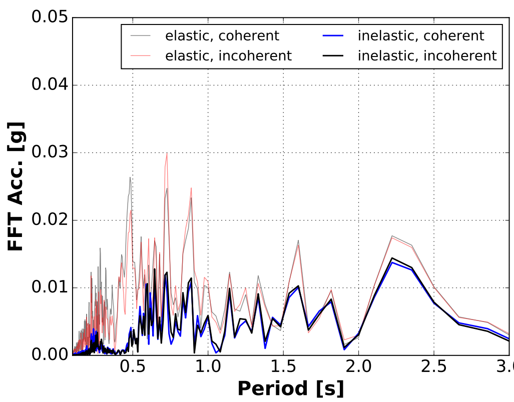

(c) FFT Acceleration at the 1st floor

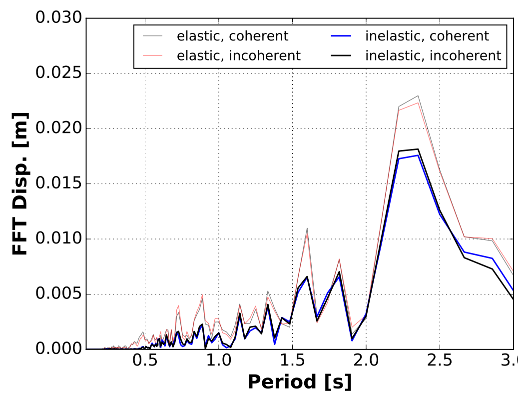

(d) FFT Displacement at the 1st floor

Figure 4.113: The 1st floor, low steel building, Baseline Motion 120711 and 120712, elastic Soil Material Model SM-EL1 and inelastic Soil Material Model SM-EP1, X direction. PFA: elastic coherent 0.65g, elastic incoherent 0.55g, inelastic coherent 0.20g and inelastic incoherent 0.17g.

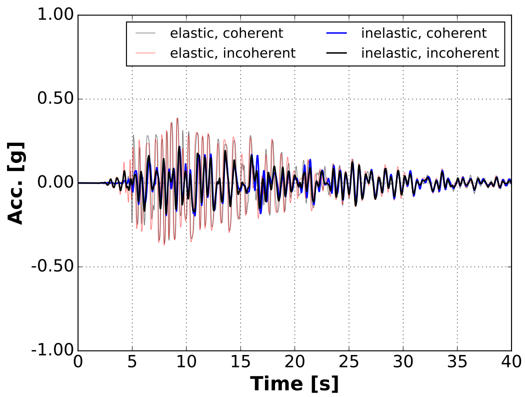

(a) Acceleration at the roof level

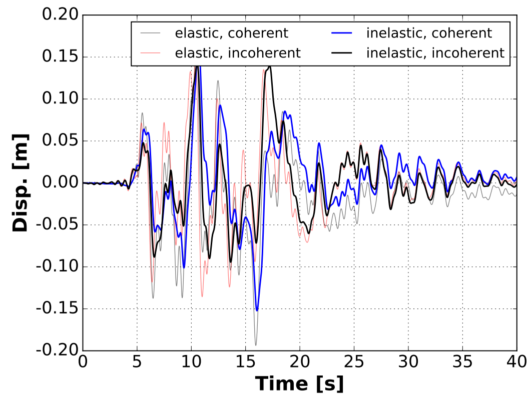

(b) Displacement at the roof level

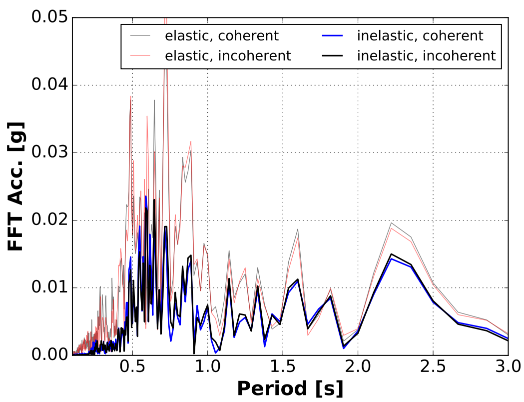

(c) FFT Acceleration at the roof level

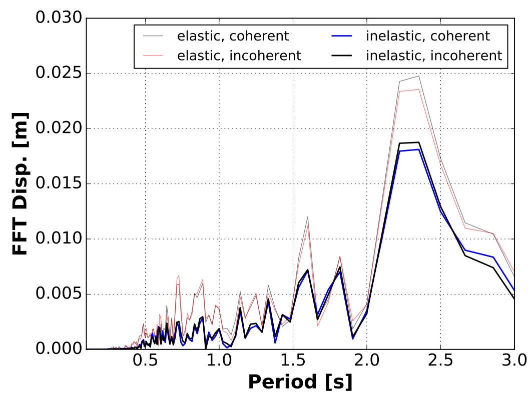

(d) FFT Displacement at the roof level

Figure 4.114: The roof level, low steel building, Baseline Motion 120711 and 120712, elastic Soil Material Model SM-EL1 and inelastic Soil Material Model SM-EP1, X direction. PFA: elastic coherent 0.39g, elastic incoherent 0.39g, inelastic coherent 0.22g and inelastic incoherent 0.22g.

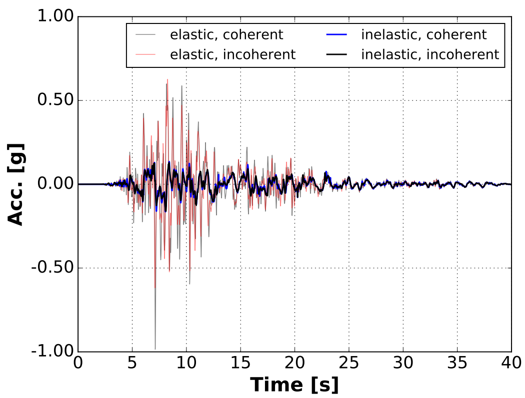

(a) Acceleration at foundation surface

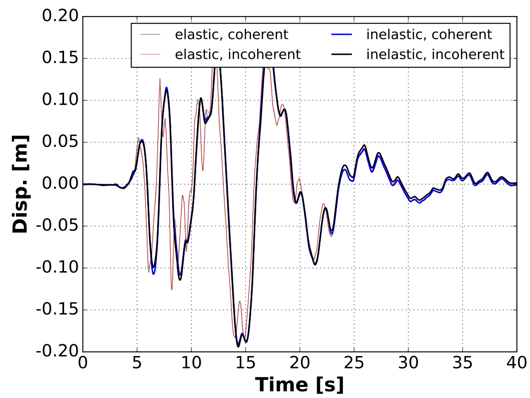

(b) Displacement at foundation surface

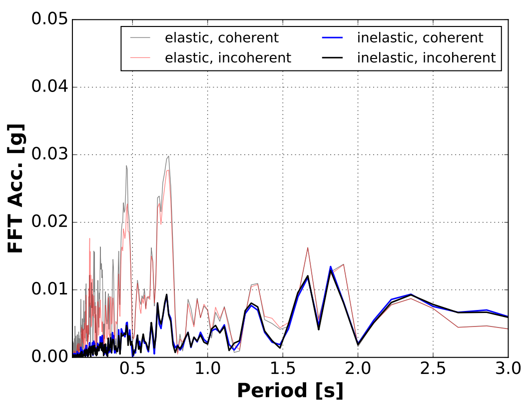

(c) FFT Acceleration at foundation surface

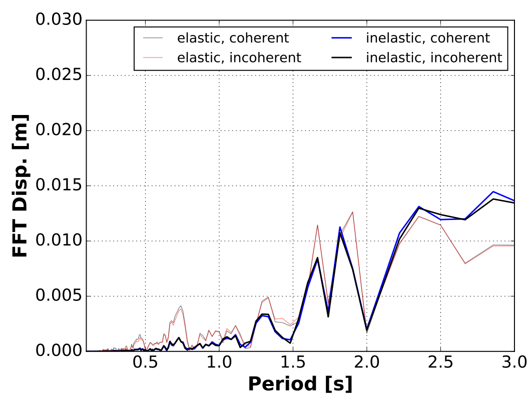

(d) FFT Displacement at foundation surface

Figure 4.115: Foundation surface, low steel building, Baseline Motion 120711 and 120712, elastic Soil Material Model SM-EL1 and inelastic Soil Material Model SM-EP1, Y direction. PGA: elastic coherent 0.98g, elastic incoherent 0.63g, inelastic coherent 0.16g and inelastic incoherent 0.16g.

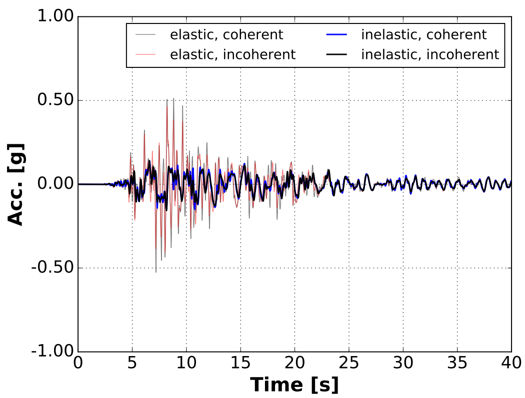

(a) Acceleration at the 1st floor

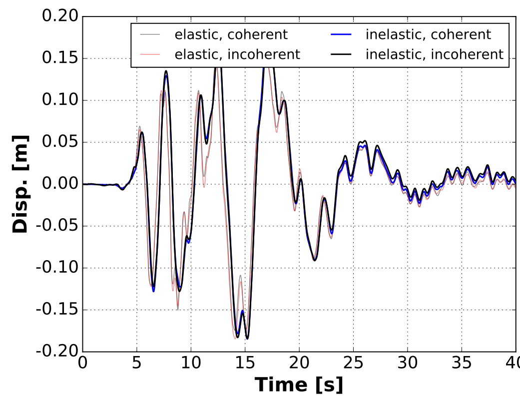

(b) Displacement at the 1st floor

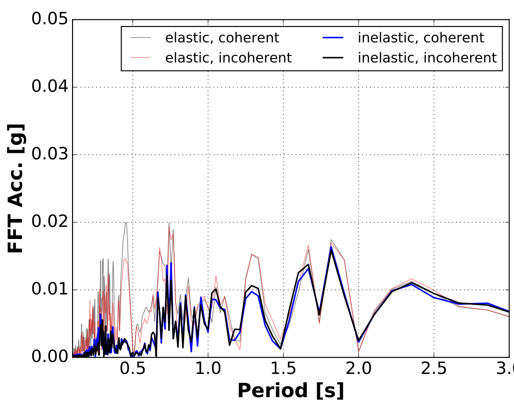

(c) FFT Acceleration at the 1st floor

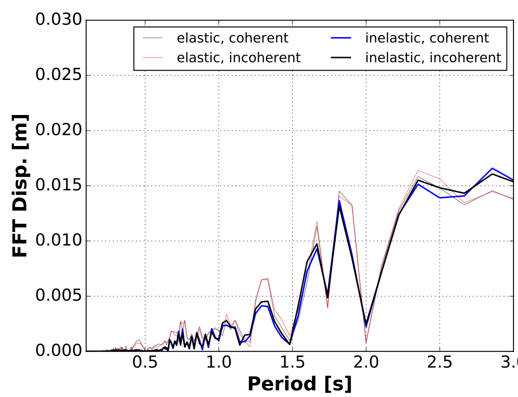

(d) FFT Displacement at the 1st floor

Figure 4.116: The 1st floor, low steel building, Baseline Motion 120711 and 120712, elastic Soil Material Model SM-EL1 and inelastic Soil Material Model SM-EP1, Y direction. PFA: elastic coherent 0.53g, elastic incoherent 0.46g, inelastic coherent 0.15g and inelastic incoherent 0.16g.

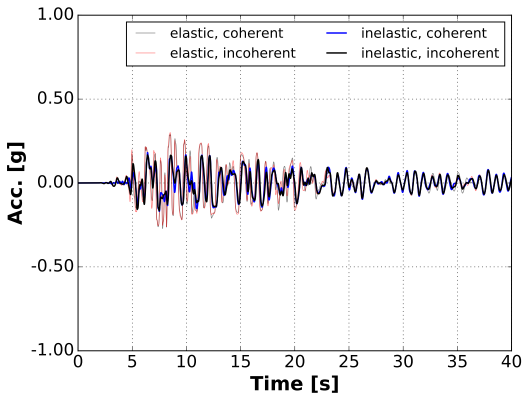

(a) Acceleration at the roof level

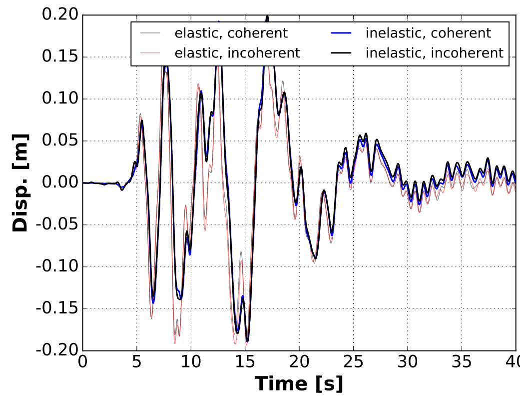

(b) Displacement at the roof level

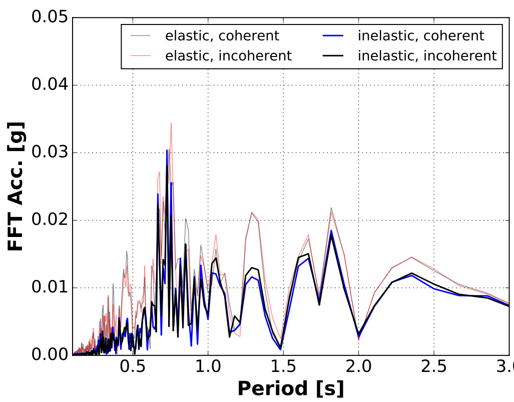

(c) FFT Acceleration at the roof level

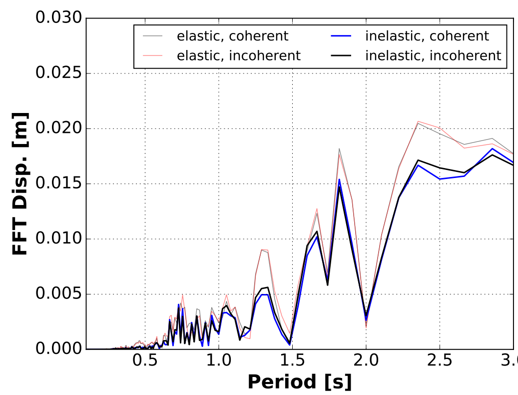

(d) FFT Displacement at the roof level

Figure 4.117: The roof level, low steel building, Baseline Motion 120711 and 120712, elastic Soil Material Model SM-EL1 and inelastic Soil Material Model SM-EP1, Y direction. PFA: elastic coherent 0.29g, elastic incoherent 0.30g, inelastic coherent 0.18g and inelastic incoherent 0.17g.

Table 4.9 shows the input peak acceleration at the ground surface and peak acceleration response (PGA) for different cases. It is important to note that the ground surface peak acceleration, shown in Table 4.9 as surface input, is the free-field motions that were used to perform deconvolution (Kramer, 1996) to a certain depth, and then motions from a depth are propagated upward through a linear and/or nonlinear soil and soil-structure system. A note on locations of seismic motion measurement points is provided in section 4.1.5 on Page 76. It is also noted that all the results for structural response (Foundation surface, First floor, Roof level) presented in Table 4.9 are obtained in the middle of the model, at respective elevations.

Table 4.9: Comparison of input and response PGAs and PFAs for different simulation cases of low steel building, Baseline Motion 120711 and 120712, elastic Soil Material Model SM-EL1 and inelastic Soil Material Model SM-EP1.

		Elastic coherent	Elastic incoherent	Inelastic coherent	Inelastic incoherent
	Free Field Surface input	0.95	0.95	0.95	0.95
PGA/PFA [g]	Foundation surface	0.95	0.88	0.14	0.15
X positive	First floor	0.65	0.55	0.14	0.16
	Roof floor	0.39	0.39	0.22	0.22
	Free Field Surface input	0.99	0.99	0.99	0.99
PGA/PFA [g]	Foundation surface	0.98	0.60	0.15	0.14
X negative	First floor	0.61	0.47	0.20	0.17
	Roof level	0.36	0.37	0.20	0.19
	Free Field Surface input	0.62	0.62	0.62	0.62
PGA/PFA [g]	Foundation surface	0.60	0.63	0.14	0.13
Y positive	First floor	0.51	0.46	0.14	0.14
	Roof level	0.29	0.30	0.18	0.17
	Free Field Surface input	0.98	0.98	0.98	0.98
PGA/PFA [g]	Foundation surface	0.99	0.62	0.16	0.16
Y negative	First floor	0.53	0.41	0.15	0.16
	Roof level	0.27	0.26	0.17	0.17

Figure 4.118 and 4.119 compare acceleration FFT between free-field motion and foundation surface of the 2-story low steel building.

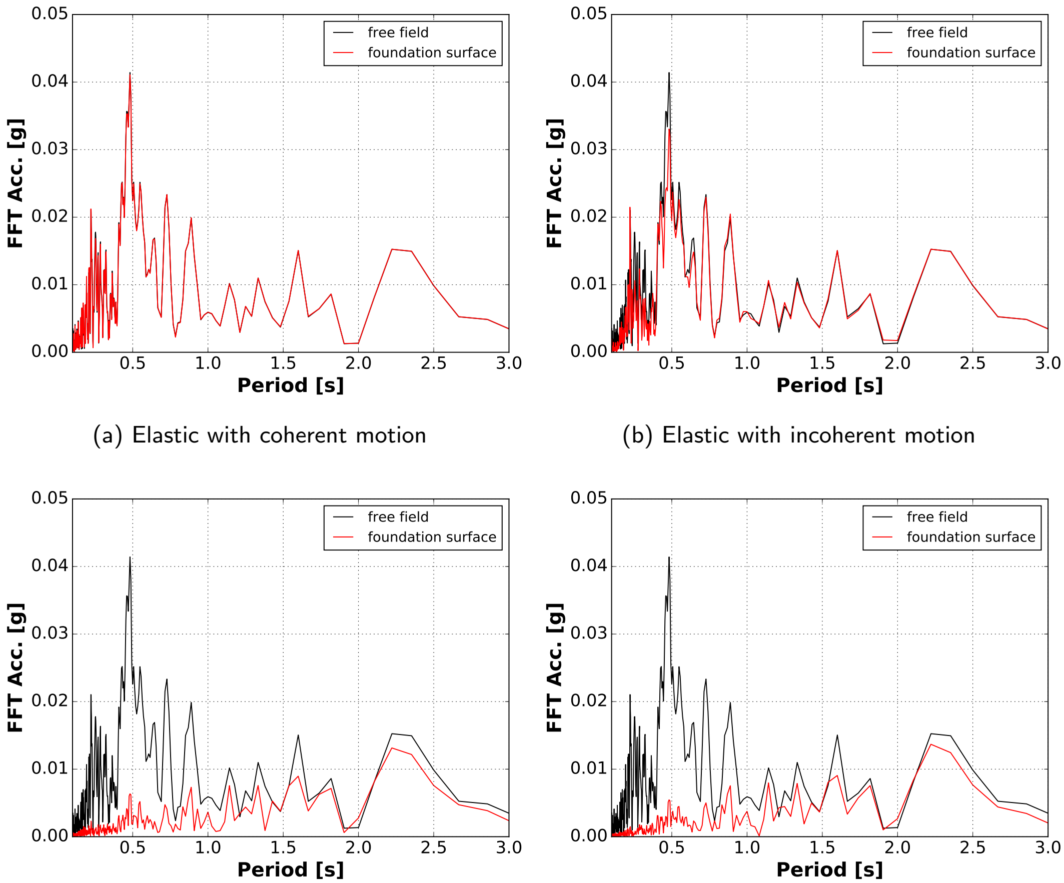

(a) Elastic with coherent motion

(b) Elastic with incoherent motion

(c) Inelastic with coherent motion

(d) Inelastic with incoherent motion

Figure 4.118: Comparison of acceleration FFT between free-field and foundation surface, X direction, Baseline Motion 120711 and 120712, Soil Material Model SM-EP1.

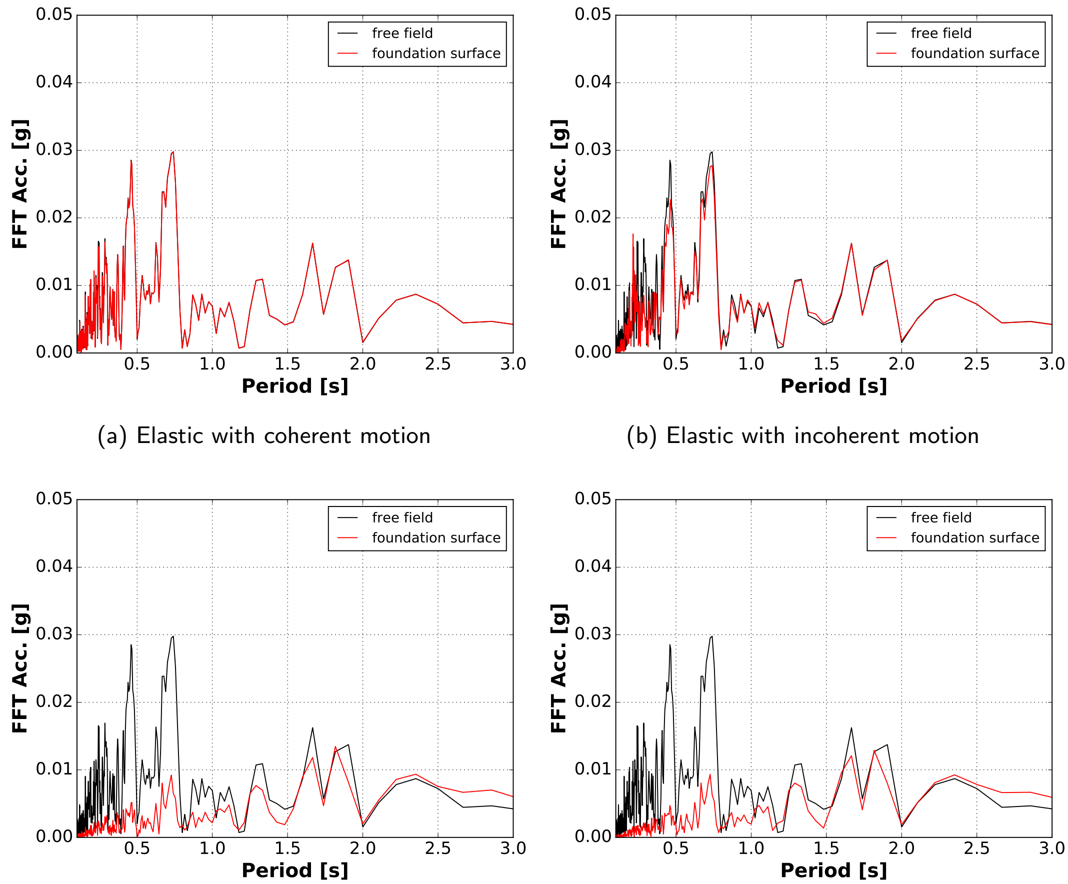

(a) Elastic with coherent motion

(b) Elastic with incoherent motion

(c) Inelastic with coherent motion

(d) Inelastic with incoherent motion

Figure 4.119: Comparison of acceleration FFT between free-field and foundation surface, Y direction, Baseline Motion 120711 and 120712, Soil Material Model SM-EP1.

Figure 4.120 compares the ratio of acceleration FFT between foundation surface of the two-story, low steel frame building and free-field motions.

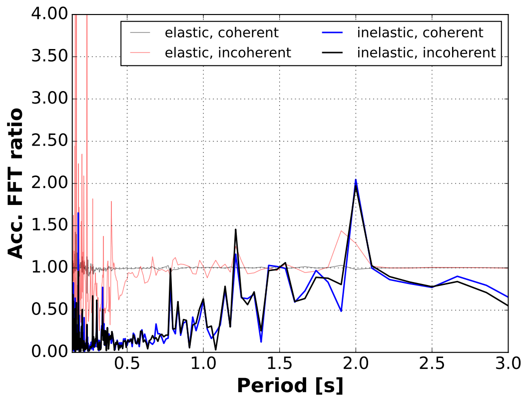

(a) X direction

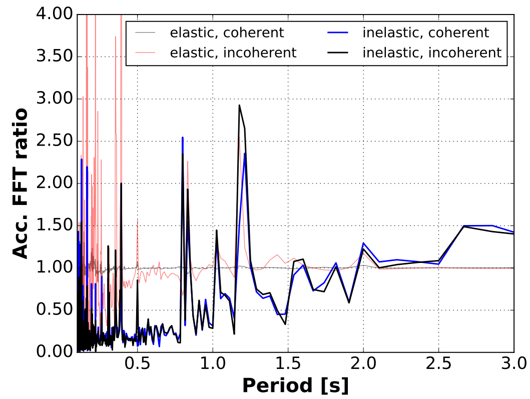

(b) Y direction

Figure 4.120: Comparison of acceleration FFT ratio between foundation surface of the 2 story, low steel frame building and free-field motions, Baseline Motion 120711 and 120712, elastic Soil Material Model SM-EL1 and inelastic Soil Material Model SM-EP1.

Figure 4.121 and 4.122 compare acceleration FFT response of foundation surface of low steel building under coherent and incoherent motion within elastic simulation and inelastic simulation.

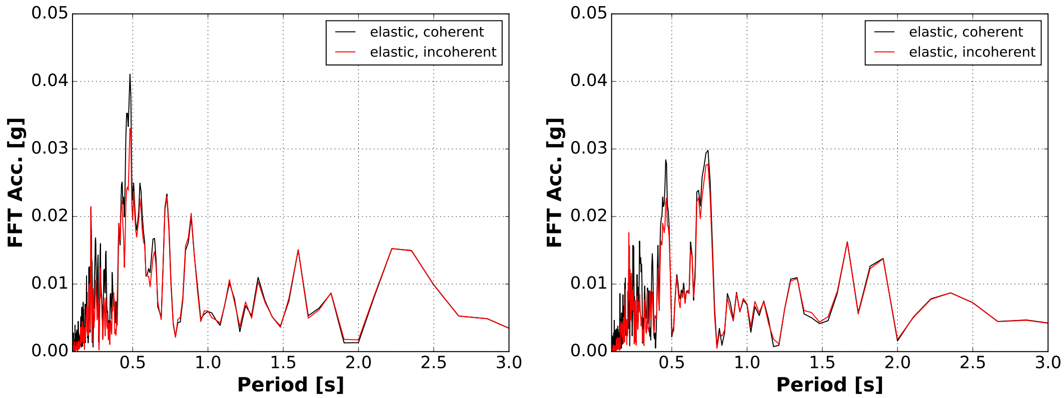

(a) X direction (b) Y direction

Figure 4.121: Comparison of acceleration FFT of foundation surface between elastic, coherent case and elastic, incoherent case, Baseline Motion 120711 and 120712, elastic Soil Material Model SM-EL1: (a) Longitudinal X direction (b) Transverse Y direction.

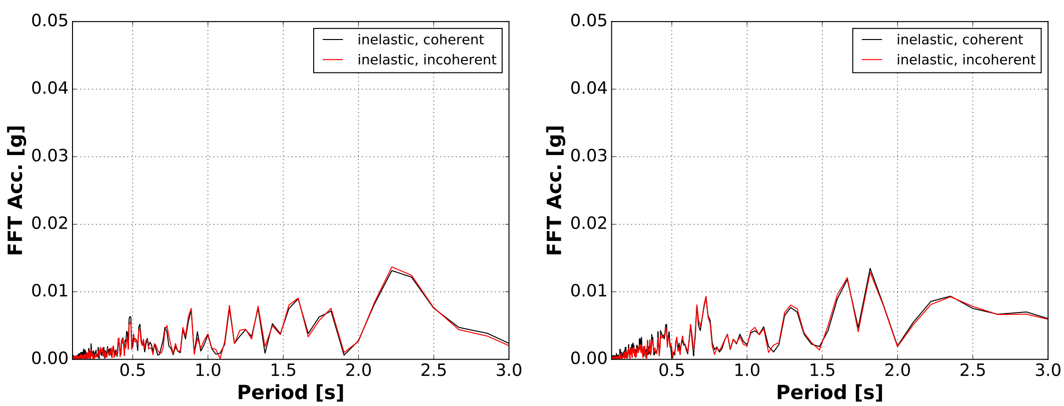

(a) X direction (b) Y direction

Figure 4.122: Comparison of acceleration FFT of foundation surface between inelastic, coherent case and inelastic, incoherent case, Baseline Motion 120711 and 120712, Soil Material Model SM-EP1: (a) Longitudinal X direction (b) Transverse Y direction.

Figure 4.123 shows the acceleration FFT ratio of foundation surface under coherent and incoherent motion $u_{\text{foundation,incoherent}}/u_{\text{foundation,coherent}}$ within elastic and inelastic simulations.

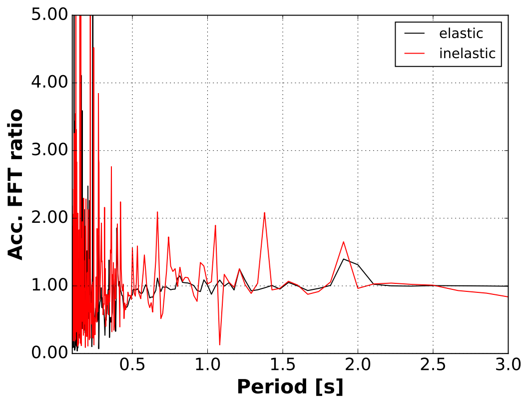

(a) X direction

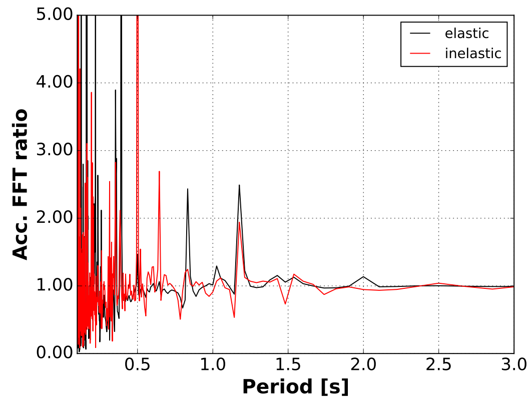

(b) Y direction

Figure 4.123: Ratio of acceleration FFT of foundation surface under coherent and incoherent motions within elastic and inelastic simulations, Baseline Motion 120711 and 120712, Soil Material Model SM-EP1: (a) Longitudinal X direction (b) Transverse Y direction.

Figure 4.124 and 4.125 compare response spectra of free-field motion and foundation surface in both longitudinal (X) direction and transverse (Y) direction.

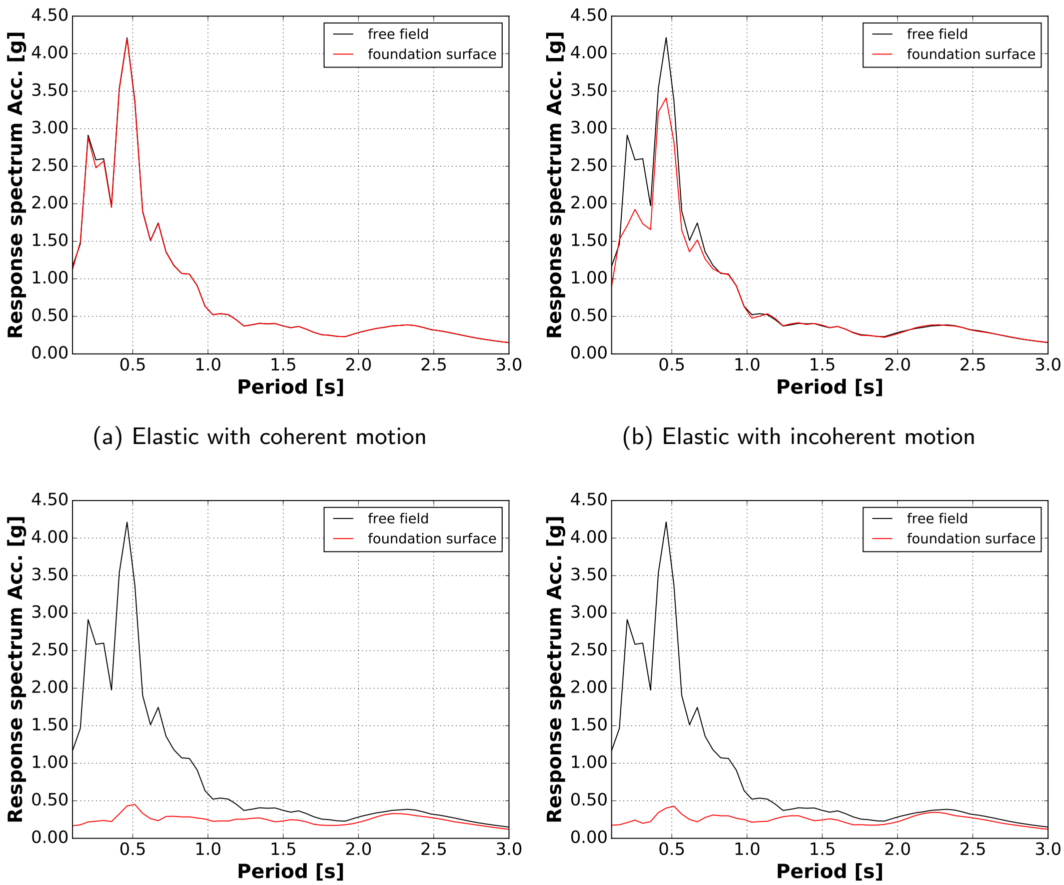

(a) Elastic with coherent motion

(b) Elastic with incoherent motion

(c) Inelastic with coherent motion

(d) Inelastic with incoherent motion

Figure 4.124: Comparison of response spectra between foundation surface and free-field, X direction, Baseline Motion 120711 and 120712, Soil Material Model SM-EP1.

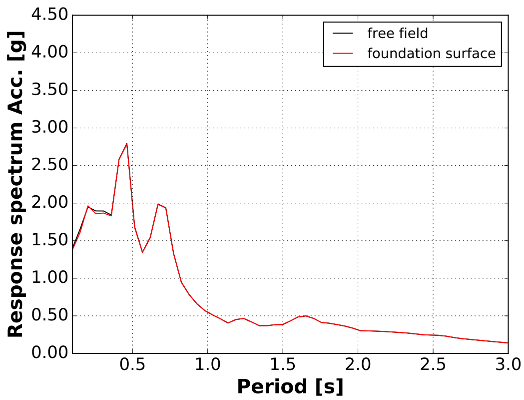

(a) Elastic with coherent motion

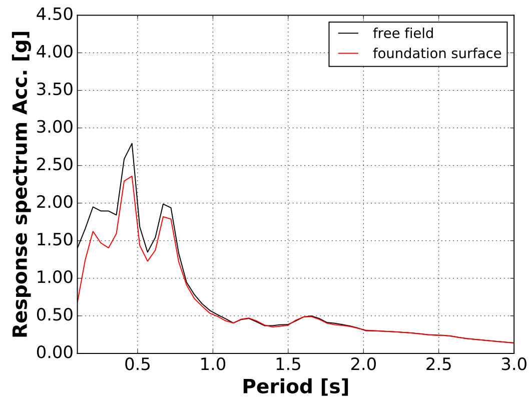

(b) Elastic with incoherent motion

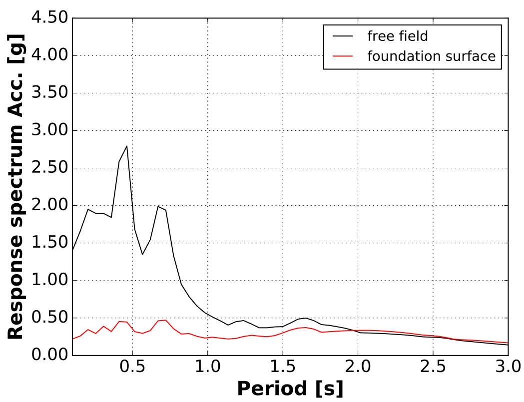

(c) Inelastic with coherent motion

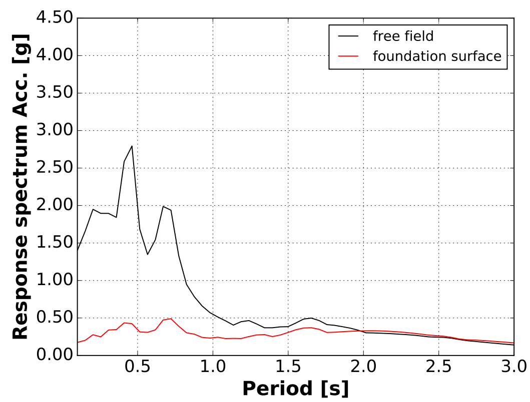

(d) Inelastic with incoherent motion

Figure 4.125: Comparison of response spectra between foundation surface and free-field, Y direction, Baseline Motion 120711 and 120712, Soil Material Model SM-EP1.

Figure 4.126 compares the ratio of response spectra (RRS) between foundation surface response and free-field.

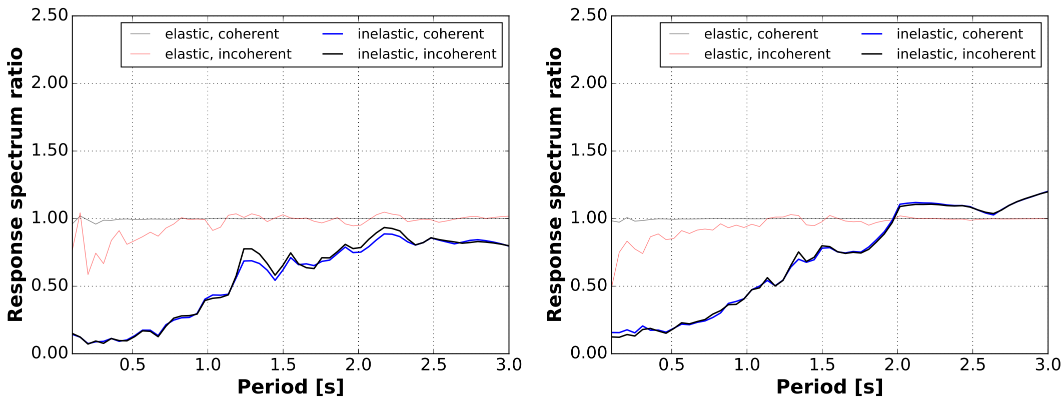

(a) X direction (b) Y direction

Figure 4.126: Comparison of ratio of response spectra (RRS) between foundation surface of the 2 story, low steel frame building and free-field motions, Baseline Motion 120711 and 120712, elastic Soil Material Model SM-EL1 and inelastic Soil Material Model SM-EP1.

Figure 4.127 and 4.128 compare acceleration FFT between roof level and foundation surface of the 2-story low steel building.

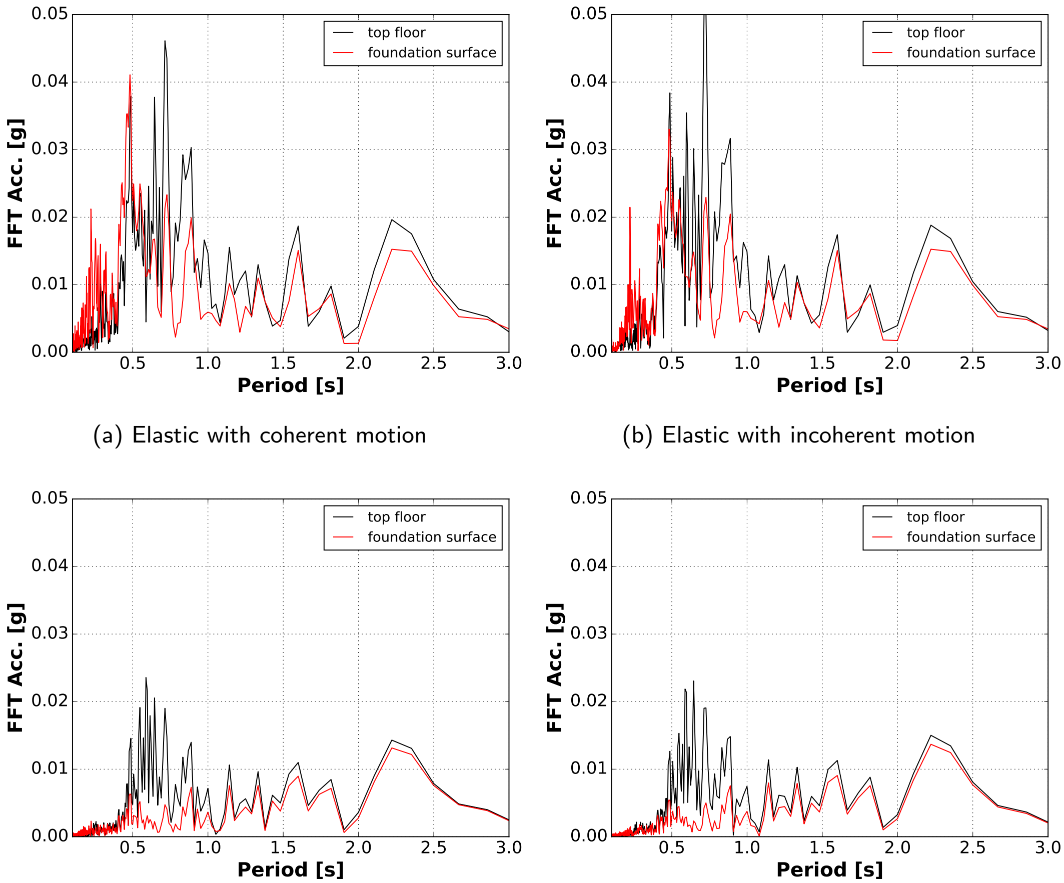

(a) Elastic with coherent motion

(b) Elastic with incoherent motion

(c) Inelastic with coherent motion

(d) Inelastic with incoherent motion

Figure 4.127: Comparison of acceleration FFT between the roof level and foundation surface, X direction, Baseline Motion 120711 and 120712, Soil Material Model SM-EP1.

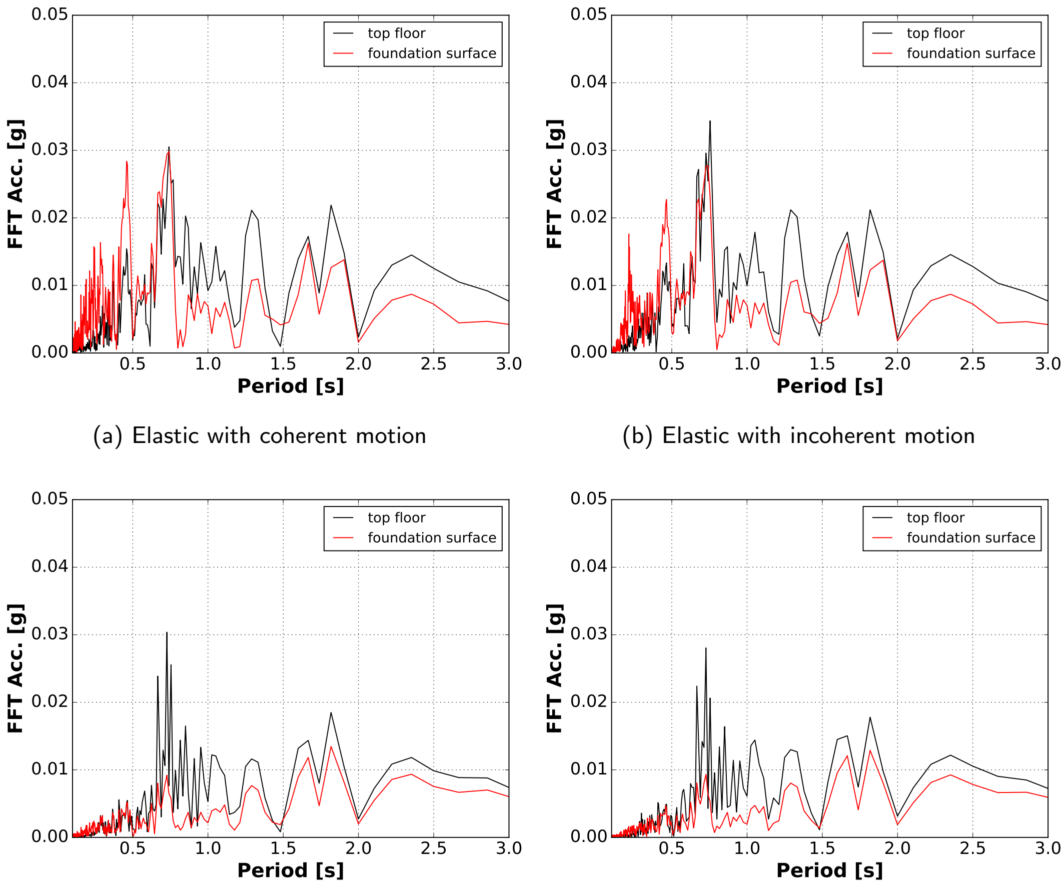

(a) Elastic with coherent motion

(b) Elastic with incoherent motion

(c) Inelastic with coherent motion

(d) Inelastic with incoherent motion

Figure 4.128: Comparison of acceleration FFT between the roof level and foundation surface, Y direction, Baseline Motion 120711 and 120712, Soil Material Model SM-EP1.

Figure 4.129 compares the ratio of acceleration FFT between roof level and foundation surface of the 2 story, low steel frame building.

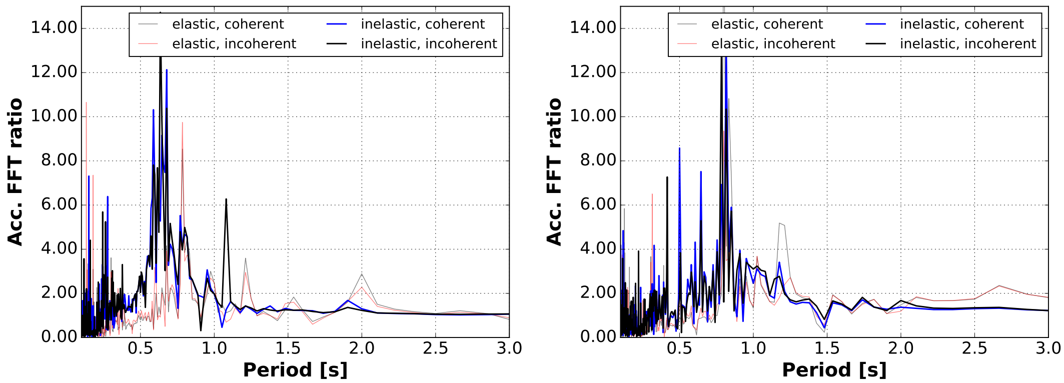

(a) X direction

(b) Y direction

Figure 4.129: Comparison of acceleration FFT ratio between roof level and foundation surface of the 2 story, low steel frame building, Baseline Motion 120711 and 120712, elastic Soil Material Model SM-EL1 and inelastic Soil Material Model SM-EP1.

Figure 4.130 compares the base shear of two-story, low steel frame building for four different cases in both longitudinal and transverse direction.

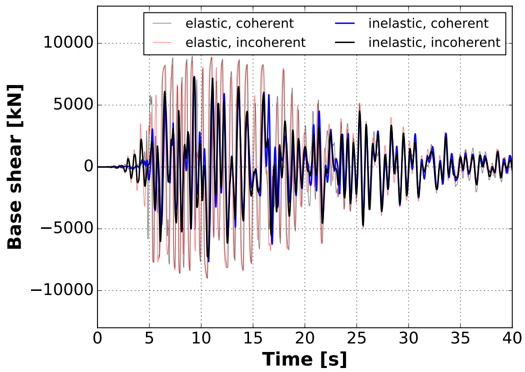

(a) Longitudinal base shear (X direction)

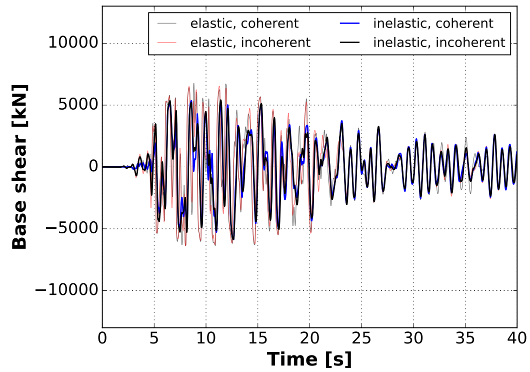

(b) Transverse base shear (Y direction)

Figure 4.130: Comparison of base shear of low, steel frame building, Baseline Motion 120711 and 120712, elastic Soil Material Model SM-EL1 and inelastic Soil Material Model SM-EP1.

Spread foundation vs Slab foundation

Dynamic responses of three different types of foundation are compared: Independent spread foundation, connected spread foundation, and mat-slab foundation.

Figure 4.131 and 4.132 compare dynamic response of foundation surface of the 2-story low steel building for three different types of foundations.

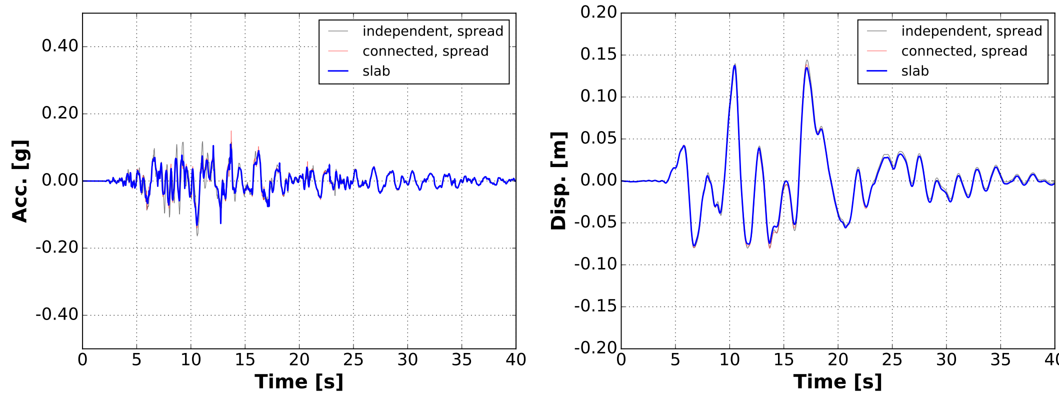

(a) Acceleration at foundation surface

(b) Displacement at foundation surface

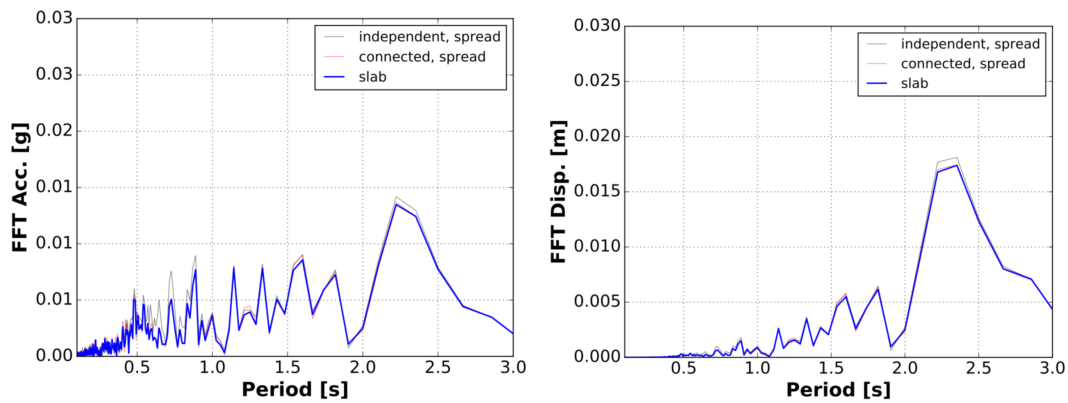

(c) FFT Acceleration at foundation surface

(d) FFT Displacement at foundation surface

Figure 4.131: Comparison of foundation surface responses for different types of foundation, X direction, Baseline Motion 120711 and 120712, Soil Material Model SM-EP1.

Figure 4.133 compares response spectra of foundation surface response of the two-story, low steel frame building for different types of foundation.

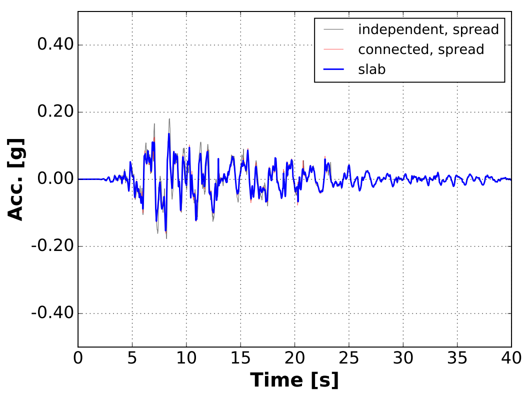

(a) Acceleration at foundation surface

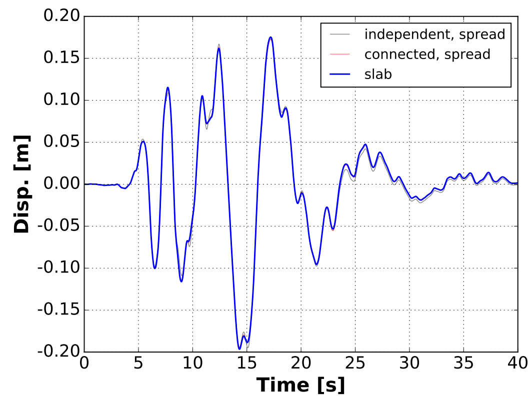

(b) Displacement at foundation surface

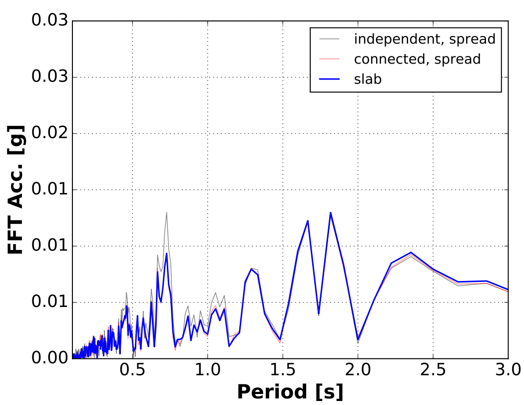

(c) FFT Acceleration at foundation surface

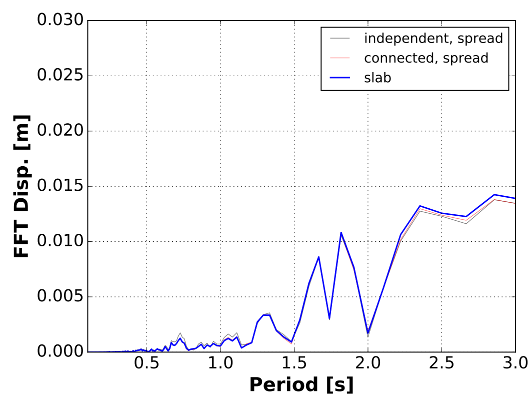

(d) FFT Displacement at foundation surface

Figure 4.132: Comparison of foundation surface responses for different types of foundation, Y direction, Baseline Motion 120711 and 120712, Soil Material Model SM-EP1.

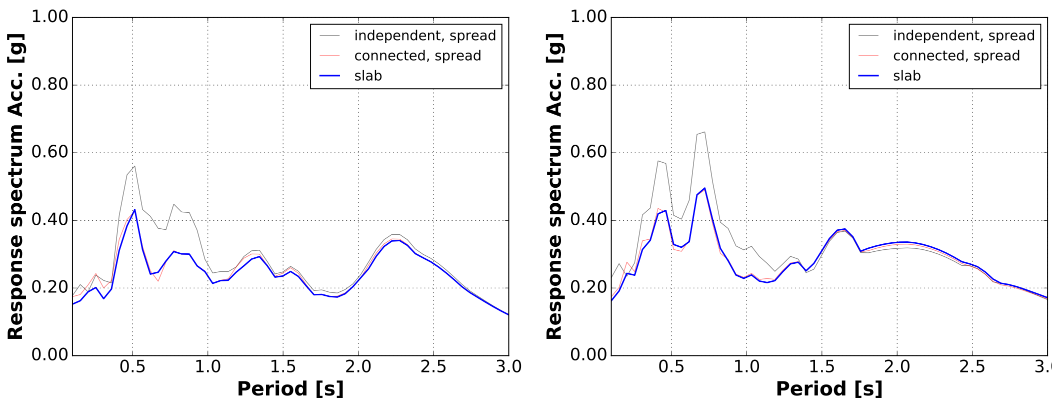

(a) X direction (b) Y direction

Figure 4.133: Comparison of spectra acceleration of foundation surface responses for different types of foundation, Baseline Motion 120711 and 120712, Soil Material Model SM-EP1.

Design Earthquake vs. Maximum Considered Earthquake

Figures 4.134 and 4.135 compare the base averaging effects (ratio of acceleration FFT and response spectra between foundation surface and free-field) under Design Earthquake (DE) and Maximum Considered Earthquake (MCER). It is noted that the scaling factor between MCER and DE is 2.74.

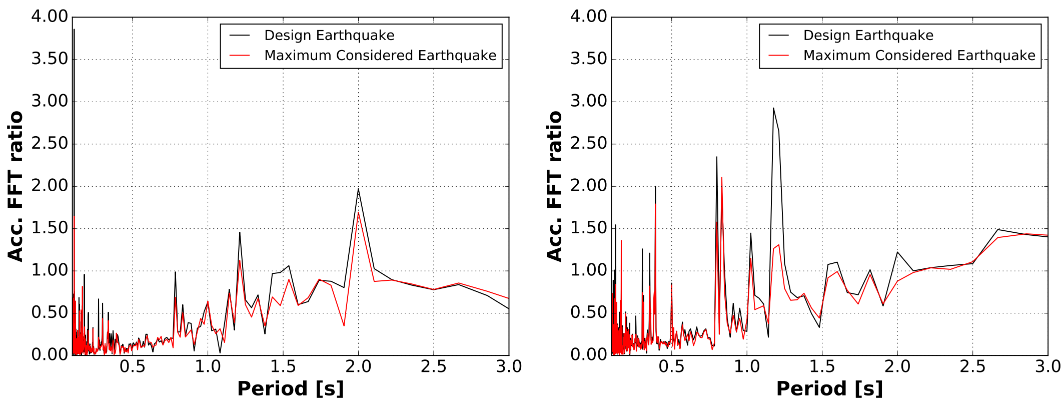

(a) X direction (b) Y direction

Figure 4.134: Comparison of acceleration FFT ratio between foundation surface and free-field for Design Earthquake and Maximum Considered Earthquake, Soil Material Model SM-EP1.

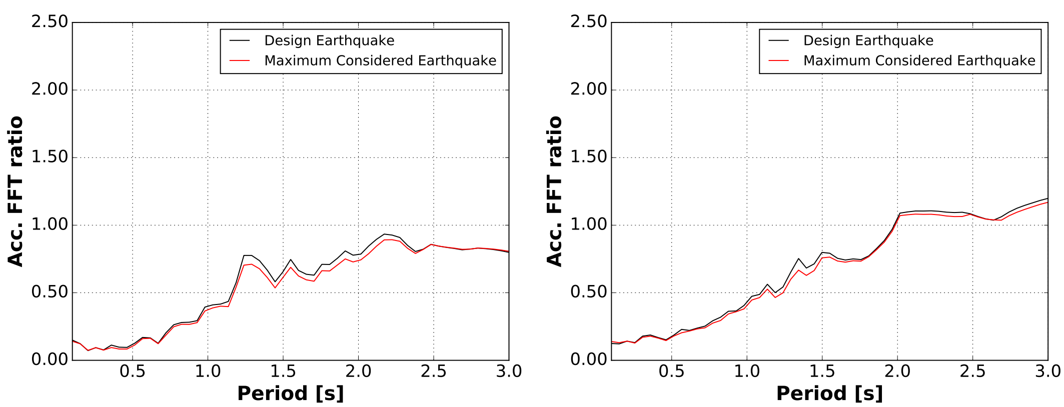

(a) X direction (b) Y direction

Figure 4.135: Comparison of spectra acceleration between foundation surface and free-field for Design Earthquake and Maximum Considered Earthquake, Soil Material Model SM-EP1.

4.5.4 Earthquake Soil-Structure Interaction Results - 1C coherent motion

Elastic vs Inelastic

Figure 4.136 to Figure 4.138 compare the elastic and inelastic response of two-story steel frame building with spread foundation.

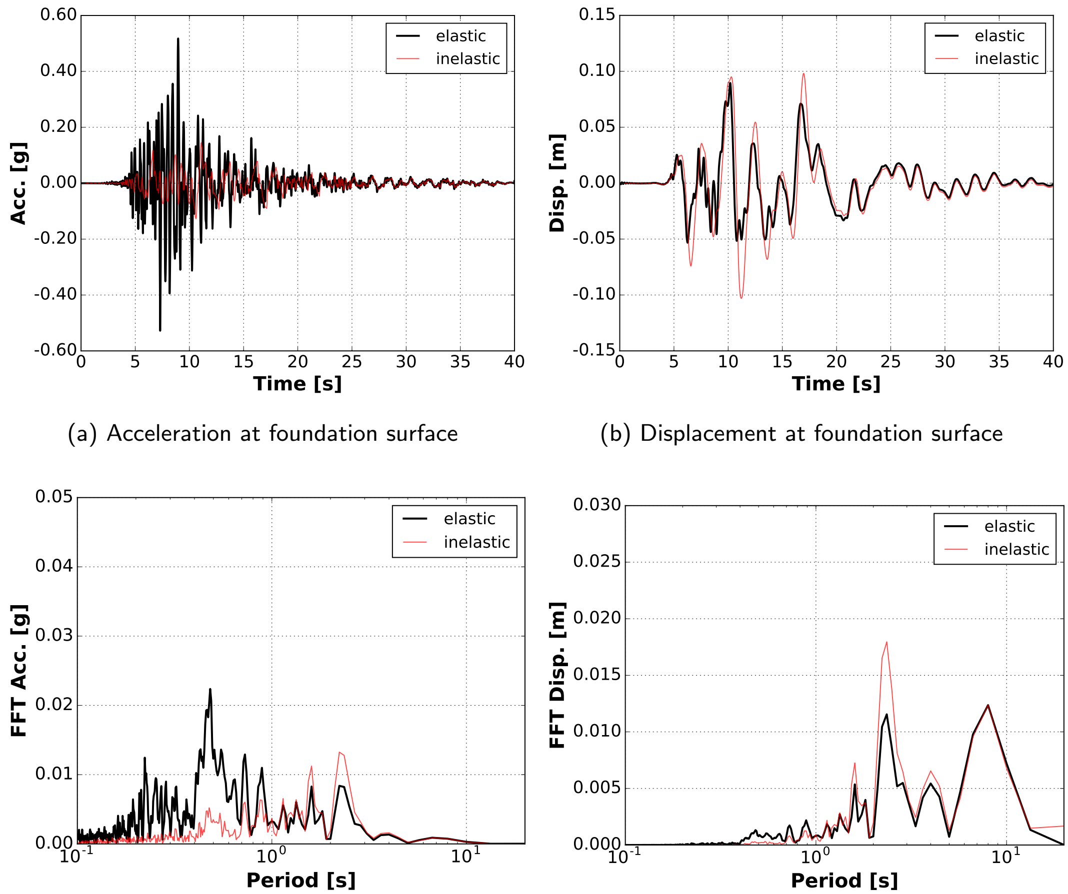

(a) Acceleration at foundation surface

(b) Displacement at foundation surface

(c) FFT Acceleration at foundation surface

(d) FFT Displacement at foundation surface

Figure 4.136: Elastic vs inelastic, foundation surface, low steel building, spread foundation, baseline coherent motion 120711, elastic Soil Material Model SM-EL1 and inelastic Soil Material Model SM-EP1, X direction.

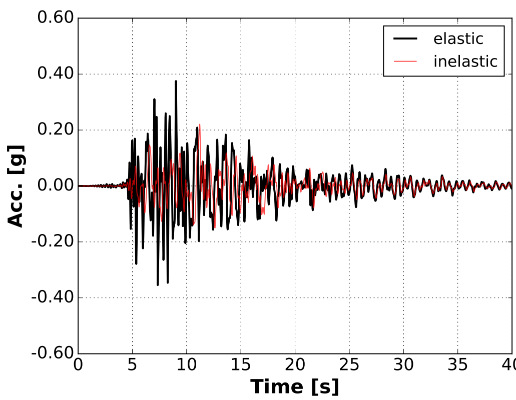

(a) Acceleration at the first floor

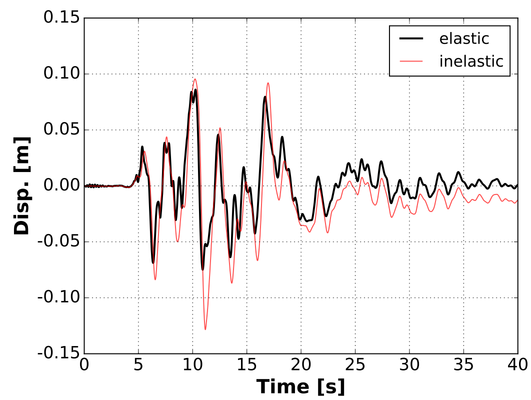

(b) Displacement at the first floor

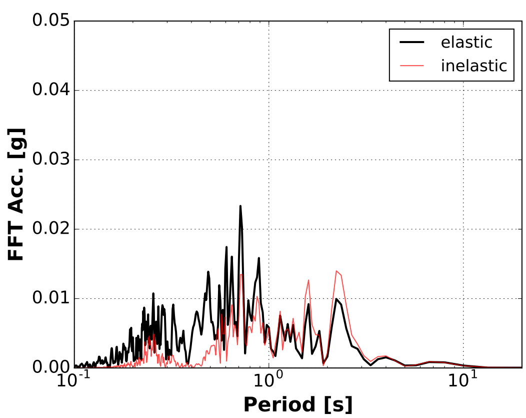

(c) FFT Acceleration at the first floor

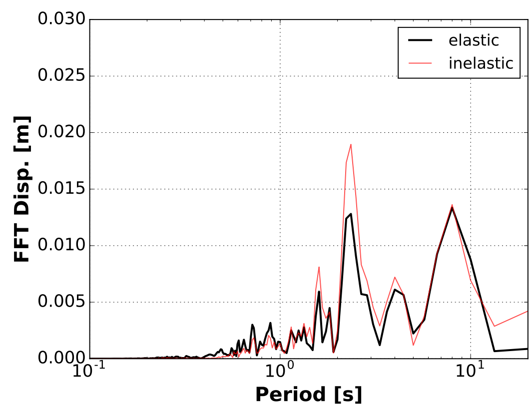

(d) FFT Displacement at the first floor

Figure 4.137: Elastic vs inelastic, first floor, low steel building, spread foundation, baseline coherent motion 120711, elastic Soil Material Model SM-EL1 and inelastic Soil Material Model SM-EP1, X direction.

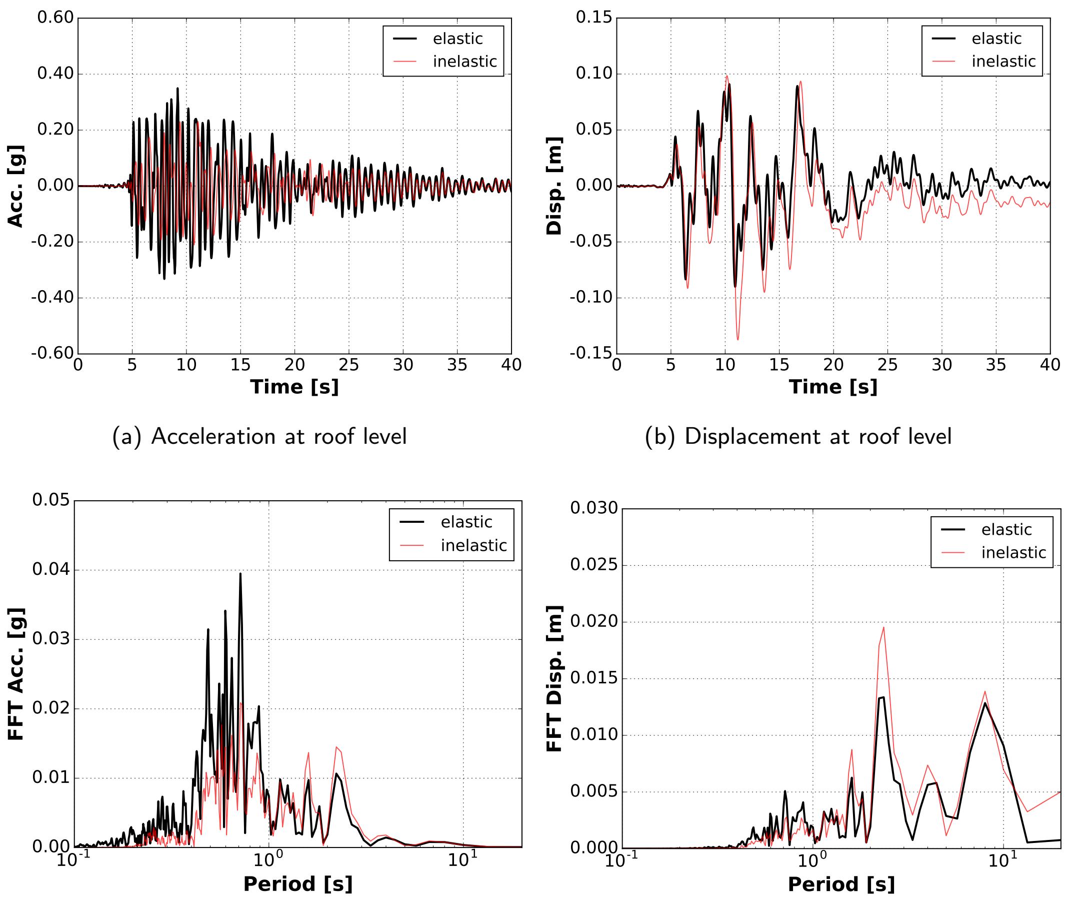

(a) Acceleration at roof level

(b) Displacement at roof level

(c) FFT Acceleration at roof level

(d) FFT Displacement at roof level

Figure 4.138: Elastic vs inelastic, roof level, low steel building, spread foundation, baseline coherent motion 120711, elastic Soil Material Model SM-EL1 and inelastic Soil Material Model SM-EP1, X direction.

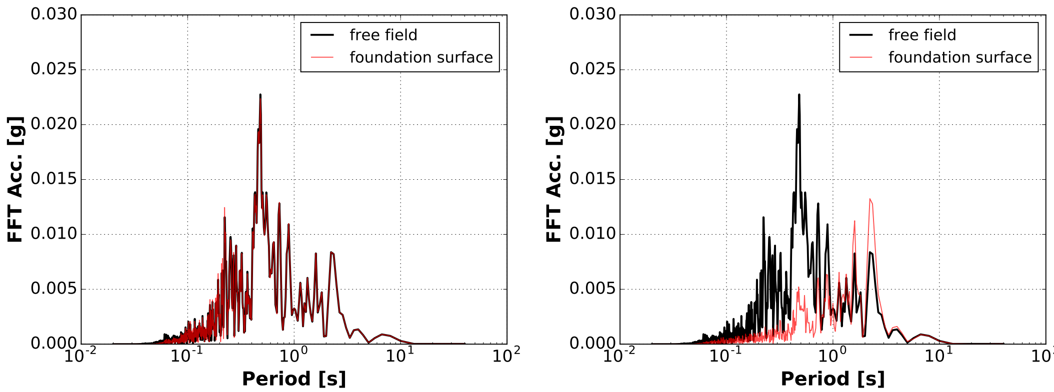

(a) Free-field vs Elastic SSI

(b) Free-field vs Inelastic SSI

Figure 4.139: Acc FFT: free-field vs foundation surface, low steel building, spread foundation, baseline coherent motion 120711, baseline coherent motion 120711, X direction: (a) Elastic Soil Material Model SM-EL1 (b) Inelastic Soil Material Model SM-EP1.

Spread foundation vs Slab foundation

Figure 4.140 to Figure 4.142 compare the inelastic response of low steel building with spread foundation and mat-slab foundation.

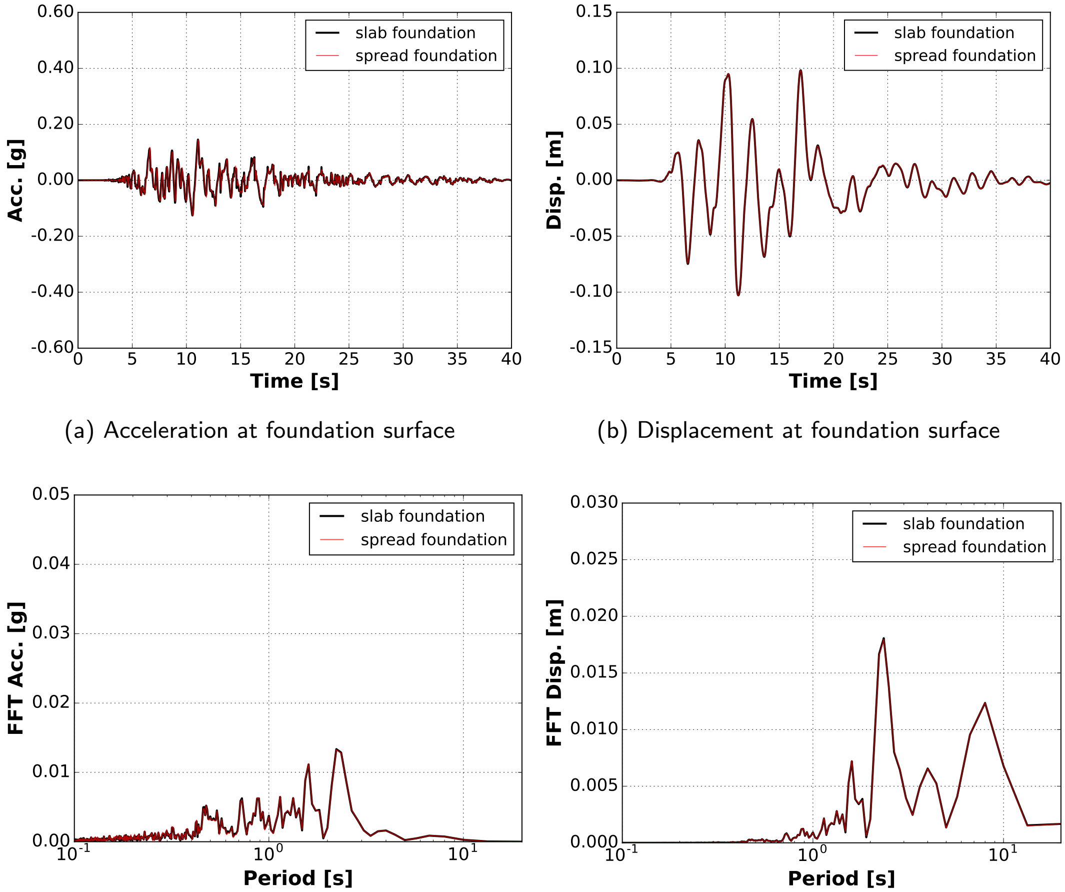

(a) Acceleration at foundation surface

(b) Displacement at foundation surface

(c) FFT Acceleration at foundation surface

(d) FFT Displacement at foundation surface

Figure 4.140: Spread vs mat-slab foundation, inelastic response, foundation surface, low steel building, baseline coherent motion 120711, Soil Material Model SM-EP1, X direction.

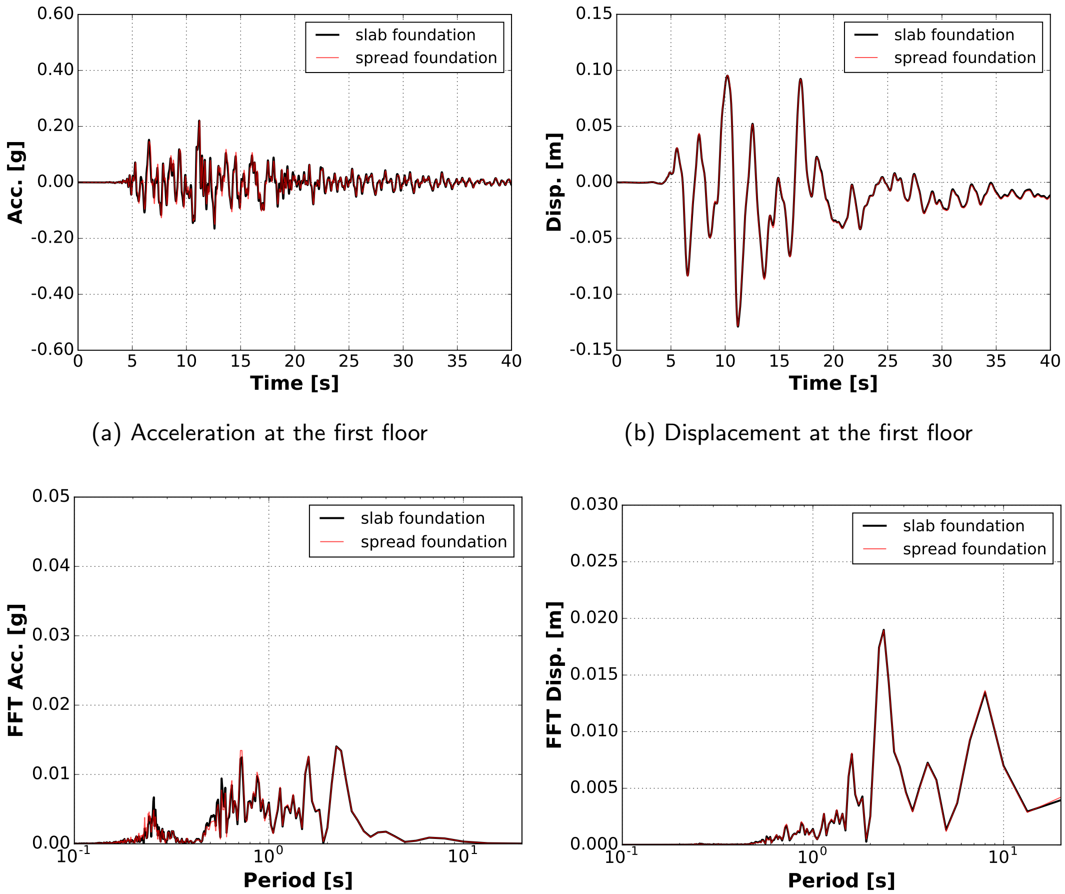

(a) Acceleration at the first floor

(b) Displacement at the first floor

(c) FFT Acceleration at the first floor

(d) FFT Displacement at the first floor

Figure 4.141: Spread vs mat-slab foundation, inelastic response, first floor, low steel building, baseline coherent motion 120711, Soil Material Model SM-EP1, X direction.

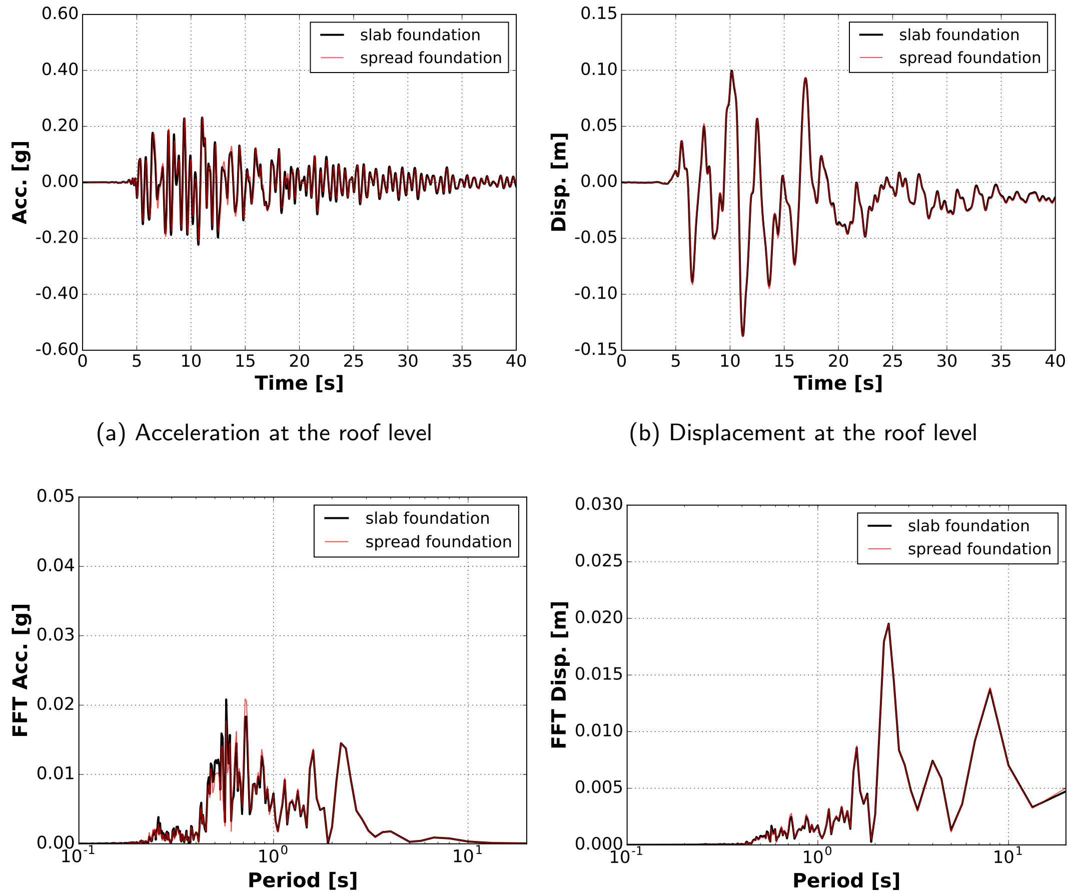

(a) Acceleration at the roof level

(b) Displacement at the roof level

(c) FFT Acceleration at the roof level

(d) FFT Displacement at the roof level

Figure 4.142: Spread vs mat-slab foundation, inelastic response, roof level, low steel building, baseline coherent motion 120711, Soil Material Model SM-EP1, X direction.

4.5.5 Earthquake Soil-Structure Interaction under 1C Incoherent Motion

This section provides comparative results for soil-structure interaction analysis of low steel building under both 1C coherent and incoherent motions.

- Linear elastic soil and nonlinear fiber-based structural modeling with spread foundation

  Figures 4.143 to 4.145 present the dynamic response of the low, steel building with spread foundation under both coherent and incoherent motion. Elastic Soil Material Model SM-EL1 is used here.

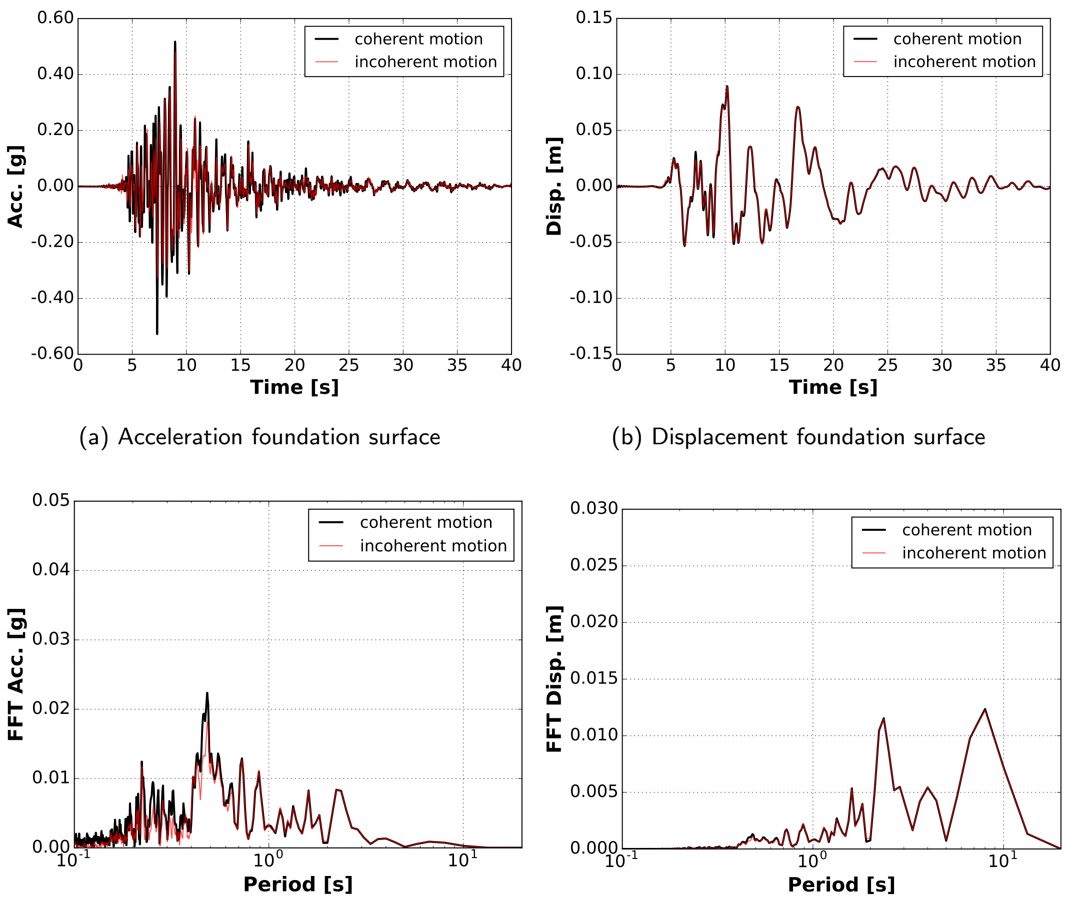

(a) Acceleration foundation surface

(b) Displacement foundation surface

(c) FFT Acceleration foundation surface

(d) FFT Displacement foundation surface

Figure 4.143: Coherent vs Incoherent of Baseline Motion 120711, elastic Soil Material Model SM-EL1, foundation surface, low steel building, spread foundation, X direction.

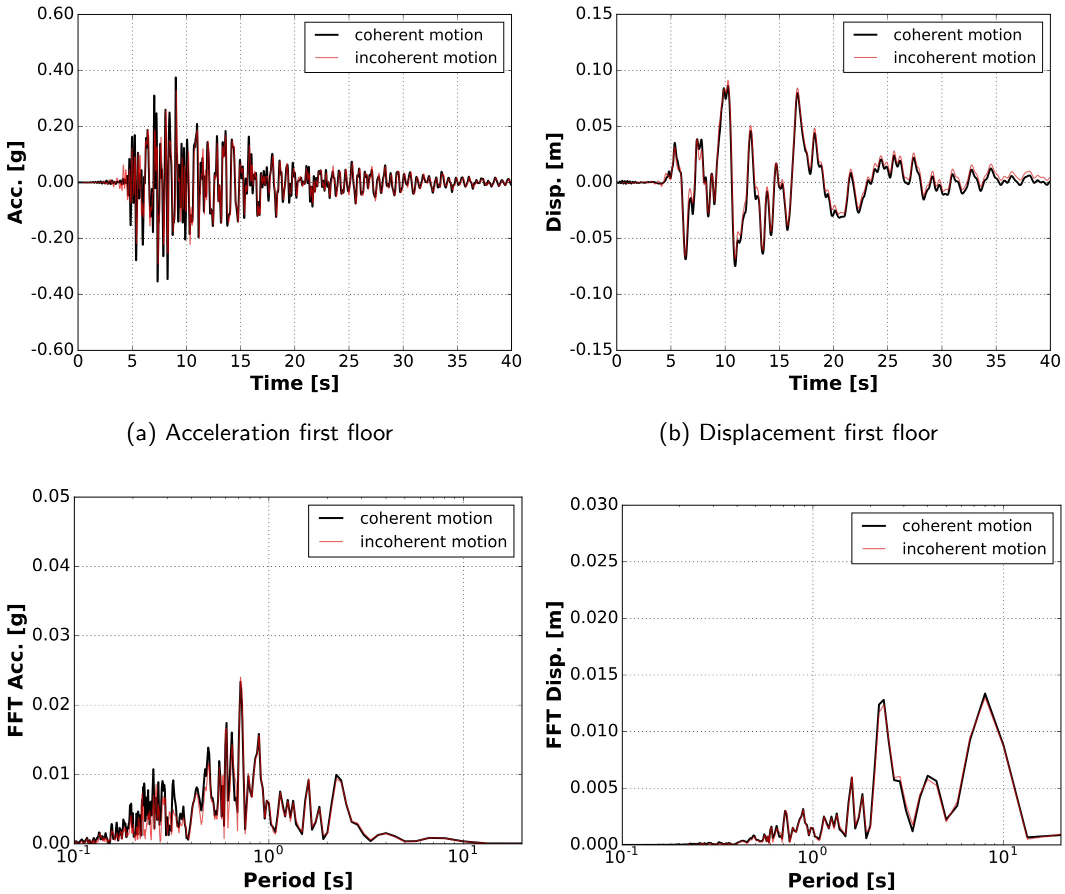

(a) Acceleration first floor

(b) Displacement first floor

(c) FFT Acceleration first floor

(d) FFT Displacement first floor

Figure 4.144: Coherent vs Incoherent Baseline Motion 120711, elastic Soil Material Model SM-EL1, first floor, low steel building, spread foundation, X direction.

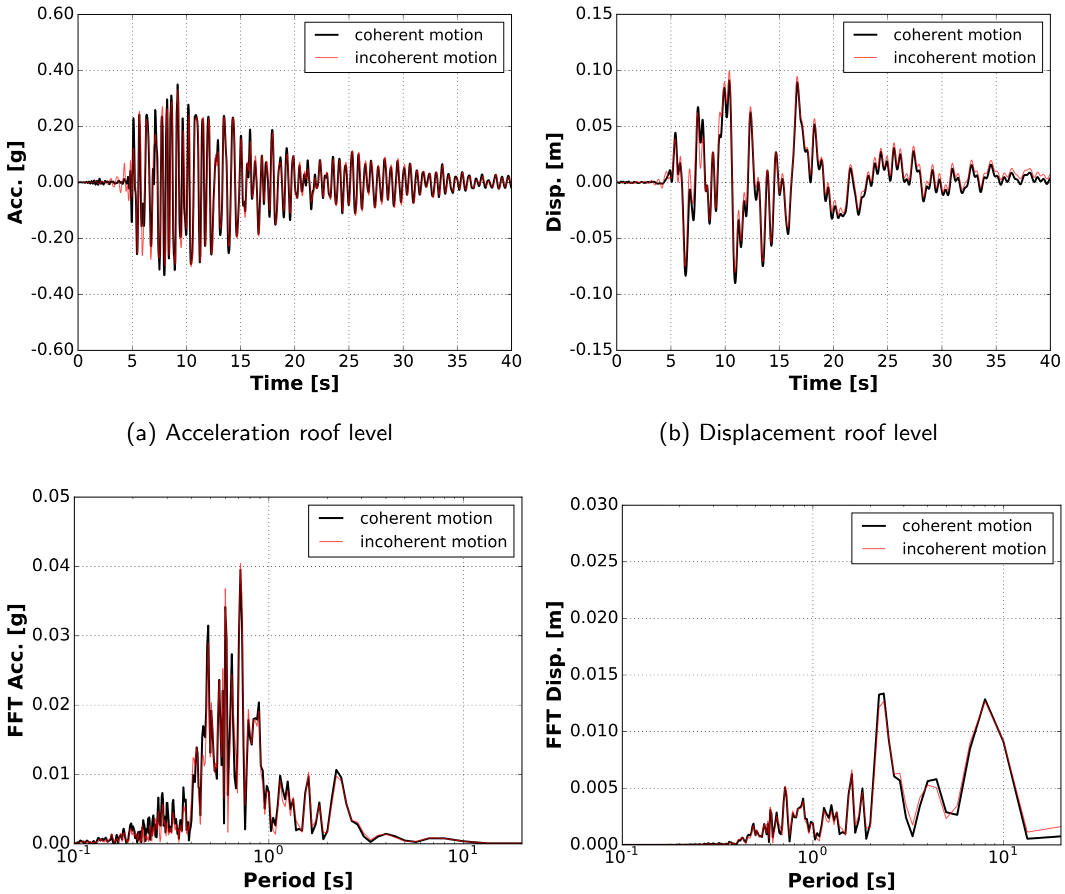

(a) Acceleration roof level

(b) Displacement roof level

(c) FFT Acceleration roof level

(d) FFT Displacement roof level

Figure 4.145: Coherent vs Incoherent Baseline Motion 120711, elastic Soil Material Model SM-EL1, roof level, low steel building, spread foundation, X direction.

- Nonlinear inelastic soil and nonlinear fiber-based structural modeling with spread motion

  Figure 4.146 to 4.148 present the dynamic response of the low, steel building with spread foundation under both coherent and incoherent motion. Inelastic behavior of soil is simulated.

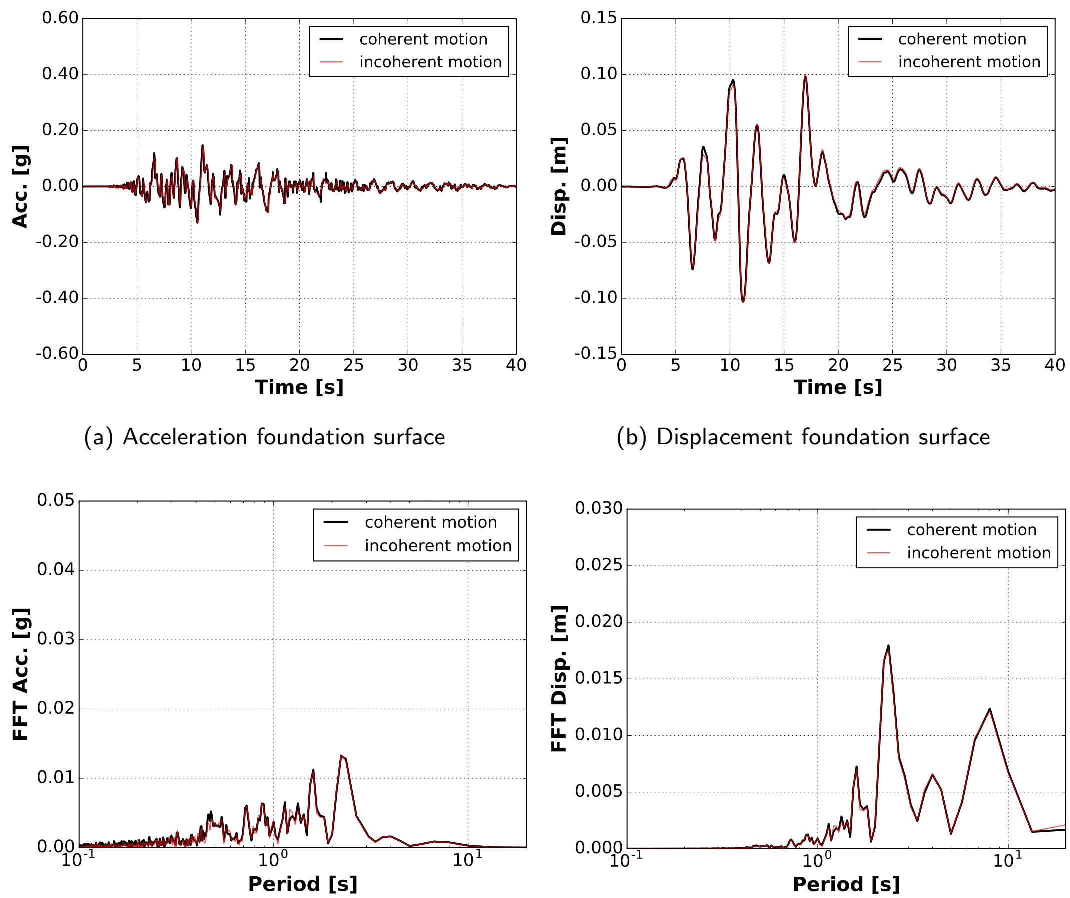

(a) Acceleration foundation surface

(b) Displacement foundation surface

(c) FFT Acceleration foundation surface

(d) FFT Displacement foundation surface

Figure 4.146: Coherent vs Incoherent Baseline Motion 120711, inelastic response, Soil Material Model SM-EP1, foundation surface, low steel building, spread foundation, X direction.

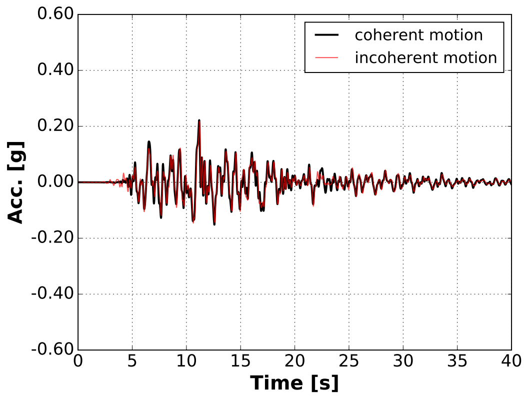

(a) Acceleration first floor

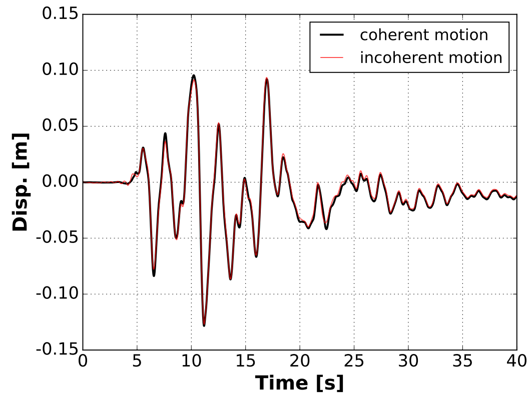

(b) Displacement first floor

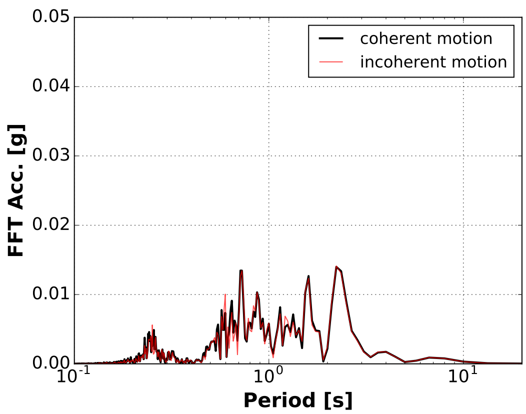

(c) FFT Acceleration first floor

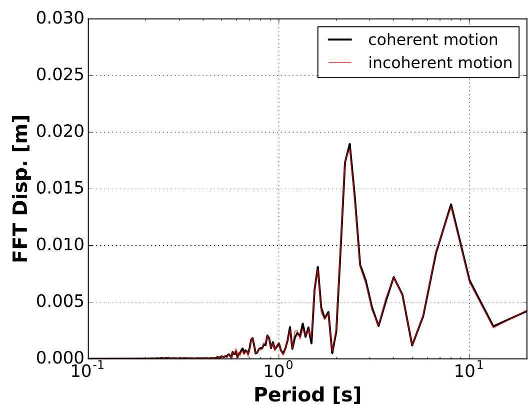

(d) FFT Displacement first floor

Figure 4.147: Coherent vs Incoherent Baseline Motion 120711, inelastic response, Soil Material Model SM-EP1, first floor, low steel building, spread foundation, X direction.

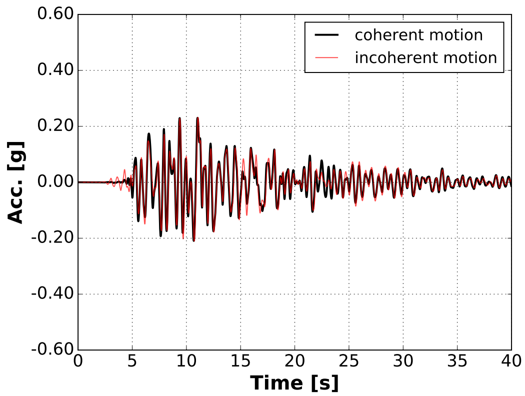

(a) Acceleration roof level

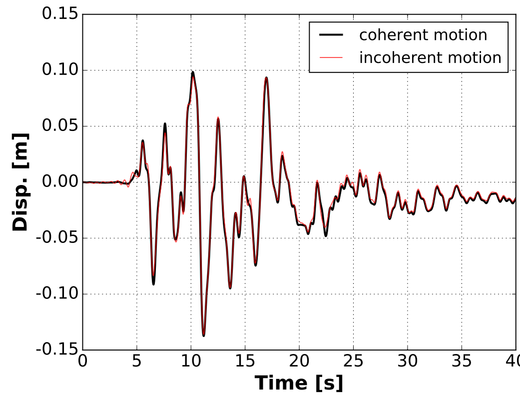

(b) Displacement roof level

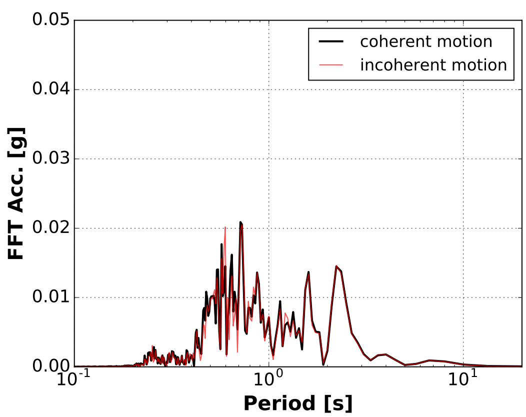

(c) FFT Acceleration roof level

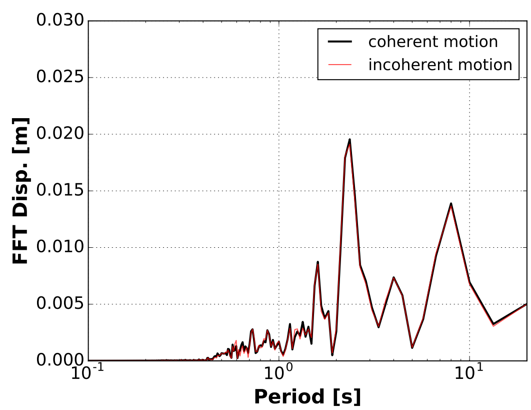

(d) FFT Displacement roof level

Figure 4.148: Coherent vs Incoherent Baseline Motion 120711, inelastic response, Soil Material Model SM-EP1, roof level, low steel building, spread foundation, X direction.

- Nonlinear inelastic soil and nonlinear fiber-based structural modeling with a mat-slab foundation

  Figures 4.149 to 4.151 present the dynamic response of the low, steel building with mat-slab foundation under both coherent and incoherent motion. Inelastic behavior of soil is simulated.

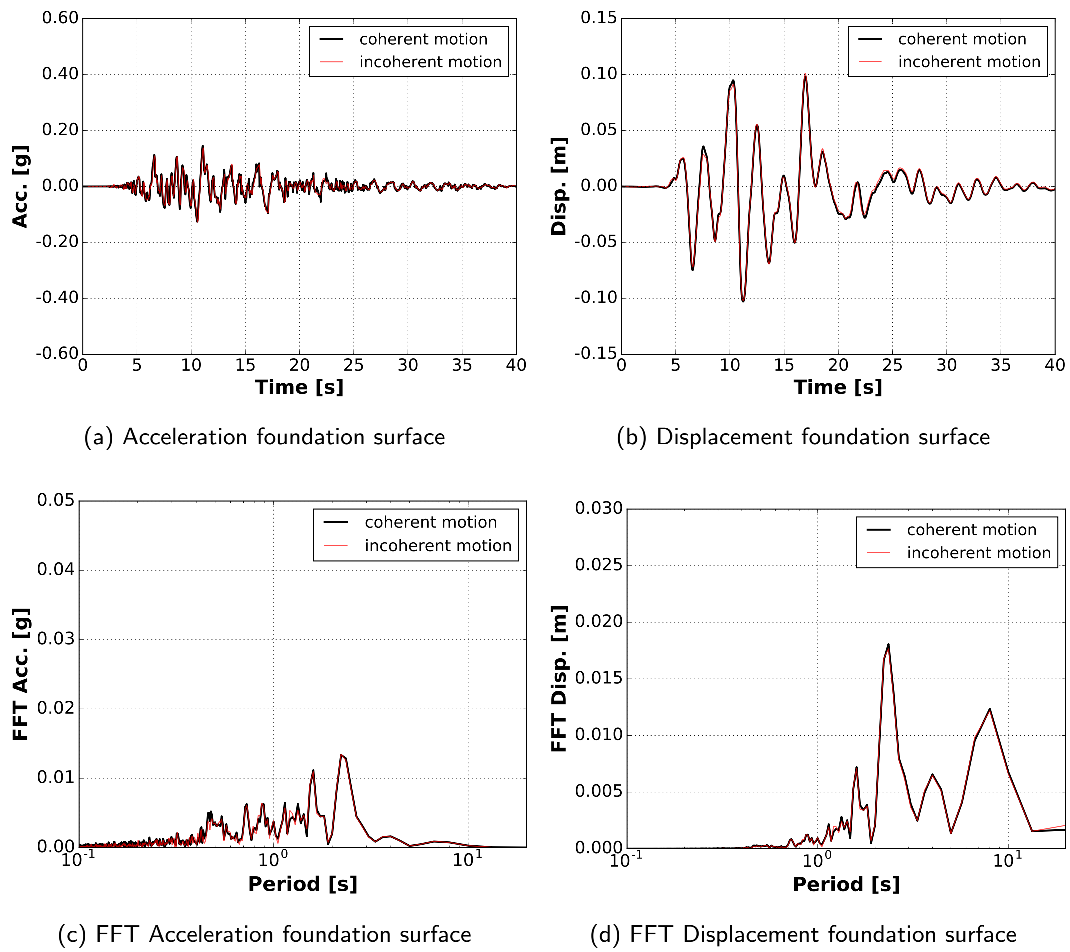

Figure 4.149: Coherent vs Incoherent Baseline Motion 120711, inelastic response, Soil Material Model SM-EP1, foundation surface, low steel building, mat-slab foundation, X direction.

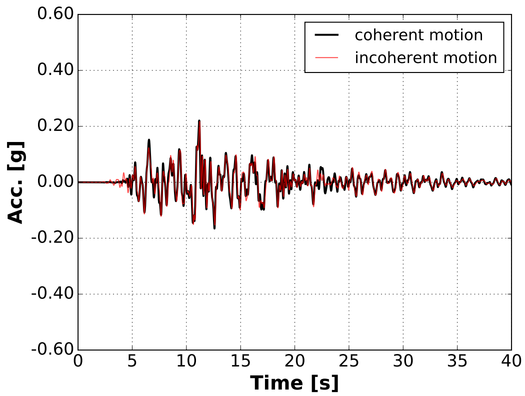

(a) Acceleration the first floor

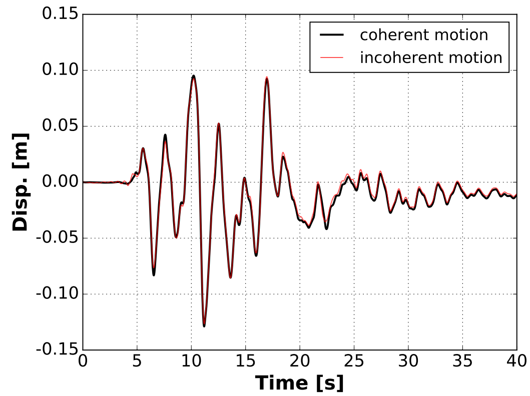

(b) Displacement the first floor

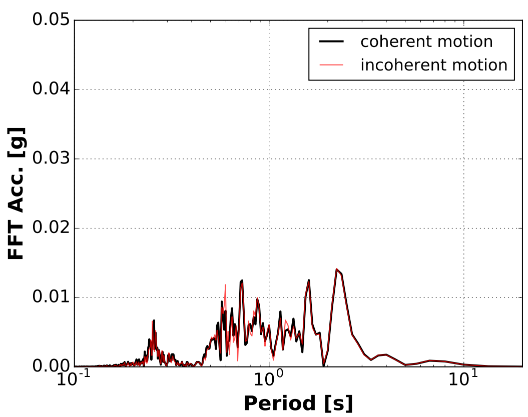

(c) FFT Acceleration the first floor

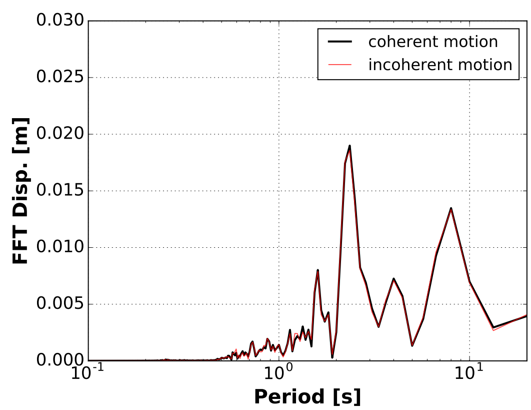

(d) FFT Displacement the first floor

Figure 4.150: Coherent vs Incoherent Baseline Motion 120711, inelastic response, Soil Material Model SM-EP1, 1st floor, low steel building, mat-slab foundation, X direction.

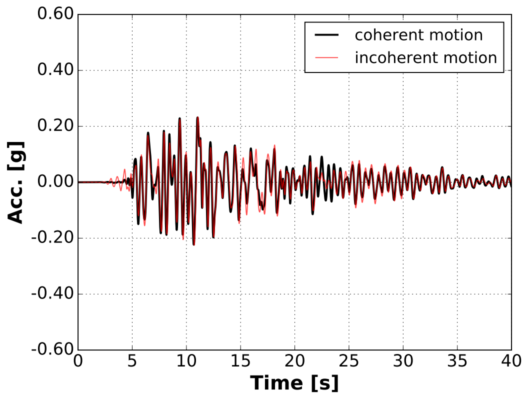

(a) Acceleration roof level

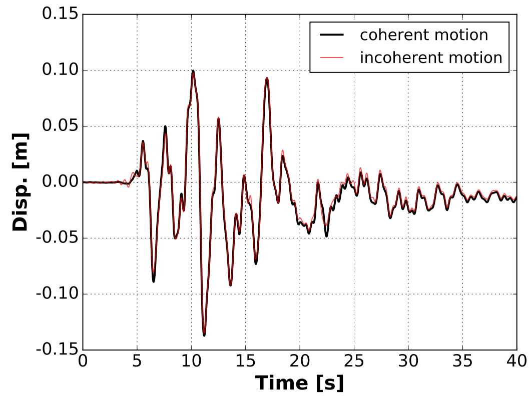

(b) Displacement roof level

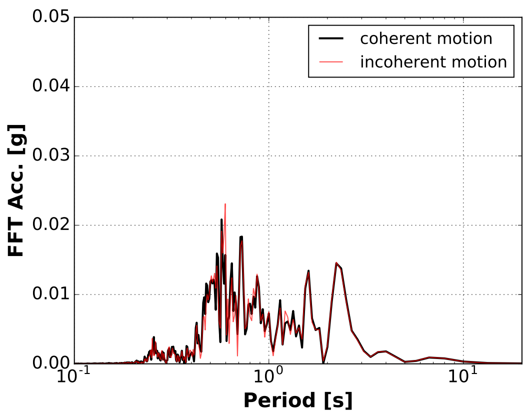

(c) FFT Acceleration roof level

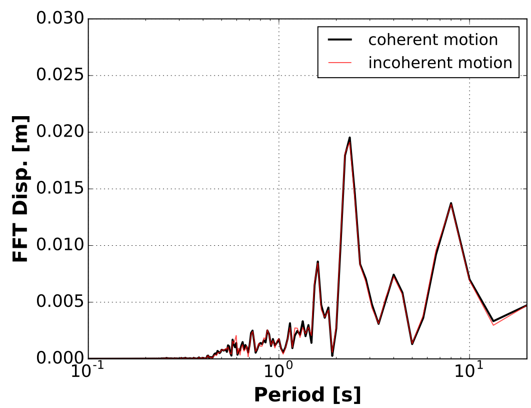

(d) FFT Displacement roof level

Figure 4.151: Coherent vs Incoherent Baseline Motion 120711, inelastic response, Soil Material Model SM-EP1, roof level, low steel building, mat-slab foundation, X direction.

4.5.6 ESSI with Linear and Nonlinear/Inelastic Models, The ratio of Response Spectrum

- Ratio of Response Spectrum (RRS)

  Code-based spectra modification (ASCE/SEI 7-16) factors considering kinematic SSI is shown in Figure 4.152.

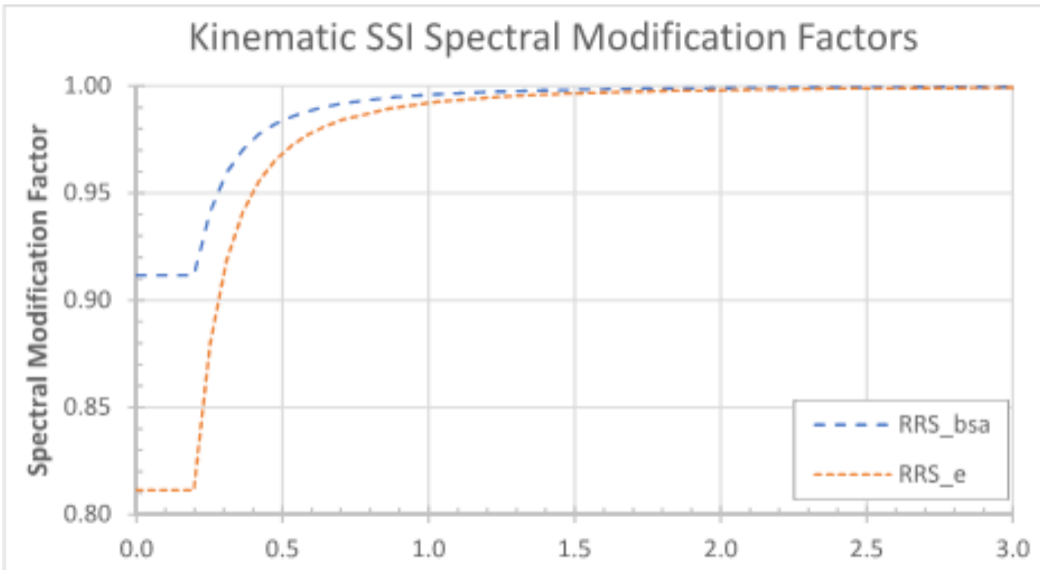

Figure 4.152: Code based spectra modification factors considering kinematic SSI.

The response spectra of foundation surface and far-field response for the case with elastic material (SM-EL2) and bonded contact, under baseline coherent motion 120711 and 120712 are shown in Figure 4.153 (a) and corresponding RRS are shown in Figure 4.153 (b).

The response spectra of foundation surface and far-field response for the case with elastic material (SM-EL2) and bonded contact, under baseline incoherent motion 120711 and 120712 are shown in Figure 4.154 (a) and corresponding RRS are shown in Figure 4.154 (b).

The response spectra of foundation surface and far-field response for the case with inelastic material (SM-EP3) and bonded contact, under baseline incoherent motion 120711 and 120712, are shown in Figure 4.155 (a) and corresponding RRS are shown in Figure 4.155 (b).

The response spectra of foundation surface and far-field response for the case with inelastic material (SM-EP3) and soft contact, under baseline incoherent motion 120711 and 120712 is shown in Figure 4.156(a) and corresponding RRS is shown in Figure 4.156(b).

The response spectra of foundation surface and far-field response for the case with inelastic material (SM-EP3) and soft contact, under baseline input motion, scaled by 1.3 are shown in Figure 4.157

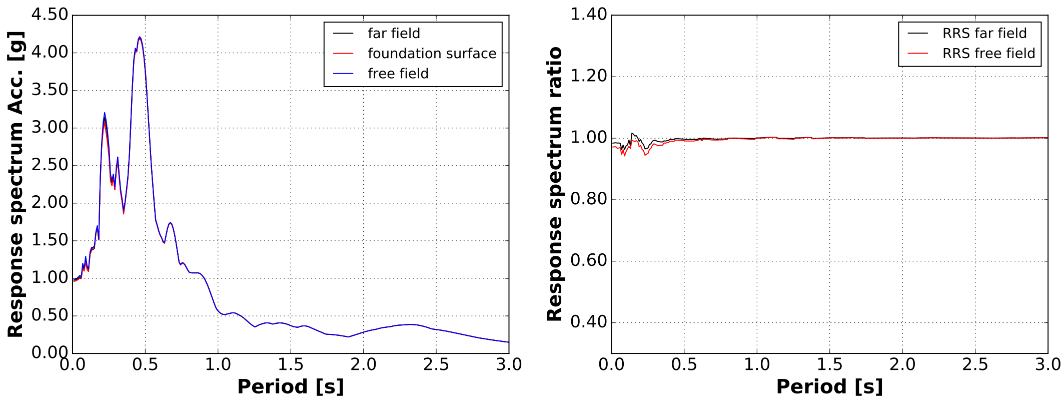

(a) Response spectra (b) Ratio of response spectra

Figure 4.153: Response spectrum and RRS for the case with elastic material SM-EL2 and bonded contact, X direction, baseline coherent motion 120711 and 120712.

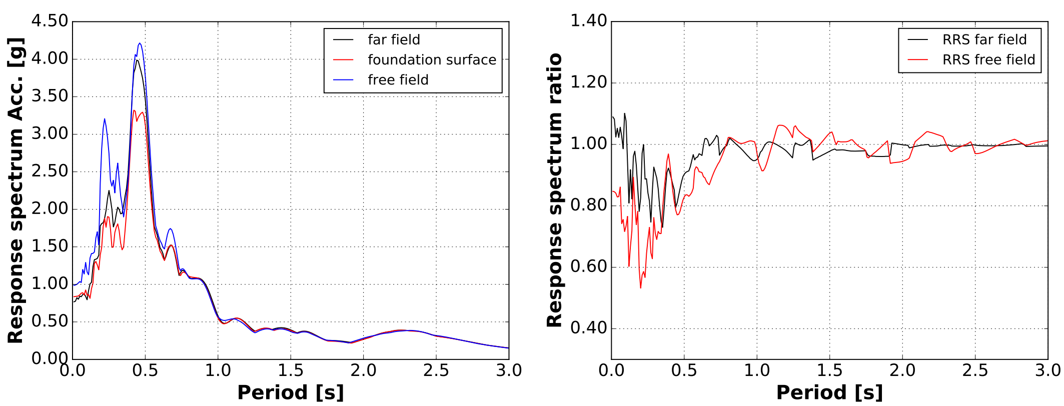

(a) Response spectra (b) Ratio of response spectra

Figure 4.154: Response spectrum and RRS for the case with elastic material SM-EL2 and bonded contact, X direction, baseline incoherent motion 120711 and 120712.

(a) and corresponding RRS are shown in Figure 4.157(b). Note that in this case, the overall scale factor is $1.3 \times 1.82 = 2.366$.

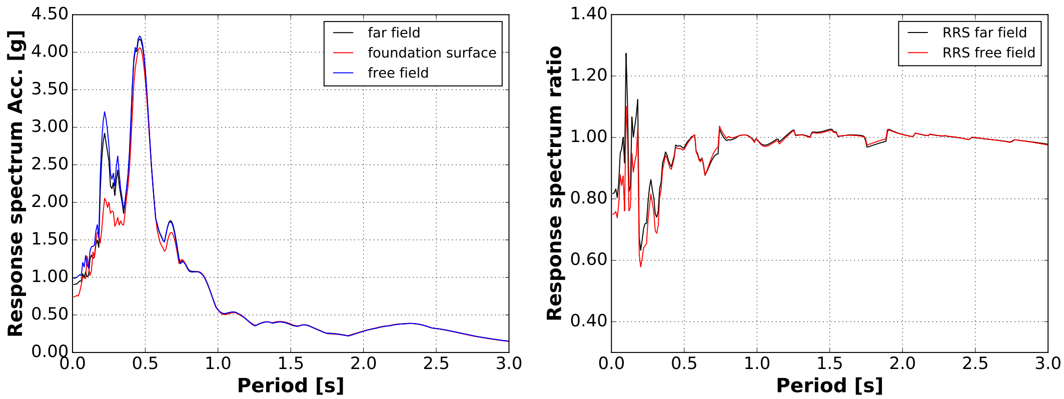

(a) Response spectra (b) Ratio of response spectra

Figure 4.155: Response spectrum and RRS for the case with inelastic Soil Material Model SM-EP3, and bonded contact, X direction, baseline incoherent motion 120711 and 120712.

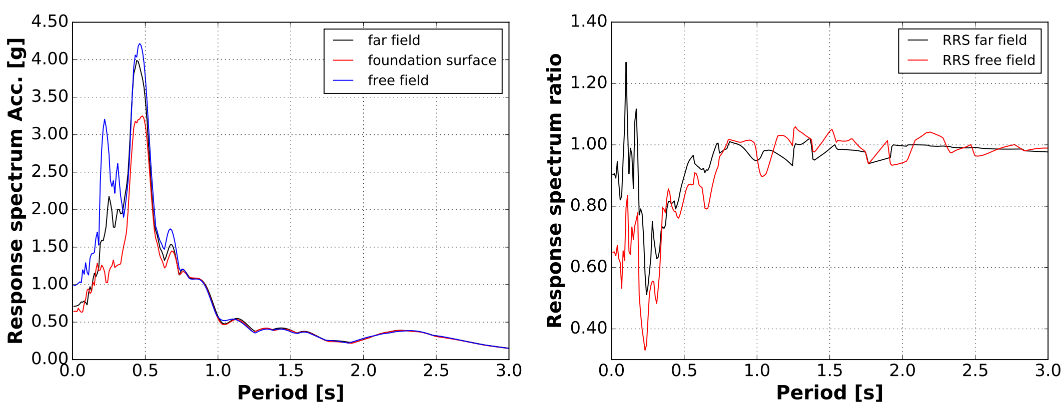

(a) Response spectra (b) Ratio of response spectra

Figure 4.156: Response spectrum and RRS for the case with inelastic Soil Material Model SM-EP3 and soft contact, X direction, baseline incoherent motion 120711 and 120712.

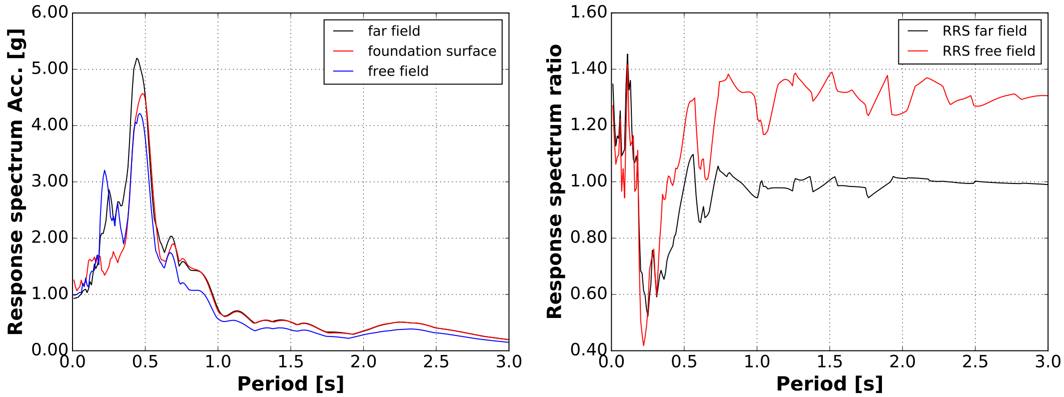

(a) Response spectra

(b) Ratio of response spectra

Figure 4.157: Response spectrum and RRS for the case with inelastic Soil Material Model SM-EP3 and soft contact, X direction, incoherent motion 120711 and 120712 with a overall scale factor of 2.366.

4.5.7 Plastic Energy Dissipation

This section presents energy dissipation analysis results for the low steel building, inelastic model, under 120711 incoherent motion. Modeling presented here is based on recent work by Yang et al. (2018), Yang et al. (2019a), Yang et al. (2019c), Yang et al. (2019b).

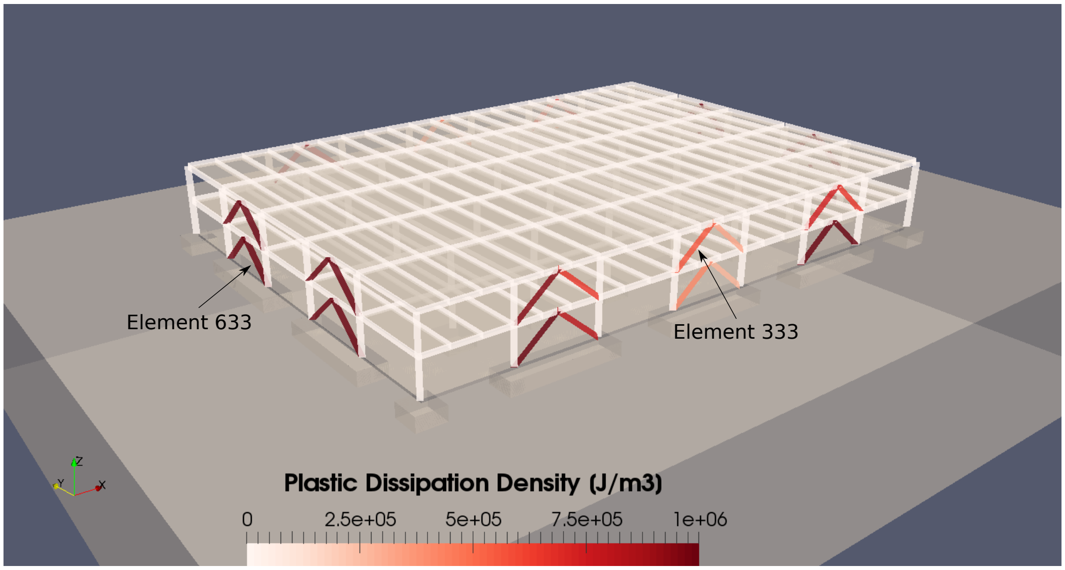

Figure 4.158: Plastic energy dissipation density in the low steel building, inelastic model, 120711 incoherent motion. Color map cutoff at 1000000 $\mathrm{J/m^3}$.

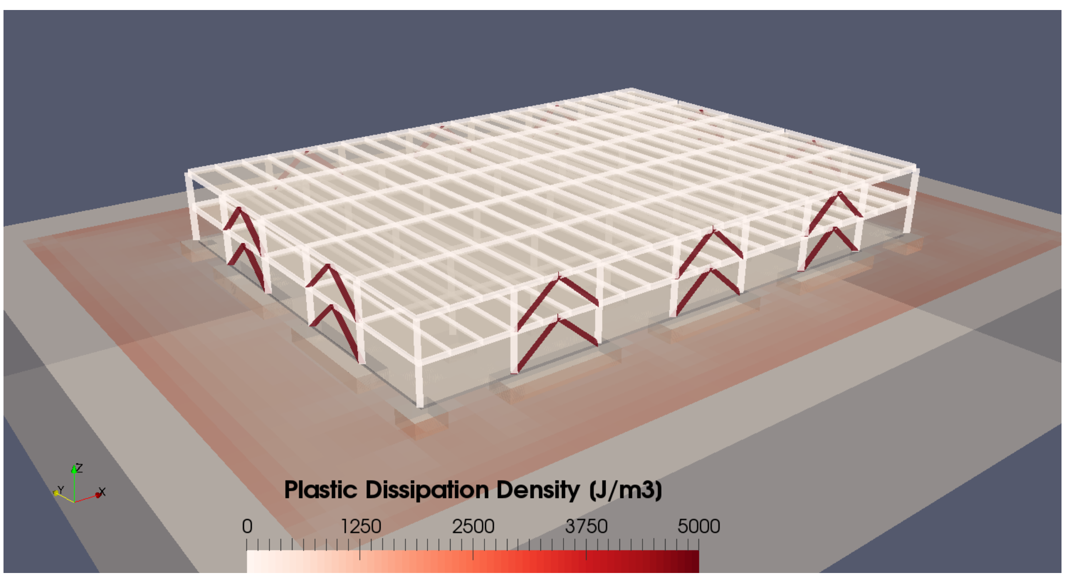

Figure 4.159: Plastic energy dissipation density in the low steel building, inelastic model, 120711 incoherent motion. Color map cutoff at 5000 $\mathrm{J/m^3}$.

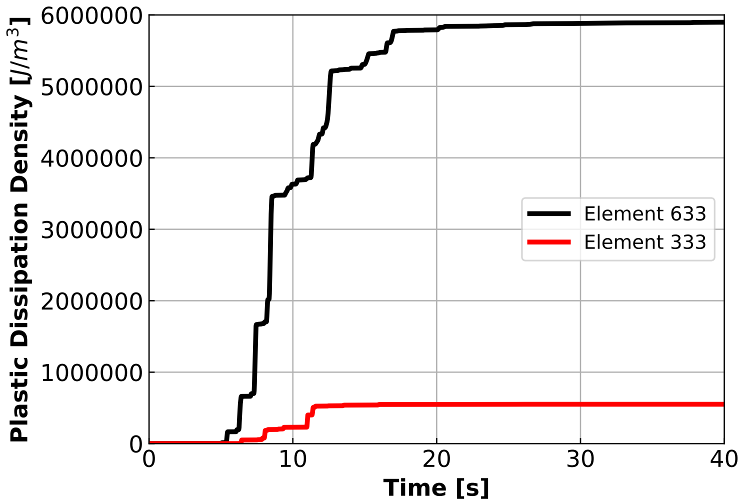

Figure 4.160: Plastic dissipation density time history for Element 633 and Element 333 (see Figure 4.158) in the low steel building, inelastic model, 120711 incoherent motion.

It is important to note earlier work by Crouse and McGuire (2001), Trifunac et al. (2001b), Trifunac et al. (2001a), and Trifunac (2005), that influenced our work on energy dissipation for soil-structure systems during earthquakes.

4.6 Tall, Concrete Building

Unless otherwise specified, a scale factor of 3.65 is used for the ESSI simulations present in this section. Seismic Records 120111 and 120112, scaled by 3.65, are noted as the baseline surface input motion in the figure captions shown in this section.

4.6.1 Eigen Analysis, Tall, Concrete Building

Table 4.10 presents the first 20 eigen periods and frequencies for tall, concrete building.

Table 4.10: Eigen analysis results for tall, concrete building

	Eigen periods [s]	Eigen frequencies [Hz]
1	2.1140	0.4730
2	1.5997	0.6251
3	1.5903	0.6288
4	0.7245	1.3803
5	0.7132	1.4022
6	0.7087	1.4110
7	0.5550	1.8017
8	0.5229	1.9124
9	0.5006	1.9977
10	0.4671	2.1411
11	0.4301	2.3252
12	0.3833	2.6088
13	0.3798	2.6327
14	0.3625	2.7584
15	0.3597	2.7800
16	0.3593	2.7836
17	0.3384	2.9552
18	0.3194	3.1308
19	0.3105	3.2210
20	0.3072	3.2551

Figure 4.161 presents first eight eigen modes for the tall building.

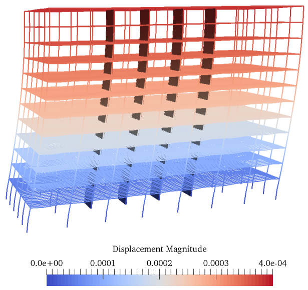

(a) 1st mode

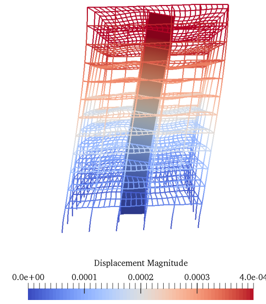

(b) 2nd mode

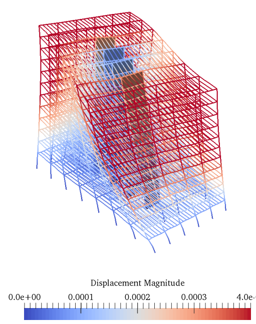

(c) 3rd mode

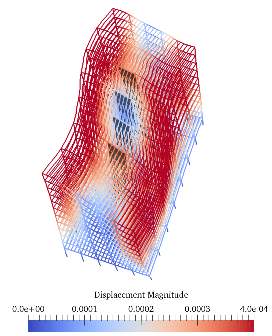

(d) 4th mode

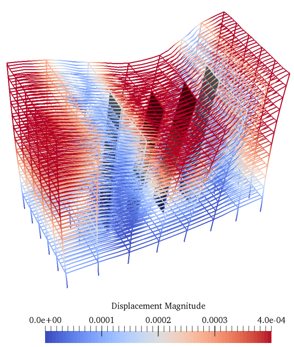

(e) 5th mode

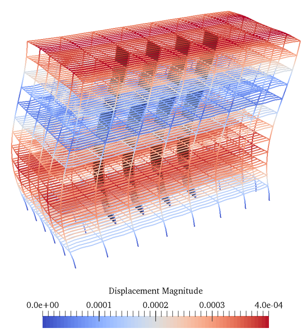

(f) 6th mode

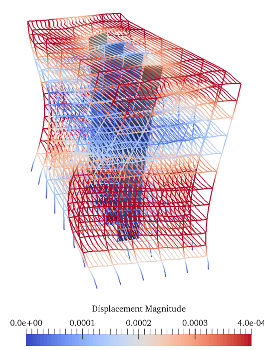

(g) 7th mode

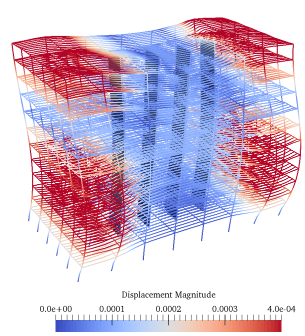

(h) 8th mode

Figure 4.161: The first eight eigen modes for the tall building.

4.6.2 Earthquake Soil-Structure Interaction Results - $2 \times 1C$ Coherent and $2C$ Incoherent Motion

Simulation results from four cases are compared: elastic soil with coherent motion (denoted as elastic, coherent), inelastic soil with coherent motion (denoted as inelastic, coherent), elastic soil with incoherent motion (denoted as elastic, incoherent) and inelastic soil with incoherent motion.

Figure 4.162 to 4.167 show the dynamic response of the 12-story reinforced concrete building subjected to $2 \times 1C$ coherent and $2C$ incoherent motion from Baseline Motion 120111 and 120112.

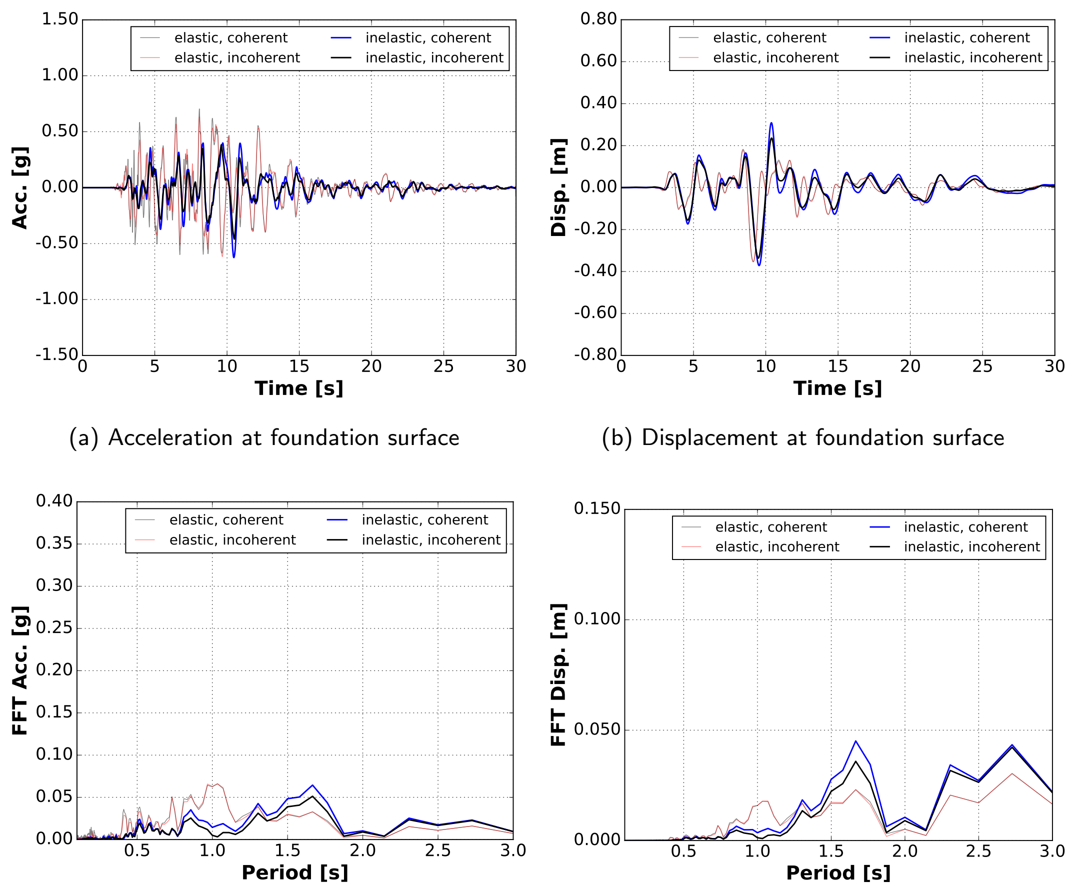

(a) Acceleration at foundation surface

(b) Displacement at foundation surface

(c) FFT Acceleration at foundation surface

(d) FFT Displacement at foundation surface

Figure 4.162: Foundation surface, tall reinforced concrete building, Baseline Motion 120111 and 120112, elastic Soil Material Model SM-EL2 and inelastic Soil Material Model SM-EP4, X direction. PGA: elastic coherent 0.70g, elastic incoherent 0.63g, inelastic coherent 0.63g and inelastic incoherent 0.46g.

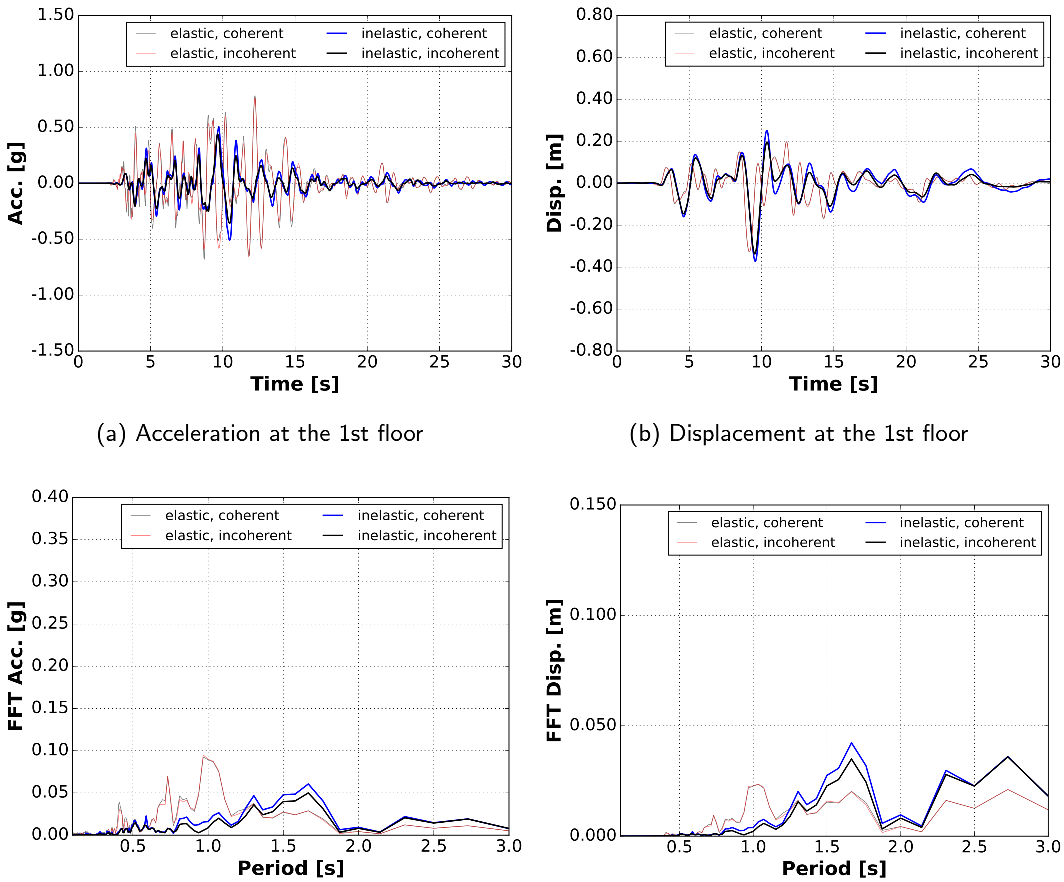

(a) Acceleration at the 1st floor

(b) Displacement at the 1st floor

(c) FFT Acceleration at the 1st floor

(d) FFT Displacement at the 1st floor

Figure 4.163: The 1st floor, tall reinforced concrete building, Baseline Motion 120111 and 120112, elastic Soil Material Model SM-EL2 and inelastic Soil Material Model SM-EP4, X direction. PFA: elastic coherent 0.78g, elastic incoherent 0.76g, inelastic coherent 0.51g and inelastic incoherent 0.44g.

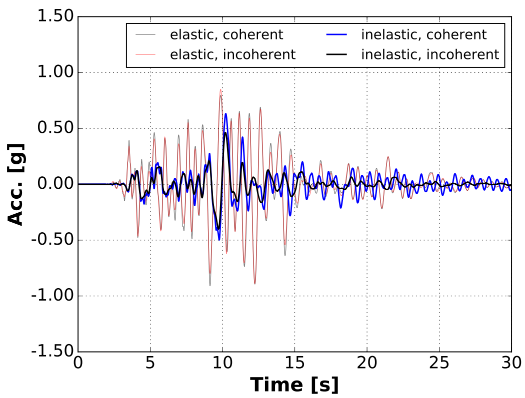

(a) Acceleration at the top floor

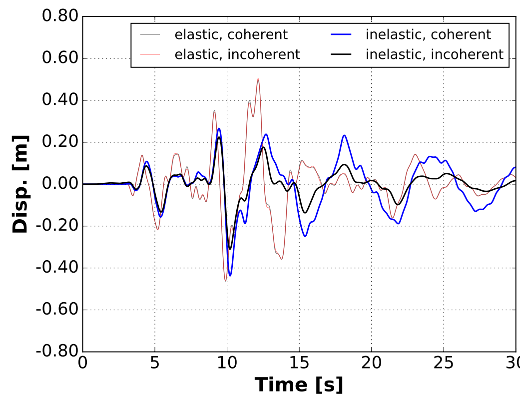

(b) Displacement at the top floor

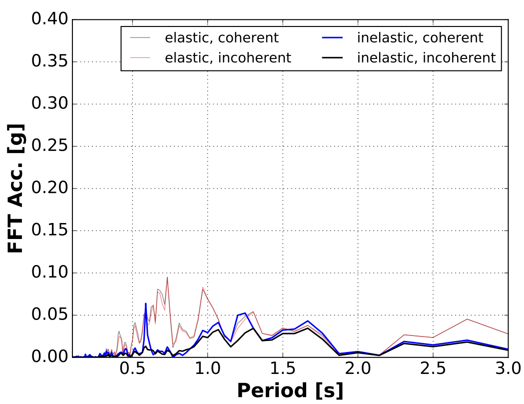

(c) FFT Acceleration at the top floor

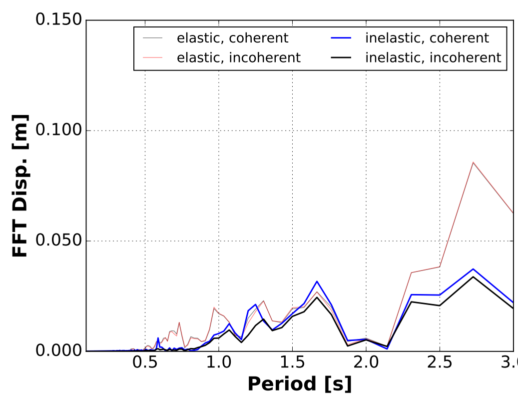

(d) FFT Displacement at the top floor

Figure 4.164: The top floor, tall reinforced concrete building, Baseline Motion 120111 and 120112, elastic Soil Material Model SM-EL2 and inelastic Soil Material Model SM-EP4, X direction. PFA: elastic coherent 0.91g, elastic incoherent 0.89g, inelastic coherent 0.63g and inelastic incoherent 0.46g.

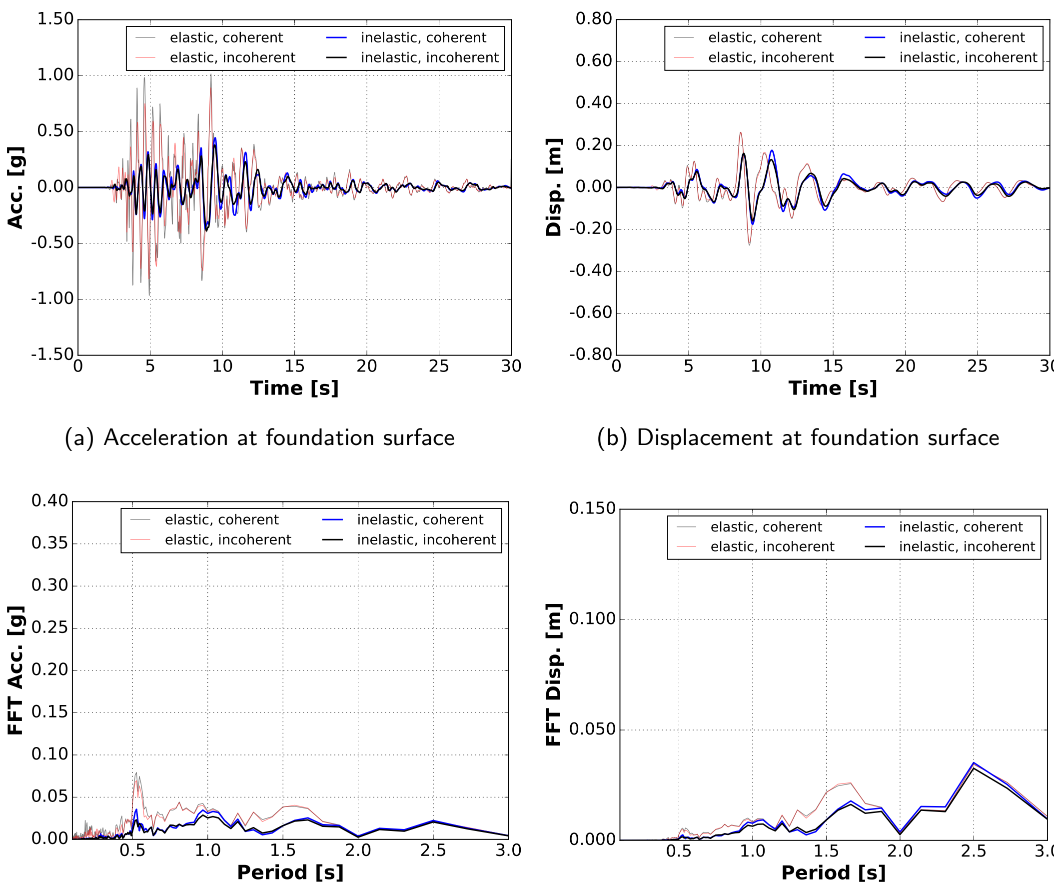

(a) Acceleration at foundation surface

(b) Displacement at foundation surface

(c) FFT Acceleration at foundation surface

(d) FFT Displacement at foundation surface

Figure 4.165: Foundation surface, tall reinforced concrete building, Baseline Motion 120111 and 120112, elastic Soil Material Model SM-EL2 and inelastic Soil Material Model SM-EP4, Y direction. PGA: elastic coherent 1.02g, elastic incoherent 0.89g, inelastic coherent 0.44g and inelastic incoherent 0.39g.

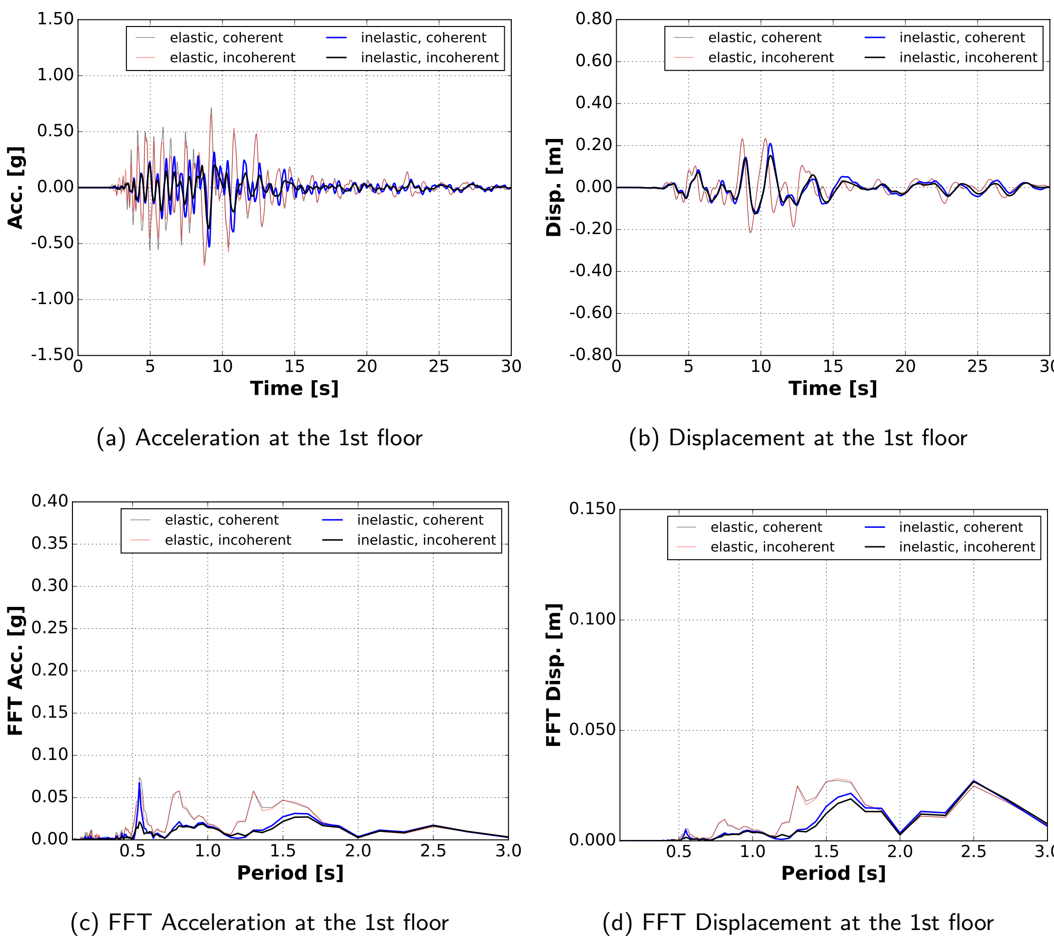

(a) Acceleration at the 1st floor

(b) Displacement at the 1st floor

(c) FFT Acceleration at the 1st floor

(d) FFT Displacement at the 1st floor

Figure 4.166: The 1st floor, tall reinforced concrete building, Baseline Motion 120111 and 120112, elastic Soil Material Model SM-EL2 and inelastic Soil Material Model SM-EP4, Y direction. PFA: elastic coherent 0.71g, elastic incoherent 0.70g, inelastic coherent 0.53g and inelastic incoherent 0.37g.

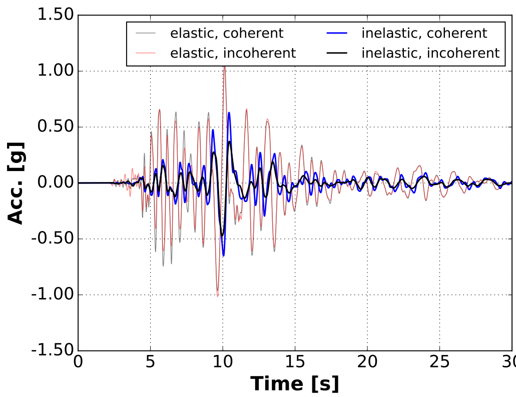

(a) Acceleration at the top floor

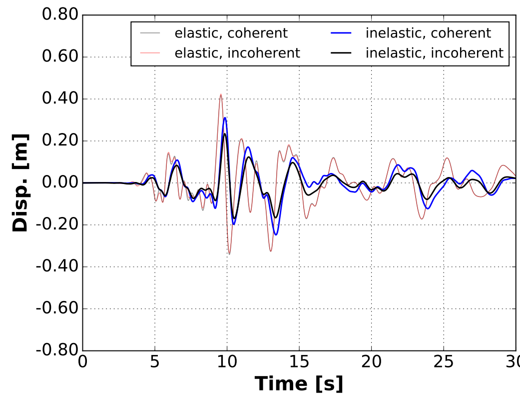

(b) Displacement at the top floor

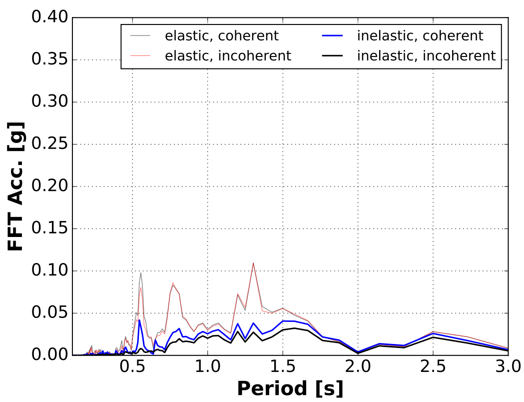

(c) FFT Acceleration at the top floor

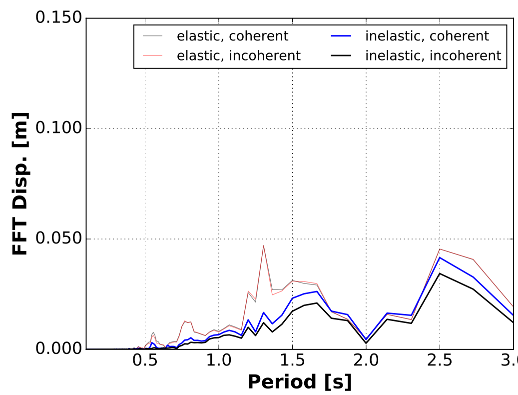

(d) FFT Displacement at the top floor

Figure 4.167: The top floor, tall reinforced concrete building, Baseline Motion 120111 and 120112, elastic Soil Material Model SM-EL2 and inelastic Soil Material Model SM-EP4, Y direction. PFA: elastic coherent 1.10g, elastic incoherent 1.07g, inelastic coherent 0.65g and inelastic incoherent 0.47g.

Table 4.11 shows the input peak acceleration at the ground surface and peak ground acceleration response (PGA) and peak floor acceleration response (PFA) among different cases of the tall reinforced concrete building, for seismic motion scaling factor of 3.65. A note on locations of seismic motion measurement points is provided in section 4.1.5 on page 76. It is noted again that the ground surface peak acceleration, shown in Table 4.11 as surface input, is the free-field motions that were used to perform deconvolution (Kramer, 1996) to a certain depth, and then motions from a depth are propagated upward through a linear and/or nonlinear soil and soil-structure system.

Table 4.11: Comparison of input and response PGAs/PFAs for different simulation cases of tall reinforced concrete building, inelastic Soil Material Model SM-EP4, Baseline Motion 120111 and 120112 with scale factor 3.65.

		Elastic coherent	Elastic incoherent	Inelastic coherent	Inelastic incoherent
	Free Field Surface input	0.97	0.97	0.97	0.97
PGA/PFA [g]	Foundation surface	0.70	0.63	0.40	0.38
X positive	First floor	0.78	0.76	0.51	0.44
	Top floor	0.79	0.85	0.63	0.46
	Free Field Surface input	0.66	0.66	0.66	0.66
PGA/PFA [g]	Foundation surface	0.60	0.62	0.63	0.46
X negative	First floor	0.68	0.66	0.51	0.36
	Top floor	0.91	0.89	0.50	0.40
	Free Field Surface input	1.25	1.25	1.25	1.25
PGA/PFA [g]	Foundation surface	1.02	0.89	0.44	0.38
Y positive	First floor	0.71	0.66	0.32	0.21
	Top floor	1.10	1.07	0.63	0.37
	Free Field Surface input	1.10	1.10	1.10	1.10
PGA/PFA [g]	Foundation surface	0.97	0.82	0.37	0.39
Y negative	First floor	0.67	0.70	0.53	0.37
	Top floor	0.96	1.02	0.65	0.47

Figure 4.168 and 4.169 compare acceleration FFT between free-field motion and foundation surface of the 12-story tall concrete building.

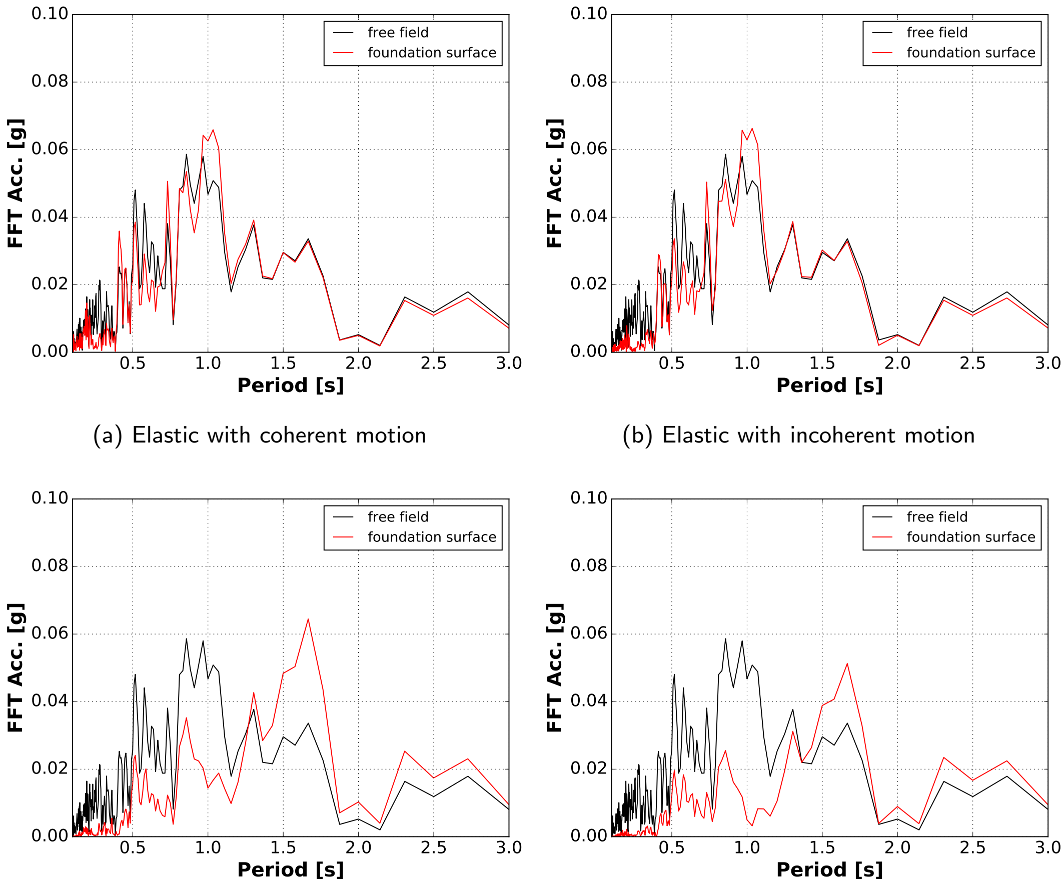

(a) Elastic with coherent motion

(b) Elastic with incoherent motion

(c) Inelastic with coherent motion

(d) Inelastic with incoherent motion

Figure 4.168: Comparison of acceleration FFT between free-field and tall building foundation surface, elastic Soil Material Model SM-EL2 and inelastic Soil Material Model SM-EP4, Baseline Motion 120111 and 120112, X direction.

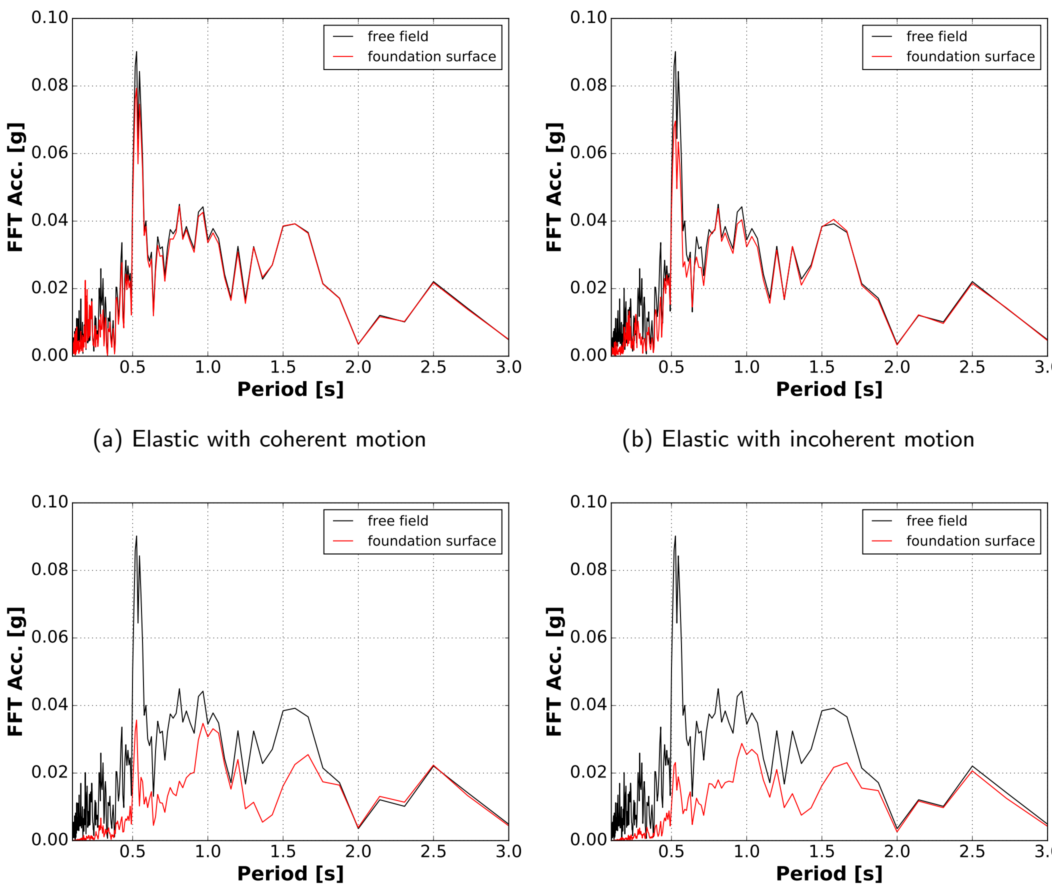

(a) Elastic with coherent motion

(b) Elastic with incoherent motion

(c) Inelastic with coherent motion

(d) Inelastic with incoherent motion

Figure 4.169: Comparison of acceleration FFT between free-field and tall building foundation surface, elastic Soil Material Model SM-EL2 and inelastic Soil Material Model SM-EP4, Baseline Motion 120111 and 120112, Y direction.

Figure 4.170 compares the ratio of acceleration FFT between free-field and foundation surface of the 12 story, tall concrete building.

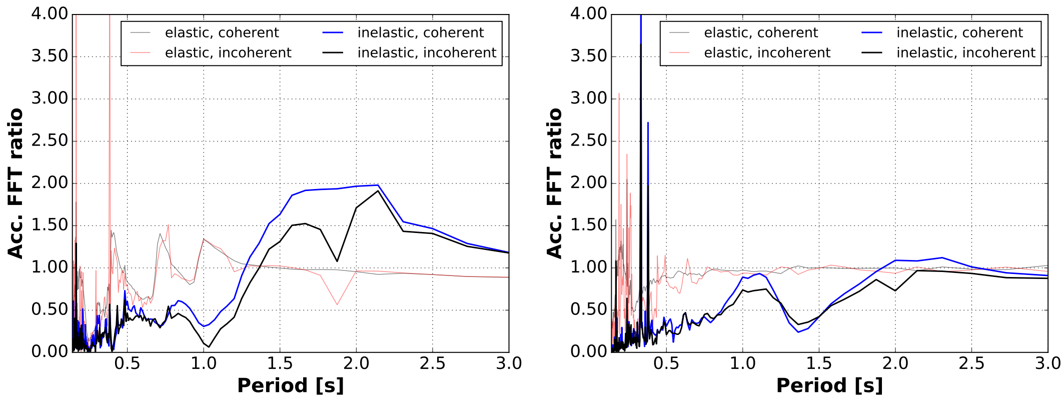

(a) X direction (b) Y direction

Figure 4.170: Comparison of acceleration FFT ratio between foundation surface of the 12 story, tall concrete building and free-field, elastic Soil Material Model SM-EL2 and inelastic Soil Material Model SM-EP4, Baseline Motion 120111 and 120112.

Figure 4.171 and 4.172 compare acceleration FFT response of foundation surface of tall concrete building under coherent and incoherent motion within elastic simulation and inelastic simulation.

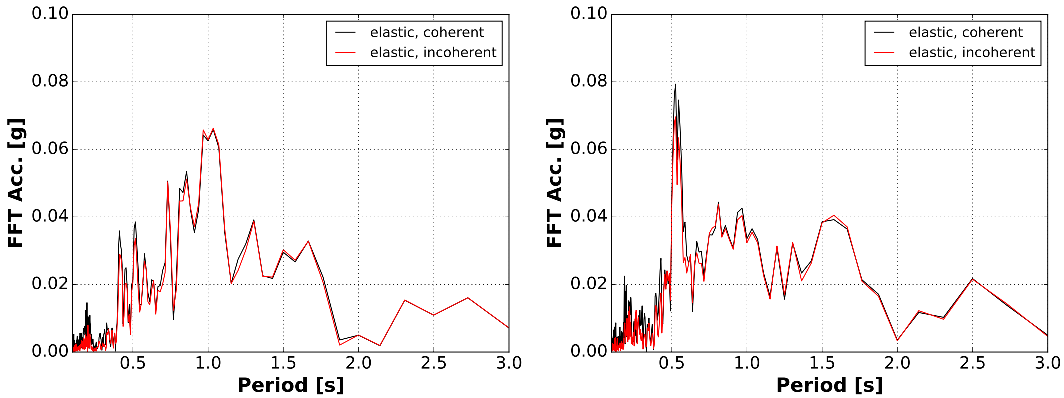

(a) X direction (b) Y direction

Figure 4.171: Comparison of acceleration FFT of foundation surface between elastic, coherent case and elastic, incoherent case, Baseline Motion 120111 and 120112, elastic Soil Material Model SM-EL2: (a) Longitudinal X direction (b) Transverse Y direction.

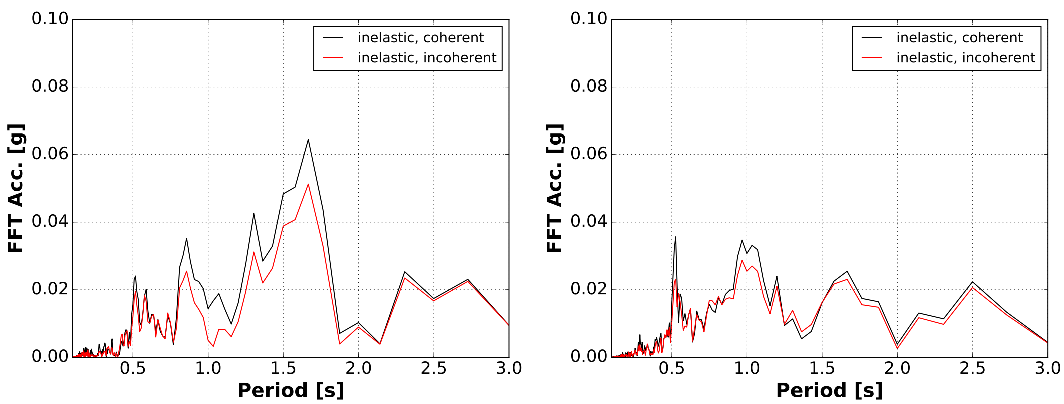

(a) X direction (b) Y direction

Figure 4.172: Comparison of acceleration FFT of foundation surface between inelastic, coherent case and inelastic, incoherent case, inelastic Soil Material Model SM-EP4, Baseline Motion 120111 and 120112: (a) Longitudinal X direction (b) Transverse Y direction.

Figure 4.173 shows the acceleration FFT ratio of foundation surface under coherent and incoherent motion $u_{\text{foundation,incoherent}}/u_{\text{foundation,coherent}}$ within elastic and inelastic simulations.

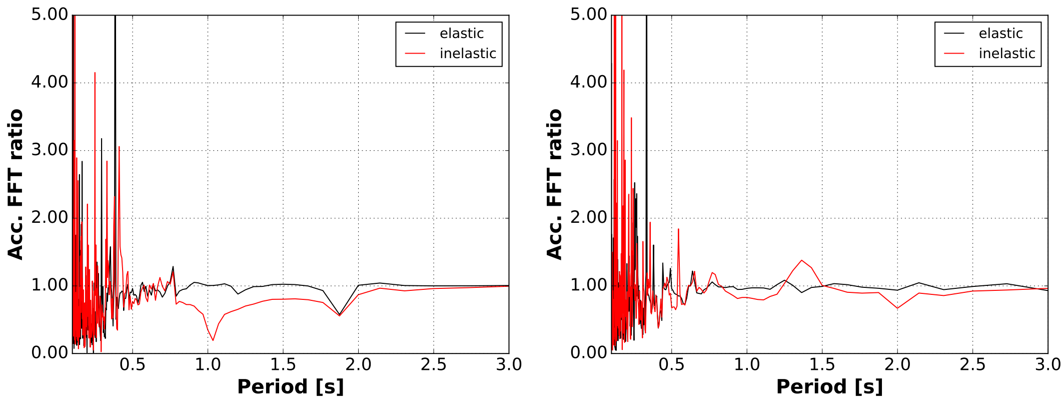

(a) X direction

(b) Y direction

Figure 4.173: Ratio of acceleration FFT of foundation surface under coherent and incoherent motions within elastic and inelastic simulations, elastic Soil Material Model SM-EL2 and inelastic Soil Material Model SM-EP4, Baseline Motion 120111 and 120112: (a) Longitudinal X direction (b) Transverse Y direction.

Figure 4.174 and 4.175 compare response spectra of free-field motion and foundation surface in both longitudinal (X) direction and transverse (Y) direction.

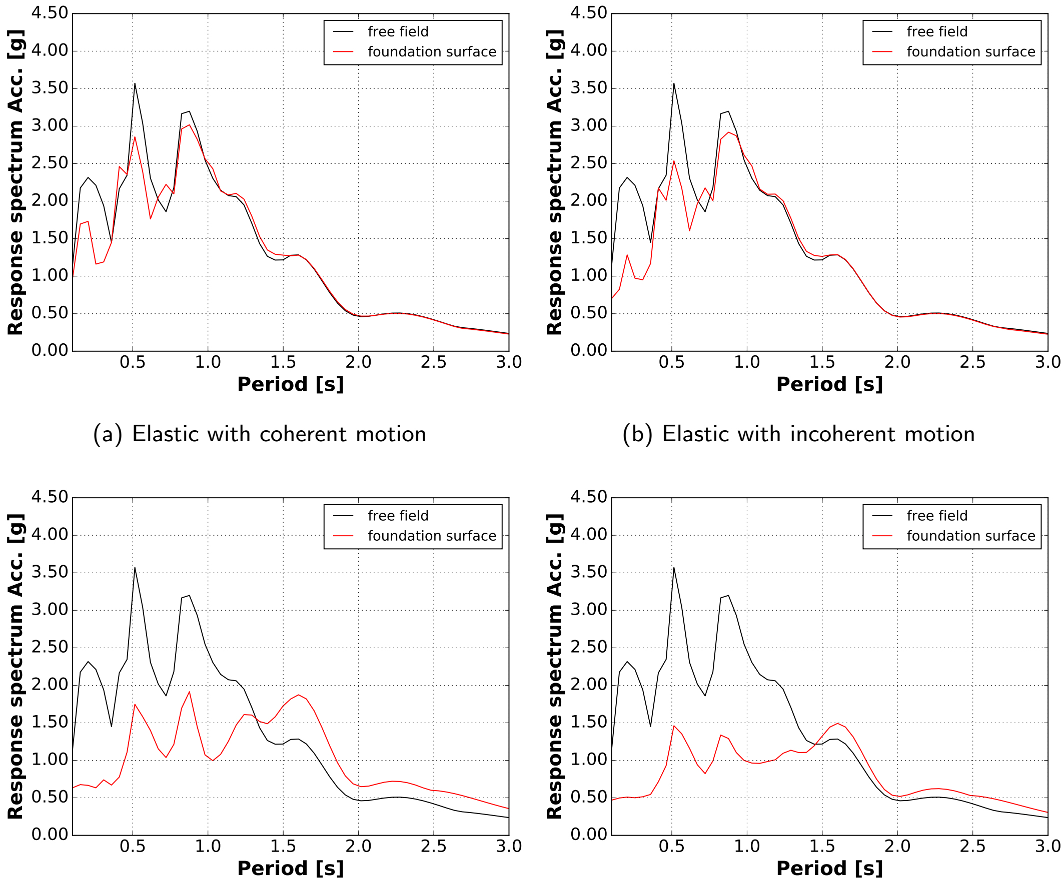

(a) Elastic with coherent motion

(b) Elastic with incoherent motion

(c) Inelastic with coherent motion

(d) Inelastic with incoherent motion

Figure 4.174: Comparison of response spectra between foundation surface of tall building and free-field, inelastic Soil Material Model SM-EP4, Baseline Motion 120111 and 120112, X direction.

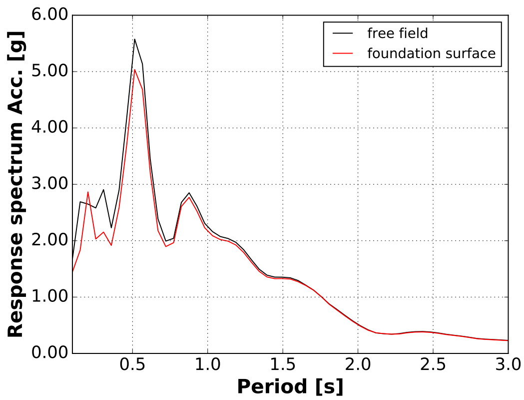

(a) Elastic with coherent motion

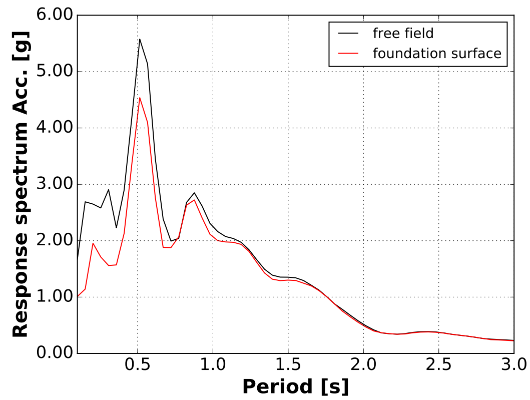

(b) Elastic with incoherent motion

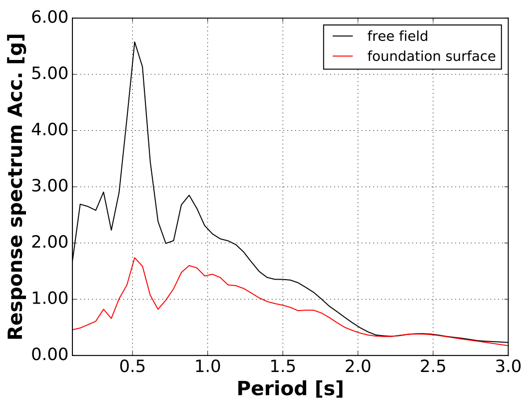

(c) Inelastic with coherent motion

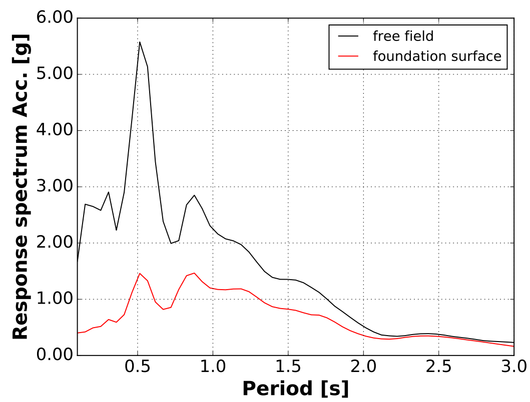

(d) Inelastic with incoherent motion

Figure 4.175: Comparison of response spectra between foundation surface of tall building and free-field, inelastic Soil Material Model SM-EP4, Baseline Motion 120111 and 120112, Y direction

Figure 4.176 compares the ratio of response spectra (RRS) between foundation surface response and free-field.

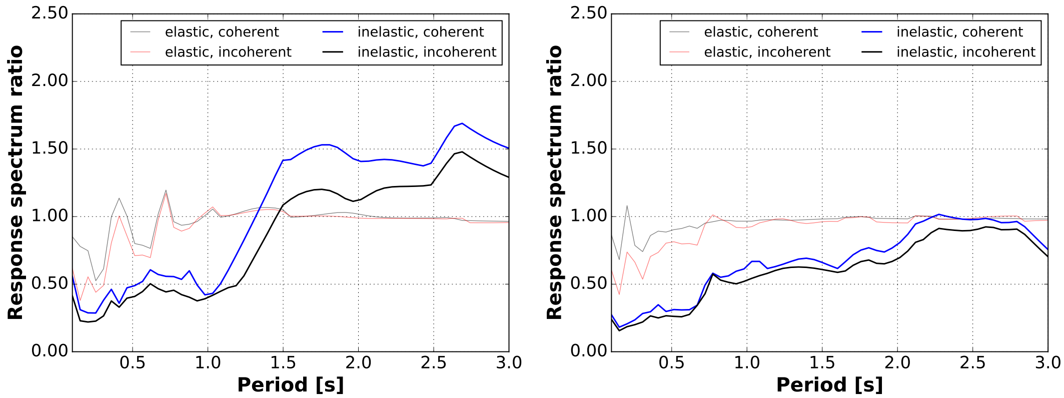

(a) X direction

(b) Y direction

Figure 4.176: Comparison of ratio of response spectra (RRS) between foundation surface of tall building and free-field motions, elastic Soil Material Model SM-EL2 and inelastic Soil Material Model SM-EP4, Baseline Motion 120111 and 120112.

Figure 4.177 and 4.178 compare acceleration FFT between top floor and foundation surface of the 12-story tall concrete building.

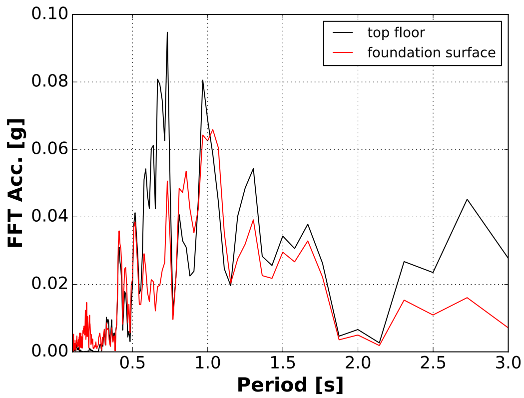

(a) Elastic with coherent motion

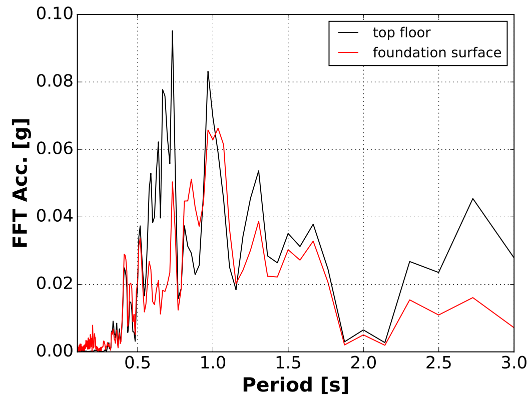

(b) Elastic with incoherent motion

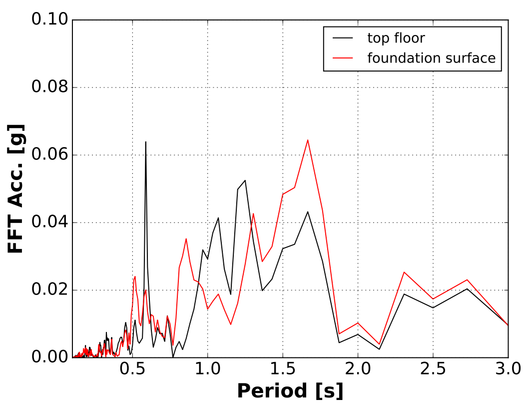

(c) Inelastic with coherent motion

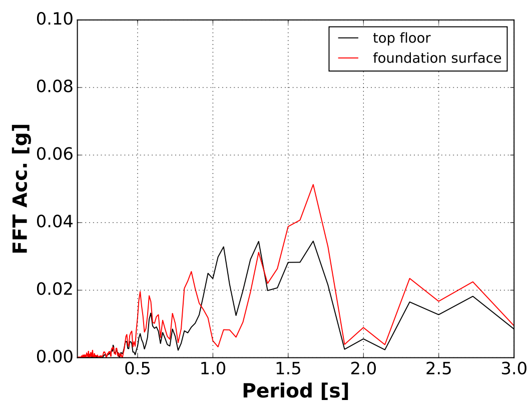

(d) Inelastic with incoherent motion

Figure 4.177: Comparison of acceleration FFT between the top floor and foundation surface, inelastic Soil Material Model SM-EP4, Baseline Motion 120111 and 120112, X direction

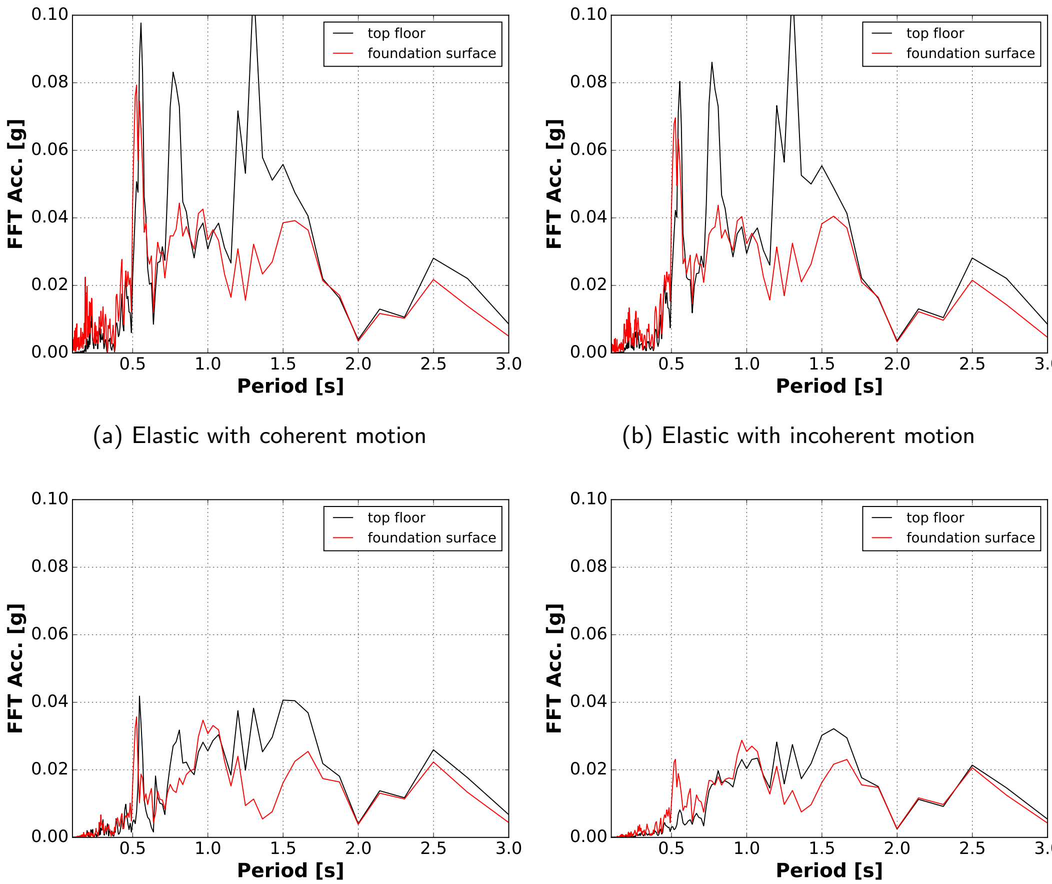

(a) Elastic with coherent motion

(b) Elastic with incoherent motion

(c) Inelastic with coherent motion

(d) Inelastic with incoherent motion

Figure 4.178: Comparison of acceleration FFT between the top floor and foundation surface, inelastic Soil Material Model SM-EP4, Baseline Motion 120111 and 120112, Y direction

Figure 4.179 compares the ratio of acceleration FFT between top floor and foundation surface of the 12 story, tall concrete building.

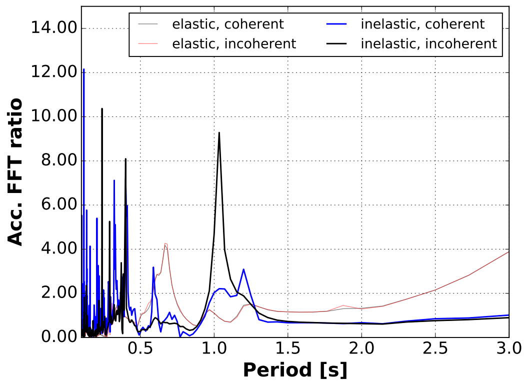

(a) X direction

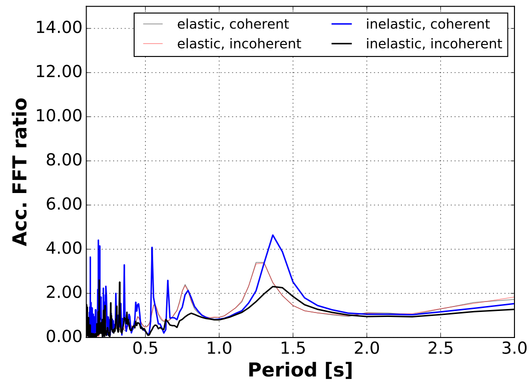

(b) Y direction

Figure 4.179: Comparison of acceleration FFT ratio between top floor and foundation surface of the 12 story, tall concrete building, elastic Soil Material Model SM-EL2 and inelastic Soil Material Model SM-EP4, Baseline Motion 120111 and 120112.

4.6.3 No-Contact/Interface Slip/Gap vs Slip/Gap Contact/Interface

Dynamic responses of different types of contact/interface behavior are compared:

- Bonded contact/interface with no-slip, no-gap, where foundation is "glued" to the soil, and
- Stress-based soft contact/interface with nonlinear shearing/ gap interface behavior, where foundation and soil are allowed to separate, and foundation can slip over soil if friction resistance is overcome.

The same Baseline Motions 120111 and 120112, inelastic Soil Material Model SM-EP4, are adopted.

Figure 4.180 and 4.181 compare dynamic response of foundation surface of the 12-story tall reinforced concrete building for different types of contact/interface behavior.

Figure 4.182 compares response spectra of foundation surface response of the tall building for different types of contact/interface behavior.

Figure 4.183 and 4.184 compare dynamic response of foundation surface of the 12-story tall reinforced concrete building for different types of contact behavior.

Figure 4.185 compares response spectrum of top floor response of the tall building for different types of contact behavior.

Figure 4.186 compares acceleration FFT ratio between the top floor and foundation surface response of the tall building for different types of contact behavior.

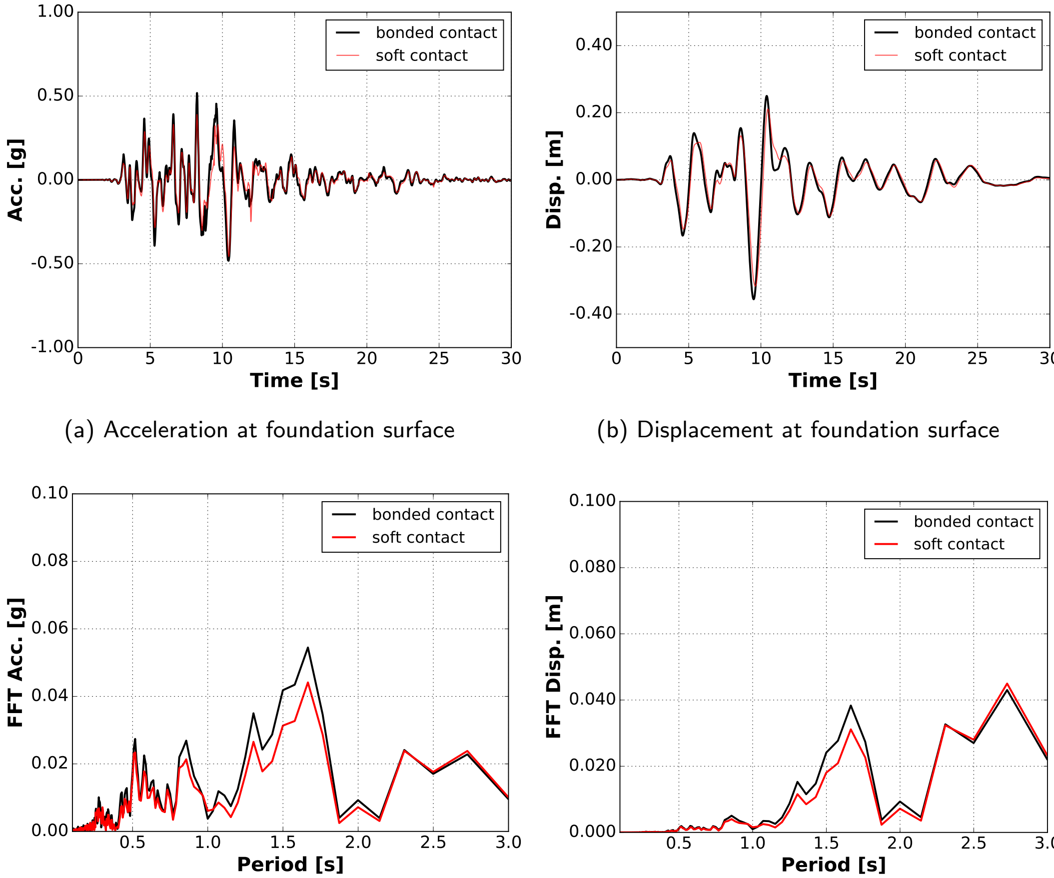

(a) Acceleration at foundation surface

(b) Displacement at foundation surface

(c) FFT Acceleration at foundation surface

(d) FFT Displacement at foundation surface

Figure 4.180: Comparison of foundation surface responses of the tall building for different contact/interface behavior, inelastic Soil Material Model SM-EP4, Baseline Motion 120111 and 120112, X direction

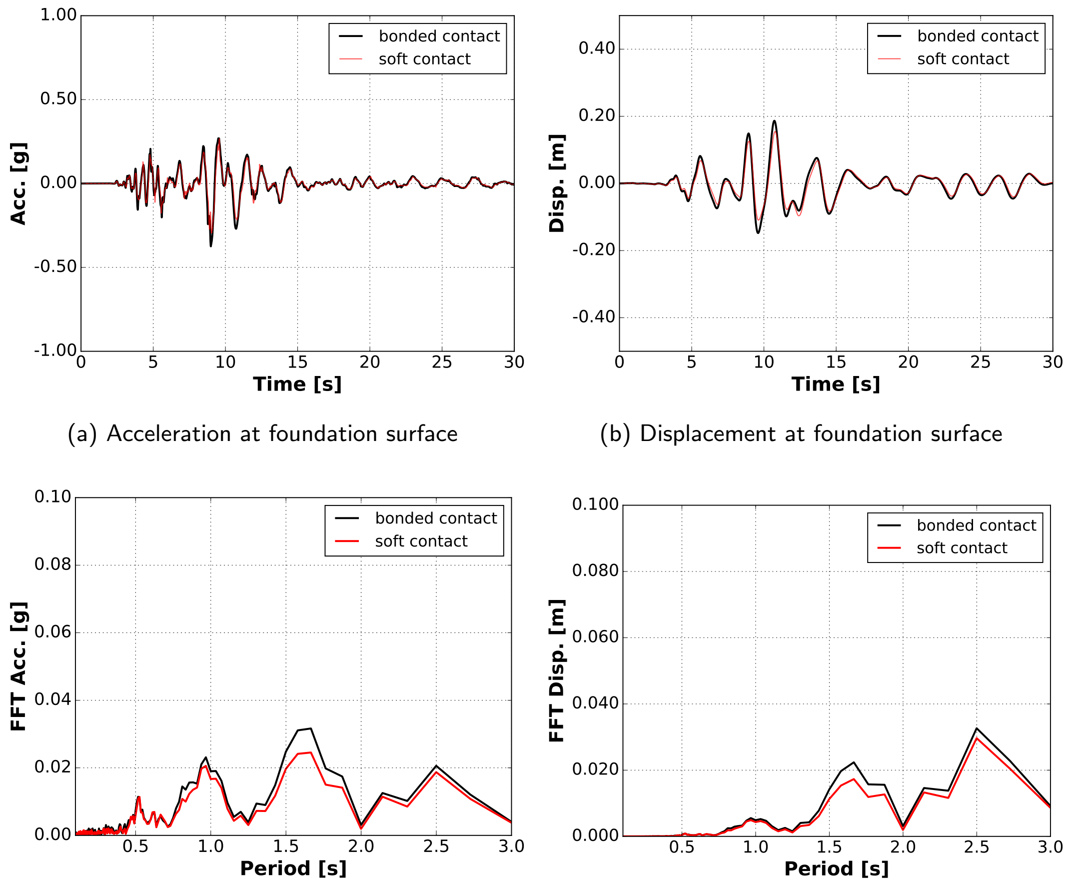

(a) Acceleration at foundation surface

(b) Displacement at foundation surface

(c) FFT Acceleration at foundation surface

(d) FFT Displacement at foundation surface

Figure 4.181: Comparison of foundation surface responses of the tall building for different contact/interface behavior, inelastic Soil Material Model SM-EP4, Baseline Motion 120111 and 120112, Y direction

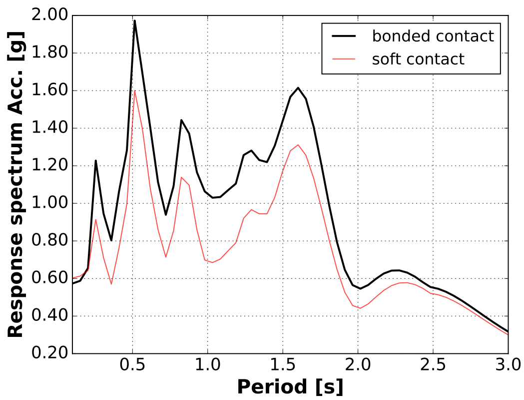

(a) X direction

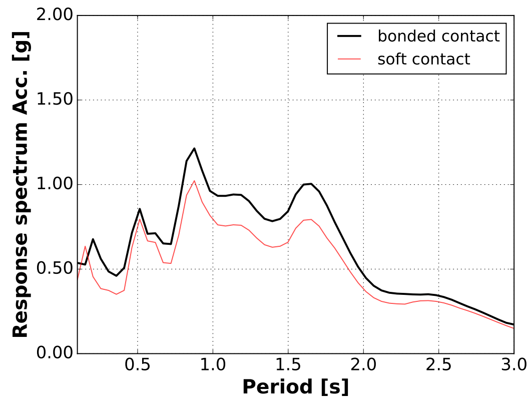

(b) Y direction

Figure 4.182: Comparison of spectral acceleration of foundation surface responses for different contact/interface behavior, inelastic Soil Material Model SM-EP4, Baseline Motion 120111 and 120112.

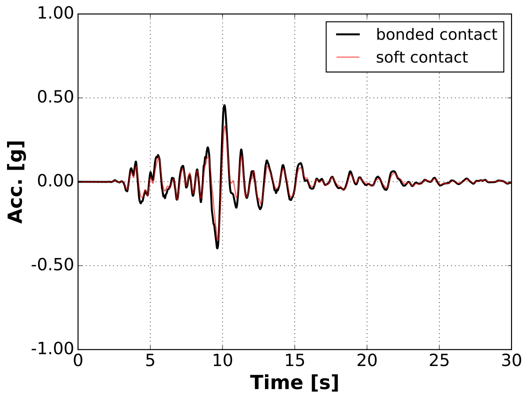

(a) Acceleration at foundation surface

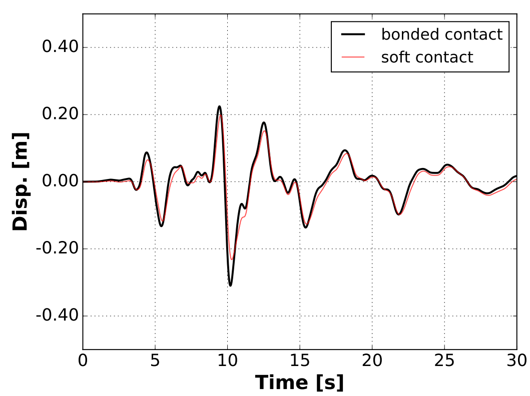

(b) Displacement at foundation surface

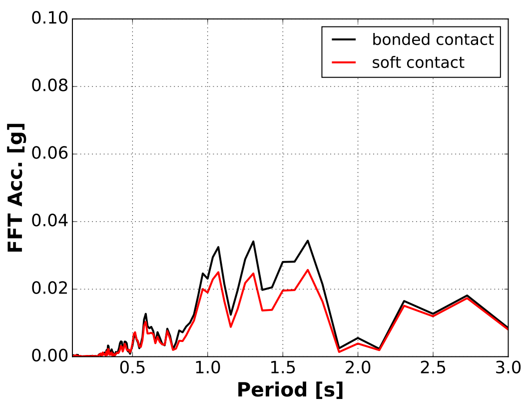

(c) FFT Acceleration at foundation surface

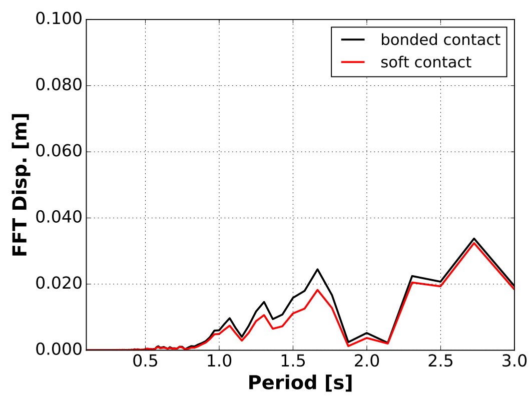

(d) FFT Displacement at foundation surface

Figure 4.183: Comparison of top floor responses of the tall building for different contact behavior, inelastic Soil Material Model SM-EP4, Baseline Motion 120111 and 120112, X direction.

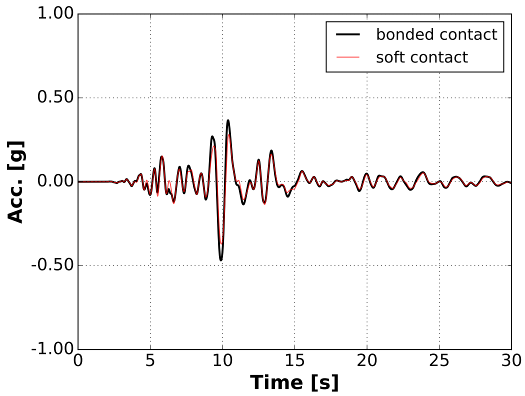

(a) Acceleration at foundation surface

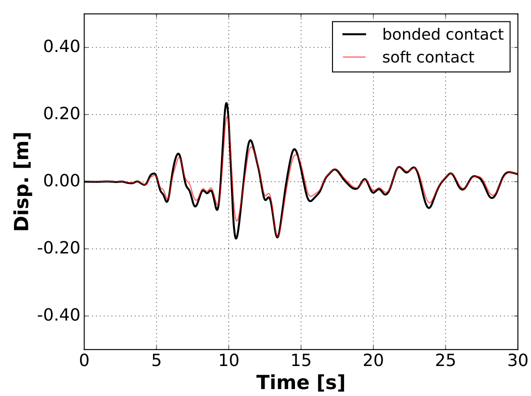

(b) Displacement at foundation surface

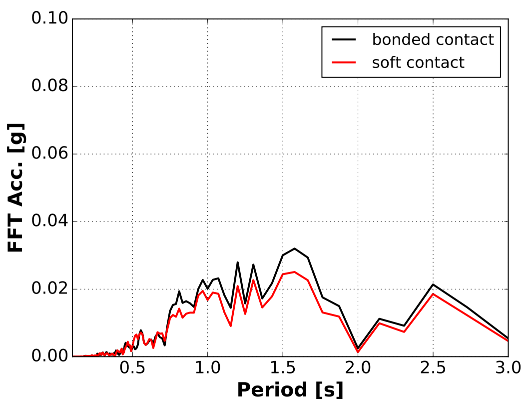

(c) FFT Acceleration at foundation surface

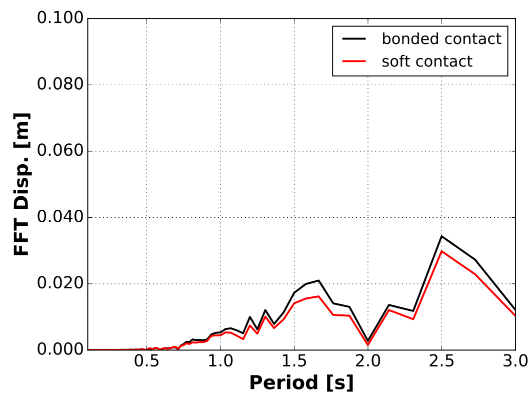

(d) FFT Displacement at foundation surface

Figure 4.184: Comparison of top floor responses of the tall building for different contact behavior, inelastic Soil Material Model SM-EP4, Baseline Motion 120111 and 120112, Y direction.

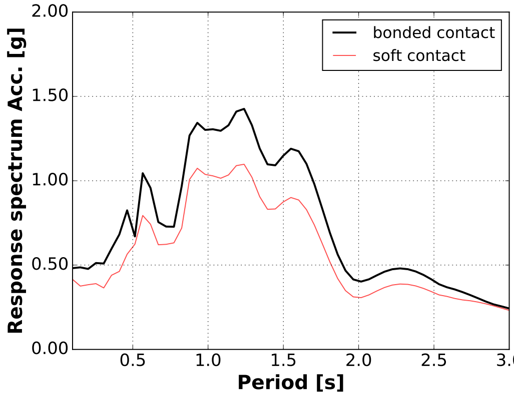

(a) X direction

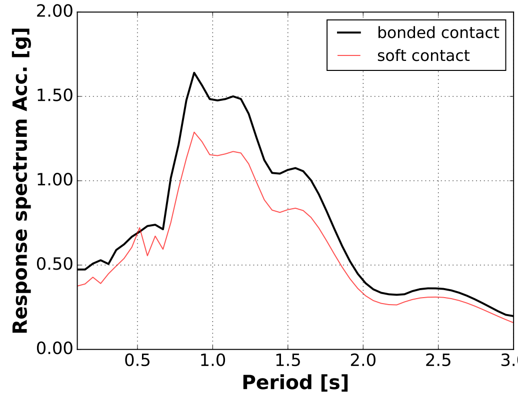

(b) Y direction

Figure 4.185: Comparison of spectrum acceleration of top floor responses for different contact behavior, inelastic Soil Material Model SM-EP4, Baseline Motion 120111 and 120112.

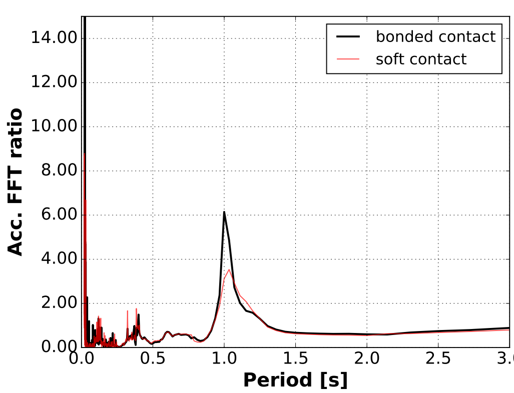

(a) X direction

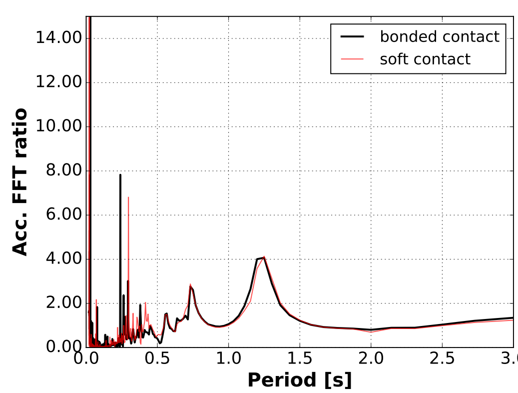

(b) Y direction

Figure 4.186: Comparison of acceleration FFT ratio between top floor and foundation surface for different contact behavior, inelastic Soil Material Model SM-EP4, Baseline Motion 120111 and 12011.

4.6.4 Earthquake Soil-Structure Interaction Results - 1C Coherent Motion

Figures 4.187 to 4.189 compare the elastic and inelastic response of the tall concrete building under 1C seismic excitation shown in Figure 4.2 (a) and (b).

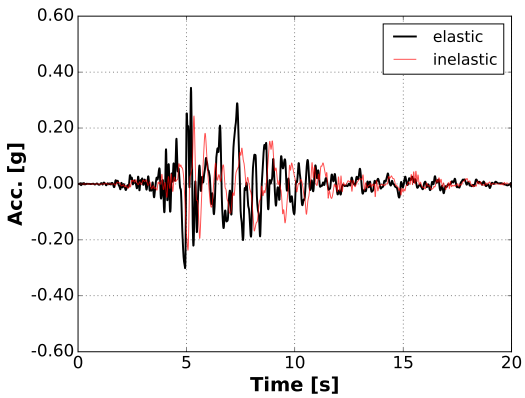

(a) Acceleration at foundation surface

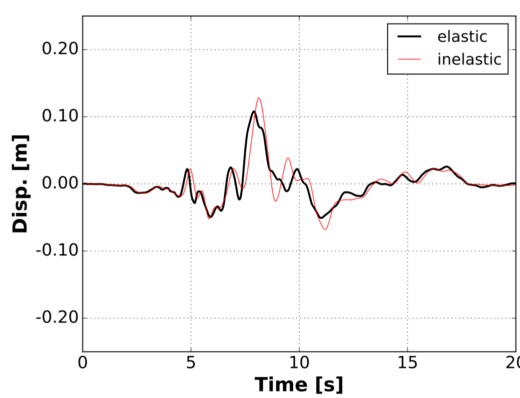

(b) Displacement at foundation surface

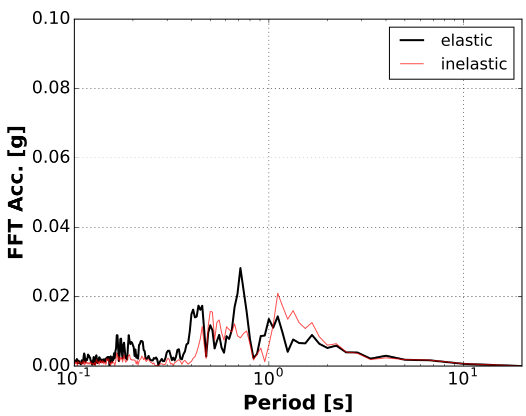

(c) FFT Acceleration at foundation surface

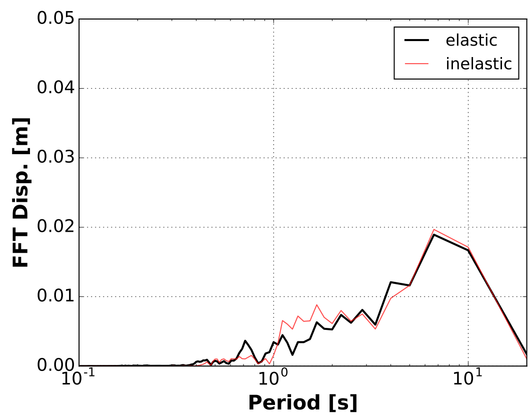

(d) FFT Displacement at foundation surface

Figure 4.187: Elastic vs inelastic, foundation surface, tall concrete building, elastic Soil Material Model SM-EL2 and inelastic Soil Material Model SM-EP4, Baseline Coherent Motion 120122.

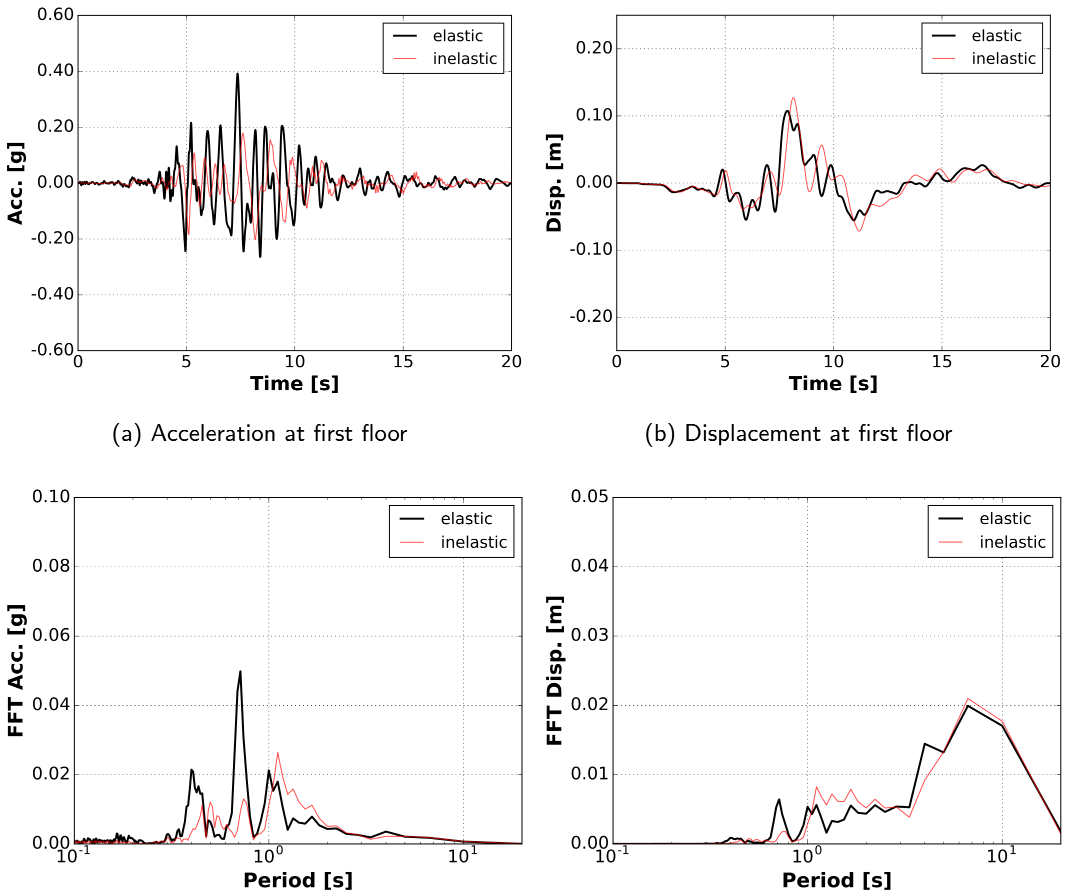

(a) Acceleration at first floor

(b) Displacement at first floor

(c) FFT Acceleration at first floor

(d) FFT Displacement at first floor

Figure 4.188: Elastic vs inelastic, first floor, tall concrete building, elastic Soil Material Model SM-EL2 and inelastic Soil Material Model SM-EP4, Baseline Coherent Motion 120122.

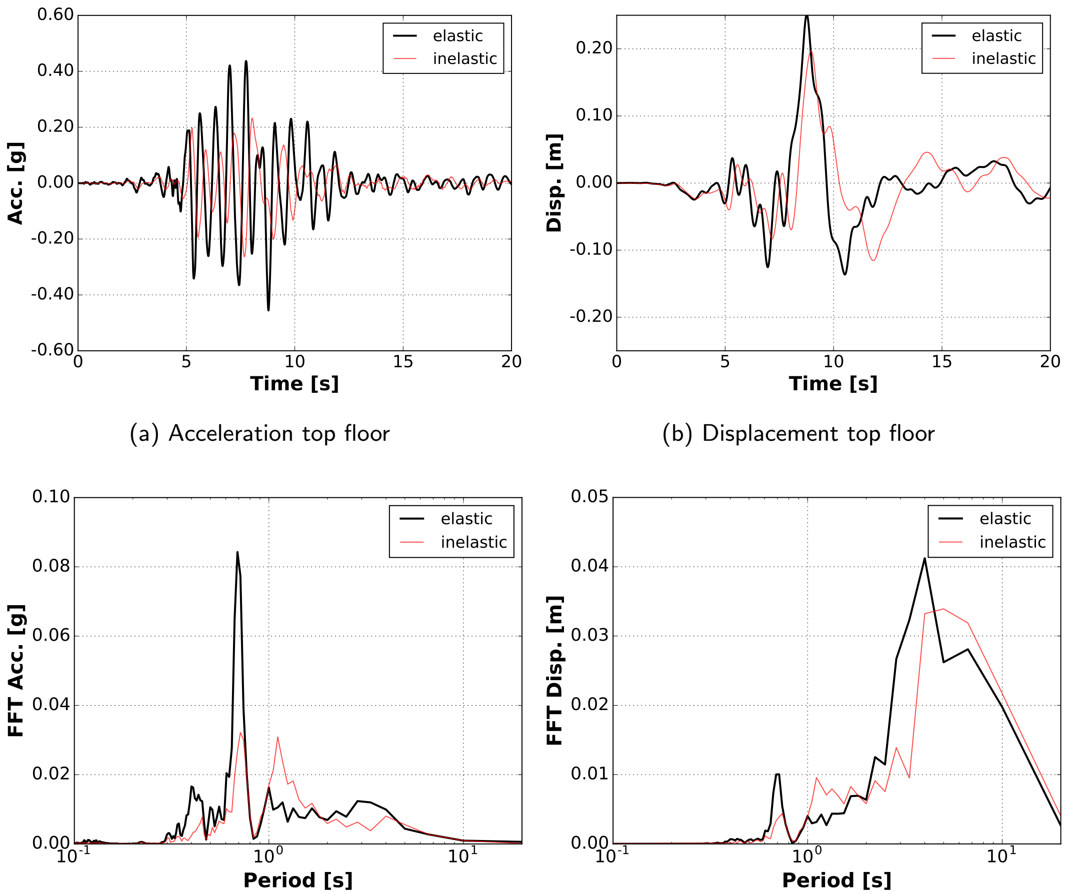

(a) Acceleration top floor

(b) Displacement top floor

(c) FFT Acceleration top floor

(d) FFT Displacement top floor

Figure 4.189: Elastic vs inelastic, top floor, tall concrete building, elastic Soil Material Model SM-EL2 and inelastic Soil Material Model SM-EP4, Baseline Coherent Motion 120122.

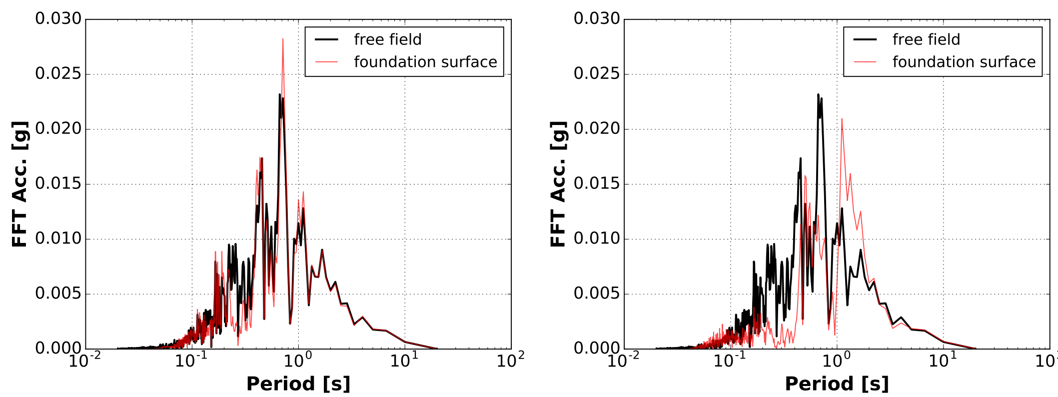

(a) Free-field vs Elastic SSI

(b) Free-field vs Inelastic SSI

Figure 4.190: Acc FFT: free-field vs foundation surface response, elastic Soil Material Model SM-EL2 and inelastic Soil Material Model SM-EP4, Baseline Coherent Motion 120122, tall concrete building: (a) Elastic (b) Inelastic.

4.6.5 Earthquake Soil-Structure Interaction Results - 2C Incoherent Motion with Scaling Factor 1.94

A smaller seismic motion scaling factor of 1.94 is applied to 2C incoherent motions. Nonlinear earthquake soil-structure interaction analysis results are shown below. Figure 4.191 shows the displacement and acceleration response of the foundation surface of the tall building. Figure 4.192 shows the displacement

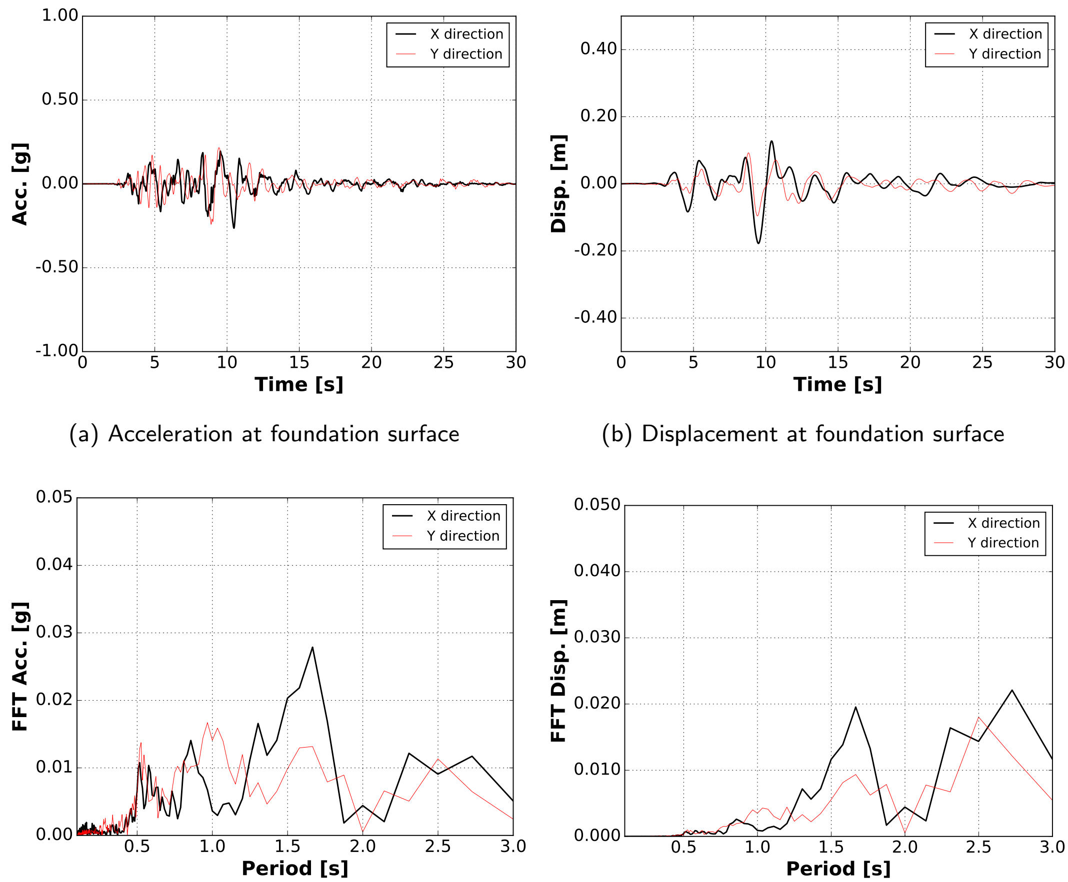

(a) Acceleration at foundation surface

(b) Displacement at foundation surface

(c) FFT Acceleration at foundation surface

(d) FFT Displacement at foundation surface

Figure 4.191: Foundation surface, tall concrete building, inelastic Soil Material Model SM-EP4, Record Incoherent Motion 120111 and 120112 scaled by 1.94.

and acceleration response of the first floor of the tall building. Figure 4.193 shows the displacement and acceleration response of the top floor of the tall building. Figure 4.194 compares the spectral acceleration of the free-field surface input and foundation response of the tall building. The ratio of spectral acceleration between foundation surface and free-field motion is shown in figure 4.195.

It is noted that due to inelastic soil structure interaction effects, reduction of acceleration demand is

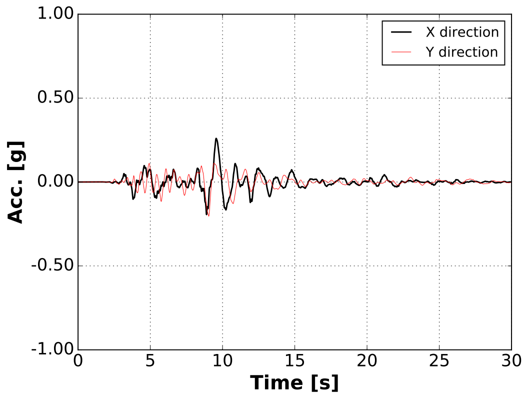

(a) Acceleration at 1st floor

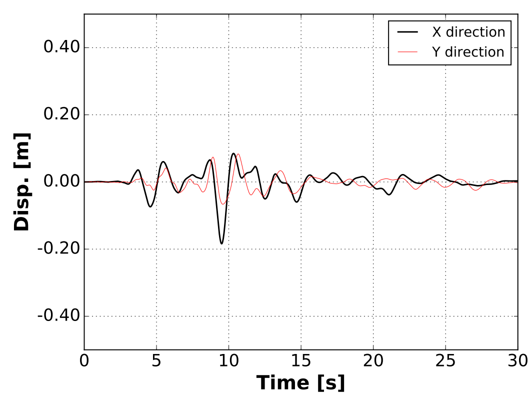

(b) Displacement at 1st floor

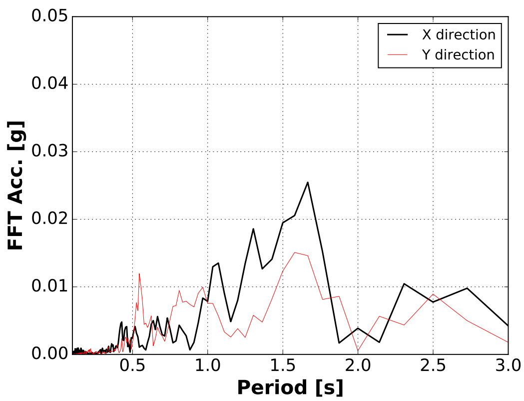

(c) FFT Acceleration at 1st floor

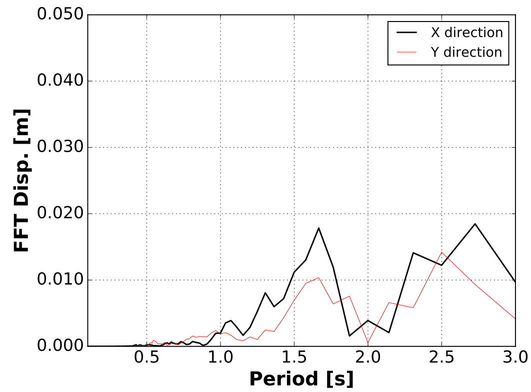

(d) FFT Displacement at 1st floor

Figure 4.192: The 1st floor, tall concrete building, inelastic Soil Material Model SM-EP4, Record Incoherent Motion 120111 and 120112 scaled by 1.94.

observed, again, especially at low periods.

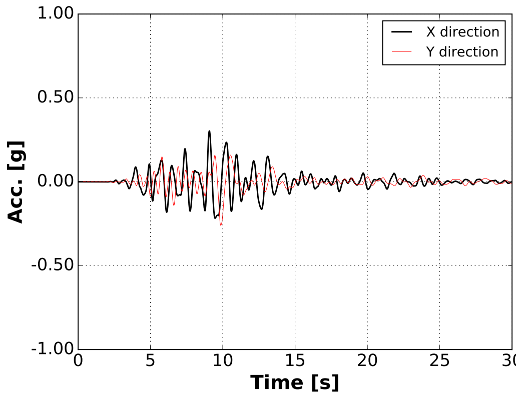

(a) Acceleration at top floor

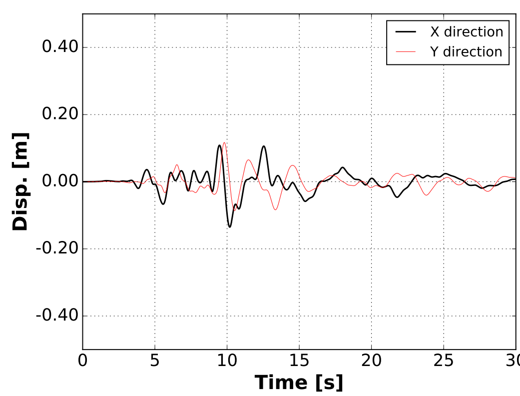

(b) Displacement at top floor

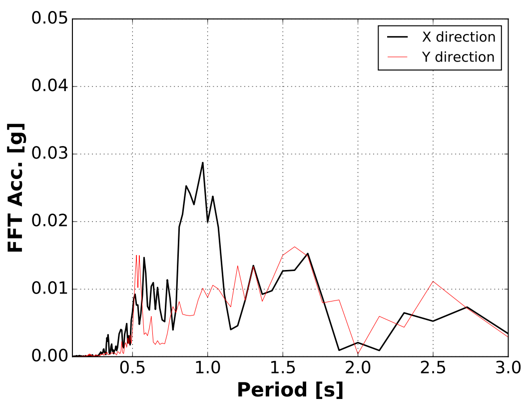

(c) FFT Acceleration at top floor

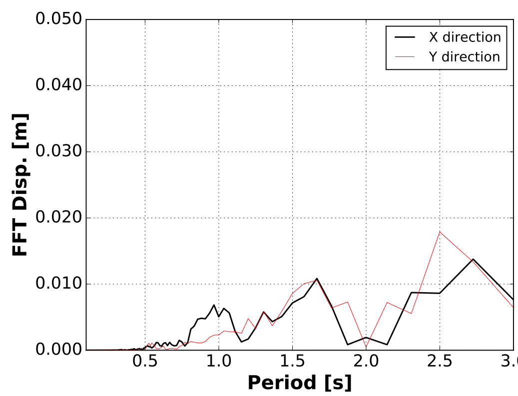

(d) FFT Displacement at top floor

Figure 4.193: The top floor, tall concrete building, inelastic Soil Material Model SM-EP4, Record Incoherent Motion 120111 and 120112 scaled by 1.94.

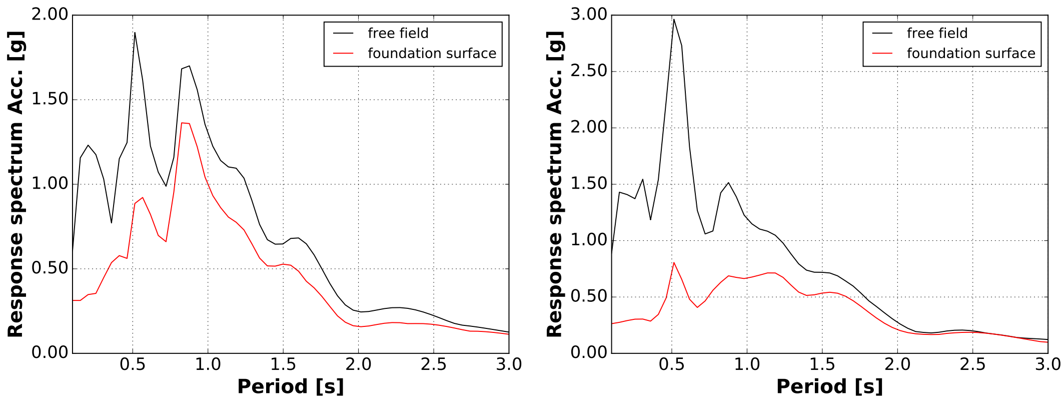

(a) X direction

(b) Y direction

Figure 4.194: Free-field vs foundation surface, tall concrete building, inelastic Soil Material Model SM-EP4, Record Incoherent Motion 120111 and 120112 scaled by 1.94.

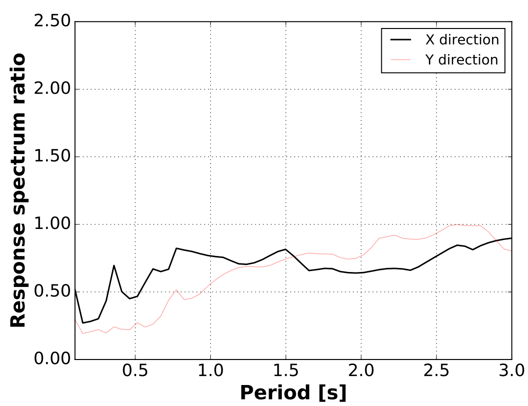

Figure 4.195: Free-field vs foundation surface, tall concrete building, inelastic Soil Material Model SM-EP4, Record Incoherent Motion 120111 and 120112 scaled by 1.94.

Table 4.12 shows the input peak acceleration at the ground surface (PGAs) and peak floor acceleration response (PFA) for different cases of the tall reinforced concrete building for a motions scale factor of 1.94. A note on locations of seismic motion measurement points is provided in section 4.1.5 on page 76. It is noted yet again that the ground surface peak acceleration, shown in Table 4.12 as surface input, is the free-field motions that were used to perform deconvolution (Kramer, 1996) to a certain depth, and then motions from a depth are propagated upward through a linear and/or nonlinear soil and soil-structure system. It is also noted that Table 4.12 does not show results for an inelastic coherent case as these results are not available. Locations of seismic motion measurement points are shown in section 4.1.5 on page 76.

Table 4.12: Comparison of input and response PGAs/PFAs for different simulations cases of tall reinforced concrete building, inelastic Soil Material Model SM-EP4, Record Motion 120111 and 120112 scaled by 1.94.

		Elastic coherent	Elastic incoherent	Inelastic coherent	Inelastic incoherent
	Free Field Surface input	0.52	0.52	–	0.52
PGA/PFA [g]	Foundation surface	0.37	0.33	–	0.20
X positive	First floor	0.41	0.40	–	0.26
	Top floor	0.42	0.45	–	0.30
	Free Field Surface input	0.35	0.35	–	0.35
PGA/PFA [g]	Foundation surface	0.32	0.33	–	0.26
X negative	First floor	0.36	0.35	–	0.19
	Top floor	0.48	0.47	–	0.22
	Free Field Surface input	0.67	0.67	–	0.67
PGA/PFA [g]	Foundation surface	0.54	0.47	–	0.22
Y positive	First floor	0.38	0.35	–	0.11
	Top floor	0.58	0.57	–	0.16
	Free Field Surface input	0.58	0.58	–	0.58
PGA/PFA [g]	Foundation surface	0.52	0.44	–	0.24
Y negative	First floor	0.36	0.37	–	0.20
	Top floor	0.51	0.54	–	0.26

Chapter 5

Results Discussion

Modeling and simulation results presented in above sections are briefly discussed below.

- Ventura Hotel, seismic motions are fairly weak,
  - Simulation of observed behavior for Northridge earthquake with Real-ESSI shows very good agreement,
  - Real-ESSI results show a bit higher frequencies in response,
  - Real-ESSI results show some discrepancy in response, increased response after 30 seconds, particularly in X direction
  - Variability in response for different levels of damping is presented as well,
  - Variability in response for different stiffness reductions for structural members is presented too,
- Low, steel building
  - Reduction of accelerations due to inelastic response when compared to elastic response, particularly for soft soil model SM-EP1, less reduction for stiffer soil model SM-EP2 and less reduction for stiffer soil model SM-EP3. However, reduction are present for al three models.
  - Increase in displacements due to inelastic response when compared to elastic response
  - Reduction in frequency content due to inelastic response when compared to elastic response
  - Similar response for spread foundation and slab foundation models
  - Reduction of acceleration demand is less influenced by incoherent motions
  - Reduction of acceleration demand is more influenced by soil and interface/contact inelastic response

  - Good match of code based RRS factors with calculated RRSs for elastic, no-interface/contact models with incoherent motions, see Section 4.5.6 on page 228
  - Calculated RRS for inelastic soil models and inelastic interfaces/contacts can influence RRSs even more, with RRS values going down to 0.6, even for stiffer soil SM-EP3, see page 230

- Tall, concrete building,

  - Reduction of accelerations due to inelastic response, sometimes significant, see table 4.11 on page 242, and figures in sections 4.6.2, 4.6.3 and 4.6.4
  - Increase in displacements due to inelastic response
  - Reduction in frequency content due to inelastic response
  - Reduction of acceleration demand is less influenced by incoherent motions
  - Reduction of acceleration demand is more influenced by soil and interface/contact inelastic response
  - Simulations are still ongoing for this building with stronger soil and results will be added shortly

Chapter 6

Suggested Future Work

Work on modeling and simulation of earthquake soil structure interaction (ESSI) behavior of soil-building systems during ATC-144 project revealed a number of interesting question. A partial list of these questions, problems, that justify further work and investigation, are listed below.

- Additional nonlinear, inelastic modeling and analysis of response of buildings designed using standard, ASCE-7 based design procedures. In particular, a more in depth investigation of nonlinear soil and nonlinear structural effects on ESSI response,
- Investigation of influence of non-vertically propagating seismic waves, including influence of surface translational and surface rotational waves on response of low and tall buildings,
- Investigation of behavior of buildings with BRB (Buckling Restraint Braces) systems, particularly when more than two BRBs are present per level/floor within each frame/direction.
- Detailed investigation of coherent versus incoherent seismic motion input effects on building systems, including traveling wave effects.
- Investigation of soil stiffness and soil nonlinear/inelastic behavior effects on ESSI response of low and tall buildings.
- Investigation of foundation design (shallow, embedded, spread, mat-slab, piles, etc.) effects on ESSI response of low and tall buildings.
- Further investigation of deconvolution methods for nonlinear, inelastic wave propagation.

Bibliography

T. Ancheta, J. Stewart, and N. Abrahamson. Frequency dependent windowing: A non-stationary method for simulating spatially variable earthquake ground motions. Earthquake Spectra, 2012. in review.

T. D. Ancheta. Engineering characterization of spatially variable earthquake ground motions. PhD thesis, University of California at Los Angeles, 2010.

T. D. Ancheta, J. P. Stewart, and N. A. Abrahamson. Engineering characterization of earthquake ground motion coherency and amplitude variability. In 4th IASPEI/IAEE International Symposium, 2011.

K.-J. Bathe. Finite Element Procedures in Engineering Analysis. Prentice Hall Inc., 1996. ISBN 0-13-301458-4.

J. Bielak, K. Loukakis, Y. Hisada, and C. Yoshimura. Domain reduction method for three–dimensional earthquake modeling in localized regions. part I: Theory. Bulletin of the Seismological Society of America, 93(2):817–824, 2003.

D. Boore. Orientation-independent nongeometric-mean measures of seismic intensity from two horizontal components of motion. Bulletin of the Seismological Society of America, 100(4):1830–1835, 2010.

C. Crouse and J. McGuire. Energy dissipation in soil-structure interaction. Earthquake Spectra, 17(2): 235–259, May 2001.

FEMA. Quantification of building seismic performance factors. Technical Report P-695, Applied Technology Council for the Federal Emergency Management Agency, Washington DC, 2009.

J. F. Hall. Problems encountered from the use (or misuse) of Rayleigh damping. Earthquake engineering & structural dynamics, 35(5):525–545, 2006.

B. Jeremić, G. Jie, Z. Cheng, N. Tafazzoli, P. Tasiopoulou, F. Pisanò, J. A. Abell, K. Watanabe, Y. Feng, S. K. Sinha, F. Behbehani, H. Yang, and H. Wang. The Real-ESSI Simulator System. University of California, Davis, 1988-2020. http://real-essi.us/.

B. Jeremić, Z. Yang, Z. Cheng, G. Jie, N. Tafazzoli, M. Preisig, P. Tasiopoulou, F. Pisanò, J. Abell, K. Watanabe, Y. Feng, S. K. Sinha, F. Behbehani, H. Yang, and H. Wang. Nonlinear Finite Elements: Modeling and Simulation of Earthquakes, Soils, Structures and their Interaction. Self Published, University of California, Davis, CA, USA, and Lawrence Berkeley National Laboratory, Berkeley, CA, USA, 1989-2021. ISBN 978-0-692-19875-9. URL: http://sokocalo.engr.ucdavis.edu/~jeremic/LectureNotes/.

S. L. Kramer. Geotechnical Earthquake Engineering. Prentice Hall, Inc, Upper Saddle River, New Jersey, 1996.

B. Lizundia, T. Ancheta, C. Crouse, R. Hanson, S. Harris, A. Hortacsu, B. Jeremić, M. Mahoney, L. Star, J. Stewart, and M. Valley. Improved design guidance for soil-structure interaction. In Proceedings of the 17th World Conference on Earthquake Engineering, number Proceedings No C004321,, Sendai, Japan, 2021.

L. Star. personal communication with B. Lizundia and B. Jeremić,. 30Dec2019, 29Jan2020, 2019, 2020.

J. P. Stewart and A. F. Stewart. Analysis of soil-structure interaction effects on building response from earthquake strong motion recordings at 58 sites. Technical Report UCB/EERC-97/01, University of California at Berkeley, 1997.

M. Trifunac. Power design method. In Proceedings Earthquake Engineering in the 21st Century, Skopje, Ohrid, Macedonia, August 27 - September 1 2005. IZIIS.

M. Trifunac, T. Hao, and M. Todorovska. On energy flow in earthquake response. Technical Report CE 01-03, University of Southern California, Los Angeles, California, 2001a.

M. D. Trifunac, T. Ying Hao, and M. I. Todorovska. Energy of earthquake as a design tool. In Proceedings of 13th Mexican Conference on Earthquake Engineering, XIII MCEE, pages 1–49, Guadalajara, Mexico, 31th October – 3rd November 2001b.

H. Yang, S. K. Sinha, Y. Feng, D. B. McCallen, and B. Jeremić. Energy dissipation analysis of elastic-plastic materials. Computer Methods in Applied Mechanics and Engineering, 331:309–326, 2018.

H. Yang, Y. Feng, H. Wang, and B. Jeremić. Energy dissipation analysis for inelastic reinforced concrete and steel beam-columns. Engineering Structures, 197:109431, 2019a. ISSN 0141-0296. doi: https://doi.org/10.1016/j.engstruct.2019.109431. URL http://www.sciencedirect.com/science/article/pii/S0141029618323459.

H. Yang, H. Wang, Y. Feng, and B. Jeremić. Plastic energy dissipation in pressure-dependent materials. ASCE Journal of Engineering Mechanics, 2019b. In Print.

H. Yang, H. Wang, Y. Feng, F. Wang, and B. Jeremić. Energy dissipation in solids due to material inelasticity, viscous coupling, and algorithmic damping. ASCE Journal of Engineering Mechanics, 145 (9), 2019c.

C. Yoshimura, J. Bielak, and Y. Hisada. Domain reduction method for three–dimensional earthquake modeling in localized regions. part II: Verification and examples. Bulletin of the Seismological Society of America, 93(2):825–840, 2003.